Imperial College London

Engineered Scaffolds for the Preservation of Gliding Tissue Interfaces

Rachael Helen Harrison

Submitted in Accordance with the Requirement for the

Degree of Doctor of Philosophy and the Diploma of Imperial College London

The Department of Materials

Imperial College London

January 2016

Abstract

The production of modular scaffolds that allow for the facile spatial localisation of a variety of interchangeable functional groups gives a toolbox of options for tissue engineering. Furthermore, the need to re-engineer a system for each specific application or function is eliminated. A modular scaffold system based on the versatility of the electrospinning processing technique, chemical modification of bioresorbable poly-ε-caprolactone (PCL) and a controlled free radical polymerization technique is proposed.

An antifouling surface is prepared by grafting a poly(oligoethylene glycol) bottlebrush (pOEGMA) from a surface initiating group on silicon wafers and electrospun PCL scaffolds. The surface initiated polymerization method provides versatility which allows for wide variety of monomer units to be selected for bespoke scaffolds and tailored to particular applications, including fluorescent labelling. The antifouling ability of the pOEGMA functionalization is explored and characterised with protein and cell assays. The chemical and mechanical stability of the pOEGMA functionalized scaffolds is explored in a simulated physiological environment over 10 weeks. Following which the chemical and material properties are re-characterised and found to be maintained.

A dual functional bilayer scaffold with an antifouling, non-cell adhesive surface and an opposing cell-adhesive surface is then produced. The pOEGMA coating provides the antifouling surface whilst the cell adhesive side is prepared by end-functionalizing the PCL with the cyclic cell binding Arg-Gly-Asp-Ser (RGDS) peptide. Spatial control of the functionality through the mat is achieved by sequential electrospinning of the functionalized polymers. The opposing properties of the surfaces are demonstrated through cell culture and florescent labelling to illustrate clear spatial segregation.

Gliding surfaces such as those found in the musculoskeletal systems, the tendon for example, are vulnerable to tethering from scarring following surgical and traumatic injury. This scaffold could offer protection from these scars through the control of cellular migration and may lead to improved patient outcomes.

Declaration of Originality

I, Rachael H Harrison, declare that the original scientific content contained within this thesis was acquired and analysed by me at Imperial College London, UK, unless otherwise stated. All collaborative efforts and contributions by others are stated in the "Statement of Contribution" below.

Statement of Contribution

Mr Tarik Abdelmoula, PhD student, Physics, assisted in the measurement and interpretation of the ellipsometry data.

Dr Nadav Amdursky, postdoctoral scientist in the group, assisted with all AFM measurements and related data interpretation.

Dr Robert Chapman, postdoctoral scientist in Prof Stevens's groups, synthesised and provided the biotinylated–peg monomer and provided draft text for the synthesis steps which are included for completeness in section 3.2.3.4. He provided characterisation figures 7-1 and 7-2. Dr Chapman also synthesised the peg3ma-ibu monomer and provided draft text for section I.2.2.2.

Dr Lesley Chow, postdoctoral scientist in Prof Stevens's group, synthesised the cRGDS peptide in Chapter 4 and coupled it to the PCL-malamide that I had produced. She provided draft text for the synthesis in section 4.2.2.1 and 4.2.2.2.

Mr Moht Mahat, fellow PhD student in Prof Stevens's group, ran the XPS measurements, data analysis and interpretation included in Chapter 2 and Chapter 3. He provided draft text for section 2.3.3.1.2 and provided XPS panels of Figures 2-9 and 3-7.

Mr Paresh Parmar, fellow PhD student in Prof Stevens's group assisted in the FTIR measurements in Chapter 4 and provided Figure 4-5. Furthermore he provided Figure 4-4.

Dr Anna Regoutz, postdoctoral scientist in the department, ran the XPS measurements, data analysis and interpretation included in Chapter 5. She provided draft text the XPS aspect of section 5.2.2.2 and provided Figures 5-4, 5-5, and 5-6.

Dr Chris Spicer, postdoctoral scientist in Prof Stevens's group, synthesised and provided the amino-Cy5 dye for labelling of the cRGDS, used in Chapter 4. He provided the text and characterisation Figures included in Appendix G which have been included for completeness.

Dr Joe Steele, former PhD student in Prof Steven's group, for sectioning all the histology samples on the microtome and for his assistance with all the confocal imaging and production of the images in Figures 3-12 and 4-8. Furthermore, he calculated the pressure experienced by scaffolds during mechanical testing and provided draft text for this in Appendix H, included for completeness.

Acknowledgments

I would like to thank Professor Molly Stevens for taking me on as a PhD candidate given my clinical rather than purely scientific background, and for her guidance and support over the last 3 years. I would also like to thank her for building a research group that inspires innovative and collaborative working; bringing fantastic people together from all disciplines and giving them the freedom and support to explore their ideas.

I would also like to thank Dr Iain Dunlop and Mr Shehan Hettiaratchy for their support, mentorship and supervision. Together they have inspired and taught me things well beyond the scope of my PhD, and together with Molly have changed the way I view my in future in both my personal and professional life. I would particularly like to thank H for his mentorship that precedes this PhD. He is one of the (few) clinicians that lead me to buck the trend and follow my dream in entering into Plastics training when so many told me not to. You also supported and encouraged my decision to undertake this PhD when so many tried to dissuade me from this path. I would not be where I am now if our paths had not crossed (in Costa, how appropriate!) and I will be forever grateful. I hope that as I build my career that we can continue to collaborate on projects.

I would also like to thank the many members of the Stevens Group at Imperial College London without whom this work would not have been possible. Dr Rob Chapman and Dr Adam Gormley for their supervision and mentorship in particular, and together with Dr Lesley Chow and Dr Jean-Philippe St-Pierre for their inspiration and kind patience for a simple surgeon. Thank you also to Miss Sabrina Skeete, Mr Alex Kirby and Dr Ben Pierce for keeping the lab running so smoothly. Thank you too to my many friends in the Stevens group and beyond, especially Joe Steele, Karla-Luise Herpoldt and Anu Solanki who shared the journey, and many lunches along the way. I also fondly remember those who have not seen me come to the end of this journey.

Funding for this work has come from many sources, including the Blond Fellowship from the Royal College of Surgeons of England through the Research Fellowship programme, the Rosetrees Trust, and the bursary scheme at Imperial College London which is supported by the EPSRC.

Finally to those closest to me; to my family, thank you for all the support you have given me throughout my adventures both in education, professionally, and personally. I really don't think there is any more you could have done and there is no doubt in my mind that without you I would not be where I am today….not so bad for someone who used to write backwards when they were not concentrating eh?!

I probably should mention Sam Wright. You started this process as my boyfriend and finish it as my husband. Your unwavering support of my career, whether clinical or academic, is second to none. With you by my side I feel like I can take on the world and win; you give me the confidence to dare to compete. Thank you for always making me celebrate the wins…however small.

Table of Contents

Abstract 3
Declaration of Originality 5
Statement of Contribution 6
Acknowledgments 7
List of Figures 13
List of Tables 19
List of Abbreviations 20

Chapter 1 : Tissue Engineering and Regenerative Medicine: a versatile approach for treatment design 23

1.1Tissue engineering and regenerative medicine 23
1.1.1 Biomaterials within tissue engineering 24
1.2Gliding tissues and interfaces 25
1.2.1 How tissue engineering could be used to preserve a gliding surface 25
1.3 A modular and versatile approach to scaffold design 26
1.3.1 Introduction to polymers and radical polymerisation 29
1.3.2 Scaffold fabrication 38
1.3.3 Scaffold surface functionalization: polymer brush grafting from electrospun fibres 40
1.3.4 Spatial control of functional groups 44
1.3.5 Cell binding surfaces 47
1.4 The damaged tendon: a model system 49
1.4.1 Tendon: structure, function and anatomy 49
1.4.2 Tendon Healing 53
1.4.3 Treatment Strategies and Complications 55
1.5 Bilayer scaffold design and scaffold adaptations for the tendon model 69
1.5.1 Poly-ε-caprolactone, the polymer chosen for the bulk scaffold 70
1.5.2 Electrospinning as a processing technique 71
1.5.3 Monomer selection for surface functionalization 71
1.6 Summary 75
1.7 References 76

Chapter 2 : Controlled Radical Polymerisation 95
2.1 Introduction 95
2.2 Materials and Methods 95
2.2.1 Materials 95
2.2.2 ATRP polymerisation in solution 96
2.2.3 ARGET ATRP polymerisation in solution 97
2.2.4 Polymer brush grafting from 2-dimentional silicon surfaces 98
2.3 Results and Discussion 103
2.3.1 Polymerisation of HEMA and OEGMA in solution with ATRP 103
2.3.2 ARGET ATRP polymerisation in solution 104
2.3.3 Polymer brush grafting from 2D silicon surfaces 108
2.4 Conclusions 113
2.5 References. 114

Chapter 3 : Surface Grafted Polymerisation 116
3.1 Polymerisation from 3D surfaces 116
3.2 Materials and Methods 117
3.2.1 Materials 117
3.2.2 Grafting pOEGMA from functionalised 3D electrospun fibres 118
3.2.4 Assessment of antifouling ability of PCL-pOEGMA scaffolds 122
3.2.5 Statistical Analysis 127
3.3 Results and Discussion 128
3.3.1 Grafting pOEGMA from functionalised electrospun fibres 128
3.3.2 Assessment of the antifouling ability of PCL-pOEGMA scaffolds 135
3.4 Conclusions 143
3.5 References 144

Chapter 4 : Bilayer scaffolds 147
4.1 Spatial control of functional groups and bilayer scaffold generation 147
4.2 Materials and Methods 149
4.2.1 Materials 149
4.2.2 End functionalization of PCL with cyclised RGDS peptide motif 149
4.2.3 Assessment of cell binding of PCL-cRGDS scaffold 152
4.2.4 Layered electrospinning for the production of bilayer scaffolds 153
4.2.5 Characterisation of bilayered scaffold 154
4.2.6 Statistical Analysis 156

4.3 Results and Discussion 157
4.3.1 End functionalization of PCL with cyclised RGDS peptide motif 157
4.3.1.3 Electrospinning of PCL-cRGDS 159
4.3.2 PCL-cRGDS scaffolds promote cell adhesion of tenocytes 160
4.3.3 Spatially controlled polymerisation within electrospun scaffolds 163
4.3.4 Characterisation of bilayered scaffold 163
4.4 Conclusions 166
4.5 References. 167

Chapter 5: Scaffold stability ..... .170
5.1 Assessing scaffold integrity *in vitro* for a demanding *in vivo* environment 170
5.1.1 Stability and degradation of the pOEGMA surface 170
5.2 Materials and Methods 173
5.2.1 Materials 173
5.2.2 Assessment of degradation and stability of pOEGMA in solution and from scaffolds 173
5.2.3 Statistical Analysis 175
5.3 Results and Discussion 176
5.3.1 Degradation and stability of pOEGMA in solution and on scaffolds 176
5.4 Conclusions 189
5.5 References. 190

Chapter 6 : Conclusions and Future Directions 192
6.1 Conclusions 192
6.2 Future directions 194
6.2.1 Exploring and expanding the mechanical properties 194
6.2.2 Drug releasing polymer brushes 195
6.2.3 Applying the versatile design for a different application: an engineered blood vessel 196
6.3 References 197

Chapter 7 : List of appendices 199
Appendix A 200
Appendix B 216
Appendix C – Purification of Cu(I)Br 226
Appendix D – SOP for ARGET ATRP in solution 227
Appendix E – ToF-SIMS analysis of silicon surfaces 232

Appendix F - Method and assessment of adsorbed polymer removal from scaffolds 233
Appendix G – Characterization of the biotin monomer.....235
Appendix H – Synthesis of amino-cy5 dye.....237
Appendix I: Mechanical testing of scaffolds 242
Appendix J: Calculating the contact pressure on scaffolds exerted by mechanical testing 247
Appendix K : Drug Releasing Scaffolds.....249
Appendix L : Permission for reproduction of Figure 7-10 from Ricciotti et al.[301].....276
Appendix M : List of publications.....278
References 281

List of Figures

Figure 1-1: Schematic of the key features in the modular and versatile scaffold design. 28
Figure 1-2: Schematic to outline the steps of initiation, propagation and termination through (i) combination or (ii) disproportionation, found in free radical polymerisation, adapted from[34].....30
Figure 1-3: Schematic of ATRP (adapted from[34]).....31
Figure 1-4: Schematic of ARGET ATRP (adapted from[3]).....34
Figure 1-5: Schematic of polymer brush grafting to, form and through surfaces. 35
Figure 1-6: Electrospinning fabrication of scaffolds. (A) Schematic of the electrospinning set up onto a rotating mandrel. (B) Handling an electrospun mat. (C) A bright field microscopy image of a histological section of an electrospun mat with an SEM image of the fibres inset. 39
Figure 1-7: Schematic representation of the different approaches for producing polymer brushes from electrospun scaffold surfaces.....42
Figure 1-8: The approach outlined in this thesis for the production of surface initiated polymer brush grafting from electrospun fibres with spatial control. See legend from Figure 1-6. 43
Figure 1-9: Surface initiated polymer bottlebrush grafting from 2D and 3D functionalised surfaces by ARGET ATRP. (A) Schematic of ARGET ATRP controlled radical polymerisation from surfaces. (B) Schematic of functionalised 2D silicon surfaces before (i) and after (ii) grafting with pOEGMA bottlebrushes. (C) Schematic of functionalised 3D electrospun fibres before (i) and after (ii) grafting with pOEGMA bottle brushes. 44
Figure 1-10: The hierarchical structure of a tendon, adapted from the literature[1].....50
Figure 1-11: Anatomy of the flexor tendons. (A)The FDS chiasm (B) The pulley system in the thumb (C) The FDS and FDP in the finger with 3 annular pulleys demonstrated. Illustrations copyright Donnald Sammut, reproduced with permission (www.donnaldsammut.com).....52
Figure 1-12: The bilayer scaffold design with an antifouling surface and a cell adhesive surface.....72
Figure 1-13: Schematic of the adaptions of the modular scaffold for a primary flexor tendon repair. Central photograph adapted from http://www.atlantaequine.com/images/tendon_sheath_dissection.jpg.....73
Figure 1-14: Flow chart showing the aims of this work and the key components at each stage.....74

Figure 2-1: Structures and schematic of radical addition polymerisation with the EBIB initiator of HEMA to pHEMA (A) and OEGMA to pOEGMA (B) in solution.....92
Figure 2-2: Schematic of pOEGMA grafting from 2D silicon surfaces. Chemical structures of APTES-Ini presenting polymerisation initiating group for grafting of OEGMA from the silicon surface (i) with schematic (iii). Chemical structure of the resultant pOEGMA bottlebrush from the 2D silicon surface (ii) with schematic (iii). 99
Figure 2-3: Reaction scheme for the functionalization of ATPES with Ini. 99
Figure 2-4: Polymerisation of HEMA by ATRP. (i) Kinetics plot of polymer conversion by ^{1}H-NMR. (ii) SEC of HEMA polymer produced at 2 hours with dispersity ($Đ$), M_n and conversion (X) by ^{1}H-NMR inset. 103

Figure 2-5: SEC analysis of pHEMA by ARGET ATRP with different catalysts. Cu(II)Cl exhibits superior control of polymerisation (*Đ*, by SEC analysis) and conversion (X, by ^{1}H-NMR) when compared to Cu(II)Br for use in ARGET ATRP polymerisations with HEMA. 104
Figure 2-6: Optimisation of ARGET ATRP with through changing molar equivalents of the reducing agent (AScA). Conversion by ^{1}H-NMR (X) together with M_n and dispersity (*Đ*) as produced through SEC analysis are inset.....106
Figure 2-7: Polymerisation kinetics of HEMA and OEGMA by ARGET ATRP. (i) Logarithmic conversion of HEMA and OEGMA by ^{1}H-NMR. (ii) SEC analysis of the resultant polymers produced from ARGET ATRP polymerisations of OEGMA with initiator:reducing agent ratios of 150:0.12 and 150:0.15 at a reaction time of 60 minutes.....107
Figure 2-8: Measurement of the height of the dry brush. (i) Height of dry brush as measured by AFM (n = 3, error bars SD) and ellipsometry (n = 2, error bars SD) of pOEGMA grafted from 2D silicon surfaces. (ii) AFM scratch test and representative profile (iii) of pOEGMA grafting from silicon wafers. Theoretical polymer contour length = 24.7 nm. Extracted from Harrison *et al*.[2] 109
Figure 2-9: XPS analysis of the surface initiated pOEGMA bottlebrushes from silicon wafers. XPS analysis of silicon wafers functionalised with APTES-Ini with controls (dashed, bottom trace), silicon functionalised with APTES-Ini that underwent polymerisation with no reducing agent, (ascorbic acid, AScA, dotted middle trace) and pOEGMA grafting from a silicon wafer (top trace). Conversion by ^{1}H-NMR is included above each trace (left). Si-APTES-pOEGMA sample with the C 1*s* peaks fitted (right).....110
Figure 2-10: Water contact angle measurement of silicon wafers functionalised with (i) APTES-Ini and (ii) following surface initiated grafting with pOEGMA. 112

Figure 3-1: Surface initiated polymer bottlebrush grafting from 2D and 3D functionalised surfaces by ARGET ATRP. (A) Schematic of ARGET ATRP controlled radical polymerisation from surfaces. (B) Schematic of functionalised 2D silicon surfaces before (i) and after (ii) grafting with pOEGMA bottlebrushes. (C) Schematic of functionalised 3D electrospun fibres before (i) and after (ii) grafting with pOEGMA bottle brushes. 116
Figure 3-2: End functionalised PCL-diol with the initiating group BIBB (PCL-Ini).....118
Figure 3-3: Electrospinning experimental set up for the production of electrospun scaffolds. The polymer solution within a syringe is loaded onto a programmable syringe driver (left) and a voltage applied to the mounted needle. An earth wire or opposing voltage is applied to a metal collector, here a rotating mandrel, covered in aluminium foil. The apparatus is completely contained within a fume hood.....119
Figure 3-4: Structure of the biotinylated PEG monomer 120
Figure 3-5: ^{1}H-NMR (400MHz, $CDCl_3$) of PCL-Ini 129
Figure 3-6: SEM images of control PCL scaffolds and modified PCL scaffolds (PCL-Ini) with 9% (w/w) and 17% (w/w). 130
Figure 3-7: Demonstration and characterization of surface initiated polymer brush growth from functionalized 3D electrospun scaffolds, initially published in Harrison *et al.*[282] (A) High resolution C 1*s* core-level spectra of pOEGMA grafting from electrospun scaffolds with 9% and 17% (w/w) PCL-Ini before (left) and after (right) grafting of pOEGMA. Conversion by ^{1}H-NMR (X) is inset. (B) Water contact angle measurement of (i) electrospun PCL/PCL-Ini and (ii) PCL-pOEGMA with inset schematics. (C) Representative SEM micrograph of electrospun PCL-pOEGMA fibres..... 131

Figure 3-8 Fluorescent labelling and histological sectioning of PCL-pOEGMA and PCL-p(OEGMA-*co*-biotin) scaffolds following incubation with streptavidin-fluorescein, demonstrating even distribution of polymer across the scaffold cross section. Electrospun scaffolds of PCL-Ini 9% (w/w) underwent polymerisation with OEGMA (left) and OEGMA in conjunction with the biotinylated monomer (right) and were both subsequently labelled with streptavidin-fluorescein. Following which, the scaffolds were embedded and histologically sectioned. Bright field images (upper) and fluorescence images (lower) show clear signal on the PCL-p(OEGMA-*co*-biotin) fibres. Conversion of the sacrificial initiator by ^{1}H-NMR in included (X). Initially published in Harrison *et al.*[282] 133
Figure 3-9: Confirmation of covalent attachment of pOEMGA to 3D electrospun scaffolds. (A) Water contact angle images of a control scaffold (with no initiating group) and 17% (w/w) PCL-Ini following polymerisation with OEGMA and the biotinylated monomer. The control scaffold remains hydrophobic after washing, suggesting little remaining surface pOEGMA (A). (B) Electrospun scaffolds of 17% (w/w) PCL-diol (control) and 17% (w/w) PCL-Ini underwent polymerisation with the biotninylated monomer and subsequent streptavidin-fluorescein labelling. Bright field images (upper) and fluorescence images (lower) show minimal signal on control fibres and labelling of pOEGMA-*co*-biotin. Conversion of the sacrificial initiator by ^{1}H-NMR is included (X). Adapted from Harrison *et al.*[282] 135
Figure 3-10: Antifouling ability of 17% (w/w) PCL-diol control scaffolds and 17% (w/w) PCL-pOEGMA scaffolds when incubated with a panel of fluorescently bound biomolecules. BSA, fibronectin, HA, CS and heparin were incubated with scaffolds for 18 hours before being washed. Fluorescence from absorbed biomolecules was read using a plate reader. $^{**}p < 0.005$, N = 4 with 3 technical replicates. Error bars show standard deviation. 137
Figure 3-11 P1 bovine tenoytes in culture flasks before seeding on scaffolds. 138
Figure 3-12: An MTT calibration curve was performed to allow the estimation of cell numbers from absorbance signal. Serial dilutions were performed on a single cell suspension of bovine tenocytes to give a series of known cell numbers ranging from 100 000 to 3125 cells. N = 3 with 3 technical replicates using 3 different animals. Normalised means are displayed with error bars showing the standard deviation. 139
Figure 3-13: Assessment of cell adhesion to antifouling pOEGMA scaffolds and PCL control scaffolds. (A) Representative confocal microscopy images of bovine tenocytes cultured for 7 days on electrospun 17% (w/w) PCL-diol control scaffolds (i) and PCL-pOEGMA scaffolds (ii). Cell nuclei stained with draq5 (purple) and actin with phalloidin (green). (B) Metabolic activity of bovine tenocytes cultured on scaffolds for 7 days was assessed by MTT assay. Estimated cell numbers are stated for each bar. Significant difference $^{**}\ p < 0.01$, error bars represent standard deviation. N = 3, with a minimum of 3 internal replicates. 140
Figure 3-14: Fluorescence microscopy images showing cell morphology on PCL control and PCL-pOEGMA scaffolds after 24 hours in culture. (A) Representative image of bovine tenocytes on PCL-pOEGMA scaffolds (A) and PCL control scaffolds (B). (C) Cellular aggregates were occasionally seen on PCL-pOEGMA scaffolds indicating preferential cell-cell adhesion rather than cell-surface adhesion. Cellular nuclei stained with DAPI (blue) and actin with phalloidin (red).....141

Figure 4-1: The bilayer scaffold design with an antifouling surface and a cell adhesive surface.....148

Figure 4-2: Synthesis scheme of cRGDS, adapted from Parmar *et al.* and initially published in Harrison *et al.*[308,309] 149
Figure 4-3: Synthesis scheme of the PCL-cRGDS end-functionalised polymer, adapted from Chow *et al.* and initially published in Harrison *et al*[307,308] 151
Figure 4-4: ESI of the cRGDS peptide confirming the correct mass of the product (MW 577) which is from the same batch previously published in Parmar *et al.*, Figure S3[309] and in Harrison *et al.*, Figure S8[308] 158
Figure 4-5: FTIR of the solid PCL-cRGDS, cRGDS, and control PCL-diol demonstrating successful coupling of the cRGDS to the PCL through the demonstration of the amide (C=O) bonds (boxed). Initially published in Harrison *et al.*[308] 159
Figure 4-6: Representative SEM images of a control PCL scaffold (PCL-diol, left), and scaffolds modified with PCL-cRGDS in a low (middle) and high (right) concentration demonstrating no difference in fibre morphology following the addition of the cRGDS moiety. 160
Figure 4-7: Representative fluorescence microscopy images of bovine tenocytes seeded on PCL-cRGDS electrospun scaffolds at a high (3 mg.mL-1) and a low (1 mg.mL-1) PCL-cRGDS concentration. Bovine tenocytes were seeded onto scaffolds and cultured for 24 hours before assessment. Cells were stained with DAPI (blue, cell nuclei) and phalloidin (red, cell actin) and imaged on a fluorescence microscope. 161
Figure 4-8: Cell-adhesive and non cell-adhesive properties of functionalised electrospun scaffolds, initially published in Harrison *et al.*[308] (A) Representative images of bovine tenocytes cultured on electropsun PCL-cRGDS and PCL-pOEGMA scaffolds for 7 days. Cell nuclei stained with draq5 (purple) and cell actin with phalloidin (green). (B) Metabolic activity of bovine tenocytes cultured on scaffolds for 7 days is assessed by MTT assay. Estimated cell numbers are stated for each bar. *** Significant difference (p <0.0001) N = 3 with 5 internal replicates.....162
Figure 4-9: Dual functionality scaffolds demonstrated by fluorescent labelling of functional groups, adapted from Harrison *et al.*[308]. Fluorescence microscopy images of cross sections of bilayered scaffolds formed with opposing PCL-Ini and PCL-cRGDS electrospun fibre layers. Post-processing polymerisation was used to produce a PCL-p(OEGMA-*co*-biotin) surface (A-B). Overlaid fluorescence images of histological cross sections labelled with streptavidin-fluorescein (green) on the p(OEGMA-*co*-biotin) and with Cy5 (red) for the PCL-cRGDS show well defined spatial resolution of the moieties. Insets (left) show the bright field and single channel fluorescence images with 100 µm scale bars.....16 4
Figure 4-10: Representative images of bovine tenocytes seeded on bilayer scaffolds following post-processing polymerisation and 7 days of tissue culture before being stained with DAPI (blue) for cell nuclei and imaged with fluorescence microscopy. Cell adhesion is supported by the PCL-cRGDS surface and only minimally by the PCL-pOEGMA surface of the scaffold.....165

Figure 5-1: Chemical structure and schematic of modified 14 kDa PCL-ini with pOEGMA polymer brush grafted from either end. (A) Chemical structure with the ester bonds identified where hydrolysis may occur. Red shaded regions indicate the ester linkages binding a whole polymer bottlebrush to the PCL, originating from the initiator group, and green shaded regions indicating the ester bond binding a “branch” or single OEGMA unit to the bottlebrush backbone. (B) Schematic representation of the polymer structure with the

PCL (blue, 1) portion, the structural contribution of the BiBB initiator (red, 2), and the pOEGMA bottlebrush (green, 3). 170
Figure 5-2: Peg3ma mono-disperse monomer degradation by ^{1}H-NMR in dPBS at pH 6.0, 7.4 and 8.1 over 10 weeks 177
Figure 5-3: Normalised C 1*s* XPS characterisation of the 17% (w/w) PCL-pOEGMA scaffolds and the 17% (w/w) PCL-diol matched controls before (0 weeks) and following 10 weeks incubation in PBS. (A) Representative survey spectra of a control scaffold following 0 weeks incubation demonstrating no observable scaffold contamination and clean samples. C 1*s* spectra of the control 17% (w/w) PCL-diol scaffolds (B) and the 17% PCL-pOEGMA scaffolds (C) before (0 weeks), and following 10 week incubation in PBS. (N = 2) 178
Figure 5-4: XPS peak fits for the C 1*s* spectra for the 17% (w/w) PCL-diol controls (left) and the 17% (w/w) PCL-pOEGMA scaffolds (right) following 0 (upper) and 10 weeks (lower) incubation in PBS demonstrating the relative contributions of the different groups to the shape of the spectra. 180
Figure 5-5: C 1*s* components quantified using peak fits from the 17% (w/w) PCL-diol controls and 17% (w/w) PCL-pOEGMA samples over 10 weeks of incubation in PBS. The relative atomic percentages demonstrate the progressive loss of the C-O ether signal from the 17% (w/w) PCL-pOEGMA samples indicating some loss of the polymer brush. Two scaffolds (N = 2) were analysed for time 0 and 10 weeks, otherwise single scaffolds were analysed (N = 1). 2 points were measured from each scaffold and the guidelines are based on the average values from these points. Error bars demonstrate an assumed error of 5%. 181
Figure 5-6: Representative fluorescence microscopy images of PCL-pOEGMA-*co*-biotin scaffolds incubated for 10 weeks in PBS at 37^{o}C. Scaffolds were labelled with streptavidin-fluorescein before imaging. 182
Figure 5-7: Water contact angle measurements for 17% (w/w) PCL-diol (control) and 17% (w/w) PCL-pOEGMA scaffolds before (time 0) and after incubation in PBS for 10 weeks....182
Figure 5-8: Representative SEM images of scaffolds before (time 0) and after 10 week incubation in PBS at 37^{o}C. 17% (w/w) PCL-pOEGMA and matched control scaffolds show no difference in fibre morphology before and after incubation. 183
Figure 5-9: Antifouling ability of 17% (w/w) PCL-diol control scaffolds and 17% (w/w) PCL-pOEGMA scaffolds when incubated with fluorescently labelled BSA. Scaffolds from the same polymerisation were maintained *in vacuo* or incubation in PBS at physiological conditions for 10 weeks before assessment. The polymerisation had a conversion (X) of 73% by ^{1}H-NMR and MW 19000. (** $p < 0.005$, *** $p < 0.001$). N = 4. Error bars show standard deviation. 184
Figure 5-10: An MTT calibration curve was performed to allow for the estimation of cell numbers from absorbance readings. Serial dilutions were performed on a single cell suspension of bovine tenocytes to give a series of known cell numbers ranging from 100 000 to 3125 cells. Using a single animal donor, 3 independent ladders were produced and read in triplicate. Normalised means are displayed with error bars showing standard deviation. 185
Figure 5-11: Assessment of cell adhesion to antifouling pOEGMA scaffolds and PCL control scaffolds before and after incubation in PBS for 10 weeks to assess potential loss of antifouling function. Cells cultured on scaffolds for 7 days. (A) Representative fluorescence microscopy images of bovine tenocytes seeded on scaffolds having been stained with DAPI (blue) for cell nuclei. (B) Metabolic activity of bovine tenocytes cultured on scaffolds for 7 days was assessed by MTT assay. Estimated cell numbers are started for each bar. Significant difference ** $p < 0.01$, *** $p < 0.001$. Single animal cell line with N = 5 scaffolds

read in technical triplicates. Error bars represent standard deviation (SD) and error in cell number is SD in calculated cell number. 186

Figure 7-1: ToF-SIMS heat maps depicting the bromine coverage of silicon samples before and after polymerisation with OEGMA. Si-APTES-Ini (left) is a pre-polymerisation sample; a silicon wafer has been functionalized with APTES and the bromine containing initiating group has been reacted onto the surface. The Si-pOEGMA samples (middle and right) are post polymerisation samples. 232
Figure 7-2: ESI-MS for the biotin-PEG monomer. Calculated 875.5 (M+H+), found 875.5. ..235
Figure 7-3: ^{1}H-NMR of biotin-PEG monomer. 235
Figure 7-4: Synthesis scheme for compound 1. 237
Figure 7-5: Synthesis of Cy5.HCL 2 from compound 2 238
Figure 7-6: Synthesis of amino Cy5 3 from Cy5.HCL 2 239
Figure 7-7 : ESI-MS for the amino Cy5 dye. Calculated 525.4 M+, Found 525.4. 240
Figure 7-8: ^{1}H NMR characterisation of amino-Cy5. Please see above for peak assignments 241
Figure 7-9: Custom built hydration chamber for the uniaxial compression testing of the scaffolds. 243
Figure 7-10: Uniaxial, unconfined load testing of matched electrospun 17% (w/w) PCL-diol scaffolds (A, upper) and 17% (w/w) PCL-pOEGMA scaffolds (B, lower) with a range of normal forces from 1 N to 40 N using a hemispherical indentor at a rate of 10 Hz for 1000 cycles. Representative SEM images showing the resultant change in fibre morphology at the central point of loading is shown. Scale bars 50 µm. 246
Figure 7-11: Schematic representation of the indenter probe striking the sample in the unconfined uniaxial compression testing. 247
Figure 7-12: The biosynthetic pathway of prostanoids. Reproduced with permission from Ricciotti, E, and Fitzgerald G. Prostaglandins and Inflammation. Arterioscler Thromb Vasc Biol. 2011 May; 31 (5) Figure 1, p986. 250
Figure 7-13: A schematic representation of the intended drug releasing monomer within the surface initiated polymer bottlebrush system. 256
Figure 7-14: The synthesis of HPMAm-ibuprofen 257
Figure 7-15: The synthesis of peg3ma-ibu 258
Figure 7-16: ^{1}H-NMR (400MHz, $CDCL_3$) of HPMAm-ibu monomer with peak assignments. 263
Figure 7-17: Mass spectroscopy for the HPMAm-ibu monomer. Calculated 332.20, found 333.20. 264
Figure 7-18: ^{1}H-NMR (400MHz, $CDCl_3$) of peg3ma-ibu monomer 265
Figure 7-19: Drug release from the p(OEGMA-*co*-peg3ma-ibu) polymer in solution by ^{1}H-NMR. 270
Figure 7-20: Surface grafting of PCL-p(OEGMA-co-peg3ma-ibu) is confirmed with change in water contact angle (right) and compared to PCL-pOEGMA scaffolds (centre). 273
Figure 7-21 Calibration curve of known concentrations of ibuprofen and the absorbance on UV-vis spectroscopy. 273

List of Tables

Table 1-1: Factors involved in tendon development, formation and healing (adapted from the literature[132]).....51
Table 1-2: Differing roles of TGF (adapted from[132]). 58
Table 1-3: Pharmacological agents used to modulate tendon adhesion *in vitro* and *in vivo* .62

Table 2-1: The C-O signal internsity of 2D silicon surfaces as measured by XPS and the corresponding polymer M_n and $Đ$. 111
Table 2-2 : C 1*s* breakdown for the 2D silicon surfaces as measured by XPS 111

Table 3-1: The panel of biomolecules used to assess antifouling of the pOEGMA surface and their properties. 123
Table 3-2: C-O signal intensity of 3D electrospun scaffolds as measured by XPS and the corresponding polymer M_n and $Đ$. 132
Table 3-3: C 1*s* signal breakdown for the 3D electrospun scaffolds as measured by XPS. ...132

Table 5-1: XPS C 1*s* peak fit results for the 17% (w/w) PCL-diol control scaffolds and the 17% (w/w) PCL-pOEGMA scaffolds following 0 and 10 weeks incubation in PBS. The published binding energies are included.....180

Table 7-1: Contact angle and staining appearance of PCL-diol control and PCL-p(OEGMA-*co*-biotin) scaffolds following different washing regimes. 233
Table 7-2: Common NSAIDs and their mechanism of action 251
Table 7-3: Mechanisms for drug release from bioerodible polymers.....254
Table 7-4: ARGET ATRP of p(OEGMA-co-HPMAm-ibu) with variations in reaction time and temperature and the corresponding X, $Đ$, and M_n. 265
Table 7-5: ARGET ATRP of p(OEGMA-co-HPMAm-ibu) with variations in water content of solvent and the corresponding X, $Đ$, and M_n. 266
Table 7-6: ARGET ATRP of p(OEGMA-co-HPMAm-ibu) with variations in molar ratios of AScA and the corresponding X, $Đ$, and M_n.....267
Table 7-7: ARGET ATRP of OEGMA with HPMAm with different mol% of ibuprofen and the corresponding X, $Đ$, and M_n. 267
Table 7-8: ARGET ATRP of OEGMA with HPMAm and HPMA with different ligands and the corresponding X, $Đ$, and M_n. 269
Table 7-9: Ibuprofen release from PEGulated ibuprofen prodrugs[353]. 272

List of Abbreviations

ACN	Acetonitrile
AFM	Atomic Force Microscopy
APTES	3-(Aminopropyl)triethoxysilane
ARGET ATRP	Activators Re- Generated By Electron Transfer ATRP
AScA	Ascorbic Acid
ASCs	Adipocyte Derived Stem Cells
ATRP	Atom Transfer Radical Polymerisation
BiBB	α-Bromoisobutyryl Bromide
BMSC	Bone Marrow Derived Mesenchymal Stem Cell
BPY	2,2'-Bipyridine
COX	Cyclooxygenase
cRGDS	cyclized RGDS
Cu(I)Br	Copper (I) Bromide
Cu(II)Br	Copper (II) Bromide
D_2O	Deuterium oxide
d4-MeOD	Deuterated methanol
DAPI	4',6-diamidino-2-phenylindole
DCC	*N*, *N*-Dicyclohexylcarbodiimide
DCM	Dichloromethane
DCU	*N*, *N*-dicyclohexylurea
DEE	Diethyl ether
DIEA	*N*, *N*-Diisopropylethylamine
DiH_2O	Deionized Water
DMAP	4-(Dimethyl)aminopyridine
DMEM	Dulbecco's Modified Eagle's Medium
DMF	*N*, *N*-Dimethylformamide
DMSO	Dimethyl Sulfoxide
dPBS	Deuterated Phosphate Buffered Saline
EBIB	Ethyl-α-Bromoisobutyrate
ECM	Extracellular Matrix
EDC	1-ethyl-3(3-dimethylaminopropyl)carbodiimide
ESI	Electrospray ionization
ESI-MS	Electrospray ionization- mass spectrometry
FCS	Foetal Calf Serum
FTIR	Fourier Transform Infrared Spectroscopy
GAG	Glycosaminoglycans
HA	Hyaluronic Acid
HEMA	2-Hydroxyethyl Methacrylate
HFIP	1,1,1,3,3,3-Hexafluoro-2-Propanol
HPLC	High Performance Liquid Chromatography
HPMA	2-Hydroxypropyl Methacrylate
HPMAm	*N*-(2-Hydroxypropyl) methacrylamide
LC-MS	Liquid Chromatography-Mass Spectrometry
MMA	Methyl methacrylate
M_n	Number Average Molecular Weight
MSC	Mesenchymal Stem Cell or Multipotent Stromal Cell

MTT	Cell assay for the assessment of metabolic activity based on 3-(4,5-dimethylthiazol-2-yl)-2,5-diphenyltetrazolium bromide
M_w	Weight Average Molecular Weight
MW	Molecular weight
NaOH	Sodium Hydroxide
NGM	Normal Growth Media
NHS	*N*-hydroxysuccinimide
NMP	*N*-methyl pyrrolidone
NMR	Nuclear Magnetic Resonance
NSAID	Non-Steroidal Anti-Inflammatory Drug
PBS	Phosphate Buffered Saline
PCL	Poly-Ɛ-Caprolactone
PEG	Poly(ethylene glycol)
Peg3ma	Mono-disperse poly(ethylene glycol) monomethyl ether methacryate
PFA	Paraformaldehyde
pHEMA	Poly(2-hydroxyethyl methacrylate)
PMDETA	*N,N,N′,N′,N″*-pentamethyldiethylenetriamine
pMMA	Poly(methyl methacrylate)
pMPC	Poly[2-(methyacryloyloxy)ethyl phophorylcholine]
PMPI	P-maleimidophenyl isocyanate
pOEGMA	Poly(ethylene glycol) methyl ether methacrylate
PyBop	Benzotriazol-1-yl-oxytripyrrolidinophosphonium hexafluorophosphate
RT	Room Temperature
SEC	Size Exclusion Chromatography
SEM	Scanning Electron Microscope
SI-ATRP	Surface initiated atom transfer radical polymerisation
SOP	Standard Operating Procedure
T175	175cm^2 Cell Culture Flask
TEA	Triethylamine
TFA	Trifluoroacetic acid
TGF-β	Transforming Growth Factor Beta
THF	Tetrahydrofuran
TIS	Triisopropylsilane
TLC	Thin Layer Chromatography
TPMA	Tris[(2-pyridyl)methyl]amine
TRIS	Tris(hydroxymethyl)aminomethane
UHQ	Ultra high quality (water)
UV	Ultra violet
XPS	X-ray photoelectron spectroscopy

Chapter 1 : Tissue Engineering and Regenerative Medicine: a versatile approach for treatment design

1.1 Tissue engineering and regenerative medicine

Tissue engineering and regenerative medicine is a diverse and rapidly expanding area of research that may find its origins in the lab of Dr Eugene Bell at Massachusetts Institute of Technology (MIT) in the early 1980s. Two companies came together to collaborate on an attempt to prepare a cell-based vascular scaffold and, perhaps, lead to a new field of research[4]. This was followed by the seminal work published in Science by Langer and Vacanti in 1993 defining the field as one that endeavours to develop functional substitutes for damaged tissues using a combination of cells, engineered materials and biological cues[5].

The field evolved and condensed from a number of origins including materials and biomaterials, leading to tissue engineering, and from research into self-healing and stem cells, leading to regenerative medicine. The terms “tissue engineering” and “regenerative medicine” are now often used interchangeably as the boundaries between the disciplines become increasingly blurred. The field is also widely multidisciplinary with expertise from engineers, material scientists, biologists, chemists and clinicians to name but a few. Challenges requiring such diverse expertise include the development of engineered cartilage for the treatment of osteoarthritis in load bearing joints, such as the knee[6], where biological, chemical, mechanical and surgical inputs must all be considered in the tissue engineering material design. The multidisciplinary nature of the researchers leads to a vastly broad and diverse field and is increasingly translational with research being undertaken all the way from the lab bench to patient’s bedside. Both simpler tissues, such as skin substitutes[7,8], and more complex organ systems, such as the bladder[9] have passed successfully into long-term clinical trials. Other targets for the field, such as nerve regeneration following spinal cord injury, remain predominantly in the pre-clinical phase.

The tissue engineering and regenerative medicine field is vast and this introductory chapter cannot serve to do it justice. Areas include stem cell research including embryonic, adult and induced pluripotent (iPS) cell lines[10,11]. Scaffolds to guide repair, healing and regeneration range from natural materials, such as decellularised tissues including kidney[12] and vascular

grafts[13], to synthetically produced materials such as polymers[14] and recombinant biopolymers[15]. Cutting edge imaging and characterisation techniques are employed and advanced within the field together with diagnostics, drug delivery and device development.

Finally, the field also has a key focus on real clinical translation. Tissue engineering and regenerative medicine therapies are reaching clinical trials and making an impact on healthcare. This may lead to a dramatic shift in the way we consider healthcare in the future if the potential of autologous stem cell therapies can be achieved to provide personalised healthcare. Goals such as the ability to produce an autologous heart to alleviate the need for allogenic organ transplantation are currently some way away. Clinical success has been achieved however with autologous bladders[9] and tracheas[16,17] for example. The first clinical trial using embryonic stem cells is also underway, in this case for the treatment of retinal degenerative disease, the first of many registered with the international database Clinicaltrials.gov[18-20]. The field of tissue engineering and regenerative medicine and the emerging trends are discussed fully in the published appended 1st author review article (RH Harrison *et al.* "Tissue Engineering and Regenerative Medicine: a Year in Review" Tissue Engineering Part B: Reviews. February 2014, Appendix A)[20]. The work presented in this thesis focuses on the biomaterials aspect of tissue engineering, which will form the focus for this literature review.

1.1.1 Biomaterials within tissue engineering

Materials have been implanted into the body for over three thousand years[21] however, the period spanning the 1960s and 1970s is thought of as the beginning of the modern era of biomaterials design. At that time, scientists aimed to develop implants that performed mostly mechanical functions whilst eliciting a minimal host response[20]. The "bioinert" materials developed still have a major impact on the treatment of a number of diseases today. During the 1980s a transition occurred towards the design of biomaterials with controlled biological activity. Tissue engineering (TE) has led to another paradigm shift in our approach to biomaterials design. Complex and smart materials that promote cellular interaction to direct their biological response, or even be responsive to cells, are now being designed.

1.2 Gliding tissues and interfaces

For movement of the body to be successful, be it the flexion of a joint or peristalsis of the gut, the specialised tissues that are involved in the locomotion must be able to glide past the neighbouring tissues unimpeded. The body is elegantly arranged to facilitate such movements through the use of gliding interfaces such as those seen at joints, between muscle bellies, nerves and abdominal viscera for example. Furthermore, lubricating fluid is made and found at some of those interfaces to facilitate smooth glide between the surfaces such as synovial fluid within joints or tendon sheaths or peritoneal fluid within the abdominal cavity. These delicate and specialist surfaces are easily disrupted through trauma, infection or inflammation which may lead to the formation of adhesions.

Adhesions are bands of scar tissue that directly result from cellular ingrowth and bridging between previously gliding surfaces resulting in restriction of movement. These can cause pain and compromised function, the impact of which is dependent upon the tissues involved, the size of the scar bridge, the strength of the scarring and the location upon the tissue. This is extremely varied depending on the tissues involved, but may have a significant impact on a patient's morbidity or even mortality when involving the abdominal viscera. This work will focus on the tendons of the hand as a model of adhesion formation to guide the design of a potential novel preventive developed through a TE and regenerative medicine approach.

1.2.1 How tissue engineering could be used to preserve a gliding surface

The ability to design the properties of the cell-scaffold interface to modulate protein and cell binding is key in TE and regenerative medicine. Following injury, it is the cell and protein attachment onto gliding tissue surfaces that leads to adhesion formation and problematic scar tissue. Through the design and production of an antifouling scaffold surface the attachment of cells and proteins may be significantly modified. However, having a construct with an antifouling surface through its substance may have negative effects on the healing surface beneath and be difficult to place and maintain *in vivo*. Designing a layered structure with an opposing cell-adhesive and antifouling surfaces however, could revolutionize the outcome of the injuries and operations at these biological interfaces through their ability to

support tissue healing (cell-adhesive surface) and to reduce cell-ingrowth and protein adsorption (antifouling surface) in a spatially controlled manner.

1.3 A modular and versatile approach to scaffold design

The ability to generate a scaffold with an antifouling surface and an opposing cell adhesive surface is very attractive for a number of clinical challenges. The gliding surfaces of the musculoskeletal system that are compromised following tendon laceration, fracture, or the placement of metal work may benefit. A scaffold may be of use for the prevention of adhesions onto viscera, such as in the abdomen, pelvis or thorax following surgery or injury, for which the need has been identified and is an area of active research in the field[22,23]. Following repair of transected major nerves or even tethering of the skin following scarring onto the fascial planes may benefit from the placement of such a device. There are wider applications that could also benefit from such surface modification; scaffolds that interface with the vasculature for example are troubled with protein deposition onto the scaffold surfaces. This can lead to blood clotting and blockage of vessels, with potentially disastrous consequences.

The technology employed in this work to create the scaffold has been specifically designed and selected from the cutting edge of current knowledge to be versatile and modular in its approach. This will allow for this scaffold system to be applicable to a broad range of clinical challenges and tissues in the future. The scaffold will allow the tailored selection of modular units to create a bespoke approach for a particular need without having to redesign a scaffold from scratch (Figure 1-1).

The scaffold employs the rational design of end-functionalized polymers to give spatial control of functional groups within the bulk scaffold as produced by electrospinning. Electrospinning allows for a wide variety of controlled parameters on the micro and macro scale including scaffold size, shape and location of functional groups within the scaffold substance. One of the key functional groups used is an initiator for a controlled radical polymerisation. A state-of-the-art controlled radical polymerisation technique is used to create a bespoke surface initiated surface functionalization where the initiating groups are present. The polymerisation can be used with a wide range of monomers to select the surface properties required for the proposed purpose. Specially designed monomer units,

such as fluorescent tagging may be used. Each of the aspects of the design will be thoroughly discussed below and the adaptions to the clinical application outlined.

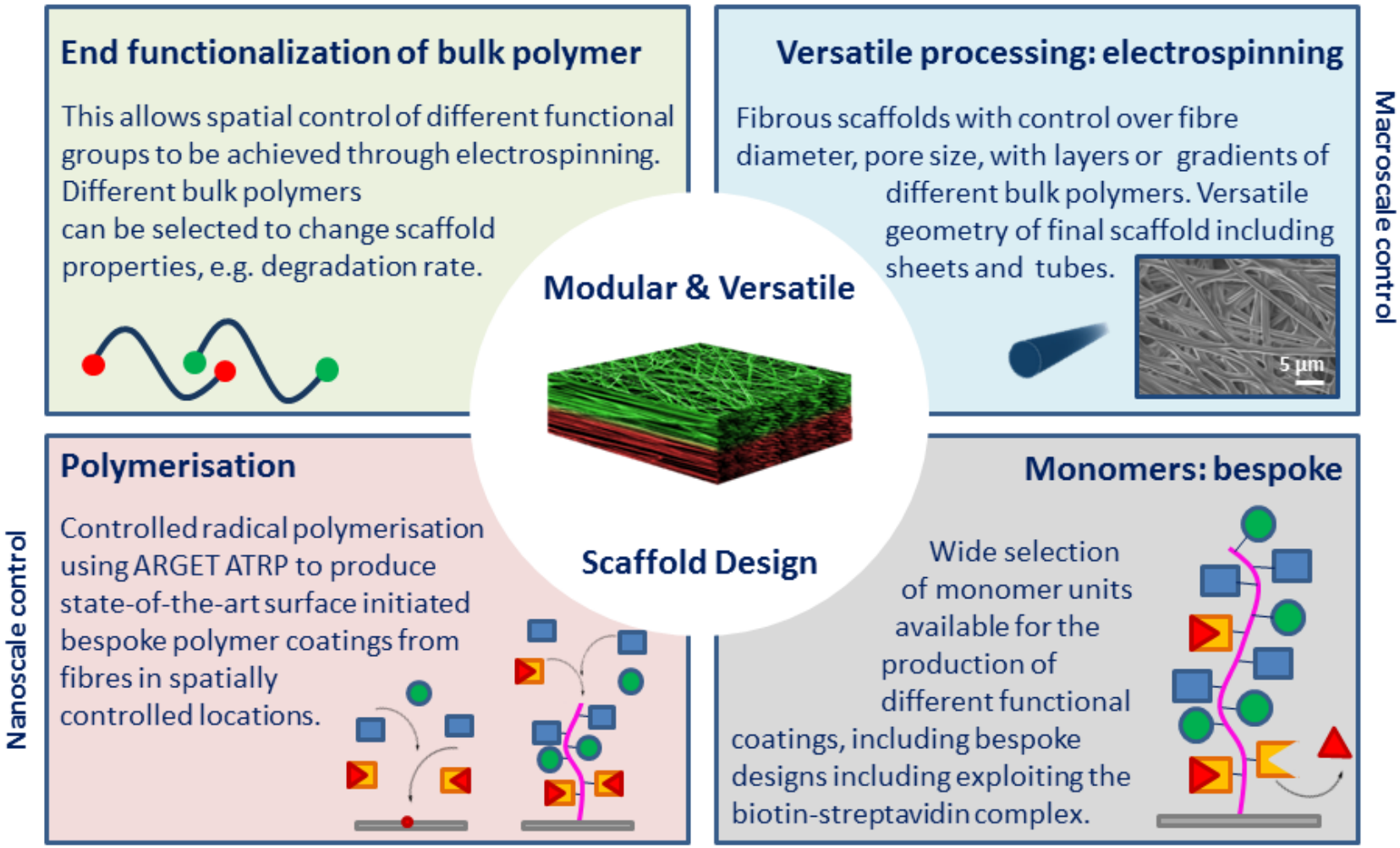

Figure 1-1: Schematic of the key features in the modular and versatile scaffold design.
Notes: Activators regenerated by electron transfer atom transfer radical polymerisation (ARGET ATRP).

1.3.1 Introduction to polymers and radical polymerisation

Polymers are commonly used and exploited in material science for a wide range of uses, including biomaterials for tissue engineering[24,25]. Polymers are extremely versatile in their design, properties, character and architecture making them good candidates for the synthesis and modification of structures.

Polymers may be produced through a variety of different approaches, one of which is *free radical polymerisation*. Radical polymerisation is extremely versatile and so has become the most widespread industrial method to produce polymers, such as rubbers and plastics[26]. This is part due to the range of monomers that be used and the reaction conditions employed. A large range of unsaturated monomers may be polymerised, or copolymerised, using radical polymerisation as most vinyl monomers may be used, including functional monomers. The reaction conditions are also mild; temperature ranges of 0 to 100^{o}C and the tolerance of water or other impurities is well tolerated. The reaction does, however, require the absence of oxygen[27].

Radical polymerisation occurs through the production of free radicals and may result in three possible outcomes. *Initiation* may occur if the radical is produced in the presence of a vinyl monomer unit, then the radical adds to the double bond of the monomer unit and leads to the formation of another radical, this time on the monomer unit itself. This radical may then attack the vinyl unit of another monomer unit, resulting in the addition of the two monomer unit together, and again, a new radical is formed now consisting of two monomer units, which is known as *propagation.* Propagation is the method by which the polymer chain is lengthened to form higher molecular weights. Termination may also occur; this occurs when two radicals react together to form a stable paired electron covalent bond and results in the loss of radical reactivity (Figure 1-2).

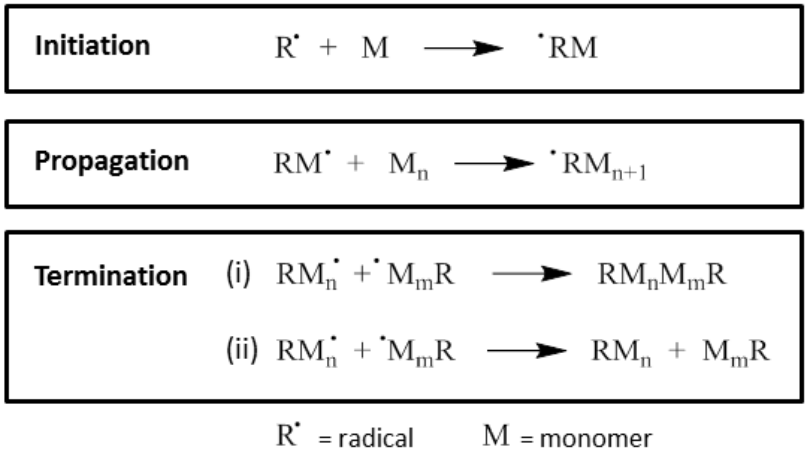

Figure 1-2: Schematic to outline the steps of initiation, propagation and termination through (i) combination or (ii) disproportionation, found in free radical polymerisation, adapted from[2].

Termination reactions result in no further monomer addition for that polymer chain. When a high concentration of radicals is present, a high rate of termination occurs and the result is the production of polymers with a wide range of molecular weights with poorly controlled architecture. These features are then reflected in the mechanical and physical properties of the resultant polymer. In order to manage a radical polymerisation reaction and produce predictable polymer molecular weights, the ratio of radical species to monomers must be significantly reduced. This reduces the chances of radical meeting and thus reduces the number of termination reactions occurring and forms the basis of controlled radical polymerisation[2].

1.3.1.1 Controlled radical polymerisation

Techniques to control radical polymerisation were developed in the 1990s[28,29]. Having control of the reaction refers to the synthesis of a polymer with a predictable molecular weight and the production of a narrow molecular weight distribution between polymer chains within the same reaction vessel, (i.e. M_w/M_n or dispersity, PDI, $Đ$ < 1.5)[30]. The polymerisation also exhibits linear evolution of M_n with conversion of monomer to polymer, which is not seen in uncontrolled systems[31]. This control further allows the end group of the polymer to be maintained which can either be used to re-initiate the polymerisation and grow the polymer chain further, or, for further functionalization through the reaction with a different compound[27].

Controlled free radical polymerisation exists in several different forms; two of the most commonly employed being *reverse addition fragmentation polymerisation* (RAFT)[32,33] and *atom transfer radical polymerisation* (ATRP)[34,35]. This work focuses on the use of ATRP and a closely related polymerisation, *activators regenerated by electron transfer atom transfer radical polymerisation* (ARGET ATRP)[36]. Controlled radical polymerisations (CRP) such as RAFT, ATRP and ARGET ATRP are facile and versatile methods for providing surface functionalization with a variety of monomers. They provide a convenient way of polymerising as most compounds with double bonds may be incorporated into the polymer in the presence of almost any other functional group, giving vast versatility[37]. This has not yet been fully exploited in scaffold functionalization in tissue engineering and represents an excellent choice to generate polymer surface coatings.

1.3.1.1.1 ATRP

The ATRP process, using a copper mediated catalyst, was co-discovered in 1995 and can produce well controlled polymerisations and is outlined in Figure 1-3[38,39].

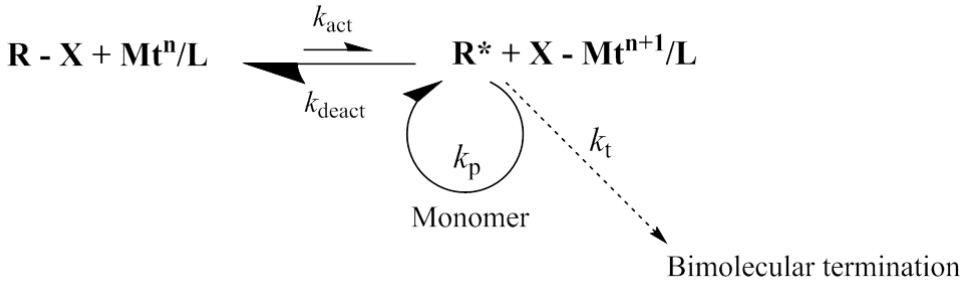

R – part of alkyl halide initiator and polymer chain
X – Cl or Br
Mt^{n} – metal catalyst
L - ligand

k_{act} – activation rate constant
k_{deact} – deactivation rate constant
k_{p} – rate constant for propagation
k_{t} – rate constant for termination
k_{ATRP} - equilibrium constant for ATRP (k_{act}/k_{deact})

Figure 1-3: Schematic of ATRP (adapted from[2]).

ATRP is a radical based polymerisation and relies on the reversible redox reaction of a dormant alkyl halide terminated polymer chain and through the transfer of a halogen to a

transition metal complex. The resultant cleavage of the carbon-halogen bond generates a free and active carbon centred radical at the chain end. The activation step is based on a single electron transfer process from the transition metal complex to the halogen atom on the initiator compound (or dormant propagating chain end). This results in oxidation of the transition metal complex. Then, in a fast and reversible reaction, the oxidized form of the transition metal catalyst reconverts the propagating radical chain end to the corresponding halogen-capped dormant species[40]. Many variables including ligand to transition metal ratio. Cu(II):Cu(I), ligand type, solvent and initiator type all influence the reaction performance and many be varied to optimise the reaction[41].

ATRP polymerisation exhibits first order kinetics in homogeneous systems accompanied with a linear increase in molecular weight of the resultant polymer with increasing conversion of monomer to polymer. Polymer molecular weight is determined by the number-average degree of polymerisation (DP_n), the ratio of consumed monomer, M, to initiator, I ($DP_n = \Delta[M]/[I]_0$)[27]. The rate of the reaction being directly influenced by temperature[42], pressure[43], solvent (polarity)[44], alkyl halide initiator and transition metal catalyst concentration[45]. The reaction is, however, sensitive to anything that could terminate the free radical process including even a low level of contamination with oxygen.

ATRP is typically carried out using organic solvents as the precise control of the reaction is limited when polar solvents, such as water, are used[36]. Several factors are seen in ATRP reactions when polar solvents, such as water, are used that lead to a loss of control. High radical concentrations occur as a results of a large ATRP equilibrium constant shifting the reaction to the right, resulting in large numbers of termination reactions[44]. Water also leads to inefficient deactivation of the propagating radicals as it can cause partial dissociation of the halide ion (X) from the deactivation complex ($X\text{-}Mt^{n+1}/L$), leading to further radical accumulation[46]. Water may also disrupt certain Cu(I)/L complexes leading to further loss of control[46]. Furthermore, polymer end group functionality can be lost through hydrolysis of the carbon-halide bond[46]. Significant efforts have been made to improve ATRP in aqueous media[47-49].

The mechanism of ATRP allows for precisely controlled polymers to be produced, including polymers with different architecture (linear, branched, etc.), and/or the composition of the

polymer chain (copolymers in blocks or gradients, etc.)[27]. Furthermore, the end group for the final polymer produced is dictated by the initiator used. This occurs as the initiator, a low molecular weight organic compound with a halogen, becomes activated with a radical at initiation. When this occurs the halogen leaves the compound. As a monomer unit is incorporated to start the polymer growth, what remains of the initiator group is found on the non-active end of the growing polymer chain with the halogen on the opposite end. As the end groups are maintained during this reaction this allows the selection of an initiator, including the possibility of one with functional group(s), to be used and a resultant end-functionalised polymer to be produced[27].

Many different monomers have been successfully polymerised using ATRP. One of the most successful group of monomers perhaps is the (meth)acrylates. This diverse group of monomers are based on acrylic acid and may contain a wide variety of functional groups that may be incorporated into the polymer, including sugar groups. Several of these monomers, such as 2-hydroxyethyl acrylate and 2-hydroxyethyl methacrylate (HEMA) are water soluble and have found applications in the biomaterials field[27].

ATRP has been successfully used to produce polymer brushes for biological systems previously, such as for in the production of haemocompatible surfaces and thermoresponsive surfaces to control cell attachment[50,51]. The ATRP process does however have some significant drawbacks when biological systems are considered; high concentrations of potentially toxic transition metal catalyst ions are used together with the use of organic solvents for the polymerisation[52]. It is critical that scaffolds designed and intended for use in biomedical applications can have such toxic contaminants removed prior to use and this can be challenging to do effectively when using a bulk scaffold.

1.3.1.1.2 ARGET ATRP

Activators regenerated by electron transfer atom transfer radical polymerisation (ARGET ATRP) is a modified form of conventional ATRP that was proposed in 2005 (Figure 1-4) and avoids the high concentrations of transition metal catalyst and organic solvents required for conventional ATRP[53]. Furthermore, ARGET ATRP is also less sensitive to small amounts of oxygen contamination offering increased ease of use, and uses the transition metal catalyst in the lower oxygen state resolving problems of storage[52].

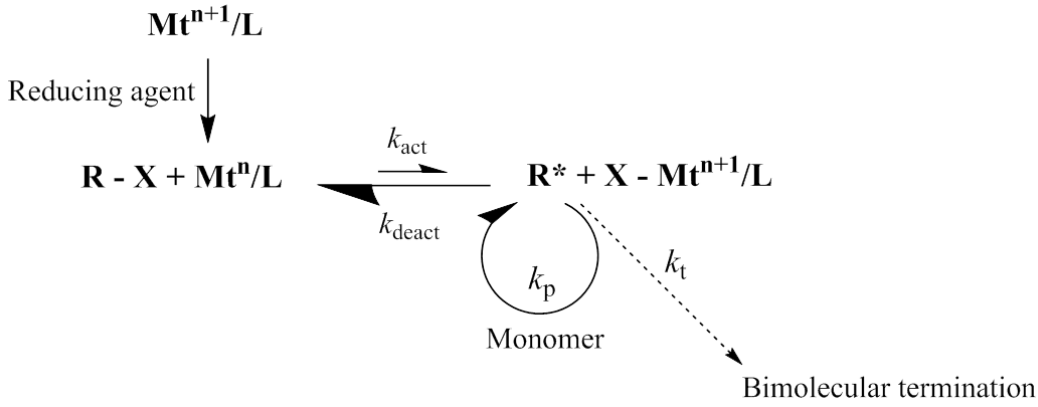

Figure 1-4: Schematic of ARGET ATRP (adapted from[3]).

ARGET ATRP differs from conventional ATRP through the use of a reducing agent, such as ascorbic acid, which is used to reduce the stable transition metal catalyst. Often, this will result in the Cu(II)/ligand complex to reduce to the Cu(I)/ligand form in solution. Following this step, the reaction proceeds through the conventional ATRP process[3]. This allows the recycling and continued production of the catalyst in the reduced state, thus allows a significantly reduced concentration of the potentially toxic catalyst to be used. This also improves some of the challenges associated with maintaining polymerisation control of ATRP in aqueous solvents, thus allowing ARGET ATRP to be successfully controlled in such solvents. As ultimately the reaction proceeds as a normal ATRP, hence ARGET ATRP maintains all of the advantages that ATRP exhibits with regard to monomer and initiator versatility, maintenance of end groups, and the ability for well controlled reactions.

ARGET ATRP in aqueous solvents can be used to prepare well controlled high molecular weight polymers and had been used to prepare antifouling surfaces to control cell behaviour *in vitro*[54].

1.3.1.2 Polymerization from 2D surfaces

Surface initiated ATRP was first reported by Huang and Wirth in 1997 with the successful grafting of poly(acrylamide) brushes from silica particles[55]. Since that time other polymerisations have also been successfully used for surface-initiated polymerisations, including RAFT and ARGET ATRP[41,56-61]. These polymerisation techniques are extremely versatile and offer excellent control over chain length, architecture, reaction kinetics, and an array of functionality as a large number of monomers may be incorporated, dictating the final surface properties[41,54].

Polymer functionalization of surfaces may be achieved through three different approaches, each with different advantages. Polymers may be *grafted to, grafted from* or *grafted through* the surface (Figure 1-5).

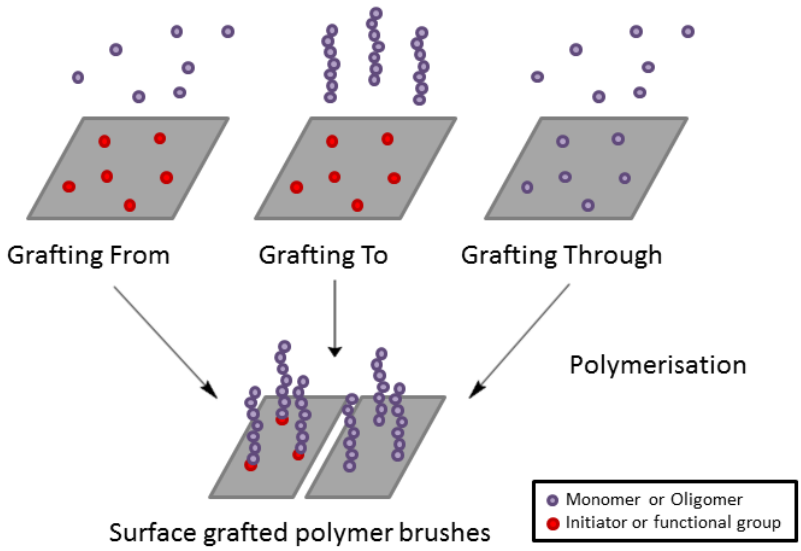

Figure 1-5: Schematic of polymer brush grafting to, form and through surfaces.

Grafting to a surface is achieved when a preformed polymer or polymer brush is attached to a surface. This is advantageous in that the polymer characteristics may be interrogated before attachment, so the exact properties of the polymer such as molecular weight and

chain length are known. The principle disadvantage of this approach is that it is difficult to achieve high grafting density of the polymer due to the steric hindrance of the presence of the polymer on the surface and surface contamination occurs with the presence of non-surface bound polymer chains persisting[41,62,63]. *Grafting through* a surface avoids the problem of steric hindrance through the covalent attachment of a monomer unit to the surface. The monomer unit becomes activated by the formation of a radical within the compound, and reacts to another monomer unit in solution, thus growing the polymer from the surface. The attachment of the desired monomer unit may however be challenging in part because you cannot control the position the chain attaches, so another approach is *grafting from*. Grafting from a surface is achieved through the covalent attachment of an initiating group to the surface, which again generates a radical that reacts with a monomer unit in solution and allows the polymer to be extended from the surface. Like grafting through, this avoids the steric hindrance and resultant low grafting density seen in grafting to, and can result in high-density surface functionalization[64,65]. For this reason, this technique was employed in this work.

Grafting polymers from surfaces within a solution can lead chemical gradients being established within the reaction vessel that may lead to a local loss of control of the reaction. Adjacent to the reacting surface there will be a high local concentration of radicals and consummation of the various reacting units. The low local concentration of the deactivating Cu(II) species leads to a local loss of control[41]. This can be mitigated through the use of a sacrificial initiator in solution as this will lead to the formation of polymer throughout the solution as well as on the functionalised surface. This has the additional advantage that the polymer in solution has been shown to exhibit the same characteristics as the polymer on the surface and so may be used as a surrogate marker for surface polymer characterisation, thus allowing optimisation of the molecular weight on the surface grafted polymer[66]. The number of initiating groups on the surface needs to be negligible compared to the initiating groups in solution to not affect the behaviour of the polymerisation[41,66]. The use of a sacrificial initiator however does have a drawback as the generation of free polymer in solution may act as a contaminant on the surface and needs to be effectively removed to leave only the surface bound polymer to ensure accurate characterisation.

1.3.1.3 Polymer brushes

The monomer or monomers chosen for a polymerisation ultimately dictate the properties of the polymer produced. The polymers described above have primarily been from single monomer units and produce a linear polymer. *Oligomers* are units that are made up of several monomer units. If a number of oligomer units are polymerised together the resultant polymer is not a linear chain, but made of a bottlebrush structure. Each oligomer branches outwards from a backbone chain that has been formed by the polymerisation and this can lead to a high density structure. Polymer brushes have been used to produce low friction and antifouling surfaces both within industrial and biological systems for some time[41,54,67]. Such properties are of benefit in tissue engineering.

An example of such a oligomer is poly(ethylene glycol) methyl ether methacrylate, OEGMA.

1.3.1.4 OEGMA

OEGMA is an oligomer unit made up of repeating poly(ethylene glycol) (PEG) units modified with a methacrylate group. PEG, and the associated oligomer OEGMA are of interest in this work as they are known to be antifouling to both cell and protein adhesion and have been used extensively for industrial and medical applications for surface functionalization and in for drug delivery[68-70]. The polymer has been used in FDA approved devices and is known to be biocompatible and excreted in the urine. PEG and OEGMA may also be modified for the preparation of biologically relevant conjugates in a facile manner, making it a good candidate for surface functionalization of tissue engineered scaffolds[71]. Furthermore, OEGMA has been successfully polymerised using ARGET ATRP in aqueous solution previously, facilitating the translation to its polymerisation from surfaces more facile[3].

1.3.1.5 Drug pendant polymers

As discussed above, the selection of a controlled radical polymerisation process allows the inclusion of a wide variety of monomer units into the resultant polymer brush. This leads to the potential to include a drug releasing moiety into the surface bound polymer brush producing a drug pendant polymer, adding another layer of functionality to the scaffold where required.

Tissue engineering is well suited to drug delivery and considerable work has been done in this area, particularly involving drug eluting stents for cardiovascular disease[72,73], use of active wound dressings that release growth factors or other agents such as vitamins or minerals into wounds[74], or to reduce the inflammatory response to injury including those designed for use in tendon engineering[75,76]. Many different strategies have been employed to capture drugs within scaffolds all with differing properties and release profiles. These include the simple, such as a hydrolysable ester linkage[77] to the more complex including liposomes[78], hydrogels[79] and nanoparticle delivery[80]. Drug delivery as part of the scaffold system presented within this thesis is presented in Appendix K.

1.3.2 Scaffold fabrication

Within nature and the body nothing can be found in a standard size or shape. No two tissues are identical either on the macro- or nano-scale. A processing technique needed to be identified that gave the flexibility on both these scales to produce scaffolds with the correct architectural properties for the desired application. Whilst the work presented in this thesis involves the production of scaffolds in sheets, the ability to produce other architectures is essential for future work.

1.3.2.1 Electrospinning

A versatile processing technique that resulted in robust and easily handled scaffolds was identified, electrospinning. Electrospinning is a technique whereby fine fibres that mimic the topography of native extracellular matrix (ECM) can be produced. It is used widely for bulk scaffold preparation in the field of tissue engineering and regenerative medicine[81-84].

Electrospinning is a processing technique that has been adapted from the textiles industry, for a comprehensive review please see cited reviews[85,86]. Electrospinning is a method that can be used to generate polymer fibres with diameters that may vary from several microns to under 100 nm using a high voltage electrostatic field. The polymer solution or melt within a plastic syringe is set up on an automatic syringe driver with an associated metal needle. A voltage is applied to the needle and an opposing voltage, or an earth wire, is applied to a metal collector plate in air which may be either static or dynamic. The liquid polymer is drawn from the needle due to the voltage differential and becomes unstable. This process,

known as whipping, causes the polymer jet to bend into expanding loops as it travels towards the collector. This movement stretches the polymer into thinner and finer fibres as the solvent evaporates (Figure 1-6, A). The resultant continuous fibres produces are deposited on the collector producing 3D networks of non-woven fibres of tuneable size, orientation, composition and density. These features, together with those outlined in Figure 1-6 make electrospun scaffolds attractive candidates for surgical implants. Electrospun scaffolds are flexible and easy to handle (Figure 1-6, B) in contrast to polymer films which can be brittle and non-pliable. Furthermore, the scaffolds are porous due to the structure of the fibre network (Figure 1-6, C). This is also key as it may allow the diffusion of tissue fluid through the scaffold to the tissue surface beneath, facilitating gas and nutrient exchange for the cells[86]. Electrospinning can, however, be unpredictable at times as the fibre formation is directly linked to solvent evaporation. This is affected by different external factors including relative humidity, temperature, and ambient conditions which can be challenging to control and require consideration to the positioning of the machine.

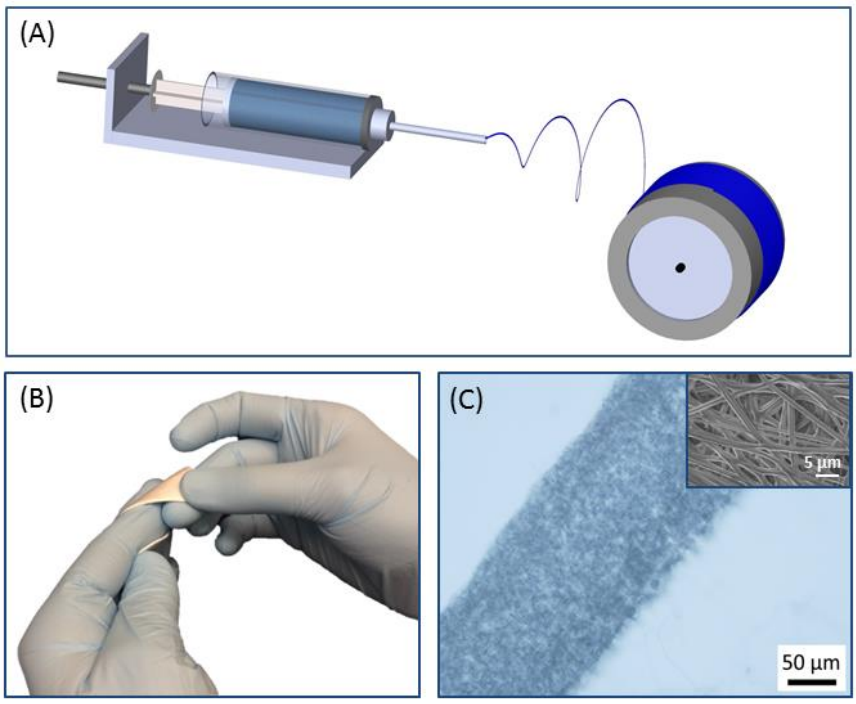

Figure 1-6: Electrospinning fabrication of scaffolds. (A) Schematic of the electrospinning set up onto a rotating mandrel. (B) Handling an electrospun mat. (C) A bright field microscopy image of a histological section of an electrospun mat with an SEM image of the fibres inset.

Electrospinning is extremely versatile in the processing set up allowing for scaffolds with a huge variety of materials and levels of complexity to be produced. Natural polymers such as collagen[87], gelatin[88] or silk fibrotin[89] have been electrospun as well as many synthetic polymers including poly(glycolic acid)[90], poly(lactide)[91] and poly-ε-caprolactone (PCL)[92]. More sophisticated approaches, such as the use of ice crystals to template for pore sizes between fibres[93], and electrospinning with living cells to produce live scaffolds have been achieved[94]. Simpler processes, such as dissolving different substances within the polymer solution have been used to produce modified fibres that may act as releasing conduits for drug delivery[75,95], bioactive glasses[96], or nanoparticles for example[83].

Recently, a sophisticated but facile methodological development has enabled the control of spatial location of polymers within a scaffold using electrospinning. This has allowed the generation of scaffolds with spatially arranged functionalization through layering of different polymers during the electrospinning process[97-102]. This exciting development of a controlled method for producing zonally arranged functional groups within a continuously produced scaffold allows for the possibility of a hierarchically arranged structure that can modulate cell behaviour in a specific way within each functional zone. Electrospinning and the use of fibres also allows for the production of varying architecture and due to the fibre size, provides a large surface area. With the adequate provision of high density functionalization, a dramatic change in surface properties may be produced both on the macroscopic, or bulk level, and at the cell-scaffold interface in a spatially controlled manner. This could lead to highly effective surface functionalization.

1.3.3 Scaffold surface functionalization: polymer brush grafting from electrospun fibres

Polymer brushes have been grafted from a wide variety of 3D structures using a range of polymerisation techniques and monomer units. These techniques have typically been applied to industrial systems and not to biological ones. Furthermore, they are unable to generate spatially controlled production of surface functionalization, rather resulting in bulk change.

Silica is probably the most commonly exploited surface when considering polymerisation with ATRP, but many others have been studied including metals and metal oxides, semiconductors, carbon-based materials, clay minerals, and synthetic polymers[41,65]. In parallel, the chemical modification of nanofibers, often prepared using electrospinning is becoming more common place as potential candidates for applications such as sensing, ion exchange membranes, functional textiles, catalysis, biomaterials, tissue engineering and drug delivery[103]. Several different approaches have been employed for the engraphment of polymer brushes to the surface of electrospun fibres (Figure 1-7). Once again, these result in bulk change and cannot be used to form spatially discrete areas of functionalization or the production of bilayers, both of which are possible with the system presented in this thesis.

Typically, for indications directed towards biomedical applications, the *grafting from* approach is used for the polymerisation and the initiating group is incorporated following production of the electrospun scaffold (Figure 1-7, A) [50,104-108]. This approach has resulted in good bulk grafting of polymer but accurate spatial control over functional groups is not achievable. An alternative approach has been to undertake the polymerisation during the electrospinning step (Figure 1-7, B), or through electrospinning with the pre-formed polymer required for the surface functionalization within the electrospinning solution or melt (Figure 1-7, C). Wang *et al*. produced nanofibers of poly(urethane) and poly(ethylene glycol) methacrylate (PEGMA) that underwent photo-induced polymerisation and crosslinking during the electrospinning process[109]. They suggest that the majority (90 wt%) of the PEGMA remains on the surface of the fibres with 10 wt% contained within them, although from the paper it is unclear exactly how they reached these numbers.

Grafahrend *et al.* synthesised polymers functionalised with either PEG or RGDS before electrospinning them to produce a scaffold containing both the PEG and RGDS functional groups throughout the bulk of the structure[110]. This approach could be used to generate spatial control over surface functionalization. They demonstrated change in water contact angle and differing properties with regard to cell attachment, but lack robust evidence for the presence of the PEG or RGDS groups reliably at the fibre surface. This approach, whilst simpler to perform, is limited by the enrichment of the desired polymer on the fibre surface, again, a feature that is optimised in the approach presented in this work.

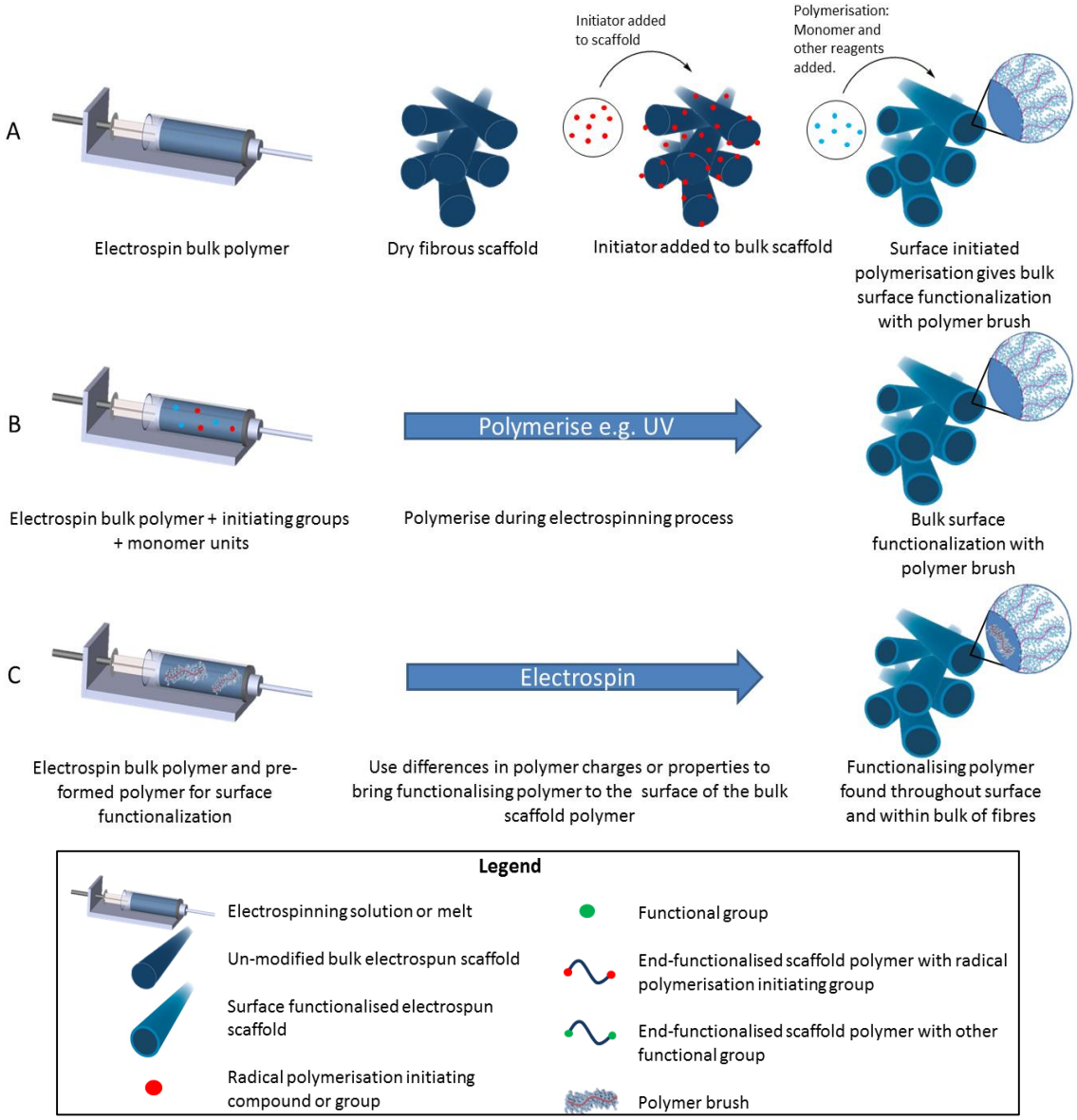

Figure 1-7: Schematic representation of the different approaches for producing polymer brushes from electrospun scaffold surfaces.

The strategy developed in this thesis offers significant advantages to this by incorporating the initiator as an end-group to the polymer prior to electrospinning to allow precise control over the spatial position of the functional groups without disrupting the fiber architecture (Figure 1-8). Furthermore, through the selection of an appropriate initiating group and set up of the polarity of the electrospinning apparatus, electrostatic attraction leads to surface enrichment of the fibres and ultimately is likely to produce adequate polymer brush density[111].

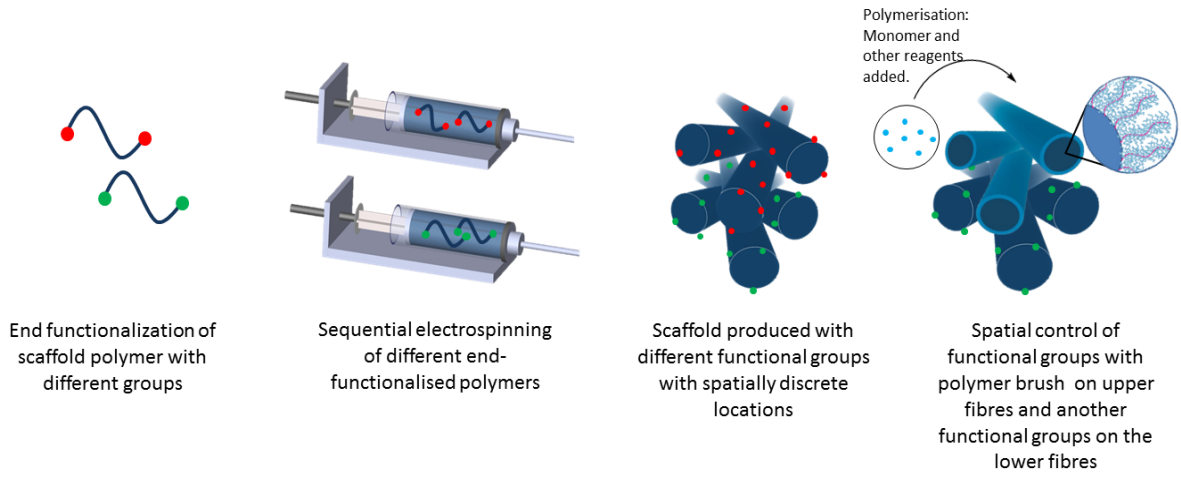

Figure 1-8: The approach outlined in this thesis for the production of surface initiated polymer brush grafting from electrospun fibres with spatial control. See legend from Figure 1-7.

Surface initiated-ATRP (Si-ATRP) has been published in the literature for the polymerization of styrene[111], 2-hydroxyethyl methacrylate[64] and *N,N*-isopropylacrylamide[112] from fibre surfaces and has not been employed for biomedical application. To the best of my knowledge this work is the first time that ARGET ATRP has been used to produce surface-initiated polymer brush grafting from electrospun fibres[97].

1.3.3.1 Antifouling polymers for surface functionalization

Antifouling surfaces have been explored and exploited for a wide range of applications from the biomedical, such as contact lenses, biosensors, and drug delivery, to marine applications such as the coating of the hulls of ships. Polymer brushes have be posed as a convenient way of providing an ultrathin antifouling coating in a controlled manner.

PEG, and the associated OEGMA oligomer, have been explored and used widely for antifouling surface functionalization, as discussed above in section 1.3.1.4. They can be used to generate hydrophilic, ultra-hydrated polymer layers that provide an effective enthalpic and entropic barrier to nonspecific protein absorption. The thermodynamic theory for the antifouling behaviour is that if a protein absorbs onto a hydrophilic polymer brush, water molecules associated within the polymer chains will be released into the bulk and the polymer chain is therefore compressed. The increase in enthalpy due to chain dehydration and decreased entropy due to chain compression are both unfavourable[41]. Theoretical studies predict that an enhanced resistance to nonspecific protein binding and cell adhesion will occur with increasing chain length and grafting density[113]. The theoretical basis for the antifouling action has been reflected in the rational design of our approach and choices of both materials and processing.

1.3.3.2 Grafting antifouling polymer brushes from 3D electrospun scaffolds

Antifouling surfaces have been generated from electrospun fibres only three previous times in the literature, primarily for the purposes of water purification, and before this work had not been applied to biomaterials for tissue engineered scaffolds. In two approaches, the antifouling action was provided through the polymer selection, a triblock polystyrene copolymer polystyrene-*b*-poly(ethylene-*r*-butylene)-*b*-polyisoprene[114] and poly(vinylidene) fluoride[115], neither of which would be suitable for biomaterial synthesis. The final approach used interfacial polymerisation of bisphenol A and trimesoyl chloride onto polysulphone electrospun membranes to produce a thin-film polyester layer of a few microns around each of the fibres. This polymerisation technique, which is based on the polymerisation that occurs between two reactive monomers at the interface of two immiscible liquids, lacks the control over both polymer characteristics and spatial control that we require within our system[116].

The design of the polymer brush system proposed in this work has been such to maximise the antifouling performance. Our approach of pre-functionalizing PCL with end-functional groups before electrospinning also offers a facile and versatile method for maintaining scaffold architecture, functionality, and material properties whilst having precise control over the spatial location and molecular weight of the grafted polymer (Figure 1-9). The

density of the functional groups may also be modified in a facile manner by simply changing the concentration of the PCL conjugates. The selection of the α-Bromoisobutyryl Bromide (BiBB) initiator and electrospinning set up promotes maximal surface enrichment of initiating groups for polymerisation combined with the grafting to approach leads to a high density of polymer brush chains on the surface. Furthermore, through the selection of the oligomeric monomer of PEG, poly(ethylene glycol) methyl ether methacrylate (OEGMA) a polymer brush of pOEGMA is produced, that leads to a vastly higher density of PEG being displayed on the surface for superior performance. This is the first time that pOEGMA has been grafted from PCL fibres, and the first time an antifouling surface has been successfully produced from electrospun fibres for a biomaterial application.

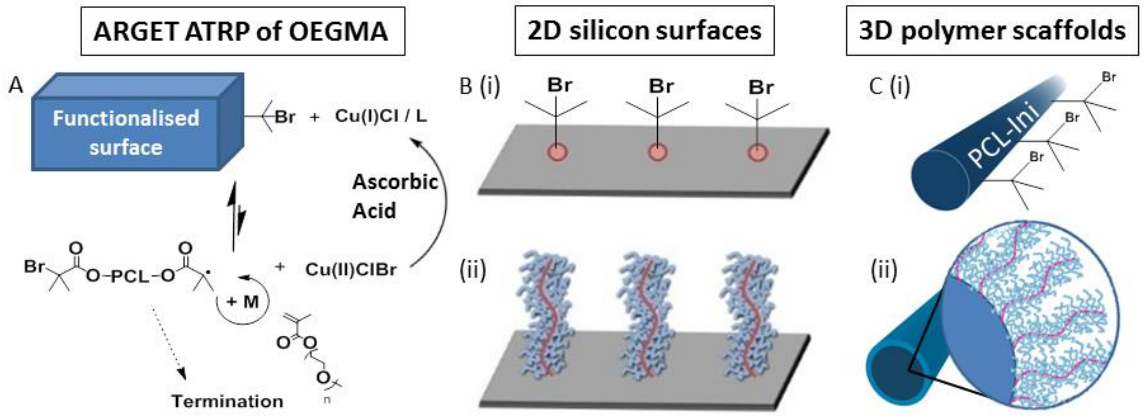

Figure 1-9: Surface initiated polymer bottlebrush grafting from 2D and 3D functionalised surfaces by ARGET ATRP. (A) Schematic of ARGET ATRP controlled radical polymerisation from surfaces. (B) Schematic of functionalised 2D silicon surfaces before (i) and after (ii) grafting with pOEGMA bottlebrushes. (C) Schematic of functionalised 3D electrospun fibres before (i) and after (ii) grafting with pOEGMA bottle brushes.

1.3.4 Spatial control of functional groups

Native tissues are typically heterogeneous and often exhibit hierarchical organisation[2]. The generation of scaffolds that can mimic such properties is critical for tissue engineering applications and relies on the ability to spatially control functional groups. The ability to produce changing functionality across a scaffold provides differing cues to cells at the cell-scaffold interface and may provide optimised signalling to the cells and ultimately lead to desirable cell behaviour and outcomes.

Gliding tissue interfaces, such as the surface of a tendon, ligament or muscle are examples of locations where a scaffold with an antifouling surface and an opposing cell-binding surface may be advantageous. The antifouling surface is designed to resist cell adhesion that may result in detrimental scar tethering. The opposing cell adhesive surface allows integration of the scaffold into the recipient site and may be designed to support native cell growth and integration. Thus encouraging the production of native ECM and ultimately the replacement of the scaffold with native tissue during which time the function of the gliding interface is maintained.

Electrospinning was chosen for the production of scaffolds as it is extremely versatile. The fibre morphology, porous structure, resultant high surface area for functionalization and potential for spatial control confirm this processing technique as a good choice for scaffold production. Developing a controlled method that allows zonally organised functional groups within a continuously produced scaffold allows the production of hierarchical structures that can modulate cell behaviour within each functional zone. Different polymers, with differing properties, have been electrospun in layers or gradients to provide opposing surfaces in the literature by a few researchers[99-102,117,118] and this work builds upon previous work done within our group whereby sequential electrospinning was used to achieve functional gradients of two different peptides within a PCL scaffold which led to the specific binding and spatial organisation of glycosaminoglycans across the thickness of a scaffold[117].

1.3.4.1 Electrospinning for spatial control

Industrial applications of the production of liquid jets in the presence of intense electric fields have been investigated since the 1920s and were more thoroughly investigated in 1995 by Doshi and Reneker for the production of fibres in sheets or as tubular structures[85]. Kidoaki *et al*. expanded from this work in 2004 to use multi-layering and mixed electrospinning techniques to produce both sheets and tubular structures to explore the versatility of the system[118].

Electrospun scaffolds using the techniques of multi-layering or mixing have been explored by a few groups to direct cell behaviour across scaffolds. Mechanical and cell adhesive gradients have been prepared for example, increasing concentrations of modified methacrylated hyaluronic acid (to increase cross-linking and thus mechanical strength) were

electrospun with another polymer incorporating the RGD peptide with an opposing concentration gradient[119]. Further examples include a scaffold to maintain separation but support the growth of different cell and tissue types was produced through electrospinning[100] in addition to a bilayer scaffolds proposed for use as artificial blood vessels[101].

Electrospun scaffolds with a cell adhesive surface and an opposing antifouling surface have been proposed in the literature previously. Arnal-Pastor *et al*. generated scaffolds with opposing properties of cell adhesion by electrospinning hyaluronic acid (HA) fibres onto a previously electrospun mat of poly(L-lactic acid) (PLLA). PLLA is known for its cell binding properties and supports cell growth in contrast to HA which is known to be non-cell adhesive[102]. Mollet *et al*. used polymers based on ureido-pyr-imidinone (UPy) units to make UPy functionalised polymers and peptides. Bilayered scaffolds were produced using electrospinning to produce bilayers of either UPy-PCL and UPy-PCL / UPy-PEG or UPy-PCL / UPy-PEG / UPy-RGD and UPy-PCL / UPy-PEG to produce an cell adhesive layer (PCL or RGD) and a non-cell adhesive layer (PEG)[1200]. A bilayer scaffold for use in tendon repair as a replacement flexor sheath has also been proposed by Liu *et al.* employing a layered, sequential electrospinning approach. The inner, non-cell adhesive surface was prepared using PCL loaded with an HA microgel to allow controlled release of HA from the PCL fibres. HA is a known lubricant and may promote tendon glide. The outer surface of the scaffold was PCL alone. A clear demarcation of the layers was demonstrated with SEM and the scaffolds were implanted into an animal model with some success[98].

1.3.5 Cell binding surfaces

Scaffolds made of synthetic polymers often exhibit appropriate architecture for hosting cells, such as pore size, but they often lack or have a low level of biological activity for the promotion of cell-scaffold interactions[121]. A number of approaches have been used to manipulate this various ECM proteins such as fibronectin, gelatin, collagen or laminin have been incorporated into these scaffolds to promote cell adhesion and proliferation[122]. A few ECM proteins are known to mediate cell-cell and cell-scaffold interactions, one of which is the peptide motif Arg-Gly-Asp-Ser (RGDS). This sequence has been widely published within the literature as a cell-adhesive biomolecule that promotes cell adhesion through integrin

binding of fibronectin for a number of cell types and may be bound to polymers[122-125]. Fibroblasts, of which tenocytes are a specialised form, are such a cell type[110]. Typically within the literature a linear form of the RGDS peptide is used for the promotion of cell adhesion but I elected to use a cyclised variety (cRGDS) as it represents the natural presentation of the ligand in fibronectin[126].

1.4 The damaged tendon: a model system

Hand and wrist injuries are extremely common with isolated injuries alone making up some 6.6% of accident and emergency attendances per year in the UK[127]. Injury to tendons both within and outside of the hand are also common with more than 30 million injuries occurring globally on an annual basis[128]. Division of a tendon following traumatic injury is reliant on surgical repair for restoration of function, the outcome of which is often compromised due to adhesion (scar) formation (4%) or rupture of repair (4%). There are several sites and tissues in the hand that adhesions may form following injury and/or surgery. Flexor tendon adhesions typically from the tendon to adjacent tissue structures such as the flexor sheath following direct trauma to the tendon within the distal hand or fingers, or to other structures such as muscles, periosteum or following implanted metal work for other injuries. In such cases, most patients experience some degree of reduced movement and function[129]. Even a small reduction in function of the hand may have an impact on the patient's ability to work and function. Various studies have examined the work-time lost following hand injuries[130,131]. Wong demonstrates an average of 6.8 weeks off work (range of 0 to 16.6 weeks) following tendon injury in a cohort of hand injury patients in Hong Kong[130]. This represents significant work-time lost in this patient group.

Damaged ligaments or tendons may lead to joint instability that can progress to early onset osteoarthritis, pain, disability and the need for early joint replacement surgery. A high social and economic burden accompanies this, especially as the typical patient may be young and within work. The hypocellular and relatively avascular nature of tendons and ligaments means that their healing potential is limited and injuries need to be protected and mobilised in splints for long periods[132]. Any implant or device used within such a system needs to be able to withstand the mechanical forces placed upon it and be functional within them[133]. This particular part of tissue engineering have been coined "functional tissue engineering" to reflect this aspect[134].

1.4.1 Tendon: structure, function and anatomy

Tendons are specialist tissues made up of densely packed fibrous connective tissue that transmit the force generated by skeletal muscle to (typically) bone thus allowing movement[132]. They function like springs, storing energy while contributing to joint stability.

Tendons are hypocellular but are characterised by the presence of specialist fibroblast cells (tenoblasts / tenocytes) and ECM. They are not passive tissues and are responsive to changes in mechanical stimulus through physical training or disuse[135]. The cells exhibit a low metabolic rate which is essential for function as it allows tendons to be loaded for long periods of time without the risk of ischaemia[136]. Tendons do have some intrinsic blood supply through the vinculi, however they also receive nutritional support as they are bathed in synovial like fluid that provides nutrition, gas exchange and lubrication as they glide through the synovial sheaths[132].

The ECM of the tendon is predominantly made up of collagen type I (α_1) which is arranged in a hierarchical structure to produce fibrils, fibre bundles, fascicles and tendon units that run parallel to the tendon axis[1] (Figure 1-10). When in the unloaded state the collagen fibres form a wavy crimp like pattern, so large it can be visualised using an electron microscope[137]. The crimp structure allows some deformation of the collagen without tissue tension. This is seen in a typical stress-strain curve of tendons[138].

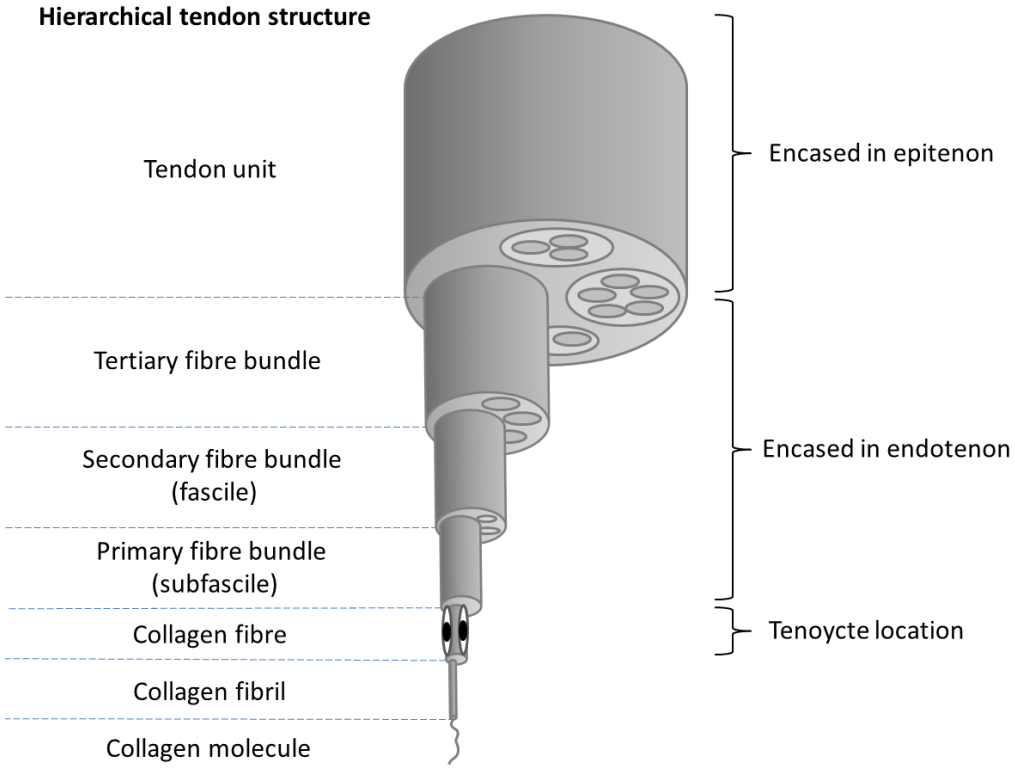

Figure 1-10: The hierarchical structure of a tendon, adapted from the literature[1].

A number of important transcription factors exist that have important roles in tendon and ligament formation, development and healing. These are outlined in Table 1-1.

Table 1-1: Factors involved in tendon development, formation and healing (adapted from the literature[132]).

Transcription factor	Impact	Citation
TGF-β	Inducer of tendon markers in mesenchymal stem cells. Significant role in tendon development.	139
Scleraxis	Considered a specific marker for tendon progenitor cells. Associated with tendon differentiation and ECM organisation. Participates in the formation of force-transmission.	140
Decorin	Most abundant proteoglycan in tendons; binds TGF and EGF. Stabilises and aligns collagen fibrils during fibrinogensis and contributes to tendon strength and elasticity.	141 142
Tenomodulin	Regulator of tenocyte proliferation. Involved in collagen fibril maturation. Highly expressed in tendon stem/progenitor cells.	143 144
Fibromodulin	Binds to type I collagen. Facilitates formation of mature large collagen fibrils. Involved in modulation of tendon strength.	141
Biglycan	Role in regulation of collagen fibrillogenesis during tendon development. Involved in the organisation of the tendon stem/progenitor cells niche and fate.	142
Collagen I	Major component of tendons providing tensile stiffness.	145
Collagen III	Structurally similar to collagen I. Important role in collagen I fibrillogenesis.	142

In the human hand, each finger (index, middle, ring and little) is serviced by two long flexor tendons; flexor digitorum profundus (FDP), the deep flexor, and flexor digitorum superficialis (FDS), the superficial flexor (Figure 1-11).

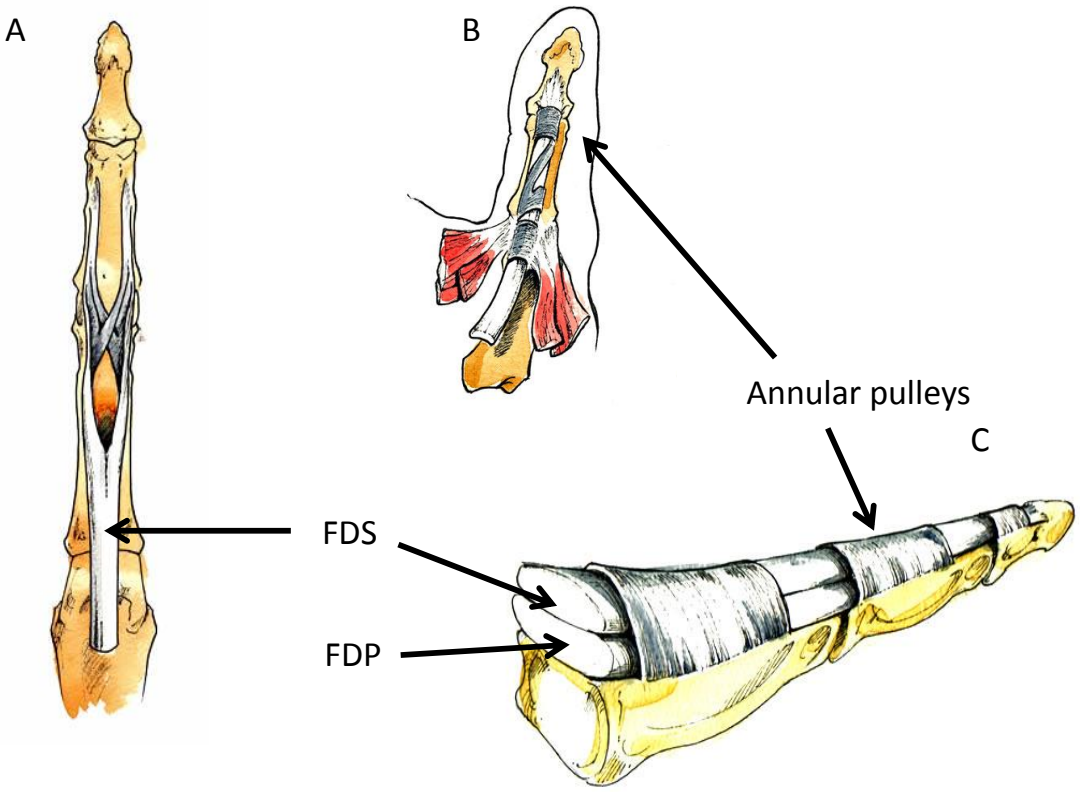

Figure 1-11: Anatomy of the flexor tendons. (A)The FDS chiasm (B) The pulley system in the thumb (C) The FDS and FDP in the finger with 3 annular pulleys demonstrated. Illustrations copyright Donnald Sammut, reproduced with permission (www.donnaldsammut.com).

The four FDS tendons arise from a common muscle belly in the superficial forearm and gain access to the palm through the carpal tunnel. They travel towards the fingers deep to the palmar fascia, but superficial to the FDP tendons and then pass into the flexor sheath to travel up the fingers. The FDS tendons bifurcate proximal to their insertion to allow transmission of the FDP tendon between the equal slips. The slips spiral around the profundus tendon to insert onto the anterior surface of the middle phalanx.

The four FDPs are similar also arising from a shared muscle belly in the forearm, the tendons also passing through the carpal tunnel to gain access to the palm. The tendon to each finger

remains deep to the FDS tendon as it enters the synovial (or flexor) sheath at the first annular (A1) pulley. At the level of the A2 pulley, the FDP passes through the FDS bifurcation and continues to the distal phalanx at which point it inserts onto the bone.

The synovial, or flexor sheath, is a fibro-osseous tunnel that guides the long flexors to their insertions on the fingers and thumb[146]. It has several thickenings along its length that make up the five annular and three paired cruciate pulleys in the fingers, with a single oblique pulley in the thumb. It provides an almost friction free surface for the tendons to glide against and anchors them to the bones to provide maximal movement of the joints (preventing the "bow-string" effect). This arrangement provides the maximal biomechanical advantage for the tendons. Within the sheath, a lubricating fluid, is produced by the sheath and bathes the tendons. This is similar to synovial fluid, the fluid produced and found in articulating joints that reduces friction between the moving surfaces. This fluid is important for tendon nutrition and healing[147].

1.4.2 Tendon Healing

In general tendons heal like all other tissues. An initial inflammatory phase (lasting 48-72 hours) precedes a regenerative (5 days to 4 weeks) then remodelling phase[136,148,149]. The damaged ECM is broken down to allow for the formation of a new network. Collagen III synthesis initially predominates over collagen I. Collagen III is composed of small fibrils and is deficient in cross linking. This allows for rapid production, important in the acute phase, but has a reduced mechanical strength when compared to collagen I. After approximately 6 weeks the newly synthesised ECM begins to remodel. During this time, consolidation and maturation occurs as collagen III is replaced by collagen I. This process may continue for up to a year. Regenerated tendon tissue, once tendon unity has occurred but before the remodelling process is complete, has been shown to have a higher cell density but reduced collagen fibre organisation when compared to the pre-injury state. This risks re-rupture, adhesions and sub-functionality[150]. Following primary tendon repair, the most likely time for tendon rupture is day 5-10 and 6 weeks post-operatively[151]. Much debate has existed around exactly how a tendon heals. Two mechanisms have been proposed, namely the extrinsic and intrinsic models.

1.4.2.1 Extrinsic Model of Tendon Healing

Traditionally it was thought that a tendon had no innate healing ability and that adhesion formation was an essential process whereby fibroblasts migrated to the injured site to heal and remodel the injury; leaving a trail of collagen bridges behind them[152,153]. It was thought, therefore, that adhesion formation was not only an inevitable consequence of tendon injury but also an essential one, without which tendon healing would not occur. This theory was challenged on the basis that blood vessels were often seen in tendons, and so since they had a blood supply they must possess healing potential. This belief led to the identification of intrinsic healing.

1.4.2.2 Intrinsic Model of Tendon Healing

Synovial fluid diffusion provides nutrition to the tendon through imbibition, whereby the fluid is forced into the interstices of the tendon through small conduits in the tendon surface through the action of flexion and extension of the digit[154]. Matthews and Richards provided experimental evidence of intrinsic healing in their classic paper in 1974[155]. Intrinsic healing relies upon the resident tenocytes within the tendon proliferating and producing new ECM to heal the defect. This may be achieved without any support from an extrinsic process as demonstrated by Matthews and Richards in their further work[156]. Partial tenotomies were performed without damage to the flexor sheath in rabbits. Tendons were not sutured or immobilised and healing occurred without adhesion formation. Further investigation led to groups assessing healing in a live, sutured tendon placed into the synovial cavity of a rabbit knee joint as a “tissue culture in situ” system. Proliferation of tenocytes and collagen deposition was observed[157,158]. Tenocytes resident within the tendon ECM have been shown to produce more mature and longer collagens than their epitenon counterparts[159].

The process of intrinsic healing relies upon an adequate nutritional support from the bathing synovial fluid and disruption to that support which results in necrosis[132]. This problem was encountered in the early days of hand surgeons trying to address the issue of adhesion formation using mechanical barriers, which lead to delayed healing or even necrosis in several early attempts[160,161].

1.4.2.3 Current Proposed Mechanism of Tendon Healing

Tendon healing is understood to be contributed to by both extrinsic and intrinsic factors. Strickland proposed that the relative contribution of each would likely depend of the factors that relate to both the injury and surgical repair[154]. This has been supported by several *in vitro* and *in vivo* studies assessing tendon healing with a live tendon grafts[162]. Interestingly, histological analysis of healing demonstrated that adhesion formation around the healing site occurred not only from fibroblast migrating into the gliding space (particularly around day 7), but also from tenocytes migrating out from the tendon surface. This migration of cells was seen at day 7, but increased significantly at day 14. The goal therefore of adhesion reduction is to prevent or reduce the migration of cells both from the tendon surface and from the synovial sheath into the gliding space.

1.4.2.4 Impact of Repair and Mobilisation on Tendon Healing

Surgical repair of tendons employs a suture technique to hold tendon ends together to allow healing whilst providing some mechanical support. Wong *et al*. assessed the impact of a single suture on the blood supply to a lacerated tendon in both a mouse (avascular) and a rabbit (vascular) tendon model[163]. Tendons analysed up to 14 days post operatively demonstrated a clear avascular zone when a suture had been applied and knotted. Upon examination of the literature they comment that several authors had observed degeneration adjacent to sutures in tendon repairs, but this had not been fully explained or addressed. The absence of the acellular zone in untied samples further supports the tension in the suture being responsible.

In current practice, patients with tendon repairs undergo early active mobilisation typically on day 1 post procedure. Mobilisation favours intrinsic healing through potential disruption of adhesion formation through migration of fibroblasts and neovascularisation, and supports a more rapid recovery of tendon strength[164,165].

1.4.3 Treatment Strategies and Complications

Treatment of tendon injuries, where there has been transection of >30% of the tendon substance, is through direct suture[166,167]. Typically core and epitedinous sutures are used to repair most injuries. However the type of suture material, number of core strands and

optimum technique that should be used is a source of much debate between surgeons. Tendon repairs are immobilised in a splint, often initially utilizing a plaster of paris splint, then a moulded thermoplastic splint. These splints are made in such a way to allow limited and protected movement of the injured digits. Current evidence supports early active postoperative mobilisation under the guidance of a specialist hand therapist to limit adhesion formation but protect repairs from excessive force.

Sutures, synovial sheath damage and immobilisation all contribute to adhesion formation. With the exception of sheath damage (dependant on anatomical site) both other variables are guaranteed in tendon surgery. Infection and re-operation may also contribute. Severe adhesions typically complicate 4% and patients with a persistent reduced tendon excursion due to adherent tendon repairs may need to go on to have flexor tenolysis surgery[129]. The aim of this procedure is to free the tendon from adhesions and allow gliding. This secondary surgical procedure is effective only in 67% of cases and stimulates further adhesion formation and scarring[168].

1.4.3.1 Tendon Adhesions: Research Areas

A large range of approaches have been used to try and tackle the problem of adhesion formation following surgery. This work focuses exclusively on adhesions associated with tendon injury, but there has been extensive research into other areas of adhesion formation, such as following abdominal or gynaecological surgery.

A wide range of approaches have been taken to try and tackle the problem of tendon adhesion formation with varying degrees of success and is outlined in a published review[169]. They can broadly be divided into several key areas; lubricants, gene therapy, pharmacological agents, and mechanical barriers (including tissue engineered approaches). Results are typically mixed. Tendon healing can be precarious and many approaches have led to an increase in postoperative ruptures; possibly due to compromised healing as a result of the anti-adhesion therapy.

1.4.3.1.1. Lubricants

One common approach that is employed to reduce adhesion formation is to insert a lubricating compound around the repaired tendon to facilitate smooth glide. The aim of

which is to facilitate and enhance boundary lubrication between the moving surfaces of the tendon and sheath, which naturally occurs in the un-injured state.

Hyaluronic acid (HA) is a glycosaminoglycan (GAG) polysaccharide that is a natural carbohydrate polymer and is one of the principal lubricants in synovial fluid. Together with lubricin and aggrecan, high molecular weight proteoglycans and proteins respectfully, boundary lubrication in synovial joints is enhanced. This is due to the water-trapping action of the polymers and production of a viscous fluid that keeps the cartilaginous surfaces apart and allows almost friction free movement between them. HA has been most extensively investigated for use in tendon surgery with generally encouraging results, particularly in relation to the higher molecular weights, *ex vivo*, but not always *in vivo*[170,171].

Modifications of HA including the addition of carboiimide derivatives have been tried in an animal model. The rationale is that the additional group should chemically bind to the exposed amine groups on the tendon surface thus prolonging the tissue resident time and binding strength; a limiting factor in some previous approaches. The results were mixed with tendons treated with the modified HA not achieving normal function post operatively[172]. Other compounds that have been assessed to reduce friction in tendon movement include 5-flurouracil, ADCON-T/N and lubricin[170,173].

1.4.3.1.2 Growth Factor Manipulation and Gene Therapy

A number of growth factors have been identified as potential targets for increasing strength of tendon repair through modulation of tenocytes. One such family is transforming growth factor beta (TGF-β). TGFβ is a cytokine key in the process of healing and has a broad range of activities. It is one of the cytokines released during platelet degranulation at the site of wound healing and it triggers a cascade of events including chemotaxis of other cells, angiogenesis, and collagen synthesis. It is also implicated in fibrosis, chronic inflammation and scarring[174]. It exists in three different isoforms (TGFβ1, β2 and β3), each with differing properties. Other growth factors associated with engineered tendon and ligament tissues are summarized in Table 1-2.

Table 1-2: Differing roles of TGF (adapted from[132]).

Factor	Function	Citation
TGFβ-1	Induces fibrotic change and scar formation. Possibly dominant isoform in early tendon healing.	[175,176]
TGFβ-2	Induces fibrotic change and scar formation.	
TGFβ-3	Inhibits scar formation.	
PDGF	Involved in tendon healing: controlled delivery of PDGF-BB enhanced the biological response in a canine tendon healing model.	[177]
bFGF	Promoter of tenocyte proliferation and collagen expression. Some evidence of increased adhesion formation.	[178,179] [180]
VEGF	Involved in tendon graft remodelling	[181]
GDFs or BMPs	GDF-5: increased proliferation, ECM production and expression of tenogenic markers in ASCs. GDF-5 coated sutures in rat tendon healing model led to increased ultimate tensile strength of repair. Cartilage formation occurred.	[150] [182]
HGF	Produced in vitro after plasma clot and platelet stimuli by tenocytes.	[183]

Notes: PDGF: platelet derived growth factor, bFGF: basic fibroblast growth factor, VEGF: vascular endothelial growth factor, GDF: growth/differentiation factor, BMP: bone morphogenic protein, HGF: hepatocyte growth factor.

TGF-β is likely to be a key component of adhesion formation and so its manipulation has received much interest in this field. *In vitro* models have demonstrated TGF-β inhibition through the use of a neutralising antibody on cultured tenocytes in a dose dependant manner[184,185]. TGF-β 1 has also been shown to produce significant differences in gene expression in populations of primary cells isolated from distinct regions of a rabbit tendon – endotenon, epitenon, and synovial sheath[148]. A more recent study used antisense oligonucleotides targeted against some components of the TGF signalling pathways with promising results[186]. The use of gene therapy for tendon repair has not been fully supported by the literature, with studies reporting no significant increase, or even a reduction in the tensile strength of treated tendons[187,188]. Topical application of growth factors to tendon injuries through the use of platelet rich plasma (PRP), which may be considered as a concentrated pool of growth factors, has been tried. A number of studies have suggested an improvement in mechanical properties and healing following tendon repair[189-191], with another suggesting it may be a useful activator of circulation-derived cells for enhancement

of the initial healing process[192]. A randomised single-blind clinical trial of the use of PRP in Achilles tendon repair however, has not supported its use in humans[193]. Studies discussed later comparing the use of cell implantation complemented with and without PRP showed no difference in cellular activity or tendon strength with its use[194]. Caliari *et al*. assessed a number of growth factor supplementation strategies and interestingly demonstrated that single factor supplementation lead to a dose-dependent trade-off between driving tenocyte proliferation (PDGF-BB and insulin like growth factor-1 [IGF-1]) and maintenance of a tenocyte phenotype (GDF-5, bFGF)[194]. Perhaps this finding, in part, explains some of the differences found in the literature.

Heparin is known to absorb and regulate the release of growth factors and has been used for this purpose in tissue engineered scaffolds[195]. This approach has been utilised in a number of tissue engineering applications previously and has been applied to tendon healing by Manning *et al*.[177] who used a combination of PDGF-BB coupled with adipocyte stem cells within a heparin/fibrin-based growth factor delivery system and showed the potential for improved outcome in tendon repair in a canine model. Heparin has even recently been used in a clinical trial of 100 patients with tendon injuries. Unfractionated heparin was injected into tendon ends before surgical repair. The findings showed no clear advantage for this use of heparin, but a significantly increased risk of tendon rupture with its use[196].

1.4.3.1.3 Pharmacological Agents

Research into reducing tendon adhesions with pharmacological agents is well established. Bora *et al.* in 1972 tried using a number of agents known to alter collagen biosynthesis in a rat model of tendon injury[197]. Unfortunately two of the agents were toxic and many animals died. Many other agents have been tested and are outlined in Table 1-3.

Non-steroidal anti-inflammatory drugs (NSAIDs) are drugs that produce antipyretic, analgesic and anti-inflammatory effects. This is achieved through reduction in the production of prostaglandins through the inhibition of cyclooxygenase (COX). The potential for NSAIDs to be a useful adjunct in the modulation of tendon adhesion following injury and repair was recognised many years ago. In the classic works by Kulick *et al.* published in 1984 and 1986, the outcome from using injectable[198] and oral ibuprofen[199] in primates was

evaluated. The initial paper was successful in reducing tendon adhesion in a primate model when ibuprofen was injected at the site of repair. The follow up work, however, using oral ibuprofen suggested that adhesions were indeed still reduced in the repaired tendon but the ultimate tensile strength was also adversely affected. Ibuprofen has recently been used by several groups as a part of a multifaceted approach for prevention of tendon adhesion in tendon injury. One study used a tissue engineering approach of a long-term drug delivery system. Modified mesoporous silica nanoparticles were loaded with ibuprofen then electrospun into a polymer scaffold of poly(L-lactic acid) (PLLA)[75] . An *in vitro* drug release profile demonstrated release of approximately 6% in the first six hours followed by a more sustained release occurring with 91% having been released at 100 days. Controls of a PLLA electrospun scaffold, and a co-spun PLLA-ibuprofen scaffold, and no scaffold were used. At four weeks histology showed dense adhesions in the control group and the PLLA scaffold group. Both scaffolds containing ibuprofen demonstrated low levels of adhesion. This was maintained at eight weeks with the exception of the PLLA-ibuprofen scaffold (short term release) which demonstrated some inflammation and adhesion formation. The group postulated this was due to the inflammatory reaction of the PLLA scaffold starting to dissolve and that the ibuprofen release had ceased. The PLLA nanoparticle loaded ibuprofen scaffold demonstrated superior results throughout. Biomechanical analysis revealed little difference in ultimate tensile strength of tendons.

Liu *et al.* again used an electrospun fibrous membrane in a drug delivery system[200]. In this study, ibuprofen was loaded into a poly(L-lacticacid)-polyethelene glycol (PELA) biblock co-polymer by co-dissolving the drug and polymer before performing the electrospinning process. Poly(ethylene glycol) is known to have anti cell adhesion properties. *In vitro* drug release studies demonstrated a burst release over the first two days followed by a sustained release over the following days. The drug release is dependent on the polymer degradation. Animal testing in a leghorn chicken model revealed superior anti-adhesion properties of the PELA-ibuprofen scaffold when compared to controls (both PELA membrane alone, and no scaffold) at 21 days. Biomechanical analysis showed work of flexion was significantly different between both PELA membranes and the surgical control, and between the PELA membrane and PELA-ibuprofen membrane which had the lowest levels of adhesion. No significant different was seen between maximal tensile strength. These approaches use the

combination of a physical barrier (the electrospun fibres) combined with the anti-inflammatory action of the ibuprofen to obtain these results. Liu *et al*.'s approach furthermore has an anti-adhesive tendency due to the polymer choice. In both studies the operated limbs were splinted. The group went on to also use celecoxib loaded membranes with some success[201] and more recently are developing a membrane to release naproxen[202].

A few drug trials have been undertaken to address the problem of adhesions following tendon laceration. A recent multicentre, randomised parallel group study was undertaken in Europe with 138 patients undergoing zone 1 or 2 flexor tendon repair surgery[203]. Patients were treated with either a viscous gel of sodium hyaluronate containing PXL01 (treatment arm) or a sodium chloride control. PXL01 is a synthetic peptide derived from human lactoferrin that is known to have antimicrobial and anti-inflammatory properties[204,205]. This first-in-patient phase II trial showed it was safe, well tolerated and did not lead to an increase in tendon rupture. The full analysis set showed no significant difference at 6 or 12 months between groups, but subset analysis supported the use of PXL01 at 6 months. Unfortunately the trial did not include a treatment arm with administration of the sodium hyaluronate gel alone and due to losses to follow up was under powered after the 12 week time point.

Table 1-3: Pharmacological agents used to modulate tendon adhesion *in vitro* and *in vivo*

Drug type	Agent	Application	Model	Result	
Pyrimidine antimetabolite	5-Flurouracil	Topical intra operative	Rabbit Chicken	Reduction in adhesion formation and reduced TGF-β1. No adverse effect of tendon or wound healing identified. Lower doses supported by *in vivo* work. Reduction of MMPs (especially 2 and 9) found suggesting limited synovial fibroblast migration and adhesion reduction.	[206,207] [208,209] [210,211]
		Topical intra operative	CLINICAL TRIAL	Results support improved outcome (reduced adhesion formation and no tendon ruptures) in treatment group compared to controls.	[212]
		Drug delivery via gelatin hydrogel	Chicken	Continuous drug delivery system with investigation of different dosages. Study supporting low dose release system for optimal results (10mg/1.5ml) for adhesion reduction. Tensile testing not performed.	[213]
Antioxidant	Vitamin C	Topical intra operative	Chicken	Some evidence of reduced adhesion formation at late time point of 6 weeks. Mechanical testing not performed.	[214]
Corticosteroid		Regular local administration	Rabbit	Reduction in adhesion formation but also in mechanical strength.	[215]
Agents to alter collagen biosynthesis	*Cis*-4-hydroxy-L-proline	Daily dosing	Rat	Some effect in adhesion reduction	[197]
	α,α'-dipyridyl	Daily dosing	Rat	Toxic to animals – limited growth and increased mortality	[197]
	B-aminopropionitrile-fumerate	Daily dosing	Rat	Moderate toxicity to animals – hepatocellular disease and increased mortality	[197]
	D-penicillamine	Daily dosing	Rat	Some effect in adhesion reduction	[197]

1.4.3.1.4 Mechanical Barriers

Many different groups have utilized a material or construct to physically prevent adhesion formation by maintaining separation between the healing surfaces. Broadly, they may be classified into synthetic or biological materials. A spectrum of results has been obtained but these techniques have typically been troubled with tendon necrosis leading to rupture of the repair, inflammatory foreign body reaction and ingrowth of adhesions at the material edges.

Biological membranes have been used to recreate or reconstruct the flexor sheath to maintain a gliding surface in several models. Amniotic membrane[216], autologous long saphenous vein grafts[217,218], fascial grafts[218], peritoneal grafts[219], collagen membranes[220] and even the tunica vaginalis has been tried as an autologous graft in male patients[221]. Overall results have been encouraging but generally statistically unconvincing. Biological barriers also suffer from the question of source. If the source is not autologous, then problems such as potential for disease transmission, religious and cultural acceptability and the reliability of sourcing for unscheduled surgery can occur. If autologous, increased operation time and complexity is expected. It also increases patient morbidity, may increase hospital stay and increases general anaesthetic requirements.

Synthetic membranes avoid such problems and have also been extensively investigated. Early work began with materials such as cellophane in 1963[222]. Unsurprisingly to us now, this resulted in tendon necrosis as this non porous material would have led to a suboptimal result through prevention of both extrinsic and intrinsic tendon healing, and a significant inflammatory response. Other materials such as gelatin wrapping[160], silastic sheeting[223], cellulose tubes[218], alumina sheets[224], stainless steel sheeting[225] and silicone envelopes.

Increasingly modern approaches started producing more promising results. Absorbable, oxidised regenerated cellulose (Interceed, TC-7, Johnson & Johnson, USA) subjectively improved movement and reduced adhesions was demonstrated by histology[226]. Interceed is an FDA approved material for adhesion reduction primarily used in bowel and gynaecological surgery. Hydrogel films containing hyaluronic acid and carboxymethylcellulose (e.g. Seprafilm® and Carbylan™) have been examined in a number of studies for this purpose[76,227-229]. Seprafilm® is currently used in abdominal and

gynaecological surgery for reduction in adhesion formation. Both films show reduced adhesion where Carbylan™ is described as being the most effective of the two. Unfortunately, both have handling difficulties and potentially short *in vivo* life span[76].

Poly(hydroxylethyl) methacrylate (pHEMA) membranes coated exteriorly with chondroitin sulphate (CS) were used to block adhesion formation and reduce cell attachment (and hence adhesion formation) in a rabbit model of primary tendon repair. This technique successfully reduced adhesion formation in the first six weeks[225]. Integra (Integra Life Sciences, Plainsboro, NJ) is a bovine collagen and shark cartilage glycosaminoglycan (GAG) dermal substitute currently used in clinical practice in a variety of fields. It was used to wrap primary tendon repair sites and showed experimental promise in a chicken model for reduced work of flexion[230]. Fibronectin biotubes were developed and used to wrap around a tendon defect such that not only did the construct form a physical barrier to migrating fibroblasts (and hence adhesion formation) but also the biotube acted as a donor for soluble fibronectin fragments which act as competitive inhibitors for cell adhesion. Mechanical tethering of gliding tissues was reduced but no difference was found on histological examination between treatment groups and controls[231].

An anti-adhesion barrier gel, ADCON-T/N (Gliatech, Cleveland, OH, USA) is a porcine gelatine/carbohydrate polymer, bioresorbable gel that has been shown to be effective against tendon and neural adhesion formation both *in vitro* and *in vivo*[232]. A randomised prospective clinical trial in humans for use in new zone 2 flexor tendon injuries in the hand was performed[233]. Of note, all patients had closure of the synovial sheath with lengths taken not to produce stenosis, and provided a one week course of Diclofenac Sodium (an NSAID). Both of these factors have been independently shown to reduce adhesion formation. Groups were matched, but small in number (16 in treatment group and 14 in control). No statistical difference was found between the two groups. A prospective double-blind, randomized, controlled clinical trial using ADCON-T/N in a larger sample size of 45 patients with 82 flexor tendon repairs was also performed. There was no significant difference in total active motion at 3, 6 and 12 months between groups. Time to total active movement was significantly shorter in the ADCON-T/N group suggesting an inhibition to adhesion formation, but increased rupture rate was also observed though not significant[234]. ADCON-T/N has also been used *in vitro* and compared to HA and 5-FU, with controls of phosphate

buffered saline (PBS) and bovine synovial fluid (BSF), for reduction in coefficient of friction in tendon glide[170].

A porous L-lactide-caprolactone copolymer (LLCC) membrane was used to reduce adhesion formation in a canine model. Following tenotomy, a primary repair was performed and treated with either an LLCC membrane, LLCC membrane with HA, HA solution alone, or a control group. The LLCC membrane was found to be effective in preventing adhesion formation but lead to delayed healing of the tendon[235]. This work has been extrapolated and modified to application in a bone healing model to assess prevention of tendon adhesion following plate fixation of a fracture using a poly L-lactide-co-caprolactone membrane in a rabbit model[236].

1.4.3.1.5 The use of cells for augmentation of tendon repairs

Tissue engineering and implanted scaffolds may include cells, the selection of which continues to be a source of debate. Cells may be autogenic, allogenic or xenogenic, adult, multipotent or pluripotent cells. Pluripotent cells may be from embryonic stem cells, or modulated such as induced pluripotent cells (iPS) or following nuclear transfer. Primary cells and adult stem cells have been used in a number of treatment modalities with some encouraging clinical results.

Most commonly cells are not used within an approach to reduce tendon adhesion formation. However, cells have been used in approaches to improve and augment tendon healing. Cells that have been typically employed to date have been mesenchymal stem cells (MSCs) found within bone marrow, or, more recently, adipose derived stem cells (ASCs). Like bone marrow, adipose tissue is derived from the mesoderm layer and also contains a stem cell population. These ASCs exhibit unique characteristics distinct from those seen in MSCs[237].

1.4.3.1.5.1 Mesenchymal Stem Cells

MSCs are multipotent mesenchymal nonhaematopoetic stromal cells that are derived from the embryonic mesoderm. These cells can be found in most adult tissues and organs in differing concentrations. They have received much interest in the field due to their ability to differentiate into, and contribute to the regeneration of mesenchymal tissues such as bone,

adipose, tendon, ligament, cartilage, and muscle. The rationale for the use of such cells in tissue engineering is for the production of growth factors, chemokines and as cell donors; to divide and differentiate into the appropriate cell lines to directly becomes involved in the tissue repair. MSCs also seem to be hypoimmunogenic and so are suitable for allogenic transplantation[238]. Cell sources include bone marrow, adipose tissue and deciduous teeth. Identification of MSCs with specific markers has remained elusive. No single surface marker exists, but rather a number of markers that defines a human MSC. Guidance from the International Society for Cellular Therapy outlines the proteins that a cell must, and must not express in order to be considered a MSC[239].

A number of different approaches have been used for delivery of MSCs to the tendon site. Yao *et al.* having had success and proof-of-concept with the successful transfer of viable embryonic stem cells to an *in vitro* tendon model[111,240] used bone marrow-derived MSCs (BMSCs) again on a suture delivery vehicle[240]. Fluorescently labelled allogenic BMSCs were incubated with 4-0 ethibond (braided polyester) sutures. In vivo testing using an Achilles tendon defect in a rat model was performed with blinding and an internal control. Biomechanical testing at time points up to day 28 post op demonstrated significant increase in load to failure for tendons with BMSCs for days 7 and 10 and trends towards increased strength for all other time points tested. Allogenic cells were visualised at all time points. The authors surmised that the donation of BMSCs that could differentiate into tenocytes may have "jump started" the repair process as it is known that the tendon stumps are relatively acellular after repair[163]. Whether enhance repair is due to the delivered cells taking part directly in repair, cytokine production for enhance fibroblast recruitment and stimulation, or indeed both, is unclear. Other carriers such as fibrin[241], collagen gel-suture constructs[242] and phosphate buffered saline[243] have been used and typically give increased tensile strength at one or more time points when compared to controls. This has not been without complication however, ectopic bone formation has been seen in 28% of rabbit tendons following treatment with an MSC-collagen gel construct[244].

MSCs can also be derived from peripheral blood. Using a combination of peripheral blood derived MSC and platelet rich plasma (containing a high concentration of growth factors) a group explored the potential of a synergistic action of both treatments. Whilst this paper was exploring tendenopathy rather than a laceration and surgical repair it is interesting to

note that the paper found no such response and highlighted the predominant effect of MSCs for enhanced tendon healing[245].

In all these studies, with the exception of the above, cells have been derived from a bone marrow source. A bone marrow aspirate is a painful, highly invasive procedure with a complication rate reported at 30%[246]. A low yield of BMSCs are also often attained by a single aspirate[247] If cell based therapy for tendon healing is to become a clinical reality a different cell source would need to be used.

1.4.3.1.5.2 Adipocyte Derived Stem Cells

Adipose tissue contains high concentrations of stem cells of mesenchymal lineage. They have the potential to differentiate into tenocytes and other mesenchymal cell lines as BMSCs[237]. Treatment with growth differentiation factor-5 (GDF-5, also known as bone morphogenic protein-14, BMP14) has been shown to drive tenogenesis of ASCs[150] and chondrogenesis[248].

ASCs can be readily harvested through lipoaspiration under either a local or general anaesthetic. The procedure is generally well tolerated, acceptable to patients, and has minimal complications or morbidity particularly when compared to bone marrow aspiration. Techniques and protocols for the isolation of ASCs have been developed and there are commercially available, FDA approved, machines for ASC isolation for use in the operating theatre[249,250]. This makes the use of autologous ASCs for tendon surgery a viable, clinically application option as they may not need to undergo *in vitro* processing after isolation.

Uysal *et al.* used autologous adipocyte derived stem cells (ASCs) within a platelet-rich plasma preparation in a rabbit model of tendon repair. Biomechanical evaluation of ultimate tensile strength at 4 weeks demonstrated that ASC treated tendons were significantly stronger than controls (PRP combined with surgical repair)[151]. A tissue engineering approach using AScs has already been outlined above, a scaffold with a layered PLGA mats and a heparin/fibrin hydrogel and ASCs[177].

ASCs are known to be anti-inflammatory[251,252] so it is also a possibility that their use may also reduce adhesion formation secondary to inflammation.

1.4.3.2 Combination Approaches

The ideal construct for this application would be biocompatible, allow normal tendon glide, be low profile, bioresorbable, easy to use, inexpensive, remain at the site of repair until healing was completed, provide mechanical support, be permeable to synovial fluid, and enhance healing of the repair. No approach to date has achieved this. Several different studies have produced some interesting combinations with encouraging results, for example, in one study an HA gel loaded with an NSAID (Naproxen) was tested[253]. Gel treatment, both with and without drug loading, had statistically reduced adhesions compared to controls. All medicated systems were shown to be significantly more effective than HA alone, as was adding a crosslinking agent to the gel.

Manning *et al.* used a scaffold of alternating layers of a poly(lactic-co-glycolic) acid (PLGA) electrospun nanofibrous mat and a heparin/fibrin hydrogel seeded with adipocyte derived stem cells was prepared for improving healing and reducing adhesion in primary tendon repair[177]. This approach uses a mechanical barrier, heparin to accumulate and control release of growth factors, and provides adipocyte stem cells to aid tendon healing. This initial proof-of-concept study demonstrated that the ASCs remained viable on the scaffold in vitro and that sustained delivery of PDGF-BB was supported by the scaffold. They were also tolerated *in vivo* in a canine model and viable ASCs were seen at the tendon healing site nine days after implantation. Further work to assess adhesion formation and perform biomechanical testing is expected in future work. Similarly, an electrospun mat consisting of a HA loaded PCL scaffold demonstrated promise in a chicken model[98].

Silver nanoparticles incorporated into an electrospun poly(L-lactide) (PLLA) membranes have been investigated[80,254]. This demonstrated reduced fibroblast adhesion when compared to a control without nanoparticles, and hence predicted reduced adhesion formation. They also prevented adhesion to several common gram positive and gram negative bacteria which may reduce post-operative wound infections in traumatic wounds. They also assessed the response to dextran glassy nanoparticles loaded with basic fibroblast growth factor (bFGF) electrospun with PLLA into a scaffold. This was implanted into an Achilles tendon defect in a rat model. They demonstrated enhanced intrinsic healing and release of the bFGF over a 30 day period. Adhesion formation was observed where bFGF

was used although breaking strength of adhesions was not assessed. Ultimate tensile strength of repaired tendons however was assessed and demonstrated that the control (surgical repair alone) was the strongest interestingly, although this result was not significant. In another study, an electrospun di-block copolymer membrane of poly(L-lactic acid)-poly(ethylene glycol) was tested with ibuprofen dissolved in the solvent/polymer solution prior to electrospinning to encapsulate the ibuprofen within the fibres[78]. Ibuprofen demonstrated an initial burst release followed by sustained release over 10 days. Implantation into a chicken model demonstrated a significant reduction in work of flexion (surrogate for adhesion strength) between the ibuprofen loaded mat and the plain scaffold, and the control. No difference between strength of tendon repair was found between groups.

Many additional approaches to reduce adhesion formation have been tried[255]. As our understanding and capabilities have increased, potential solutions to this problem are becoming increasingly elegant and drawing upon different areas of tissue engineering to produce increasingly translatable results. Flexor tendon injuries were described by Farhat *et al*. as "being among the more challenging problems for hand surgeons and tissue engineers alike. Not only do flexor tendons heal with poor mechanical strength, they can also form debilitating adhesions that may permanently impair hand function"[256]. This is why research in this area is so diverse and why, in the face of so much previous failure, it continues.

1.5 Bilayer scaffold design and scaffold adaptations for the tendon model

Using the modular scaffold design presented in this thesis, the design was adapted using the clinical application of a primary flexor tendon repair as a model to test the versatility of the design.

A bilayer system was designed with a cell and protein resisting antifouling surface and an opposing cell-binding surface (Figure 1-12). This is designed initially in the form of a flat sheet for *in vitro* testing (Figure 1-13) but the versatility of the electrospinning apparatus would allow the facile modification to a tubular structure in the future with opposing surface chemistries, i.e. the inner surface of the tube having an antifouling functionalization and the outer surface been cell adhesive.

1.5.1 Poly-ε-caprolactone, the polymer chosen for the bulk scaffold

Degradable biomaterials are diverse in their properties and can be selected for a particular application based on these, biodegradable polymers and are discussed in this recent review[257].

PCL was chosen to make up the bulk of the scaffold. PCL is a well characterised, bioresorbable polymer that has been used extensively in tissue engineering and produces good fibres when electrospinning. It was one of the earliest polymers synthesised in early 1930[258] and is very versatile with regard to its chemical, physical and material properties[92]. PCL undergoes degradation and complete excretion in humans[259,260]. Initially, the action of random non-enzymatic surface hydrolysis leads to schism of the polymer through the ester linkages, reducing the molecular weight in a first order manner[261]. This may be observed at a similar rate *in vitro* and *in vivo*. Once the M_n falls to < 5000 it is thought that enzymatic and phagocytic degradation by macrophages, giant cells and fibroblasts play a role in the final clearance of the material and the rate increases *in vivo*[262,263] . This mechanism of action means that PCL bioresorbs relatively slowly (months to years) and is highly dependent on the surface area of the implant. The classic work by Hutmacher *et al.* used extruded struts of PCL (1.7 mm Ø diameter)[259,262], which will have a significantly smaller surface area, and hence increased time for hydrolysis when compared to electrospun fibres. Bolgen *et al.* studied electrospun fibres for 6 months in various conditions *in vitro* and *in vivo* and demonstrated that the degradation profile of PCL still took many months[260]. The presence of the highly hydrated pOEGMA polymer brush layer surrounding the PCL fibres may accelerate the degradation of the PCL through hydrolysis due to the availability of water so close to the PCL surface, which is seen in other surface functionalization[92]. The effect of PEG on the degradation of PCL has been assessed previously in the literature and shown to increase the rate of degradation[264].

Implanted materials and those that undergo biodegradation or bioresorption typically cause an inflammatory response. This has been showed to be for only the first 2 weeks after implantation for PCL[263]. PCL has been featured in a large number of drug delivery devices, implants and sutures (including monocryl^{TM}). It has FDA approval and CE mark registration.

PCL has been successfully used as a scaffold for tendon tissue engineering, including for tendon applications[98,265].

End functionalization of PCL, in separate batches, with a polymerisation initiator and the cRGDS peptide allows for the production of a continuously produced electrospun scaffold.

1.5.2 Electrospinning as a processing technique

Electrospinning, as discussed in section 1.3.2.1 is extremely versatile. It has been selected for use as it allows the production of a versatile overall architecture and structure, the production of easily handled products, fibres with a large surface area for functionalization and the ability to produce spatially controlled functional groups within a single processing step and construct. Furthermore, the porosity of the fibres is key with a tendon application in mind to support healing. This has been investigated by Chen *et al.* who investigated the penetration of bovine serum albumin (BSA) through electrospun membranes[266]. They demonstrated that a significant reduction in BSA transport through PCL scaffolds when compared to scaffolds combined with PEG, which was independent to pore size. They proposed that the hydrophobic nature of the PCL lead to this result. They demonstrated BSA transport across the membranes when PEG was present.

1.5.3 Monomer selection for surface functionalization

Poly(ethylene glycol) (PEG) is an FDA approved, biocompatible, renally excreted polymer that has been used extensively to prevent fouling of surfaces both medically and in industry and as a drug delivery vehicle[68,69]. PEG coatings are known to be adhesion resistant to proteins and cells[70]. It is also easily functionalised for the preparation of biologically relevant conjugates[71], thus making it an ideal polymer for use in adhesion resistance. By selecting the oligomer, OEGMA a high density bottle brush can be produced. OEGMA is fully discussed in section 1.3.1.4 and the polymerisation from 3D scaffolds in 1.3.3.2.

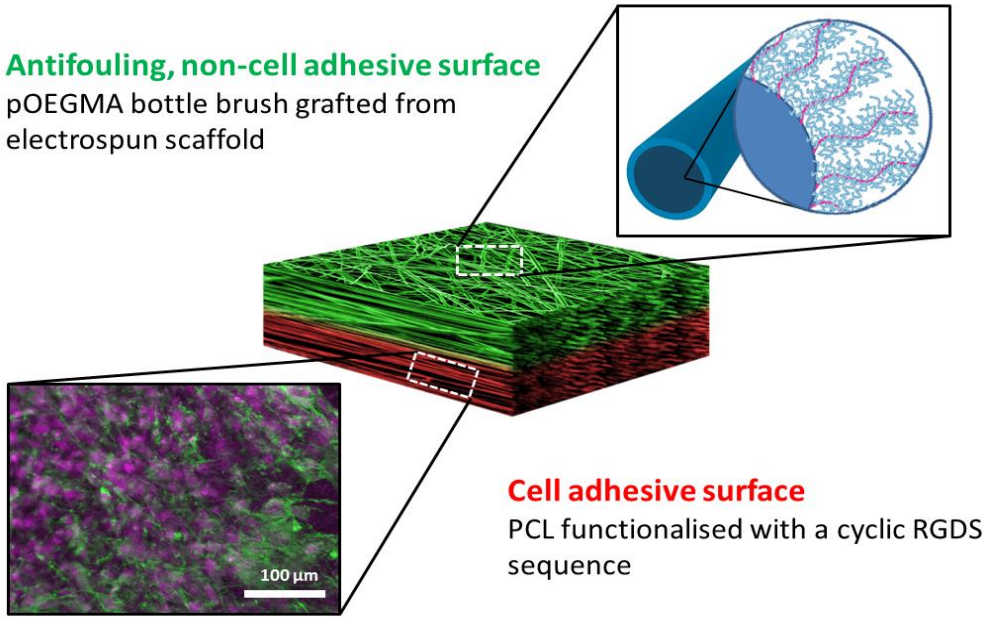

Figure 1-12: The bilayer scaffold design with an antifouling surface and a cell adhesive surface.

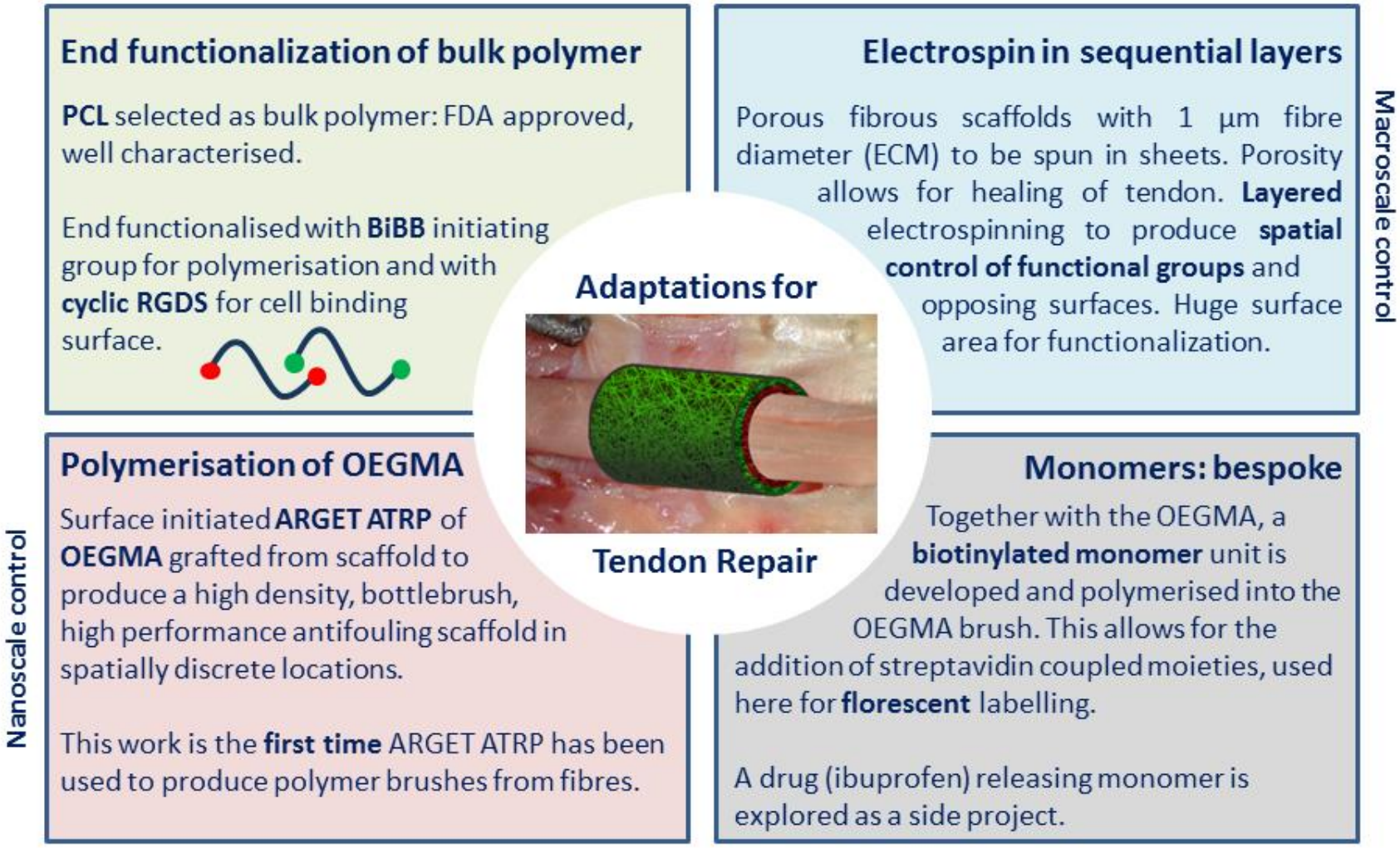

Figure 1-13: Schematic of the adaptions of the modular scaffold for a primary flexor tendon repair. Central photograph adapted from http://www.atlantaequine.com/images/tendon_sheath_dissection.jpg

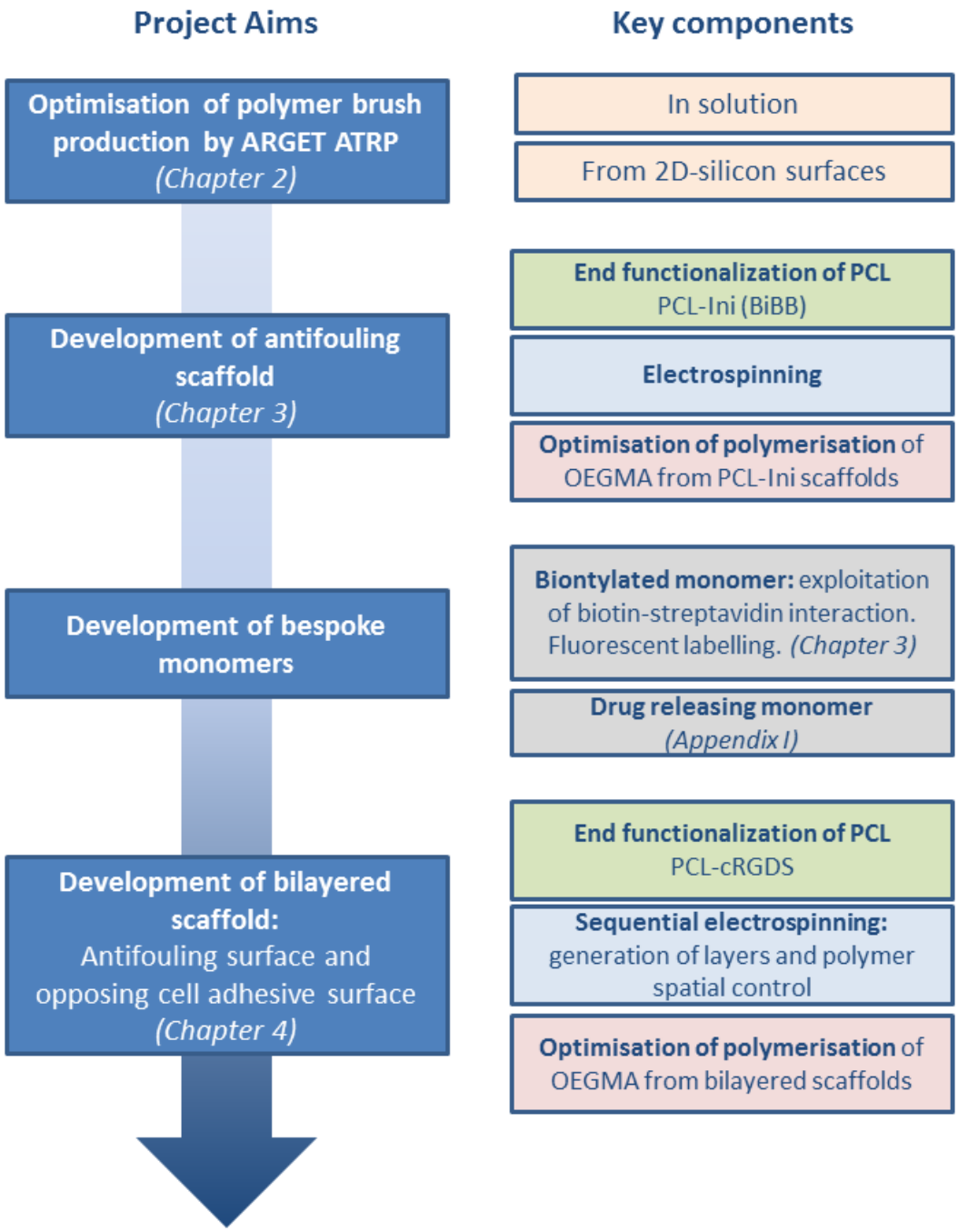

Figure 1-14: Flow chart demonstrating the project aims of this work and the key components of each stage.

1.6 Summary

The delicate gliding tissue surfaces of the body, be they of the musculoskeletal, abdominal, or pelvic in origin, are vulnerable to damage from trauma, infection or inflammation. The formation of adhesions resulting in a partial or complete obliteration of these surfaces can lead to pain, reduced function and increased patient morbidity and mortality. Tissue engineering and regenerative medicine is a multidisciplinary field that has the potential to improve outcomes in such cases.

A modular and versatile scaffold is presented for use in preservation of gliding surfaces following injury. Using specifically chosen current state-of-the-art processing and cutting edge chemistry, the scaffold is initially designed with a model system in mind; the flexor tendon of the hand. Through the application of the knowledge of the specific needs of the flexor tendon, the scaffold has been designed and optimised for use.

References: Chapter One

1 Wang, J. H. C. Mechanobiology of tendon. *Journal of biomechanics* **39**, 1563-1582, doi:10.1016/j.jbiomech.2005.05.011 (2006).

2 Billmeyer, F. W. *Textbook of Polymer Science*. Second Edition edn, (John Wiley & Sons, Inc., 1971).

3 Oh, J. K., Min, K. & Matyjaszewski, K. Preparation of poly(oligo(ethylene glycol) monomethyl ether methacrylate) by homogeneous aqueous AGET ATRP. *Macromolecules* **39**, 3161-3167, doi:10.1021/ma060258v (2006).

4 Lysaght, M. J. & Crager, J. Origins. *Tissue Eng. Part A* **15**, 1449-1450, doi:10.1089/ten.tea.2007.0412 (2009).

5 Langer, R. & Vacanti, J. P. TISSUE ENGINEERING. *Science* **260**, 920-926, doi:10.1126/science.8493529 (1993).

6 Hutmacher, D. W. Scaffolds in tissue engineering bone and cartilage. *Biomaterials* **21**, 2529-2543, doi:10.1016/s0142-9612(00)00121-6 (2000).

7 Marston, W. A., Hanft, J., Norwood, P., Pollak, R. & Dermagraft Diabet Foot Ulcer, S. The efficacy and safety of Dermagraft in improving the healing of chronic diabetic foot ulcers - Results of a prospective randomized trial. *Diabetes Care* **26**, 1701-1705, doi:10.2337/diacare.26.6.1701 (2003).

8 Eaglstein, W. H. & Falanga, V. Tissue engineering and the development of Apligraf(R), a human skin equivalent. *Clinical Therapeutics* **19**, 894-905, doi:10.1016/s0149-2918(97)80043-4 (1997).

9 Atala, A., Bauer, S. B., Soker, S., Yoo, J. J. & Retik, A. B. Tissue-engineered autologous bladders for patients needing cystoplasty. *Lancet* **367**, 1241-1246, doi:10.1016/s0140-6736(06)68438-9 (2006).

10 Takahashi, K. *et al.* Induction of pluripotent stem cells from adult human fibroblasts by defined factors. *Cell* **131**, 861-872, doi:10.1016/j.cell.2007.11.019 (2007).

11 Takahashi, K. & Yamanaka, S. Induction of pluripotent stem cells from mouse embryonic and adult fibroblast cultures by defined factors. *Cell* **126**, 663-676, doi:10.1016/j.cell.2006.07.024 (2006).

12 Song, J. J. *et al.* Regeneration and experimental orthotopic transplantation of a bioengineered kidney. *Nat. Med.* **19**, 646-651, doi:10.1038/nm.3154 (2013).

13 Olausson, M. *et al.* Transplantation of an allogeneic vein bioengineered with autologous stem cells: a proof-of-concept study. *Lancet* **380**, 230-237, doi:10.1016/s0140-6736(12)60633-3 (2012).

14 Zopf, D. A., Hollister, S. J., Nelson, M. E., Ohye, R. G. & Green, G. E. Bioresorbable Airway Splint Created with a Three-Dimensional Printer. *N. Engl. J. Med.* **368**, 2043-2045, doi:10.1056/NEJMc1206319 (2013).

15 Li, M. Y. *et al.* Electrospun protein fibers as matrices for tissue engineering. *Biomaterials* **26**, 5999-6008, doi:10.1016/j.biomaterials.2005.03.030 (2005).

16 Haag, J. C., Jungebluth, P. & Macchiarini, P. Tracheal replacement for primary tracheal cancer. *Curr. Opin. Otolaryngol. Head Neck Surg.* **21**, 171-177, doi:10.1097/MOO.0b013e32835e212b (2013).

17 Jungebluth, P. *et al.* Tracheobronchial transplantation with a stem-cell-seeded bioartificial nanocomposite: a proof-of-concept study. *Lancet* **378**, 1997-2004, doi:10.1016/s0140-6736(11)61715-7 (2011).

18 Schwartz, S. D. *et al.* Embryonic stem cell trials for macular degeneration: a preliminary report. *Lancet* **379**, 713-720, doi:10.1016/s0140-6736(12)60028-2 (2012).

19 Schwartz, S. D., Hubschman, J.-P., Heilwell, G., Pan, C. K. & Lanza, R. Embryonic stem-cell-derived retinal pigment epithelial cells for macular degeneration Reply. *Lancet* **379**, 2050-2051 (2012).
20 Harrison, R. H., St-Pierre, J.-P. & Stevens, M. M. Tissue Engineering and Regenerative Medicine: A Year in Review. *Tissue Eng. Part B-Rev.* **20**, 1-16 (2014).
21 Irish, J. D. A 5,500-year-old artificial human tooth from Egypt: A historical note. *International Journal of Oral & Maxillofacial Implants* **19**, 645-647 (2004).
22 Butler, C. E. & Prieto, V. G. Reduction of adhesions with composite AlloDerm/polypropylene mesh implants for abdominal wall reconstruction. *Plastic and Reconstructive Surgery* **114**, 464-473, doi:10.1097/01.prs.0000132670.81794.7e (2004).
23 Mohsina, A. *et al.* Bioengineered acellular dermal matrices for the repair of abdominal wall defects in rats. *Hernia* **19**, 219-229, doi:10.1007/s10029-014-1308-7 (2015).
24 Lutolf, M. P. & Hubbell, J. A. Synthetic biomaterials as instructive extracellular microenvironments for morphogenesis in tissue engineering. *Nat. Biotechnol.* **23**, 47-55, doi:10.1038/nbt1055 (2005).
25 Langer, R. & Tirrell, D. A. Designing materials for biology and medicine. *Nature* **428**, 487-492, doi:10.1038/nature02388 (2004).
26 Moad, G., Solomon, D.H. *The Chemistry of free radical polymerization*. (Pergamon, 1995).
27 Coessens, V., Pintauer, T. & Matyjaszewski, K. Functional polymers by atom transfer radical polymerization. *Progress in Polymer Science* **26**, 337-377, doi:10.1016/s0079-6700(01)00003-x (2001).
28 Matyjaszewski, K. Transition metal catalysis in controlled radical polymerization: Atom transfer radical polymerization. *Chemistry-a European Journal* **5**, 3095-3102, doi:10.1002/(sici)1521-3765(19991105)5:11<3095::aid-chem3095>3.0.co;2-# (1999).
29 Patten, T. E. & Matyjaszewski, K. Copper(I)-catalyzed atom transfer radical polymerization. *Accounts of Chemical Research* **32**, 895-903, doi:10.1021/ar9501434 (1999).
30 Wang, J. S. & Matyjaszewski, K. CONTROLLED LIVING RADICAL POLYMERIZATION - ATOM-TRANSFER RADICAL POLYMERIZATION IN THE PRESENCE OF TRANSITION-METAL COMPLEXES. *Journal of the American Chemical Society* **117**, 5614-5615, doi:10.1021/ja00125a035 (1995).
31 Tsarevsky, N. V. & Matyjaszewski, K. "Green" atom transfer radical polymerization: From process design to preparation of well-defined environmentally friendly polymeric materials. *Chemical Reviews* **107**, 2270-2299, doi:10.1021/cr050947p (2007).
32 Perrier, S. & Takolpuckdee, P. Macromolecular design via reversible addition-fragmentation chain transfer (RAFT)/Xanthates (MADIX) polymerization. *Journal of Polymer Science Part a-Polymer Chemistry* **43**, 5347-5393, doi:10.1002/pola.20986 (2005).
33 Moad, G., Rizzardo, E. & Thang, S. H. Living Radical Polymerization by the RAFT Process - A Second Update. *Australian Journal of Chemistry* **62**, 1402-1472, doi:10.1071/ch09311 (2009).

34 Matyjaszewski, K. Atom Transfer Radical Polymerization (ATRP): Current Status and Future Perspectives. *Macromolecules* **45**, 4015-4039, doi:10.1021/ma3001719 (2012).
35 Matyjaszewski, K. & Tsarevsky, N. V. Macromolecular Engineering by Atom Transfer Radical Polymerization. *Journal of the American Chemical Society* **136**, 6513-6533, doi:10.1021/ja408069v (2014).
36 Simakova, A., Averick, S. E., Konkolewicz, D. & Matyjaszewski, K. Aqueous ARGET ATRP. *Macromolecules* **45**, 6371-6379, doi:10.1021/ma301303b (2012).
37 Hawker, C. J. & Wooley, K. L. The convergence of synthetic organic and polymer chemistries. *Science* **309**, 1200-1205, doi:10.1126/science.1109778 (2005).
38 Wang, J. S. & Matyjaszewski, K. CONTROLLED LIVING RADICAL POLYMERIZATION - HALOGEN ATOM-TRANSFER RADICAL POLYMERIZATION PROMOTED BY A CU(I)CU(II) REDOX PROCESS. *Macromolecules* **28**, 7901-7910, doi:10.1021/ma00127a042 (1995).
39 Kato, M., Kamigaito, M., Sawamoto, M. & Higashimura, T. POLYMERIZATION OF METHYL-METHACRYLATE WITH THE CARBON-TETRACHLORIDE DICHLOROTRIS(TRIPHENYLPHOSPHINE)RUTHENIUM(II) METHYLALUMINUM BIS(2,6-DI-TERT-BUTYLPHENOXIDE) INITIATING SYSTEM - POSSIBILITY OF LIVING RADICAL POLYMERIZATION. *Macromolecules* **28**, 1721-1723, doi:10.1021/ma00109a056 (1995).
40 Singleton, D. A., Nowlan, D. T., Jahed, N. & Matyjaszewski, K. Isotope effects and the mechanism of atom transfer radical polymerization. *Macromolecules* **36**, 8609-8616, doi:10.1021/ma035310r (2003).
41 Barbey, R., Lavanant, L., Paripovic, D., Schu¨wer, N., Sugnaux C., Tugulu, S., Klok, H. Polymer Brushes via Surface-Initiated Controlled Radical Polymerization: Synthesis, Characterization, Properties, and Applications. *Chem. Rev.* **109**, 5437-5527 (2009).
42 Seeliger, F. & Matyjaszewski, K. Temperature Effect on Activation Rate Constants in ATRP: New Mechanistic Insights into the Activation Process (vol 42, pg 6050, 2009). *Macromolecules* **43**, 5478-5478, doi:10.1021/ma101043n (2010).
43 Mueller, L. *et al.* Synthesis of high molecular weight polystyrene using AGET ATRP under high pressure. *European Polymer Journal* **47**, 730-734, doi:10.1016/j.eurpolymj.2010.10.006 (2011).
44 Braunecker, W. A., Tsarevsky, N. V., Gennaro, A. & Matyjaszewski, K. Thermodynamic Components of the Atom Transfer Radical Polymerization Equilibrium: Quantifying Solvent Effects. *Macromolecules* **42**, 6348-6360, doi:10.1021/ma901094s (2009).
45 Tang, W. *et al.* Understanding atom transfer radical polymerization: Effect of ligand and initiator structures on the equilibrium constants. *Journal of the American Chemical Society* **130**, 10702-10713, doi:10.1021/ja802290a (2008).
46 Tsarevsky, N. V., Pintauer, T. & Matyjaszewski, K. Deactivation efficiency and degree of control over polymerization in ATRP in protic solvents. *Macromolecules* **37**, 9768-9778, doi:10.1021/ma048438x (2004).
47 Wang, X. S. & Armes, S. P. Facile atom transfer radical polymerization of methoxy-capped oligo(ethylene glycol) methacrylate in aqueous media at ambient temperature. *Macromolecules* **33**, 6640-6647, doi:10.1021/ma000671h (2000).
48 Min, K. & Matyjaszewski, K. Atom transfer radical polymerization in aqueous dispersed media. *Central European Journal of Chemistry* **7**, 657-674, doi:10.2478/s11532-009-0092-1 (2009).

49 Chung, I. D., Britt, P., Xie, D., Harth, E. & Mays, J. Synthesis of amino acid-based polymers via atom transfer radical polymerization in aqueous media at ambient temperature. *Chemical Communications*, 1046-1048, doi:10.1039/b416591h (2005).
50 Yuan, W. *et al.* Hemocompatible surface of electrospun nanofibrous scaffolds by ATRP modification. *Mater. Sci. Eng., C* **33**, 3644-3651, doi:10.1016/j.msec.2013.04.048 (2013).
51 Li, L., Zhu, Y., Li, B. & Gao, C. Fabrication of Thermoresponsive Polymer Gradients for Study of Cell Adhesion and Detachment. *Langmuir* **24**, 13632-13639, doi:10.1021/la802556e (2008).
52 Miao, J. *et al.* AGET ATRP of Water-Soluble PEGMA: Fast Living Radical Polymerization Mediated by Iron Catalyst. *Journal of Polymer Science Part a-Polymer Chemistry* **50**, 2194-2200, doi:10.1002/pola.25988 (2012).
53 Jakubowski, W. & Matyjaszewski, K. Activator generated by electron transfer for atom transfer radical polymerization. *Macromolecules* **38**, 4139-4146, doi:10.1021/ma047389l (2005).
54 Telford, A. M. *et al.* Micropatterning of Polymer Brushes: Grafting from Dewetting Polymer Films for Biological Applications. *Biomacromolecules* **13**, 2989-2996, doi:10.1021/bm3010534 (2012).
55 Huang, X. Y. & Wirth, M. J. Surface-initiated radical polymerization on porous silica. *Analytical Chemistry* **69**, 4577-4580, doi:10.1021/ac9704523 (1997).
56 Ameringer, T. *et al.* Surface grafting of electrospun fibers using ATRP and RAFT for the control of biointerfacial interactions. *Biointerphases* **8**, doi:10.1186/1559-4106-8-16 (2013).
57 Yang, W. J. *et al.* Biomimetic Anchors for Antifouling and Antibacterial Polymer Brushes on Stainless Steel. *Langmuir* **27**, 7065-7076, doi:10.1021/la200620s (2011).
58 Gao, C. & Yan, D. Hyperbranched polymers: from synthesis to applications. *Progress in Polymer Science* **29**, 183-275, doi:10.1016/j.progpolymsci.2003.12.002 (2004).
59 Zhao, H. Y., Kang, X. L. & Liu, L. Comb-coil polymer brushes on the surface of silica nanoparticles. *Macromolecules* **38**, 10619-10622, doi:10.1021/ma051822p (2005).
60 Bombalski, L., Min, K., Dong, H. C., Tang, C. B. & Matyjaszewski, K. Preparation of well-defined hybrid materials by ATRP in miniemulsion. *Macromolecules* **40**, 7429-7432, doi:10.1021/ma071408k (2007).
61 He, J. *et al.* Study and application of a linear frequency-thickness relation for surface-initiated atom transfer radical polymerization in a quartz crystal microbalance. *Macromolecules* **40**, 3090-3096, doi:10.1021/ma062613n (2007).
62 Balazs, A. C. *et al.* Theory of polymer chains tethered at interfaces. *Progress in Surface Science* **55**, 181-269, doi:10.1016/s0079-6816(97)00026-9 (1997).
63 Ruhe, J. & Knoll, N. Functional polymer brushes (Reprinted from Supramolecular Polymers, pg 565-613, 2000). *Journal of Macromolecular Science-Polymer Reviews* **C42**, 91-138 (2002).
64 Yano, T. *et al.* Precise control of surface physicochemical properties for electrospun fiber mats by surface-initiated radical polymerization. *Polymer Journal* **43**, 838-848, doi:10.1038/pj.2011.80 (2011).
65 Banerjee, S., Paira, T. K. & Mandal, T. K. Surface confined atom transfer radical polymerization: access to custom library of polymer-based hybrid materials for speciality applications. *Polymer Chemistry* **5**, 4153-4167, doi:10.1039/c4py00007b (2014).

66 Yoshikawa, C., Zhang, K., Zawadzak, E. & Kobayashi, H. A novel shortened electrospun nanofiber modified with a "concentrated" polymer brush. *Sci. Technol. Adv. Mater.* **12**, 015003/015001-015003/015007, doi:10.1088/1468-6996/12/1/015003 (2011).
67 Tugulu, S., Klok, H. Stability and Nonfouling properties of Poly(poly(ethylene glycol) methacrylate) Brushes under Cell Culture Condtions. *Biomacromolecules* **9**, 906-912 (2008).
68 Knop, K., Hoogenboom, R., Fischer, D. & Schubert, U. S. Poly(ethylene glycol) in Drug Delivery: Pros and Cons as Well as Potential Alternatives. *Angewandte Chemie-International Edition* **49**, 6288-6308, doi:10.1002/anie.200902672 (2010).
69 Yamaoka, T., Tabata, Y. & Ikada, Y. DISTRIBUTION AND TISSUE UPTAKE OF POLY(ETHYLENE GLYCOL) WITH DIFFERENT MOLECULAR-WEIGHTS AFTER INTRAVENOUS ADMINISTRATION TO MICE. *Journal of Pharmaceutical Sciences* **83**, 601-606, doi:10.1002/jps.2600830432 (1994).
70 Banerjee, I., Pangule, R. C. & Kane, R. S. Antifouling Coatings: Recent Developments in the Design of Surfaces That Prevent Fouling by Proteins, Bacteria, and Marine Organisms. *Advanced Materials* **23**, 690-718, doi:10.1002/adma.201001215 (2011).
71 Zalipsky, S. FUNCTIONALIZED POLY(ETHYLENE GLYCOL) FOR PREPARATION OF BIOLOGICALLY RELEVANT CONJUGATES. *Bioconjugate Chemistry* **6**, 150-165, doi:10.1021/bc00032a002 (1995).
72 Venkatraman, S., Boey, F. & Lao, L. L. Implanted cardiovascular polymers: Natural, synthetic and bio-inspired. *Prog Polym Sci* **33**, 853-874, doi:10.1016/j.progpolymsci.2008.07.001 (2008).
73 Wei, Y. *et al.* Surface engineering of cardiovascular stent with endothelial cell selectivity for in vivo re-endothelialisation. *Biomaterials* **34**, 2588-2599, doi:10.1016/j.biomaterials.2012.12.036 (2013).
74 Boateng, J. S., Matthews, K. H., Stevens, H. N. E. & Eccleston, G. M. Wound healing dressings and drug delivery systems: A review. *Journal of Pharmaceutical Sciences* **97**, 2892-2923, doi:10.1002/jps.21210 (2008).
75 Hu, C. *et al.* Long-term drug release from electrospun fibers for in vivo inflammation prevention in the prevention of peritendinous adhesions. *Acta biomaterialia* **9**, 7381-7388, doi:10.1016/j.actbio.2013.03.040 (2013).
76 Liu Y, S. A., Shu XZ, Prestwich GD. Prevention of peritendinous adhesions using a hyaluronan-derived hydrogel film following partial-thickness flexor tendon injury. *J Orthop Res.* **26**, 562-569 (2008).
77 Babazadeh, M., Sheidaei, M., Abbaspour, S. & Edjlali, L. Synthesis, characterization, and in vitro evaluation of new Ibuprofen polymeric prodrugs based on 2-hydroxypropyl methacrylate. *Scientia pharmaceutica* **81**, 281-296, doi:10.3797/scipharm.1204-14 (2013).
78 Ruan, L. P. *et al.* Designed amphiphilic peptide forms stable nanoweb, slowly releases encapsulated hydrophobic drug, and accelerates animal hemostasis. *Proc Natl Acad Sci U S A* **106**, 5105-5110, doi:10.1073/pnas.0900026106 (2009).
79 Drury, J. L. & Mooney, D. J. Hydrogels for tissue engineering: scaffold design variables and applications. *Biomaterials* **24**, 4337-4351, doi:10.1016/s0142-9612(03)00340-5 (2003).

80 Liu, S. *et al.* Antibacterial and anti-adhesion effects of the silver nanoparticles-loaded poly(L-lactide) fibrous membrane. *Mater. Sci. Eng. C-Mater. Biol. Appl.* **33**, 1176-1182, doi:10.1016/j.msec.2012.12.008 (2013).
81 McCullen, S. D., Autefage, H., Callanan, A., Gentleman, E. & Stevens, M. M. Anisotropic Fibrous Scaffolds for Articular Cartilage Regeneration. *Tissue Eng. Part A* **18**, 2073-2083, doi:10.1089/ten.tea.2011.0606 (2012).
82 Zhang, Y. *et al.* The impact of PLGA scaffold orientation on in vitro cartilage regeneration. *Biomaterials* **33**, 2926-2935, doi:10.1016/j.biomaterials.2012.01.006 (2012).
83 Liu, S., Qin, M., Hu, C., Wu, F., Cui, W., Jin, T., Fan, C. Tendon healing and anti-adhesion properties of electrospun fibrous membranes containing bFGF loaded nanoparticles. *Biomaterials*, doi:http://dx.doi.org/10.1016/j.biomaterials.2013.03.026 (2013).
84 Nezarati, R. M., Eifert, M. B. & Cosgriff-Hernandez, E. Effects of humidity and solution viscosity on electrospun fiber morphology. *Tissue Eng Part C Methods* **19**, 810-819, doi:10.1089/ten.TEC.2012.0671 (2013).
85 Doshi, J. & Reneker, D. H. ELECTROSPINNING PROCESS AND APPLICATIONS OF ELECTROSPUN FIBERS. *Journal of Electrostatics* **35**, 151-160, doi:10.1016/0304-3886(95)00041-8 (1995).
86 Loh, Q. L. & Choong, C. Three-Dimensional Scaffolds for Tissue Engineering Applications: Role of Porosity and Pore Size. *Tissue Eng. Part B-Rev.* **19**, 485-502, doi:10.1089/ten.teb.2012.0437 (2013).
87 Rho, K. S. *et al.* Electrospinning of collagen nanofibers: Effects on the behavior of normal human keratinocytes and early-stage wound healing. *Biomaterials* **27**, 1452-1461, doi:10.1016/j.biomaterials.2005.08.004 (2006).
88 Huang, Z. M., Zhang, Y. Z., Ramakrishna, S. & Lim, C. T. Electrospinning and mechanical characterization of gelatin nanofibers. *Polymer* **45**, 5361-5368, doi:10.1016/j.polymer.2004.04.005 (2004).
89 Chen, C., Cao, C. B., Ma, X. L., Tang, Y. & Zhu, H. S. Preparation of non-woven mats from all-aqueous silk fibroin solution with electrospinning method. *Polymer* **47**, 6322-6327, doi:10.1016/j.polymer.2006.07.009 (2006).
90 You, Y. *et al.* In vitro degradation behaviour of non-porous ultra-fine poly(glycolic acid)/poly(L-lactic acid) fibres and porous ultra-fine poly(glycolic acid) fibres. *Polymer Degradation and Stability* **90**, 441-448, doi:10.1016/j.polydegradstab.2005.04.015 (2005).
91 Li, D., Frey, M. W., Vynias, D. & Baeumner, A. J. Availability of biotin incorporated in electrospun PLA fibers for streptavidin binding. *Polymer* **48**, 6340-6347, doi:10.1016/j.polymer.2007.08.027 (2007).
92 Woodruff, M. A. & Hutmacher, D. W. The return of a forgotten polymer-Polycaprolactone in the 21st century. *Prog Polym Sci* **35**, 1217-1256, doi:10.1016/j.progpolymsci.2010.04.002 (2010).
93 Simonet, M., Schneider, O. D., Neuenschwander, P. & Stark, W. J. Ultraporous 3D polymer meshes by low-temperature electrospinning: Use of ice crystals as a removable void template. *Polymer Engineering and Science* **47**, 2020-2026, doi:10.1002/pen.20914 (2007).

94 Sampson, S. L., Saraiva, L., Gustafsson, K., Jayasinghe, S. N. & Robertson, B. D. Cell Electrospinning: An In Vitro and In Vivo Study. *Small*, n/a-n/a, doi:10.1002/smll.201300804 (2013).
95 Xu, X. L., Chen, X. S., Wang, Z. F. & Jing, X. B. Ultrafine PEG-PLA fibers loaded with both paclitaxel and doxorubicin hydrochloride and their in vitro cytotoxicity. *European Journal of Pharmaceutics and Biopharmaceutics* **72**, 18-25, doi:10.1016/j.ejpb.2008.10.015 (2009).
96 Noh, K. T., Lee, H. Y., Shin, U. S. & Kim, H. W. Composite nanofiber of bioactive glass nanofiller incorporated poly(lactic acid) for bone regeneration. *Materials Letters* **64**, 802-805, doi:10.1016/j.matlet.2010.01.014 (2010).
97 Harrison, R. H. *et al.* Modular and Versatile Spatial Functionalization of Tissue Engineering Scaffolds through Fiber-Initiated Controlled Radical Polymerization. *Advanced Functional Materials* **25**, 5748-5757, doi:10.1002/adfm.201501277 (2015).
98 Liu, S. *et al.* Biomimetic Sheath Membrane via Electrospinning for Antiadhesion of Repaired Tendon. *Biomacromolecules* **13**, 3611-3619, doi:10.1021/bm301022p (2012).
99 Angarano, M. *et al.* Layered Gradient Nonwovens of In Situ Crosslinked Electrospun Collagenous Nanofibers Used as Modular Scaffold Systems for Soft Tissue Regeneration. *Advanced Functional Materials* **23**, 3277-3285, doi:10.1002/adfm.201202816 (2013).
100 Bye, F. J. *et al.* Development of bilayer and trilayer nanofibrous/microfibrous scaffolds for regenerative medicine. *Biomater. Sci.* **1**, 942-951, doi:10.1039/c3bm60074b (2013).
101 Wang, H. *et al.* Electrospun hemocompatible PU/gelatin-heparin nanofibrous bilayer scaffolds as potential artificial blood vessels. *Macromol. Res.* **20**, 347-350, doi:10.1007/s13233-012-0012-7 (2012).
102 Arnal-Pastor, M., Martinez Ramos, C., Perez Garnes, M., Monleon Pradas, M. & Valles Lluch, A. Electrospun adherent-antiadherent bilayered membranes based on cross-linked hyaluronic acid for advanced tissue engineering applications. *Mater. Sci. Eng., C* **33**, 4086-4093, doi:10.1016/j.msec.2013.05.058 (2013).
103 Agarwal, S., Wendorff, J. H. & Greiner, A. Chemistry on Electrospun Polymeric Nanofibers: Merely Routine Chemistry or a Real Challenge? *Macromolecular Rapid Communications* **31**, 1317-1331, doi:10.1002/marc.201000021 (2010).
104 Ozcam, A. E., Roskov, K. E., Genzer, J. & Spontak, R. J. Responsive PET Nano/Microfibers via Surface-Initiated Polymerization. *ACS Appl. Mater. Interfaces* **4**, 59-64, doi:10.1021/am201559f (2012).
105 Fu, G. D. *et al.* Smart Nanofibers from Combined Living Radical Polymerization, "Click Chemistry" and Electrospinning. *Acs Applied Materials & Interfaces* **1**, 239-243, doi:10.1021/am800143u (2009).
106 Menkhaus, T. J. *et al.* Electrospun nanofiber membranes surface functionalized with 3-dimensional nanolayers as an innovative adsorption medium with ultra-high capacity and throughput. *Chemical Communications* **46**, 3720-3722, doi:10.1039/c001802c (2010).
107 Feng, Q. *et al.* Electrospun Regenerated Cellulose Nanofibrous Membranes Surface-Grafted with Polymer Chains/Brushes via the Atom Transfer Radical Polymerization Method for Catalase Immobilization. *ACS Appl Mater Interfaces* **6**, 20958-20967 (2014).

108 Gualandi, C. *et al.* Advantages of Surface-Initiated ATRP (SI-ATRP) for the Functionalization of Electrospun Materials. *Macromolecular Rapid Communications* **34**, 51-56, doi:10.1002/marc.201200648 (2013).
109 Wang, H. Y. *et al.* Fabrication of PU/PEGMA crosslinked hybrid scaffolds by in situ UV photopolymerization favoring human endothelial cells growth for vascular tissue engineering. *Journal of Materials Science-Materials in Medicine* **23**, 1499-1510, doi:10.1007/s10856-012-4613-7 (2012).
110 Grafahrend, D. *et al.* Biofunctionalized poly(ethylene glycol)-block-poly(ε-caprolactone) nanofibers for tissue engineering. *J. Mater. Sci.: Mater. Med.* **19**, 1479-1484, doi:10.1007/s10856-007-3299-8 (2008).
111 Fu, G. D. *et al.* Core-sheath nanofibers from combined atom transfer radical polymerization and electrospinning. *Macromolecules* **41**, 6854-6858, doi:10.1021/ma800499h (2008).
112 Brandl, C., Greiner, A. & Agarwal, S. Quick Polymerization from Electrospun Macroinitiators for Making Thermoresponsive Nanofibers. *Macromolecular Materials and Engineering* **296**, 858-864, doi:10.1002/mame.201100031 (2011).
113 Jeon, S. I., Lee, J. H., Andrade, J. D. & Degennes, P. G. PROTEIN SURFACE INTERACTIONS IN THE PRESENCE OF POLYETHYLENE OXIDE .1. SIMPLIFIED THEORY. *Journal of Colloid and Interface Science* **142**, 149-158, doi:10.1016/0021-9797(91)90043-8 (1991).
114 Cho, Y. *et al.* Preparation and Characterization of Amphiphilic Triblock Terpolymer-Based Nanofibers as Antifouling Biomaterials. *Biomacromolecules* **13**, 1606-1614, doi:10.1021/bm300327w (2012).
115 Lee, J.-W. *et al.* Fouling-Tolerant Nanofibrous Polymer Membranes for Water Treatment. *Acs Applied Materials & Interfaces* **6**, 14600-14607, doi:10.1021/am503874b (2014).
116 Arribas, P., Khayet, M., Garcia-Payo, M. C. & Gil, L. Self-sustained electro-spun polysulfone nano-fibrous membranes and their surface modification by interfacial polymerization for micro- and ultra-filtration. *Separation and Purification Technology* **138**, 118-129, doi:10.1016/j.seppur.2014.10.010 (2014).
117 Chow, L. W. *et al.* Peptide-Directed Spatial Organization of Biomolecules in Dynamic Gradient Scaffolds. *Advanced Healthcare Materials* **3**, 1381-1386, doi:10.1002/adhm.201400032 (2014).
118 Kidoaki, S., Kwon, I. K. & Matsuda, T. Mesoscopic spatial designs of nano- and microfiber meshes for tissue-engineering matrix and scaffold based on newly devised multilayering and mixing electrospinning techniques. *Biomaterials* **26**, 37-46, doi:10.1016/j.biomaterials.2004.01.063 (2004).
119 Sundararaghavan, H. G. & Burdick, J. A. Gradients with Depth in Electrospun Fibrous Scaffolds for Directed Cell Behavior. *Biomacromolecules* **12**, 2344-2350, doi:10.1021/bm200415g (2011).
120 Mollet, B. B. *et al.* A modular approach to easily processable supramolecular bilayered scaffolds with tailorable properties. *J. Mater. Chem. B* **2**, 2483-2493, doi:10.1039/C3TB21516D (2014).
121 Zhang, Y. Z., Lim, C. T., Ramakrishna, S. & Huang, Z. M. Recent development of polymer nanofibers for biomedical and biotechnological applications. *Journal of Materials Science-Materials in Medicine* **16**, 933-946, doi:10.1007/s10856-005-4428-x (2005).

122 Chaisri, P., Chingsungnoen, A. & Siri, S. Repetitive Arg-Gly-Asp peptide as a cell-stimulating agent on electrospun poly(-caprolactone) scaffold for tissue engineering. *Biotechnol J* **8**, 1323-1331 (2013).
123 Hersel, U., Dahmen, C. & Kessler, H. RGD modified polymers: biomaterials for stimulated cell adhesion and beyond. *Biomaterials* **24**, 4385-4415, doi:10.1016/s0142-9612(03)00343-0 (2003).
124 Danesin, R. *et al.* Self-assembling peptide-enriched electrospun polycaprolactone scaffolds promote the h-osteoblast adhesion and modulate differentiation-associated gene expression. *Bone (N. Y., NY, U. S.)* **51**, 851-859, doi:10.1016/j.bone.2012.08.119 (2012).
125 Mattanavee, W. *et al.* Immobilization of Biomolecules on the Surface of Electrospun Polycaprolactone Fibrous Scaffolds for Tissue Engineering. *ACS Appl. Mater. Interfaces* **1**, 1076-1085, doi:10.1021/am900048t (2009).
126 Xu, F. J., Wang, Z. H. & Yang, W. T. Surface functionalization of polycaprolactone films via surface-initiated atom transfer radical polymerization for covalently coupling cell-adhesive biomolecules. *Biomaterials* **31**, 3139-3147, doi:10.1016/j.biomaterials.2010.01.032 (2010).
127 Hill C, R. M., Mozzam A, Brennen MD. . A regional audit of hand and wrist injuries. A study of 4873 injuries. *J Hand Surg* **23B**, 196-200 (1998).
128 Maffulli N, W. J., Almekinders LC. Types and epidemiology of tendinopathy. *Clin Sports Med* **22**, 675-692 (2003).
129 Dy, C. J., Hernandez-Soria, A., Ma, Y., Roberts, T. R. & Daluiski, A. Complications After Flexor Tendon Repair: A Systematic Review and Meta-Analysis. *J. Hand Surg.-Am. Vol.* **37A**, 543-551, doi:10.1016/j.jhsa.2011.11.006 (2012).
130 Wong, J. Y. P. Time off work in hand injury patients. *J. Hand Surg.-Am. Vol.* **33A**, 718-725, doi:10.1016/j.jhsa.2008.01.015 (2008).
131 Watts, A. M. I., Greenstock, M. & Cole, R. P. Outcome following the rehabilitation of hand trauma patients - The importance of a subjective functional assessment. *J. Hand Surg.-Br. Eur. Vol.* **23B**, 485-489, doi:10.1016/s0266-7681(98)80128-9 (1998).
132 Rodrigues, M. T., Reis, R. L. & Gomes, M. E. Engineering tendon and ligament tissues: present developments towards successful clinical products. *Journal of tissue engineering and regenerative medicine*, doi:10.1002/term.1459 (2012).
133 Group, F. T. E. C. Evaluation criteria for MSK and craniofacial tissue engineered constructs - conference report. *TISSUE ENGINEERING: Part A* **14** (2008).
134 Butler D, G. S., Guilak F. Functional tissue engineering: the role of biomechanics. *Journal of biomechanical engineering* **122**, 570-575 (2000).
135 Kjaer M, L. H., Miller BF et al. Metabolic activity and collagen turnover in human tendon in response to physical activity. *J Musculoskelet Neuronal Interact* **5**, 41-52 (2005).
136 Sharma P, M. N. Basic biology of tendon injury and healing. *Surgeon* **3**, 309-316 (2005).
137 Yang P.J, T. J. S. Engineering Orthopedic Tissue Interfaces. *TISSUE ENGINEERING: Part B* **15**, 127-141 (2009).
138 Kjaer, M. Role of extracellular matrix in adaptation of tendon and skeletal muscle to mechanical loading. *Physiol Rev* **84**, 649 (2004).

139 Pryce, B. A. *et al.* Recruitment and maintenance of tendon progenitors by TGF beta signaling are essential for tendon formation. *Development* **136**, 1351-1361, doi:10.1242/dev.027342 (2009).
140 Schweitzer, R. *et al.* Analysis of the tendon cell fate using Scleraxis, a specific marker for tendons and ligaments. *Development* **128**, 3855-3866 (2001).
141 Yoon, J. H. & Halper, J. Tendon proteoglycans: biochemistry and function. *J Musculoskelet Neuronal Interact* **5**, 22-34 (2005).
142 Banos, C. C., Thomas, A. H. & Kuo, C. K. Collagen fibrillogenesis in tendon development: Current models and regulation of fibril assembly. *Birth Defects Research* **84**, 228-244, doi:10.1002/bdrc.20130 (2008).
143 Docheva, D., Hunziker, E. B., Fassler, R. & Brandau, O. Tenomodulin is necessary for tenocyte proliferation and tendon maturation. *Molecular and Cellular Biology* **25**, 699-705, doi:10.1128/mcb.25.2.699-705.2005 (2005).
144 Murchison, N. D. *et al.* Regulation of tendon differentiation by scleraxis distinguishes force-transmitting tendons from muscle-anchoring tendons. *Development* **134**, 2697-2708, doi:10.1242/dev.001933 (2007).
145 Gelse K, P. E., Aigner T. Collagens - structure, function, and biosynthesis. *Advanced drug delivery reviews* **55**, 1531-1546 (2003).
146 Strauch, B. & Demoura, W. DIGITAL FLEXOR TENDON SHEATH - AN ANATOMIC STUDY. *J. Hand Surg.-Am. Vol.* **10A**, 785-789 (1985).
147 Lundborg, G., Holm, S. & Myrhage, R. THE ROLE OF THE SYNOVIAL-FLUID AND TENDON SHEATH FOR FLEXOR TENDON NUTRITION - AN EXPERIMENTAL TRACER STUDY ON DIFFUSIONAL PATHWAYS IN DOGS. *Scandinavian Journal of Plastic and Reconstructive Surgery and Hand Surgery* **14**, 99-107 (1980).
148 Klass B, R. K., Grobbelaar A. In Vitro Flexor Tendon Cell Response to TGF-B1:A Gene Expression Study. *J Hand Surg* **34A**, 495- 503 (2009).
149 Beredjiklian PK, F. M., Cartmell JS et al. Regenerative versus reparative healing in tendon: a study of biomechanical and histological properties in fetal sheep. *Annals of biomedical engineering* **31**, 1143-1152 (2003).
150 Park A, H. M., Kesturu GS et al. Adipose-derived mesenchymal stem cells treated with growth differentiation factor- 5 express tendon-specific markers. *Tissue engineering. Part A* **16**, 2941-2951 (2010).
151 Uysal C, T. M., Hyakusoku H, Mizuno H. Adipose-derived stem cells enhance primary tendon repair: Biomechanical and immunohistochemical evaluation. *Journal of Plastic, Reconstructive & Aesthetic Surgery* **65**, 1712-1719 (2012).
152 Skoog, T. & Persson, B. H. An experimental study of the early healing of tendons. *Plastic and reconstructive surgery (1946)* **13**, 384-399, doi:10.1097/00006534-195405000-00005 (1954).
153 Potenza, A. D. Tendon healing within the flexor digital sheath in the dog. *J Bone Joint Surg Am* **44-A**, 49-64 (1962).
154 Strickland, J. W. Development of flexor tendon surgery: Twenty-five years of progress. *J. Hand Surg.-Am. Vol.* **25A**, 214-235 (2000).
155 Matthews, P. & Richards, H. REPAIR POTENTIAL OF DIGITAL FLEXOR TENDONS - EXPERIMENTAL STUDY. *Journal of Bone and Joint Surgery-British Volume* **B 56**, 618-625 (1974).

156 Matthews, P. & Richards, H. The repair reaction of flexor tendon within the digital sheath. *The Hand* **7**, 27-29, doi:10.1016/0072-968x(75)90031-5 (1975).
157 Lundborg, G. & Rank, F. Experimental intrinsic healing of flexor tendons based upon synovial fluid nutrition. *The Journal of hand surgery* **3**, 21-31 (1978).
158 Lundborg G., R., F. Experimental studies on cellular mechanisms involved in healing of animal and human flexor tendon in synovial environment. *Hand* **12**, 3 (1980).
159 Fujita, M., Hukuda, S. & Doida, Y. Experimental study of intrinsic healing of the flexor tendon: collagen synthesis of the cultured flexor tendon cells of the canine. *Nihon Seikeigeka Gakkai zasshi* **66**, 326-333 (1992).
160 Austin RT, W. F. Flexor tendon healing and adhesion formation after Sterispon wrapping: a study in the rabbit. *Injury* **10**, 211-216 (1979).
161 Nyska, M., Porat, S., Nyska, A., Rousso, M. & Shoshan, S. DECREASED ADHESION FORMATION IN FLEXOR TENDONS BY TOPICAL APPLICATION OF ENRICHED COLLAGEN SOLUTION - A HISTOLOGICAL STUDY. *Arch Orthop Trauma Surg* **106**, 192-194, doi:10.1007/bf00452209 (1987).
162 Juneja, S. C., Schwarz, E. M., O'Keefe, R. J. & Awad, H. A. Cellular and Molecular Factors in Flexor Tendon Repair and Adhesions: A Histological and Gene Expression Analysis. *Connective tissue research* **54**, 218-226, doi:10.3109/03008207.2013.787418 (2013).
163 Wong, J. K. F., Cerovac, S., Ferguson, M. W. J. & McGrouther, D. A. The cellular effect of a single interrupted suture on tendon. *J. Hand Surg.-Br. Eur. Vol.* **31B**, 358-367, doi:10.1016/j.jhsb.2006.03.162 (2006).
164 Woo, S. L. Y. *et al.* THE IMPORTANCE OF CONTROLLED PASSIVE MOBILIZATION ON FLEXOR TENDON HEALING - A BIOMECHANICAL STUDY. *Acta Orthopaedica Scandinavica* **52**, 615-622 (1981).
165 Gelberman, R. H., Woo, S. L. Y., Amiel, D., Horibe, S. & Lee, D. INFLUENCES OF FLEXOR SHEATH CONTINUITY AND EARLY MOTION ON TENDON HEALING IN DOGS. *J. Hand Surg.-Am. Vol.* **15A**, 69-77 (1990).
166 Small, J. O., Brennen, M. D. & Colville, J. EARLY ACTIVE MOBILIZATION FOLLOWING FLEXOR TENDON REPAIR IN ZONE-2. *J. Hand Surg.-Br. Eur. Vol.* **14B**, 383-391, doi:10.1016/0266-7681(89)90152-6 (1989).
167 Cullen, K. W., Tolhurst, P., Lang, D. & Page, R. E. FLEXOR TENDON REPAIR IN ZONE-2 FOLLOWED BY CONTROLLED ACTIVE MOBILIZATION. *J. Hand Surg.-Br. Eur. Vol.* **14B**, 392-395, doi:10.1016/0266-7681(89)90153-8 (1989).
168 Strickland, J. W. Results of flexor tendon surgery in zone II. *Hand Clin* **1**, 167 (1985).
169 Burgisser, G. M. & Buschmann, J. History and performance of implant materials applied as peritendinous antiadhesives. *Journal of Biomedical Materials Research Part B-Applied Biomaterials* **103**, 212-228, doi:10.1002/jbm.b.33182 (2015).
170 McGonagle L, J. M., Dowson D, Theobald P. The Bio-Tribological Properties of Anti-Adhesive Agents Commonly Used during Tendon Repair. *JOURNAL OF ORTHOPAEDIC RESEARCH* **30**, 775-780 (2012).
171 Akasaka, T. *et al.* Hyaluronic acid diminishes the resistance to excursion after flexor tendon repair: An in vitro biomechanical study. *Journal of biomechanics* **38**, 503-507, doi:10.1016/j.jbiomech.2004.04.021 (2005).
172 Zhao C, S. Y., Amadio P, Tanaka T, Ettema A, An K. Surface treatment of flexor tendon autografts with carbodiimide-derivatized hyaluronic acid. *J Bone Joint Surg* **88-A**, 2181-2191 (2006).

173 Zhao, C. *et al.* Effects of a Lubricin-Containing Compound on the Results of Flexor Tendon Repair in a Canine Model in Vivo. *J. Bone Joint Surg.-Am. Vol.* **92A**, 1453-1461, doi:10.2106/jbjs.i.00765 (2010).
174 Roberts, A. B. & Sporn, M. B. PHYSIOLOGICAL ACTIONS AND CLINICAL-APPLICATIONS OF TRANSFORMING GROWTH-FACTOR-BETA (TGF-BETA). *Growth Factors* **8**, 1-9 (1993).
175 Chen, C. H. *et al.* Effectiveness of MicroRNA in Down-Regulation of TGF-beta Gene Expression in Digital Flexor Tendons of Chickens: In Vitro and In Vivo Study. *J. Hand Surg.-Am. Vol.* **34A**, 1777-1784, doi:10.1016/j.jhsa.2009.07.015 (2009).
176 Chan, K.-M. *et al.* Expression of transforming growth factor beta isoforms and their roles in tendon healing. *Wound Repair and Regeneration* **16**, 399-407, doi:10.1111/j.1524-475X.2008.00379.x (2008).
177 Manning, C. N. *et al.* Controlled delivery of mesenchymal stem cells and growth factors using a nanofiber scaffold for tendon repair. *Acta biomaterialia* **9**, 6905-6914, doi:10.1016/j.actbio.2013.02.008 (2013).
178 Tang, J. B. *et al.* Adeno-associated virus-2-mediated bFGF gene transfer to digital flexor tendons significantly increases healing strength. *J. Bone Joint Surg.-Am. Vol.* **90A**, 1078-1089, doi:10.2106/jbjs.f.01188 (2008).
179 Chan, B. P., Chan, K. M., Maffulli, N., Webb, S. & Lee, K. K. H. Effect of basic fibroblast growth factor - An in vitro study of tendon healing. *Clin Orthop Relat Res*, 239-247 (1997).
180 Thomopoulos, S. *et al.* The Effects of Exogenous Basic Fibroblast Growth Factor on Intrasynovial Flexor Tendon Healing in a Canine Model. *J. Bone Joint Surg.-Am. Vol.* **92A**, 2285-2293, doi:10.2106/jbjs.i.01601 (2010).
181 Petersen, W. *et al.* The angiogenic peptide vascular endothelial growth factor (VEGF) is expressed during the remodeling of free tendon grafts in sheep. *Arch Orthop Trauma Surg* **123**, 168-174, doi:10.1007/s00402-002-0462-z (2003).
182 Dines, J. S. *et al.* The effect of growth differentiation factor-5-coated sutures on tendon repair in a rat model. *Journal of Shoulder and Elbow Surgery* **16**, 215S-221S, doi:10.1016/j.jse.2007.03.001 (2007).
183 Anitua, E. *et al.* Autologous preparations rich in growth factors promote proliferation and induce VEGF and HGF production by human tendon cells in culture. *JOURNAL OF ORTHOPAEDIC RESEARCH* **23**, 281-286, doi:10.1016/j.orthres.2004.08.015 (2005).
184 Zhang AY, P. H., Ho F, Teng K, Longaker MT, Chang J. . Inhibition of TGF-beta-induced collagen production in rabbit flexor tendons. *J Hand Surg [Am]* **29**, 230 (2004).
185 Jorgensen H, M. S., Crossan J, Curtis A. Neutralisation of TGFb or binding of VLA-4 to fibronectin prevents rat tendon adhesion following transection. *Cytokine* **30**, 195-202 (2005).
186 Loiselle, A. E. *et al.* Development of Antisense Oligonucleotide (ASO) Technology Against Tgf-beta Signaling to Prevent Scarring During Flexor Tendon Repair. *Journal of Orthopaedic Research* **33**, 859-866, doi:10.1002/jor.22890 (2015).
187 Zhou, Y. *et al.* Nanoparticle-mediated delivery of TGF-beta1 miRNA plasmid for preventing flexor tendon adhesion formation. *Biomaterials* **34**, 8269-8278, doi:10.1016/j.biomaterials.2013.07.072 (2013).
188 Chen CH, Z. Y., Wu YF, Cao Y, Gao JS, Tang JB. Effectiveness of microRNA in Down-regulation of TGF-beta gene expression in digital flexor tendons of chickens: in vitro and in vivo study. *J Hand Surg Am.* **34**, 1777-1784.e1771 (2009).

189 Virchenko, O., Grenegard, M. & Aspenberg, P. Independent and additive stimulation of tendon repair by thrombin and platelets. *Acta Orthopaedica* **77**, 960-966, doi:10.1080/17453670610013295 (2006).
190 Lyras, D. N. *et al.* Does a Single Application of PRP Alter the Expression of IGF-I in the Early Phase of Tendon Healing? *Journal of Foot & Ankle Surgery* **50**, 276-282, doi:10.1053/j.jfas.2011.02.010 (2011).
191 Oryan, A., Moshiri, A., Meimandi-Parizi, A. & Maffulli, N. Role of xenogenous bovine platelet gel embedded within collagen implant on tendon healing: an in vitro and in vivo study. *Experimental Biology and Medicine* **240**, 194-210, doi:10.1177/1535370214554532 (2015).
192 Kajikawa, Y. *et al.* Platelet-rich plasma enhances the initial mobilization of circulation-derived cells for tendon healing. *Journal of Cellular Physiology* **215**, 837-845, doi:10.1002/jcp.21368 (2008).
193 Schepull, T. *et al.* Autologous Platelets Have No Effect on the Healing of Human Achilles Tendon Ruptures A Randomized Single-Blind Study. *American Journal of Sports Medicine* **39**, 38-47, doi:10.1177/0363546510383515 (2011).
194 Caliari, S. R. & Harley, B. A. C. Composite Growth Factor Supplementation Strategies to Enhance Tenocyte Bioactivity in Aligned Collagen-GAG Scaffolds. *Tissue Eng. Part A* **19**, 1100-1112, doi:10.1089/ten.tea.2012.0497 (2013).
195 Sakiyama-Elbert, S. E. & Hubbell, J. A. Development of fibrin derivatives for controlled release of heparin-binding growth factors. *Journal of Controlled Release* **65**, 389-402, doi:10.1016/s0168-3659(99)00221-7 (2000).
196 Akbari, H., Rahimi, A.A., Ghavami, Y., Mousavi, S.J., Fatemi, M.J. Effect of Heparin on Post-Operative Adhesion in Flexor Tendon Surgery of the Hand. *J Hand Microsurg* **7**, 244-249 (2015).
197 Bora Jr FW, L. J., Prockop DJ. . Inhibitors of collagen biosynthesis as a means of controlling scar formation in tendon injury. *J Bone Joint Surg* **54A**, 1501-1508 (1972).
198 Kulick, M. I., Brazlow, R., Smith, S. & Hentz, V. R. INJECTABLE IBUPROFEN - PRELIMINARY EVALUATION OF ITS ABILITY TO DECREASE PERITENDINOUS ADHESIONS. *Ann Plast Surg* **13**, 459-467, doi:10.1097/00000637-198412000-00001 (1984).
199 Kulick, M. I., Smith, S. & Hadler, K. ORAL IBUPROFEN - EVALUATION OF ITS EFFECT ON PERITENDINOUS ADHESIONS AND THE BREAKING STRENGTH OF A TENORRHAPHY. *J. Hand Surg.-Am. Vol.* **11A**, 110-120 (1986).
200 Liu, S. *et al.* Prevention of Peritendinous Adhesions with Electrospun Ibuprofen-Loaded Poly(L-Lactic Acid)-Polyethylene Glycol Fibrous Membranes. *Tissue Eng. Part A* **19**, 529-537, doi:10.1089/ten.tea.2012.0208 (2013).
201 Jiang, S. *et al.* Down-regulating ERK1/2 and SMAD2/3 phosphorylation by physical barrier of celecoxib-loaded electrospun fibrous membranes prevents tendon adhesions. *Biomaterials* **35**, 9920-9929, doi:10.1016/j.biomaterials.2014.08.028 (2014).
202 Lui YS, L. M., Loo SC. Sustained-release of naproxen sodium from electrospun-aligned PLLA-PCL scaffolds. *Journal of tissue engineering and regenerative medicine*, doi:10.1002/term.2000 (2015).
203 Wiig, M. E. *et al.* PXL01 in Sodium Hyaluronate for Improvement of Hand Recovery after Flexor Tendon Repair Surgery: Randomized Controlled Trial. *Plos One* **9**, doi:10.1371/journal.pone.0110735 (2014).

204 Ward, P. P., Uribe-Luna, S. & Conneely, O. M. Lactoferrin and host defense. *Biochemistry and Cell Biology-Biochimie Et Biologie Cellulaire* **80**, 95-102, doi:10.1139/o01-214 (2002).
205 Legrand, D., Elass, E., Pierce, A. & Mazurier, J. Lactoferrin and host defence: an overview of its immuno-modulating and anti-inflammatory properties. *Biometals* **17**, 225-229, doi:10.1023/b:biom.0000027696.48707.42 (2004).
206 Akali A, K. U., Khaw PT, McGrouther AD. . Decrease in adhesion formation by a single application of 5-fluorouracil after flexor tendon injury. *Plast Reconstr Surg* **103**, 151-158 (1999).
207 Khan, U., Kakar, S., Akali, A., Bentley, G. & McGrouther, D. A. Modulation of the formation of adhesions during the healing of injured tendons. *Journal of Bone and Joint Surgery-British Volume* **82B**, 1054-1058, doi:10.1302/0301-620x.82b7.9892 (2000).
208 Cerovac, S., Afoke, A., Akali, A. & McGrouther, D. A. Early breaking strength of repaired flexor tendon treated with 5-fluorouracil. *J. Hand Surg.-Br. Eur. Vol.* **26**, 220-223, doi:10.1054/jhsb.2000.0537 (2001).
209 Moran, S. L., Ryan, C. K., Orlando, G. S., Pratt, C. E. & Michalko, K. B. Effects of 5-fluorouracil on flexor tendon repair. *J. Hand Surg.-Am. Vol.* **25A**, 242-251, doi:10.1053/jhsu.2000.jhsu25a0242 (2000).
210 Ragoowansi, R., Khan, U., Brown, R. A. & McGrouther, D. A. Reduction in matrix metalloproteinase production by tendon and synovial fibroblasts after a single exposure to 5-fluorouracil. *British Journal of Plastic Surgery* **54**, 283-287, doi:10.1054/bjps.2000.3580 (2001).
211 Yuan, B. M. *et al.* 5-Fluorouracil loaded thermosensitive PLGA-PEG-PLGA hydrogels for the prevention of postoperative tendon adhesion. *Rsc Advances* **5**, 25295-25303, doi:10.1039/c5ra01307k (2015).
212 Mingke, G. U. O. *et al.* EFFECTS OF 5-FLUOROURACIL ON TENDON ADHESION FORMATION AFTER FLEXOR TENDON REPAIR. *Chinese Journal of Reparative and Reconstructive Surgery* **22**, 794-796 (2008).
213 Karaaltin, M. V. *et al.* The effects of 5-fluorouracil on flexor tendon healing by using a biodegradable gelatin, slow releasing system: experimental study in a hen model. *J. Hand Surg.-Eur. Vol.* **38**, 651-657, doi:10.1177/1753193412458646 (2013).
214 Hung, L.-K., Fu, S.-C., Lee, Y.-W., Mok, T.-Y. & Chan, K.-M. Local vitamin-C injection reduced tendon adhesion in a chicken model of flexor digitorum profundus tendon injury. *J Bone Joint Surg Am* **95**, e41-e41, doi:10.2106/jbjs.k.00988 (2013).
215 Kapetanos, G. THE EFFECT OF THE LOCAL CORTICOSTEROIDS ON THE HEALING AND BIOMECHANICAL PROPERTIES OF THE PARTIALLY INJURED TENDON. *Clin Orthop Relat Res*, 170-179 (1982).
216 Demirkan F, C. N., Herek O, Erkula G. The use of amniotic membrane in flexor tendon repair: an experimental model. *Arch Orthop Trauma Surg* **122**, 396-399 (2002).
217 SAKR, W. a. A., S. Prevention of Restrictive Peritendinous Adhesions in Flexor Tendon Repair with Autologous Transplanted Vein Graft. *Egypt, J. Plast. Reconstr. Surg.* **33**, 209-215 (2009).
218 Peterson WW, M. P., Dunlap J, Horwitz DS, Kahn B. . Effect of various methods of restoring flexor sheath integrity on the formation of adhesions after tendon injury. *J Hand Surg* **15A**, 48-56 (1990).

219 Oei TS, K. P., Spaas JA, Buma P. Reconstruction of the flexor tendon sheath: an experimental study in rabbits. *J Bone Joint Surg Br* **21**, 72-83 (1996).
220 Zhao, H. *et al.* Collagen membrane alleviates peritendinous adhesion in the rat Achilles tendon injury model. *Chin. Med. J.* **126**, 729-733, doi:10.3760/cma.j.issn.0366-6999.20122566 (2013).
221 CL, W. Tendinoplasty of the flexor tendons of the hand. *J Bone Joint Surg* **19**, 152-156 (1937).
222 AD., P. Critical evaluation of flexor tendon healing and adhesion formation within artificial digital sheaths: an experimental study. *J Bone Joint Surg Am* **45A**, 1217-1233. (1963).
223 Stark HH, B. J., Johnson L, Ashworth CR. The use of paratenon, polyethylene film, or Silastic sheeting to prevent restricting adhesions to tendons in the hand. *J Bone Joint Surg* **59A**, 908-913. (1977).
224 Siddiqi NA, H. Y., Ide T, Akamatsu N. Effects of hydroxyapatite and alumina sheaths on postoperative peritendinous adhesions in chickens. *J Appl Biomater* **6**, 43-53 (1995).
225 Güdemez E, E. F., Korkusuz P, Aşan E, Gürsel I, Hasirci V. Chondroitin sulfate-coated polyhydroxyethyl methacrylate membrane prevents adhesion in full-thickness tendon tears of rabbits. *J Hand Surg Am.* **27**, 293-306 (2002).
226 Temiz A, O. C., Bakunov A, Kara K, Kaleli T. A new material for prevention of peritendinous fibrotic adhesions after tendon repair: oxidised regenerated cellulose (Interceed), an absorbable adhesion barrier. *Int Orthop* **32**, 389-394 (2008).
227 Menderes A, M. F., Tayfur V, Vayvada H, Barutçu A. Prevention of peritendinous adhesions following flexor tendon injury with seprafilm. *Ann Plast Surg.* **53**, 560-564 (2004).
228 S. Isıka, S. Ö., S. Gürsesb, M. Yetmezb, M.M. Gülera, N. Selmanpakoglua, Ö. Günhanc. Prevention of restrictive adhesions in primary tendon repair by HA-membrane: experimental research in chickens. *British Journal of Plastic Surgery* **52**, 373-379 (1999).
229 Kuo, S. M., Chang, S. J., Wang, H.-Y., Tang, S. C. & Yang, S.-W. Evaluation of the ability of xanthan gum/gellan gum/hyaluronan hydrogel membranes to prevent the adhesion of postrepaired tendons. *Carbohydrate Polymers* **114**, 230-237, doi:10.1016/j.carbpol.2014.07.049 (2014).
230 Bhavsar D, S. D., Tenenhaus M. Encircling the tendon repair site with collagen-GAG reduces the formation of postoperative tendon adhesions in a chicken flexor tendon model. *J Surg Res.* **159**, 765-771 (2010).
231 Branford O, M. V., Brown R, McGrouther D, Grobbelaar A. A Novel Biomimetic Material for Engineering Postsurgical Adhesion Using the Injured Digital Flexor Tendon–Synovial Complex as an In Vivo Model. *Plast Reconstr Surg.* **121**, 781-793 (2008).
232 Palatinsky EA, M. K., Touhalisky DK, Mock JL, Hingson MT, Coker GT. ADCON-T/N reduces in vivo perineural adhesions in a rat sciatic nerve reoperation model. *J Hand Surg Br* **22**, 331-335 (1997).
233 Mentzel, M., Hoss, H., Keppler, P., Ebinger, T., Kinzl, L. and Wacher, N. The effectiveness of ADCON-T/N, a new anti-adhesion barrier gel, in fesh divisions of the flexor tendons in zone II. *J Hand Surg Br* **25B**, 590-592 (2000).

234 Golash, A. *et al.* Efficacy of ADCON-T/N after primary flexor tendon repair in zone II: A controlled clinical trial. *J. Hand Surg.-Br. Eur. Vol.* **28B**, 113-115, doi:10.1016/S0266-7681(02)00249-8/jhsb.2003.0851 (2003).
235 Hideaki, I. Porous L-lactide-caprolactone Copolymer as Anti-adhesion membrane for flexor tendon. *Medical Journal of Hiroshima University* **49**, 135-146 (2001).
236 Sato, T., Shimizu, H., Beppu, M., Takagi, M. Effects on bone union and prevention of tendon adhesion by new porous anti-adhesive poly L-lactide-co-E-caprolactone membrane in a rabbit model. *Hand Surgery* **18**, 1-10 (2013).
237 Zuk, P. A., Zhu, M., Ashjian, P., De Ugarte, D.A., Huang, J.I., Mizuno, H., Alfonso, Z.C., Fraser, J.K., Benhaim, P., and Hedrick, M.H. . Human adipose tissue is a source of multipotent stem cells. *Mol Biol Cell* **13** (2002).
238 Porada, C. D., Zanjani, E. D. & Almeida-Porad, G. Adult mesenchymal stem cells: a pluripotent population with multiple applications. *Current stem cell research & therapy* **1**, 365-369 (2006).
239 Chamberlain, G., Fox, J., Ashton, B. & Middleton, J. Concise review: Mesenchymal stem cells: Their phenotype, differentiation capacity, immunological features, and potential for homing. *Stem Cells* **25**, 2739-2749, doi:10.1634/stemcells.2007-0197 (2007).
240 Yao, J. *et al.* The Effect of Suture Coated With Mesenchymal Stem Cells and Bioactive Substrate on Tendon Repair Strength in a Rat Model. *J. Hand Surg.-Am. Vol.* **37A**, 1639-1645, doi:10.1016/j.jhsa.2012.04.038 (2012).
241 Chong, A. K. S. *et al.* Bone marrow-derived mesenchymal stem cells influence early tendon-healing in a rabbit Achilles tendon model. *J. Bone Joint Surg.-Am. Vol.* **89A**, 74-81, doi:10.2106/jbjs.e.01396 (2007).
242 Young, R. G. *et al.* Use of mesenchymal stem cells in a collagen matrix for Achilles tendon repair. *JOURNAL OF ORTHOPAEDIC RESEARCH* **16**, 406-413, doi:10.1002/jor.1100160403 (1998).
243 Huang TF, Y. T., Chiang ER, Ma H, Hsu CY, Hsu SH, Hsu YT, Hung SC. Mesenchymal stem cells from a hypoxic culture improve and engraft achilles tendon repair. *American Journal of Sports Medicine*, doi:10.1177/0363546513480786 (2013).
244 Harris, M. T. *et al.* Mesenchymal stem cells used for rabbit tendon repair can form ectopic bone and express alkaline phosphatase activity in constructs. *JOURNAL OF ORTHOPAEDIC RESEARCH* **22**, 998-1003, doi:10.1016/j.orthres.2004.02.012 (2004).
245 Martinello, T. *et al.* Effects of In Vivo Applications of Peripheral Blood-Derived Mesenchymal Stromal Cells (PB-MSCs) and Platlet-Rich Plasma (PRP) on Experimentally Injured Deep Digital Flexor Tendons of Sheep. *JOURNAL OF ORTHOPAEDIC RESEARCH* **31**, 306-314, doi:10.1002/jor.22205 (2013).
246 Sasso, R. C., LeHuec, J.C., Shaffrey, C., and Spine Interbody Research Group Suppl. Iliac crest bone graft donor site pain after anterior lumbar interbody fusion: a prospective patient satisfaction outcome assessment. *J Spinal Disord Tech* **18**, S77-S81 (2005).
247 Varma, M. J., Breuls, R.G., Schouten, T.E., Jurgens, W.J., Bontkes, H.J., Schuurhuis, G.J., van Ham, S.M., and van Milligen, F.J. Phenotypical and functional characterization of freshly isolated adipose tissue-derived stem cells. *Stem Cells Dev* **16**, 91 (2007).
248 Yang, X., Shang, H., Katz, A. & Li, X. A modified aggregate culture for chondrogenesis of human adipose-derived stem cells genetically modified with growth and

differentiation factor 5. *BioResearch open access* **2**, 258-265, doi:10.1089/biores.2013.0014 (2013).
249 Gimble, J. M., Katz, A. J. & Bunnell, B. A. Adipose-derived stem cells for regenerative medicine. *Circulation Research* **100**, 1249-1260, doi:10.1161/01.res.0000265074.83288.09 (2007).
250 Williams, S. K. *et al.* Adipose Stromal Vascular Fraction Cells Isolated Using an Automated Point of Care System Improve the Patency of Expanded Polytetrafluoroethylene Vascular Grafts. *Tissue Eng. Part A* **19**, 1295-1302, doi:10.1089/ten.tea.2012.0318 (2013).
251 Niemeyer, P. *et al.* Comparison of immunological properties of bone marrow stromal cells and adipose tissue-derived stem cells before and after osteogenic differentiation in vitro. *Tissue Eng* **13**, 111-121, doi:10.1089/ten.2006.0114 (2007).
252 Fang, B., Song, Y., Liao, L., Zhang, Y. & Zhao, R. C. Favorable response to human adipose tissue-derived mesenchymal stem cells in steroid-refractory acute graft-versus-host disease. *Transplantation Proceedings* **39**, 3358-3362, doi:10.1016/j.transproceed.2007.08.103 (2007).
253 Miller JA, F. R., Powers DL, Burns JW, Shalaby SW. Efficacy of hyaluronic acid/nonsteroidal anti-inflammatory drug systems in preventing postsurgical tendon adhesions. *J Biomed Mat Res* **38**, 25-33 (1997).
254 Chen, S. *et al.* Silver Nanoparticles/Ibuprofen-Loaded Poly(L-lactide) Fibrous Membrane: Anti-Infection and Anti-Adhesion Effects. *International Journal of Molecular Sciences* **15**, 14014-14025, doi:10.3390/ijms150814014 (2014).
255 Jiang, S., Yan, H., Fan, D., Song, J., Fan, C. Multi-layer electrospun membrane mimicking tendon sheath for prevention of tendon adhesions. *International Journal of Molecular Sciences* **16**, 6932-6944, doi:doi: 10.3390/ijms16046932 (2015).
256 Farhat, Y. M. *et al.* Gene Expression Analysis of the Pleiotropic Effects of TGF-beta 1 in an In Vitro Model of Flexor Tendon Healing. *PLoS One* **7**, doi:10.1371/journal.pone.0051411 (2012).
257 Nair, L. S. & Laurencin, C. T. Biodegradable polymers as biomaterials. *Progress in Polymer Science* **32**, 762-798, doi:10.1016/j.progpolymsci.2007.05.017 (2007).
258 Van Natta, F. J., Hill, J.W., Carruthers, W.H. Polymerization and ring formation, E-caprolactone and its polymers. *J Am Chem Soc* **56**, 455-459 (1934).
259 Lam, C. X. F., Savalani, M. M., Teoh, S.-H. & Hutmacher, D. W. Dynamics of in vitro polymer degradation of polycaprolactone-based scaffolds: accelerated versus simulated physiological conditions. *Biomedical Materials* **3**, doi:10.1088/1748-6041/3/3/034108 (2008).
260 Bolgen, N., Menceloglu, Y. Z., Acatay, K., Vargel, I. & Piskin, E. In vitro and in vivo degradation of non-woven materials made of poly(epsilon-caprolactone) nanofibers prepared by electrospinning under different conditions. *Journal of Biomaterials Science-Polymer Edition* **16**, 1537-1555, doi:10.1163/156856205774576655 (2005).
261 Gopferich, A., Karydas, D. & Langer, R. PREDICTING DRUG-RELEASE FROM CYLINDRIC POLYANHYDRIDE MATRIX DISCS. *European Journal of Pharmaceutics and Biopharmaceutics* **41**, 81-87 (1995).
262 Lam, C. X. F., Hutmacher, D. W., Schantz, J.-T., Woodruff, M. A. & Teoh, S. H. Evaluation of polycaprolactone scaffold degradation for 6 months in vitro and in vivo. *Journal of Biomedical Materials Research Part A* **90A**, 906-919, doi:10.1002/jbm.a.32052 (2009).

263 Woodward, S. C., Brewer, P. S., Moatamed, F., Schindler, A. & Pitt, C. G. THE INTRACELLULAR DEGRADATION OF POLY(EPSILON-CAPROLACTONE). *J Biomed Mater Res* **19**, 437-444, doi:10.1002/jbm.820190408 (1985).
264 Huang, M. H. *et al.* Degradation and cell culture studies on block copolymers prepared by ring opening polymerization of epsilon-caprolactone in the presence of poly(ethylene glycol). *Journal of Biomedical Materials Research Part A* **69A**, 417-427, doi:10.1002/jbm.a.30008 (2004).
265 Bosworth, L. A., Alam, N., Wong, J. K. & Downes, S. Investigation of 2D and 3D electrospun scaffolds intended for tendon repair. *Journal of Materials Science-Materials in Medicine* **24**, 1605-1614, doi:10.1007/s10856-013-4911-8 (2013).
266 Chen, C.-H., Chen, S.-H., Shalumon, K. T. & Chen, J.-P. Prevention of peritendinous adhesions with electrospun polyethylene glycol/polycaprolactone nanofibrous membranes. *Colloids and Surfaces B-Biointerfaces* **133**, 221-230, doi:10.1016/j.colsurfb.2015.06.012 (2015).

Chapter 2 : Controlled Radical Polymerisation

2.1 Introduction

The generation of a versatile and modular scaffold system that can be tailored in a facile way for a specific clinical need without re-engineering it, is clear and outlined in chapter one. A key aspect of the scaffold design in this thesis is the production of a polymer brush from a bulk scaffold for surface modification at the cell-scaffold interface. In order to achieve this, firstly the monomer must be chosen. The bulk of this work is focused on the generation of a high performance antifouling surface modification. This has a number of clinical applications for the preservation of gliding tissue interfaces, the compromise of which is a common surgical challenge and leads to significant adverse effects for patients. As a model system, the initial design is developed with the tendon in mind.

To maximise the versatility of the scaffold system a controlled radical polymerisation of an antifouling oligomer, OEGMA, is used to produce dense polymer bottlebrushes from surfaces. In order for this to be successfully achieved, firstly, the reaction needs to be fully optimised to ensure the polymers are successfully being produced in a reproducible manner.

This chapter outlines initial experimentation and polymerisation of two monomers: OEGMA, and a similar monomer for comparison, HEMA, in solution. The controlled radical polymerisation is initially achieved using ATRP before the progression to ARGET ATRP is made and the optimisation of the reaction. Following this, polymerisation of OEGMA bottlebrushes from 2D silicon surfaces is performed, outlined and characterised.

2.2 Materials and Methods

2.2.1 Materials

OEGMA with a M_w of the poly(ethylene glycol, PEG, unit) of 400 Da, (Polysciences, Germany) was activated through the removal of inhibitors by passing if firstly through a column filled with specialist inhibitor remover followed by a column of basic alumina oxide respectively prior to use. 2-hydroxyethyl methacrylate (HEMA) was also purchased and passed through the column of specialist inhibitor remover prior to use. Copper (II) bromide (Cu[II]Br),

copper (II) chloride (Cu[II]Cl), tris[(2-pyridyl)methyl]amine (TPMA) and ascorbic acid (AScA) were purchased and used as received. Cuprisorb^{TM} was purchased from Fish Fish Fish (UK).

Copper (I) bromide (Cu[I]Br) was initially purified to eliminate contamination with copper (II) bromide according to literature procedures (Appendix C)[267]. Triethylamine (TEA) and hexane were dried using 4Å molecular sieves, sealed and stored under a nitrogen atmosphere. 3-isocyanatopropyltrimethoxysilane (ICTS, Fluorochem Ltd, Hadfield, UK) was purchased and stored under a nitrogen atmosphere at 2^{o}C.

P-doped silicon wafers (University Wafer, Boston, USA) were sectioned as required with a diamond knife and labelled on the reverse side for identification. Wafers were ultrasonicated in acetone for 3 minutes using an ultrasonic cleaner (VWR), thoroughly rinsed with ultra-high quality water (UHQ, resistivity of 18.2 MΩ, Purite Select, Ondeo) and immersed in freshly prepared piranha solution (1:3, hydrogen peroxide: concentrated sulphuric acid) for 1 hour, before rinsing twice with UHQ water and drying under a stream of nitrogen.

All other chemical reagents were purchased from Sigma Aldrich (UK) and used as received and deuterated solvents for ^{1}H-NMR from Merck (Darmstadt, Germany) unless specifically noted.

2.2.2 ATRP polymerisation in solution

Polymerisation was initially attempted using an ATRP technique of HEMA in solution using a protocol adapted from the literature[268]. In a typical experiment, the initiator ethyl-α-bromoisobutyrate (EBiB) (1.02 mmol, 198.95 mg) and HEMA monomer (40 mmol, 5.21 g) were dissolved in methanol (5 ml) in a round bottom flask and sealed with a septum and parafilm. Stock solutions were made up of the Cu(I)Br and 2,2'-bipyridyl (BPY) in methanol and sealed with septa. Solutions were degassed with bubbling argon for 15 minutes following which the BPY ligand (2.56 mmol, 400 mg) and Cu(I)Br catalyst (1.02 mmol, 146 mg) were transferred to the reaction vessel. To the reaction vessel, a nitrogen atmosphere was applied, and the mixture stirred at room temperature. The reaction was allowed to proceed for a set period of time before being terminated with the opening of the vessel and exposure to atmospheric oxygen. Conversion was determined by proton nuclear magnetic resonance spectroscopy (^{1}H-NMR). Spectra were recorded on a Bruker Avance DPX 400

(400MHz) spectrometer with the residual solvent peak used as an internal reference. Molecular weights were determined by size exclusion chromatography (SEC). This was performed on a GPCMax VE 2001 (Viscotek) and was run with an eluent of *N,N*-Dimethylformamide (DMF) with 0.075% (w/v) at a flow rate of 0.7 mL.min^{-1} over two Polymer Standards Service (PSS^{TM}) Gram DMF columns at 35^{o}C. The molecular weights were determined using a conventional pMMA calibration without correction (Agilent Technologies, UK). Copper was removed from the samples prior to running on the SEC using heavy metal chelating beads (Cuprisorb^{TM}, Fish Fish Fish, UK) and filtered through a 0.22 µm syringe mounted polytetrafluoroethylene filter.

The protocol was also performed using OEGMA substituted for the HEMA as described above. Molar ratios of the reagents were maintained EBiB:Cu(I)Br:BPY:monomer of 1:1:2.5:40.

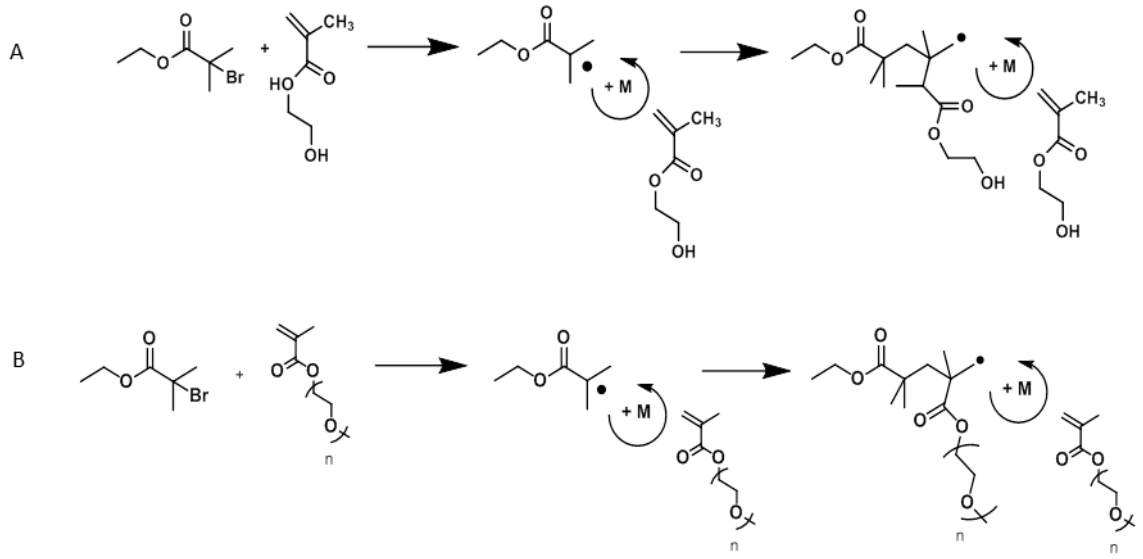

Figure 2-1: Structures and schematic of radical addition polymerisation with the EBIB initiator of HEMA to pHEMA (A) and OEGMA to pOEGMA (B) in solution.

2.2.3 ARGET ATRP polymerisation in solution

Polymerisation of OEGMA and HEMA was further established in solution using ARGET ATRP using protocols adapted from the literature[269,270]. In a typical experiment, OEGMA (1 g,

2.08 mmol), Cu(II)Cl (1.87 mg, 0.014 mmol), TPMA (4.03 mg, 0.014 mmol) and EBiB (2.71 mg, 0.014 mmol) were inserted into a round bottom flask with 8.82 mL of 1:1 (v/v) of IPA/UHQ water. This flask was sealed with a new rubber septum and parafilm before being introduced into an ice bath cool before being degassed with bubbling argon for 30 minutes. The solution was then transferred to a pre-warmed silicone oil bath, stirred at 30^{o}C and maintained under a positive nitrogen atmosphere. From a degassed stock solution of AScA in 1:1 (v/v) IPA/UHQ water a defined quantity of the reducing agent was added to the reaction mixture using a gas tight syringe and the reaction allowed to proceed for a defined period of time. Monomer to polymer conversion (X%) was determined by ^{1}H-NMR and molecular weights were determined by SEC.

Molar equivalent ratios of the reagents were maintained at monomer:Cu(II) catalyst:TPMA:EBiB: of 150:1:1:1, and an initial monomer:AScA of 150:0.15 was used. Reaction conditions were optimised, as defined by monomer conversion and polymerisation control, and was achieved through assessment of different copper catalysts (Cu(II)Cl and Cu(II)Br), solvent (water, methanol, and 50:50 IPA/UHQ water), molar ratio of reducing agent, AScA, and reaction time.

2.2.4 Polymer brush grafting from 2-dimentional silicon surfaces

Using a two-stage attachment adapted from the literature, a polymerisation initiating group was immobilised on silicon wafers to allow surface grafting of pOEGMA from the silicon wafer surface (Figure 2-2)[271,272].

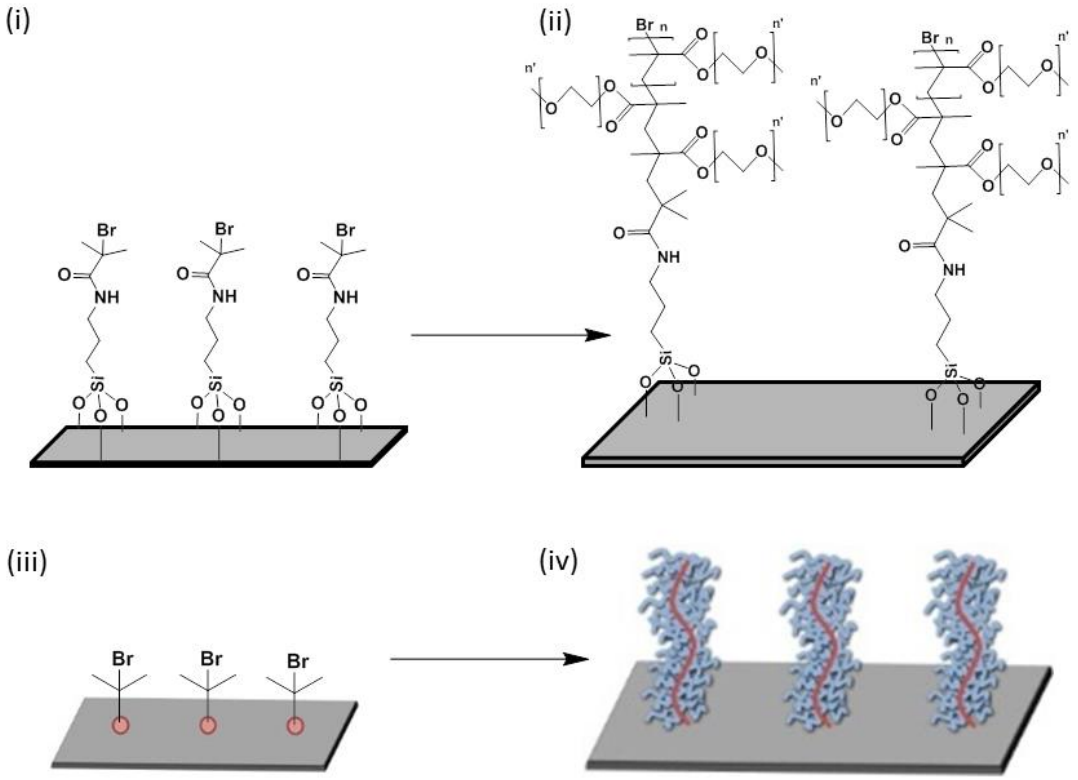

Figure 2-2: Schematic of pOEGMA grafting from 2D silicon surfaces. Chemical structures of APTES-Ini presenting polymerisation initiating group for grafting of OEGMA from the silicon surface (i) with schematic (iii). Chemical structure of the resultant pOEGMA bottlebrush from the 2D silicon surface (ii) with schematic (iii).

Silicon wafers were divided into squares of approximately 1 x 1 cm^2 pieces using a diamond knife before being cleaned and dried as described above. Once dried, wafers were treated with an oxygen plasma for 2 minutes to maximise the surface availability of hydroxyl groups using a Plasma Prep 5 (GaLa Instrumente) at power setting 5, before being functionalised with the polymerisation initiator.

2.2.4.1 Functionalization of silicon wafers with APTES and Ini

The polymerisation initiating group, α-bromoisobutyryl bromide (Ini), was immobilized on the 2D silicon surfaces using 3-(aminopropyl)triethoxysilane (APTES, Figure 2-3).

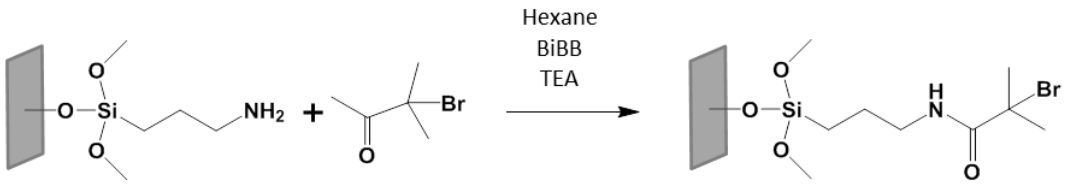

Figure 2-3: Reaction scheme for the functionalization of ATPES with Ini.

The APTES was deposited on the surface of the 2D silicon surfaces using vapor deposition using a protocol modified from the literature; modified 2D silicon wafers were placed in a glass petri dish and a glass vial containing 10 mL of anhydrous hexane and 0.25 mL of APTES was placed into the center of the dish[271]. The petri dish was placed in a dessicator to which a vacuum was applied and maintained. After 90 minutes the dessicator was vented and the wafers removed with care not to damage the upper surface. The wafers were placed into test tubes that were sealed with septa and parafilm and subsequently degassed with nitrogen. A solution of 5 mL anhydrous hexane, 0.125 mL of BiBB and 0.165 mL of anhydrous trimethylamine (TEA) was prepared and degassed with bubbling nitrogen for 15 minutes. From this solution, 5 mL was transferred using a gas tight syringe and introduced into each test tube under a nitrogen atmosphere. The reaction was allowed to proceed at room temperature for 60 minutes, following which the wafers were removed, washed with further hexane, ethanol and UHQ water, before being dried under a stream of nitrogen. Silicon wafers, Si-APTES-Ini, were stored in a vacuum dessicator and protected from light until used.

2.2.4.2 pOEGMA grafting from functionalised 2D silicon surfaces

pOEGMA polymer bottlebrushes were grafted from Si-APTES-Ini wafers using a similar protocol used to establish the kinetics of the reaction to generate polymer brush functionalised 2D silicon surfaces (Si-APTES-pOEGMA).

In a typical experiment OEGMA (340 mg, 0.7 mmol, with a M_w of the poly(ethylene glycol unit) of 400 Da, Polysciences, Germany), activated by the removal of inhibitors, was introduced into a round bottom flask with copper (II) chloride (Cu(II)Cl, 0.64 mg, 0.0047 mmol), tris[(2-pyridyl)methyl]amine (TPMA, 1.37 mg, 0.0047 mmol) and EBiB (0.92 mg, 0.0047 mmol) in 3 mL of 50:50 isopropyl alcohol (IPA)/H_2O. Following through mixing 2 mL was transferred to a test tube that contained two Si-APTES-Ini wafers back-to-back with the polished functionalised surface facing outwards. It was sealed, introduced into an ice bath, and degassed with argon for 20 minutes before ascorbic acid (AscA 0.08 mg, 0.00047 mmol) was added from a degassed solution using a gas tight syringe. Degassing was continued for a further 2 minutes. The vessel was transferred to a pre-warmed heat block at 30^{o}C and allowed to react. The reaction was terminated at 2 hours by bubbling compressed air through the liquid and 2D silicon wafers removed. The wafers were thoroughly rinsed in ethanol, then UHQ water, and dried under a stream of nitrogen. Free polymer resulting

from the sacrificial initiator in solution was analysed by SEC and ^{1}H-NMR to establish molecular weights and monomer-to-polymer conversion with a *d*4-methanol solvent (*d*4-MeOD). Polymer functionalised surface were characterised using water contact angle measurement, XPS, AFM and ellipsometry.

EBiB was used a free sacrificial initiator in solution in addition to the surface bound polymerisation initiator to aid control of the polymerisation and to allow analysis of the free polymer as a surrogate for the surface bound polymer. This has been shown in the literature to be a reliable method for controlled the M_n and M_w/M_n for the polymers grown from surfaces within the same reaction vessel[270,273,274].

2.2.4.2.1 Water contact angle measurement

Water contact angle measurements were taken using a Krüss Easy Drop DSA 100 (Hamberg, Germany) and the associated DSA1 v 1.9 software. A drop size of 7 µL of UHQ water was dropped onto scaffolds that had been immobilised on glass slides with tape. Contact angle measurements were analysed using the associated software for control and functionalised scaffolds to explore the changing surface wettability at room temperature.

2.2.4.2.2 XPS surface analysis

X-ray photoelectron spectroscopy (XPS) was used to characterize the polymer surface functionalization. The measurements were performed by M. Mahat and R. Harrison, and all data analysis and interpretation was performed by M. Mahat (PhD student in Professor Stevens's research group).

The spectra were measured using a Thermo Fisher K-Alpha XPS System (Thermo Fisher Scientific Inc.) with a monochromatic Al-Kα (energy = 1486.71 eV) X-ray source. To prepare for XPS analysis, the samples were positioned at the electron take-off angle normal to the surface with respect to the analyser in a 20 sample holder. Survey spectra were measured over a range of 0–1400 eV and recorded for each sample, then followed by high resolution spectra for C 1*s* and O 1*s*. A low energy electron/ion flood gun was used to ensure effective surface charge compensation. XPS spectra were calibrated to the adventitious C 1*s* signal (285.0 eV). Curve fitting was carried out using Thermo Avantage Software (v. 5.948) using a Shirley background. Peak areas were normalized within Thermo Avantage using atomic

sensitivity factors for the Al Kα anode ('AlWagner' library)[275] and from these areas the carbon composition and elemental ratios were determined.

2.2.4.2.3 AFM measurement of polymer brush thickness

Atomic force microscopy (AFM) measurements were taken using an Agilent Technologies 5500 atomic force microscope with a silicon probe, tip radius < 10 nm and a force constant 40 nN/m .

The thickness of the dry polymer brush on the 2D silicon wafers was measured using AFM. A scratch test was performed whereby the AFM probe tip was moved towards the sample, contact was made and the force increased until the underlying silicon wafer was contacted. The tip was then moved laterally to create a full-thickness scratch. The AFM was then used in tapping mode to create a depth profile across the scratch area. Using the associated software (Pico Image) thickness measurements of the polymer layer were made. Measurements were taken and analysed with assistance from Dr Nadav Amdursky (postdoctoral scientist in Professor Stevens' group).

2.2.4.2.4 Ellipsometry measurement of polymer brush thickness

Ellipsometry measurements were performed at room temperature using a SOPRA GESP 5 variable angle spectroscopic ellipsometer (J.A. Wollam and Co., Inc. Lincoln NE). The thickness of the dry polymer brush on the 2D silicon wafers was measured using ellipsometry. The data were recorded through incidence angles of 65^{o}-75^{o} with respect to the substrate normal, across a wavelength range from 900-1600 nm (20 nm steps). Cauchy model fits were used to analyze the ellipsometric data. Measurements were taken and analysed with assistance from Mr. Tarik Abdelmoula (PhD student, Physics).

2.3 Results and Discussion

Polymerisations in solution were initially undertaken using the HEMA monomer and using ATRP. This is a well characterised and studied reaction, and HEMA is known for its facile polymerisation. This was initially undertaken to learn and understand the techniques involved in performing such a procedure and interpreting the characterisation data.

Once ATRP polymerisations of HEMA were being reproducibly undertaken the progression was made to ARGET ATRP of HEMA, and then OEGMA. This employs a marginally more complex procedure with regards to handling of deoxygenated systems but offers significant advantages for biomedical systems as the significantly lower concentration of potentially toxic copper catalyst which may be difficult to adequately remove from a bulk scaffold.

2.3.1 Polymerisation of HEMA and OEGMA in solution with ATRP

pHEMA was successfully produced through ATRP of the HEMA monomer in solution. This was confirmed by ^{1}H-NMR spectroscopy and SEC analysis.

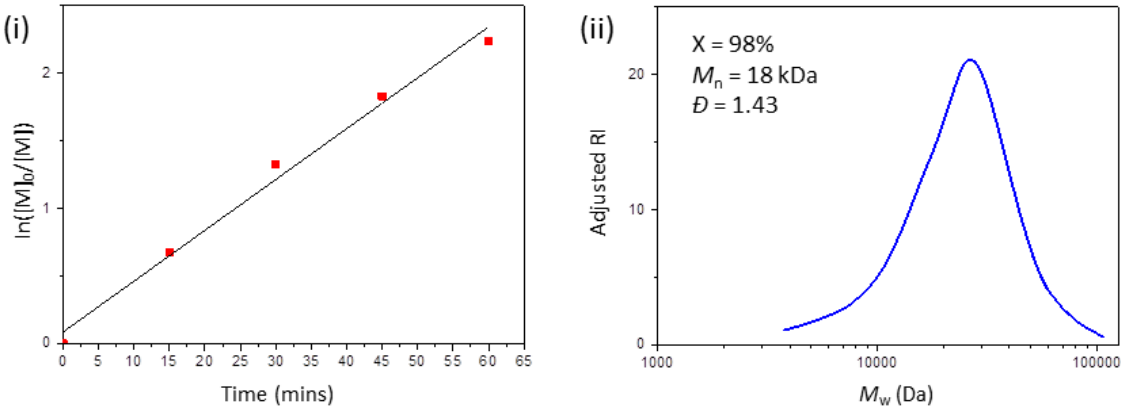

Figure 2-4: Polymerisation of HEMA by ATRP. (i) Kinetics plot of polymer conversion by ^{1}H-NMR. (ii) SEC of HEMA polymer produced at 2 hours with dispersity (*Đ*), M_n and conversion (X) by ^{1}H-NMR inset.

Monomer to polymer conversion (X) as calculated by ^{1}H-NMR demonstrates first order kinetics (Figure 2-4, i), i.e. the polymerisation rate with respect to the natural log of the monomer concentration consumed at that point of the reaction (concentration of monomer at time 0 $[M]_0$/concentration of monomer [M]) is proportional to the time that the reaction has been proceeding for. It demonstrates that the concentration of the propagating radicals

is constant (with a balance in the activating and deactivating steps of the reaction) and there is not an excess of terminating events which would be represented by a plateau. Assessment of the resultant polymer by SEC demonstrate some degree of control with a dispersity (*Đ*, M_w/M_n) of 1.43. This is shown by the breadth of the peak found by SEC (Figure 2-4, ii).

2.3.2 ARGET ATRP polymerisation in solution

The transition was made to ARGET ATRP polymerisation due to the improved biocompatibility of the reagents and the reduced sensitivity to oxygen contamination.

HEMA was successfully polymerised using ARGET ATRP. The reaction conditions were optimised with regards to the copper catalyst and solvent before the transition was made to OEGMA polymerisations. OEGMA polymerisations were optimised for AScA molar equivalents and experimental glassware.

2.3.2.1 Copper catalyst

ARGET ATRP polymerisations were undertaken using Cu(II)Cl and Cu(II)Br in identical conditions in a round bottom flask and water as the solvent. The reaction proceeded visibly

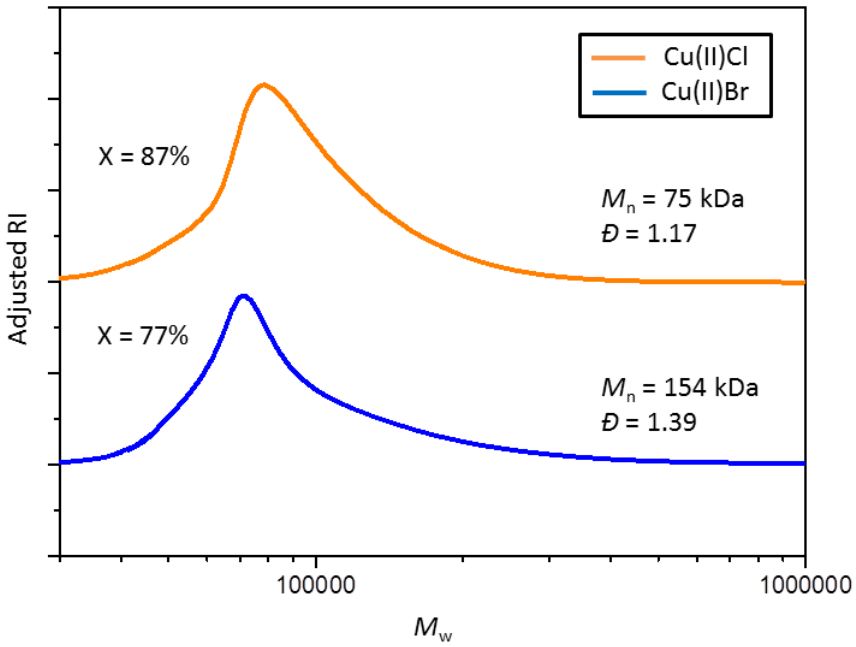

Figure 2-5: SEC analysis of pHEMA by ARGET ATRP with different catalysts. Cu(II)Cl exhibits superior control of polymerisation (*Đ*, by SEC analysis) and conversion (X, by ^{1}H-NMR) when compared to Cu(II)Br for use in ARGET ATRP polymerisations with HEMA.

rapidly and polymer was seen to precipitate out of solution so ^{1}H-NMR analysis to monitor the reaction kinetics was not successful. SEC analysis and ^{1}H-NMR were undertaken on the resultant polymer (Figure 2-5). The polymerisation is better controlled when the Cu(II)Cl catalyst is used. This is demonstrated through the lower dispersity (*Đ*) on SEC analysis when compared to Cu(II)Br. Some error in the M_n for pHEMA as calculated by the SEC is expected as it was calculated by conventional calibration from pMMA standards. The theoretical M_n for this polymerisation is 34kDa, and looking at the trends seen on the SEC, the M_n for the Cu(II)Cl reaction is 75 kDa almost double this, and for Cu(II)Br 154 kDa almost five times. This further suggests inferior control in the Cu(II)Br as it is likely that polymerisation is occurring in solution without an initiator group due to an imbalance of radicals due to the imbalance of Cu(I) and Cu(II). From this point forward the Cu(II)Cl catalyst was used for all polymerisations. This result is supported in the literature where is has been shown that a chlorine capped polymer chain is 10-100 times less active than a bromine capped chain[276], and that polymerisations using chlorinated groups proceed more slowly and with a greater level of control[277].

2.3.2.2 Optimisation of solvent

The rapid progression, precipitation of the polymer and occasional gelation of the solution was thought to be due to the solvent used to this point, water. Water can lead to a reversible dissociation of the halide ion from the deactivating complex[277,278], together with possible disproportionation of the Cu(I)/L complex seen in water, an excess of radicals may be formed and lead the reaction to be uncontrolled[278]. The solvent was modified to a 50% (v/v) diluted solution of IPA in UHQ water in line with a published protocol[270]. No further precipitation of polymer was seen and 50% (v/v) IPA was used for further reactions unless directly specified.

As the polymerisation was becoming more reproducible with HEMA the transition was made to OEGMA for further optimisation.

2.3.2.3 Molar equivalents of reducing agent

The optimal amount of reducing agent (AScA) was examined for polymerisation with OEGMA. The ideal quantity of reducing agent in the system is the minimal amount to

remove all oxygen within the reaction vessel, to promote the reduction of Cu(II) to Cu(I), and so control the polymerisation through the optimal number of free radical produced.

Excess reducing agent leads to an imbalance of the Cu(I) to Cu(II) ratio, the production of excess free radicals and so to a loss of control. Differing molar equivalents were prepared and polymerisations carried out for 3 hours in sealed glass vials. SEC and ^{1}H-NMR analysis of the resultant OEGMA polymers (Figure 2-6) demonstrated optimal control with regards to conversion (as calculated by ^{1}H-NMR) and dispersity when using 0.15 mol equivalent AScA.

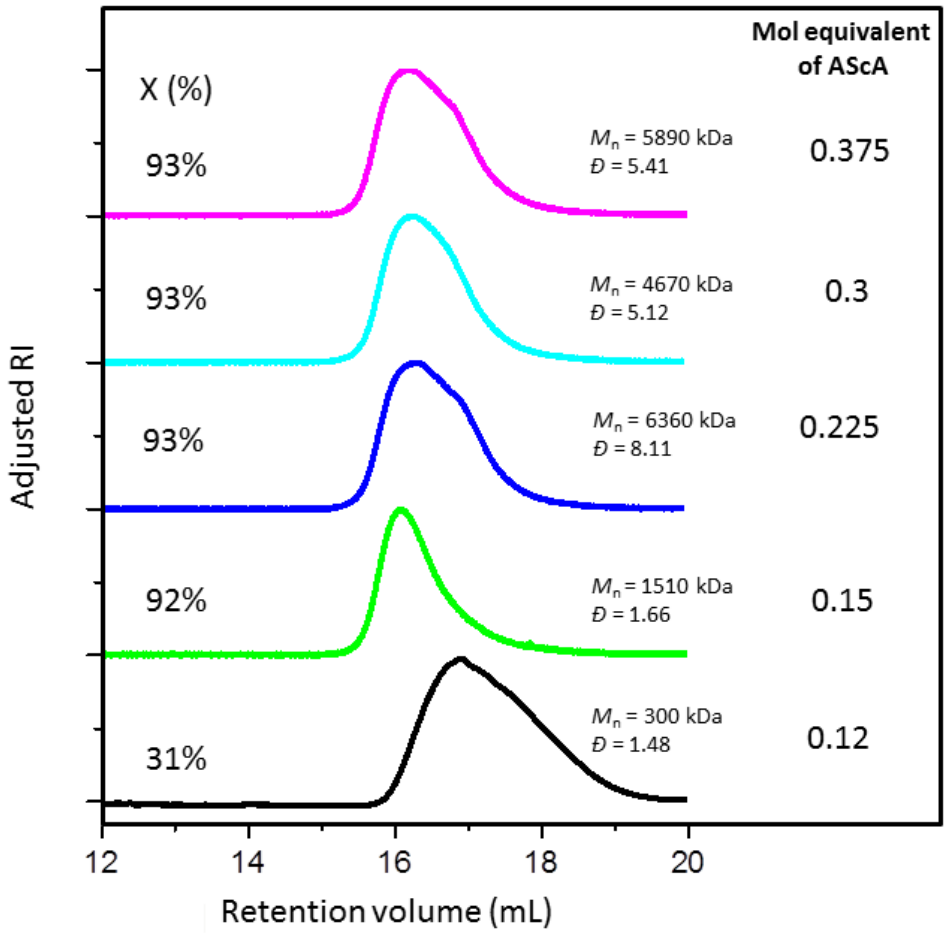

Figure 2-6: Optimisation of ARGET ATRP with through changing molar equivalents of the reducing agent (AScA). Conversion by ^{1}H-NMR (X) together with M_n and dispersity ($Đ$) as produced through SEC analysis are inset.

Using an AScA level of 0.12 and 0.15 mol equivalent the polymerisation was repeated in a round bottom flask with rubber septum to establish the kinetics of the reaction (Figure 2-7).

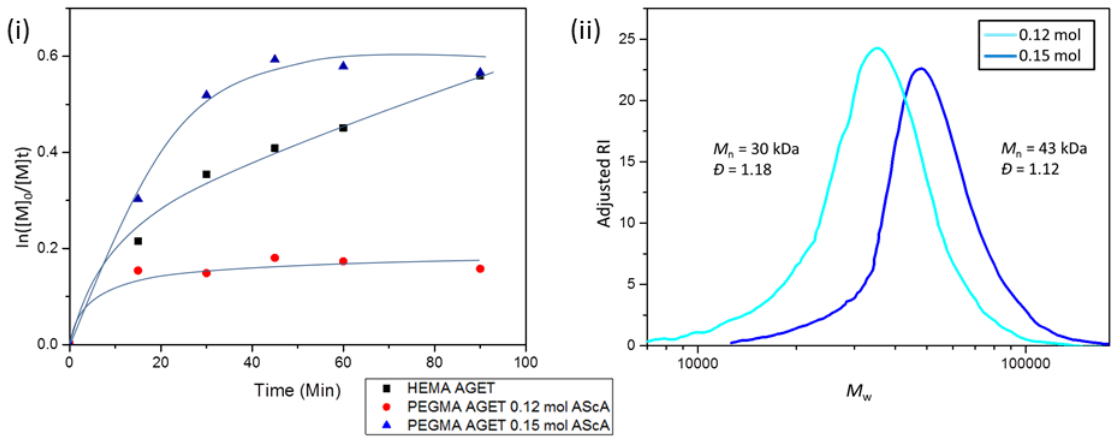

Figure 2-7: Polymerisation kinetics of HEMA and OEGMA by ARGET ATRP. (i) Logarithmic conversion of HEMA and OEGMA by ^{1}H-NMR. (ii) SEC analysis of the resultant polymers produced from ARGET ATRP polymerisations of OEGMA with initiator:reducing agent ratios of 150:0.12 and 150:0.15 at a reaction time of 60 minutes.

Interestingly, the polymerisation appears to be terminating prematurely before reaching a maximal conversion, achieving 45% (0.15 mol) and 17 % (0.12 mol) at 60 minutes. This is plotted with the data for HEMA polymerised under the same conditions. The SEC data demonstrates that this is not due to loss of control, but likely another factor, possibly contamination with oxygen leading to termination of the reaction. The data appears to suggest that we have demonstrated the optimal reaction conditions and AScA level required for a sealed system but when samples are removed, despite being held under a positive nitrogen atmosphere, there may be contamination with oxygen. Experiments conducted with a rubber septum where aliquots were removed over the course of the reaction consistently failed to achieve the conversions seen in a sealed technique despite numerous attempts. This may again due to potential contamination with oxygen due to the repeated samplings. Reactions were performed on both a schlenk line with piped nitrogen and with tanked nitrogen. Piped nitrogen consistently produced no monomer to polymer conversion (X = 0% by ^{1}H-NMR). Tanked nitrogen produced consistent results indicating possible contamination in the piped nitrogen. Due to inconsistencies in reproducibility, from this point forward all reactions were performed under a tanked argon atmosphere where possible.

From this point forward polymerisations will be undertaken in this optimised system; namely within a sealed vial, for 3 hours, utilising the Cu(II)Cl catalyst, within a solvent of 50% (v/v) IPA in UHQ water.

2.3.3 Polymer brush grafting from 2D silicon surfaces

The ultimate goal of this work is to produce an antifouling surface from polymer scaffolds for tissue engineering, generated from surface initiated ARGET ATRP of pOEGMA bottlebrushes from electropsun fibres. The characterisation of 3-dimentional surfaces is intrinsically more challenging than flat surfaces, and so, initial work was undertaken to generate surface initiated pOEGMA bottlebrushes from flat silicon wafers. This allowed the characterisation of the now highly reproducible polymerisation system in 2D before progressing to 3D surfaces. pOEGMA bottlebrushes were successfully grafted from 2D silicon wafer surfaces and characterised with a combination of techniques.

2.3.3.1 Confirmation of initiator attachment to silicon wafers

The polymerisation initiator BiBB was initially tethered to the silicon wafer using a two-step process. Vapour deposition of APTES preceded functionalising the free amine of the APTES with the BiBB initiating group. Following this, surface initiated ARGET ATRP of OEGMA was performed to graft pOEGMA bottlebrushes from the silicon surfaces (Si-APTES-pOEGMA surfaces).

2.3.3.1.1 Assessment of polymer brush thickness

Polymer brush functionalised wafers, and their associated controls were characterised for the presence of the brush and the associated thickness. The dry brush thickness coating the silicon surface was measured using AFM corroborated using ellipsometry.

An AFM scratch test was performed on dry Si-APTES-pOEGMA 2D silicon surfaces. Using tapping mode, the scratch was depth profiled to measure the polymer thickness (Figure 2-8, ii and iii). Three scratches were made and 8 to 10 depth measurements were made over each scratch. These measurements were corroborated using ellipsometry to measure the polymer layer. A difference of approximately 6.2 nm (+/- 0.038 nm, MSE 3.548, Figure 2-8, i) was demonstrated between Si-APTES-Ini functionalised controls and following polymerisation (Si-APTES-pOEGMA), supporting the deposition of a polymer layer during the polymerisation process. This is deemed to be plausible as it is less than the theoretical

polymer contour length for this polymerisation which was established to be 24.7 nm. The difference observed between the dry brush thickness as measured by ellipsometry and AFM and the theoretical thickness are likely due to the brush being collapsed on the silicon surface.

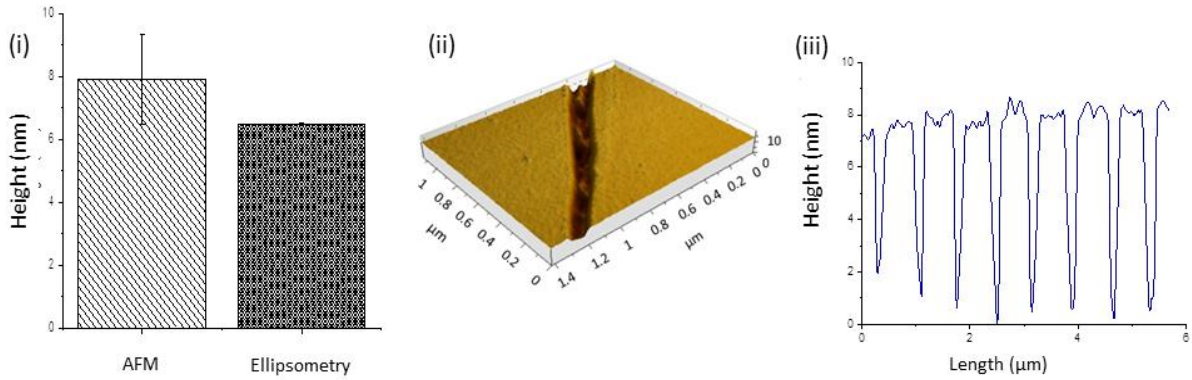

Figure 2-8: Measurement of the height of the dry brush. (i) Height of dry brush as measured by AFM (n = 3, error bars SD) and ellipsometry (n = 2, error bars SD) of pOEGMA grafted from 2D silicon surfaces. (ii) AFM scratch test and representative profile (iii) of pOEGMA grafting from silicon wafers. Theoretical polymer contour length = 24.7 nm. Extracted from Harrison *et al*.[281]

2.3.3.1.2 XPS characterisation of the surface chemistry of the Si-APTES-pOEGMA wafers

Having confirmed the presence of a deposited surface layer following the polymerisation process through AFM and ellipsometry, XPS was used to interrogate the surface chemistry of functionalised silicon wafers and their associated controls.

The Si-APTES-pOEGMA wafers were confirmed to have an organic surface coating due to the rich presence of the ether (C-O) group within the pOEGMA brush. The C-O is an excellent candidate for characterisation as it is only found in these samples within the polymer brush and may be identified in a facile manner from the other chemical groups within the sample.

High resolution spectra of the C 1*s* peak obtained from all samples were found to be well fitted by 3 peaks: 285.0 eV (C-C or C-H), 286.5 eV (C-O single bond) and 288.4 eV (carboxyl or O=CO)[279,280] as shown in Figure 2-9, A.

The fitted peaks show a clear difference between the C 1*s* peaks found on silicon wafer controls (left, bottom trace), silicon wafers functionalized with the polymerisation initiator BiBB (through APTES, left, middle trace) and wafers functionalized with surface initiated pOEGMA (Si-APTES-pOEGMA, left, upper trace, Figure 2-9).

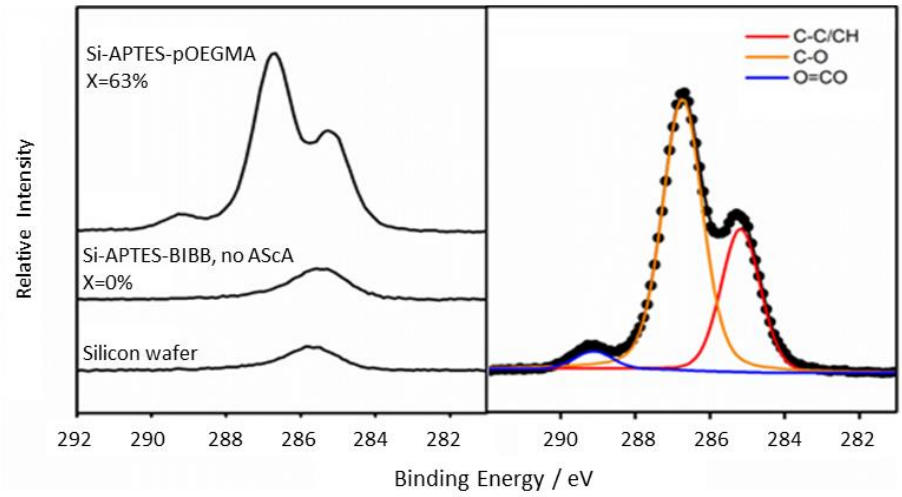

Figure 2-9: XPS analysis of the surface initiated pOEGMA bottlebrushes from silicon wafers. XPS analysis of silicon wafers functionalised with APTES-Ini with controls (dashed, bottom trace), silicon functionalised with APTES-Ini that underwent polymerisation with no reducing agent, (ascorbic acid, AScA, dotted middle trace) and pOEGMA grafting from a silicon wafer (top trace). Conversion by ^{1}H-NMR is included above each trace (left). Si-APTES-pOEGMA sample with the C 1*s* peaks fitted (right).

Analysis of the C-O composition of the 2D functionalized silicon surfaces provides good evidence for the covalent attachment of the pOEGMA brushes to the silicon surfaces. Silicon wafers functionalized with APTES (Si-APTES) and polymerisation initiator (Si-APTES-Ini) underwent two independent polymerisations of OEGMA with ARGET ATRP and were subsequently thoroughly washed in ethanol to remove unbound polymer.

The C-O signal from Si-APTES wafers shows a small increase from 12.2 to 23.9 (reaction 1) and to 15.8 (reaction 2). This is minimal in comparison to the increase in signal from Si-APTES-Ini samples which increases from 11.6 to 59.4 (reaction 1) or 56.8 (reaction 2). This supports the covalent anchoring of pOEGMA polymer brushes from Si-APTES-Ini wafers, and further demonstrates the need for the initiating group for the creation of the polymer brush layer. The C-O composition of the 2D functionalized silicon surfaces obtained from the XPS spectra are presented in Table 2-1.

Table 2-1: The C-O signal intensity of 2D silicon surfaces as measured by XPS and the corresponding polymer M_n and $Đ$.

Repeat	+/- ATRP	2D silicon surfaces		Polymer characteristics			
		Si-APTES[a]	Si-APTES-Ini[a]	X (%)	M_n (theo)[b]	M_n (SEC)[c]	$Đ$ (SEC)
1	-	12.2	11.6	-	-	-	-
2	-			-	-	-	-
1	+	23.9	59.4	78	56,200	44,800	1.12
2	+	15.8	56.8	79	56,900	45,000	1.13

Notes: [a] A single batch of silicon wafers was prepared and polymerized in two separate polymerisation reactions, so surface 1 and 2 pre-reaction on the 2D silicon wafers are the same sample. [b] Theoretical M_n calculated by ^{1}H-NMR. [c] SEC molecular weight estimated relative to polystyrene standards in DMF without correction to a universal calibration.

Table 2-2 : C 1*s* breakdown for the 2D silicon surfaces as measured by XPS

		C-C		C-O		O=CO	
Surface replicate:	**+/- ATRP**	**1**	**2**	**1**	**2**	**1**	**2**
Si-APTES	+	70.2	77.1	23.9	15.8	5.9	7.1
Si-APTES-Ini	+	33.6	34.5	59.4	56.8	7.0	8.7

The Si-APTES wafers were present within the pOEGMA polymerisation and represent the negative control for this reaction. Through the analysis of the C 1*s* spectra (Table 2-2) of the Si-APTES and the Si-APTES-Ini it is clearly demonstrated that a greater proportion of C-C groups seen on the Si-APTES samples when compared to the Si-APTES-Ini, and that these groups dominate over the signal from oxygen containing groups such as the C-O and O=CO. The opposite is seen in the Si-APTES-Ini samples, with the oxygen containing groups dominating the signal. This further supports the conclusion that pOEGMA has been successfully grafted from the Si-APTES-Ini wafers (and not from the Si-APTES wafers) as the chemical composition of the pOEGMA brush is rich in oxygen containing groups (C-O and O=CO). Furthermore, this data also demonstrates the need for the initiating group to be present for the surface initiated pOEGMA brush to be produced, the covalent anchoring of the brush on the Si-APTES-Ini wafer, and that the washing steps to remove any unbound pOEGMA formed as a result of the sacrificial initiator in solution were adequate.

2.3.3.1.3 Assessment of surface wettability following pOEGMA grafting

Further evidence for the successful grafting of pOEGMA from the 2D silicon surfaces is demonstrated through the change in surface wettability of silicon wafers. Water contact angle measurements were performed on functionalised wafers before and following polymerisation of pOEGMA with a reduction in contact angle from 63.6° +/- 2.3° on Si-APTES-Ini functionalized wafers to 36.3° +/- 5.9° (Figure 2-10), N = 3.

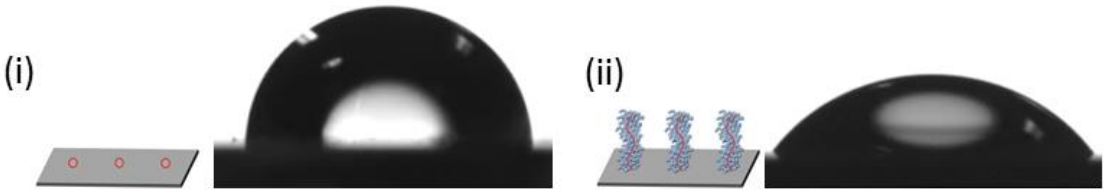

Figure 2-10: Water contact angle measurement of silicon wafers functionalised with (i) APTES-Ini and (ii) following surface initiated grafting with pOEGMA.

A reduction in water contact angle following grafting of pOEGMA brushes from the silicon surfaces is evident, but not as significant as perhaps would be expected. This may be due to a number of reasons including the number of polymer brushes tethered to the surface. A surface analysis of the bromine signal from the silicon wafers following attachment of the initiating group and following polymerisation was performed using a Time-of-Flight Secondary Ion Mass Spectrometry (ToF-SIMS) on a single set of samples. This demonstrates reasonably good and even coverage of bromine both before and after grafting (Appendix E). The bromine signal can be used as, in a well-controlled reaction, the bromine will remain present at the top of the polymer chain following termination of the reaction. These results suggest that an even coverage of polymer brushes may have been produced. However, the ToF-SIMS is unable to demonstrate whether the bromine signal is from a polymer brush or from an un-polymerised initiating group. It may be that not all of the initiating groups were successfully polymerised from, resulting in a lower grafting density than hoped, and thus the contact angle does not reduce as greatly as might be expected. The move from 2D silicon surfaces to 3D electrospun fibres produces a might greater surface area for polymer brush grafting.

2.4 Conclusions

In conclusion, from this initial and early work a reliable, reproducible and effectively controlled radical polymerisation of OEGMA using ARGET ATRP in solution has been established. Silicon wafers have been successfully functionalised with the polymerisation initiating agent through surface functionalization with APTES and reacting the initiating agent onto this surface. Surface initiated ARGET ATRP of OEGMA was then employed with the previously optimised reaction conditions to graft pOEGMA bottlebrushes from the 2D silicon surface. This surface coating was washed and dried before characterisation with AFM, ellipsometry, water contact angle and XPS which all supported the presence of the polymer layer. This system will now be extended into surface-initiated polymerisation of 3D scaffold systems using electrospun fibres.

References: Chapter 2

267 Kakwere, H., Payne, R. J., Jolliffe, K. A. & Perrier, S. Self-assembling macromolecular chimeras: controlling fibrillization of a beta-sheet forming peptide by polymer conjugation. *Soft Matter* **7**, 3754-3757, doi:10.1039/c0sm01237h (2011).

268 Robinson, K. L., Khan, M. A., Banez, M. V. D., Wang, X. S. & Armes, S. P. Controlled polymerization of 2-hydroxyethyl methacrylate by ATRP at ambient temperature. *Macromolecules* **34**, 3155-3158, doi:10.1021/ma0019611 (2001).

269 Oh, J. K., Min, K. & Matyjaszewski, K. Preparation of poly(oligo(ethylene glycol) monomethyl ether methacrylate) by homogeneous aqueous AGET ATRP. *Macromolecules* **39**, 3161-3167, doi:10.1021/ma060258v (2006).

270 Telford, A. M. *et al.* Micropatterning of Polymer Brushes: Grafting from Dewetting Polymer Films for Biological Applications. *Biomacromolecules* **13**, 2989-2996, doi:10.1021/bm3010534 (2012).

271 Dunlop, I. E. *et al.* Structure and Collapse of a Surface-Grown Strong Polyelectrolyte Brush on Sapphire. *Langmuir* **28**, 3187-3193, doi:10.1021/la204655h (2012).

272 Mecklenburg, G. *Functionalised Polymer Fibres for Orthopaedic Interfacial Tissue Engineering and Other Biomedical Applications* MPhil thesis, Imperial College London, (2014).

273 Yoshikawa, C., Zhang, K., Zawadzak, E. & Kobayashi, H. A novel shortened electrospun nanofiber modified with a "concentrated" polymer brush. *Sci. Technol. Adv. Mater.* **12**, 015003/015001-015003/015007, doi:10.1088/1468-6996/12/1/015003 (2011).

274 Brandl, C., Greiner, A. & Agarwal, S. Quick Polymerization from Electrospun Macroinitiators for Making Thermoresponsive Nanofibers. *Macromolecular Materials and Engineering* **296**, 858-864, doi:10.1002/mame.201100031 (2011).

275 D. Briggs, M. P. S. *Practical Surface Analysis. Volume 1 - Auger and X-ray Photoelectron Spectroscopy.* 2nd edn, Vol. 1 (John Wiley & Sons Ltd. UK, 1990).

276 Tang, W. *et al.* Understanding atom transfer radical polymerization: Effect of ligand and initiator structures on the equilibrium constants. *Journal of the American Chemical Society* **130**, 10702-10713, doi:10.1021/ja802290a (2008).

277 Simakova, A., Averick, S. E., Konkolewicz, D. & Matyjaszewski, K. Aqueous ARGET ATRP. *Macromolecules* **45**, 6371-6379, doi:10.1021/ma301303b (2012).

278 Tsarevsky, N. V., Pintauer, T. & Matyjaszewski, K. Deactivation efficiency and degree of control over polymerization in ATRP in protic solvents. *Macromolecules* **37**, 9768-9778, doi:10.1021/ma048438x (2004).

279 Martins, A. *et al.* Surface Modification of Electrospun Polycaprolactone Nanofiber Meshes by Plasma Treatment to Enhance Biological Performance. *Small* **5**, 1195-1206, doi:10.1002/smll.200801648 (2009).

280 Shaojun Yuan, G. X., Ariel Roguin, Swee Hin Teoh, Cleo Choong. *Advances in Biomaterials Science and Biomedical Applications*. 178-205 (InTech, 2013).

281 Harrison, R. H. et al. Modular and Versatile Spatial Functionalization of Tissue Engineering Scaffolds through Fiber-Initiated Controlled Radical Polymerization. Advanced Functional Materials 25, 5748-5757, doi:10.1002/adfm.201501277 (2015).

Chapter 3 : Surface Grafted Polymerisation

The work in this chapter has been previously prepared for publication in "Modular and Versatile Spatial Functionalization of Tissue Engineering Scaffolds through Fiber-Initiated Controlled Radical Polymerization" by **Harrison RH**, Steele JAM, Chapman R, Gormley AJ, Chow LW, Mahat MM, *et al.* published in Advanced Functional Materials in September 2015[282] (Appendix B).

3.1 Polymerisation from 3D surfaces

Biomaterials design for tissue engineering and regenerative medicine spans the simple to the complex as outlined in chapter one. In this chapter I have taken my antifouling polymer brush system from 2D surfaces and applied it to 3D electrospun scaffolds to generate an antifouling scaffold to guide cell behaviour, as outlined in Figure 3-1.

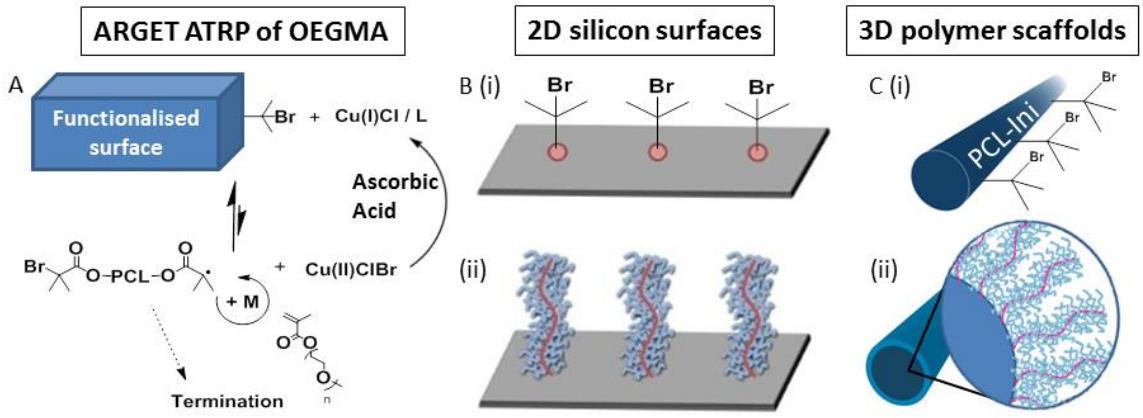

Figure 3-1: Surface initiated polymer bottlebrush grafting from 2D and 3D functionalised surfaces by ARGET ATRP. (A) Schematic of ARGET ATRP controlled radical polymerisation from surfaces. (B) Schematic of functionalised 2D silicon surfaces before (i) and after (ii) grafting with pOEGMA bottlebrushes. (C) Schematic of functionalised 3D electrospun fibres before (i) and after (ii) grafting with pOEGMA bottle brushes.

To the best of my knowledge this work is the first time that surface initiated ATRP has been used for biomedical application and ARGET ATRP has been used to produce surface-initiated polymer brush grafting from electropsun fibres[282]. Furthermore, this is the first grafting of pOEGMA from PCL fibres, and the first time an antifouling surface has been successfully produced from electropsun fibres for a biomaterial application.

3.2 Materials and Methods

3.2.1 Materials

Fluorescently labelled proteins were prepared for antifouling assays as follows. Fluorescently labelled rhodamine-heparin (rhod-hep, MW 18kDa), rhodamine-CS (rhod-CS, MW 50kDa) and fluorescein-HA (fluor-HA, MW 1,500 kDa) were purchased (Creative PEGWorks, Winston Salem, USA). Rhodamine-fibronectin (rhod-fib) and rhotamine-BSA (rhod-BSA) were kindly labelled by Dr Robert Chapman and provided for experimentation. In brief, BSA and fibronectin were coupled to Rhodamine 6B isothiocyanate and NHS-fluorescein respectively. The BSA coupling was performed in PBS (10 mg/mL) and the fibronectin coupling was performed in borate buffer (20 mM, pH 9) at 1 mg/mL protein. In each case the dye (100 equiv) was added as a solution in DMSO (100 mM), and the solution was left stirring at RT for 2 hours. Both proteins were purified from the free dye by size exclusion chromatography over sephadex G100 in PBS.

Cell materials

Bovine tenocytes were isolated from 3 animals through collagenase digestion and were then expanded by primary cell culture. Bovine lower leg joints were purchased from an abattoir (C.E. Leech, Melborne, UK) following slaughter for the food industry.

All cell consumables were purchased from Gibco® by Life Technologies and culture plastic purchased from Corning Inc. (USA) unless otherwise stated. Routine tissue culture was performed in normal growth media (NGM) and was made as follows. Dulbecco's Modified Eagle's Medium (DMEM)- GlutaMAX^{TM} supplemented with 1 g/L D-glucose and pyruvate with 10% (v/v) Fetal Calf Serum (FBS), 1% (v/v) antibiotic/antimycotic (anti/anti; containing amphotericin B, streptomycin and penicillin). NGM was refrigerated at 2-4^{o}C, used within 4 weeks of opening and warmed for 30 minutes in a 37^{o}C water bath prior to use. Cells were detached using a dissociation solution of 0.005% (v/v) trypsin-EDTA. RLT lysis buffer was purchased from Qiagen and used as received. Tissue digestion was achieved with collagenase type I purchased from Sigma (UK).

3.2.2 Grafting pOEGMA from functionalised 3D electrospun fibres

PCL was initially end-functionalised with the polymerisation initiator BIBB before electrospinning into a scaffold. An antifouling pOEGMA polymer bottlebrush was then grafted from the scaffold surface and characterised.

3.2.2.1 End functionalization of PCL with polymerisation initiator

PCL-diol (M_w 14 000 Da) was functionalized with the polymerisation initiator 2-bromoisobutyryl bromide (BiBB) using a protocol adapted from the literature to produce PCL-Ini with the chemical structure demonstrated in Figure 3-2[283].

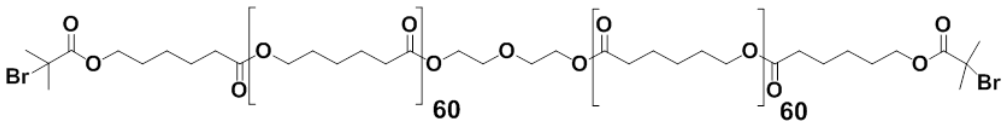

Figure 3-2: End functionalised PCL-diol with the initiating group BIBB (PCL-Ini).

In a typical run, 5 g of 14 kDa PCL-diol was introduced to 200 mL of anhydrous tetrahydrofuran (THF) in a round bottom flask and stirred at room temperature under a sealed nitrogen atmosphere. Following dissolution of the PCL, 2.9 mL TEA and 50 mg of 4-dimethylaminopyridine (DMAP) were added and the vessel was immersed into an ice bath. Following 15 minutes of cooling, 265 µL of BiBB was introduced dropwise, the ice bath removed, and the reaction stirred overnight at room temperature. The mixture was filtered to remove the side products of the reaction, and the filtrate was collected, reduced through vacuum rotary evaporation, and precipitated into cold diethyl ether. The precipitate (PCL-Ini) was isolated by vacuum filtration and dried. The product was confirmed using ^{1}H-NMR (400MHz, deuterated $CDCl_3$) using a Bruker Avance DPX 400 (400MHz) spectrometer with the residual solvent peak used as an internal reference. The PCL-Ini was then stored until needed in a vacuum desiccator, protected from light. ^{1}H NMR (400 MHz, $CDCl_3$) δ ppm: 4.24 – 4.20 (m, 4H) 4.05 (t, J = 6.7 Hz, 240H), 3.78 – 3.71 (m, 4H), 2.30 (t, J = 7.5 Hz, 244H), 1.92 (s, 0H), 1.73 – 1.55 (m, 480H), 1.46 – 1.32 (m, 252H). (see Figure 3-5 for peak assignments).

3.2.3.2 Electrospinning

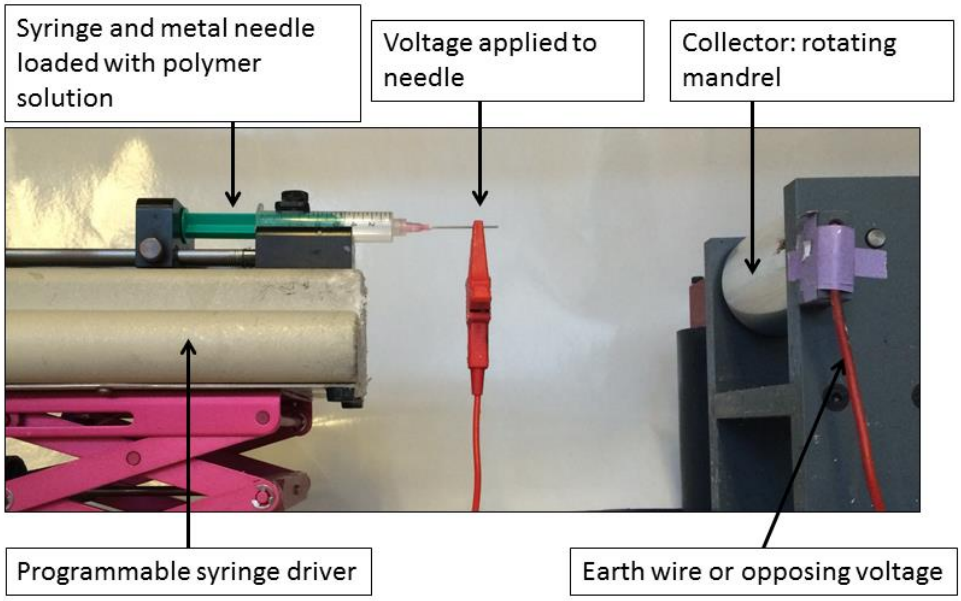

Figure 3-3: Electrospinning experimental set up for the production of electrospun scaffolds. The polymer solution within a syringe is loaded onto a programmable syringe driver (left) and a voltage applied to the mounted needle. An earth wire or opposing voltage is applied to a metal collector, here a rotating mandrel, covered in aluminium foil. The apparatus is completely contained within a fume hood.

A high (17% w/w) and a low (9% w/w) PCL-Ini:PCL ratios were electrospun into scaffolds. 12 $mg.mL^{-1}$ (9% w/w) PCL-Ini or 24 $mg.mL^{-1}$ (17% w/w) PCL-Ini was added to 12% (w/v) PCL (M_n 70,000-90,000 Da) in 1,1,1,3,3,3-hexafluoro-2-propanol (HFIP) and mixed overnight on rollers. Solutions were transferred to plastic syringes, loaded onto a programmable syringe pump (Kd Scientific, UK), and extruded at a rate of 2 $mL.hr^{-1}$ through a blunt 18-gauge stainless steel needle charged with +16kV (Glassman, Bramley, Hampshire, UK). The needle was placed at distance of 11 cm from a grounded 10 x 10 cm plate for small master scaffolds or a mandrel rotating at 0.33 m/s for large master scaffolds, each coated with aluminum foil (Figure 3-3). No difference was seen in fiber alignment or morphology between collectors. All scaffolds were electrospun under the same conditions, stored in a vacuum desiccator, and protected from light until needed.

3.2.3.3 Polymer brush grafting from electropsun fibres

Grafting of pOEGMA from PCL-Ini scaffolds was performed using the protocol outlined in Chapter 2, 2.2.3. PCL-Ini scaffolds were prepared for polymerization; they were punched from the master electrospun scaffolds using a biopsy punch to create uniform sizes before being introduced into the reaction vessel. Control scaffold of electrospun PCL containing no PCL-Ini, but the corresponding amount of unmodified 14 kDa PCL-diol were used. 9% and 17% PCL-Ini scaffolds were polymerized within the same reaction vessel to allow direct comparison and were identified by either different size, or with a small incision into the edge of the mat.

When large numbers of scaffolds were required, the amount of initiator present on the 3D electrospun surfaces was estimated and if greater than 10% of the sacrificial initiator mass, the mass of sacrificial initiator was reduced proportionally to maintain the reaction conditions. Such reactions were scaled up and performed in 10 mL solvent, and stirred within a stirred silicone oil bath.

Following polymerization, electrospun scaffolds were thoroughly washed in ethanol three times using ultrasonication for 30 seconds before rinsing with UHQ water three times. This was found to effectively remove any adsorbed polymer (Appendix F). Scaffolds were then dried and stored in a vacuum dessicator. Scaffolds were characterized with water contact angle measurements and XPS surface analysis using the protocols described in Chapter 2 (2.2.4.2.1 and 2.2.4.2.2) and scanning electron microscopy (SEM) using the LEO Gemini 1525 FEG with a 10 nm cobalt sputter.

3.2.3.4 Development of a biotinylated monomer for versatile functionalization of the polymer brush and production of p(OEGMA-co-biotin)

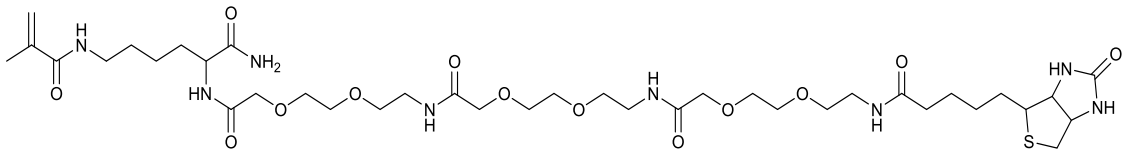

Figure 3-4: Structure of the biotinylated PEG monomer

The biotinylated PEG monomer (Figure 3-4) was kindly prepared by Dr Robert Chapman using standard solid phase peptide synthesis (SPPS) techniques. Briefly, rink amide resin (0.7 mmol/g, 1 g) was deprotected and coupled to Fmoc-Lys(Mtt)-OH (4 eq., 2h). The Mtt group was then removed with 1.5% (v/v) TFA in DCM (2 x 15 min) and the resin washed with Hünigs base in DMF 1% (v/v) and DCM after which methacryloyl chloride (8 eq., 10 min) in DCM was coupled to the free amine. Three units of Fmoc-O2Oc-OH (2 eq., 3 h) were then coupled on resin, followed by a biotin group after the final fmoc deprotection. All couplings were performed with HBTU (4 eq.) and Hünigs base (8 eq.). The monomer was cleaved from the resin with a cocktail of TFA / triisopropyl silane / H_2O (95 / 2.5 / 2.5 v/v/v, 2 h), triturated from diethyl ether and purified by HPLC (C18 column, H_2O / acetonitrile gradient). ESI-MS for C38H66N8O13S Calcd. 875.5 (M+H)+, Found 875.5 (Appendix G, Figure 7-2). ^{1}H-NMR (400 MHz, $CDCl_3$) δ ppm: 8.08 – 7.90 (s, 1H, NH), 7.75 – 7.60 (m, 3H, NH), 7.59 – 7.37 (s, 2H, NH), 7.21 – 6.93 (m, 3H, NH), 6.70 – 6.55 (m, 2H, NH), 6.44 – 6.33 (m, 2H, NH), 5.75 (s, 1H, H_2C=C), 5.41 (s, 1H, H_2C=C), 4.8 – 4.5 (m, 2H, biotin), 4.45 (m, 1H, α-Lys), 4.10 (s, 6H, -HNCO-CH_2-O-), 3.91 – 3.44 (m, 26H, O-CH_2-CH_2-, -H_2C-NHCO-), 3.43 – 3.29 (m, 1H, biotin), 3.28 – 3.17 (m, 2H, biotin), 2.43 – 2.27 (m, 2H, biotin), 1.99 (s, 3H, CH_3-C=CH2), 1.95 – 1.36 (m, 12H, biotin and Lys CH_2). See Appendix G, Figure 7-3 for peak assignment.

For 3D electropsun scaffolds that required fluorescent labelling, minor modifications were needed to the polymerisation protocol to mitigate any possible chelation of the copper catalyst due to the addition of biotinylated PEG monomer into the reaction mixture. The reaction was prepared as previously outlined, but with a 5 mol% replacement of the OEGMA monomer by the biotinylated PEG monomer, and the reaction left to proceed overnight. Samples were washed and dried as described above.

3.2.3.5 Histological sectioning, staining and imaging of PCL-pOEGMA scaffolds

Scaffolds requiring histological section and analysis were embedded in polyester wax (VWR, UK) in a method modified from the literature[284]. Scaffolds were initially incubated in a series of wax solutions maintained at 42°C, firstly for 30 minutes in a 1:1 (v/v) polyester wax and ethanol, followed by two incubations in pure polyester wax for 30 minutes and 1 hour, respectively. Scaffolds were then embedded vertically in polyester wax and allowed to set. Sections were cut at 10 µm onto untreated glass slides, dried, dewaxed with ethanol, and affixed at either end with an inert adhesive. Sections were blocked with 1% (w/w) BSA and 0.1% (w/v) tween 30 in PBS for 30 minutes, stained for 15

minutes with fluorescein-streptavidin (Vector Labs, UK) diluted to 1 μg/mL in 1% (w/w) BSA in PBS at pH 8.4, and washed three times in PBS. Slides were coverslipped for confocal microscopy with FluorSave™ fluorescent mounting media (Millipore, UK). Standard fluorescence imaging was performed on a Leica inverted optical microscope equipped with an Olympus DP70 digital camera. Confocal imaging was performed on a Leica SP5 inverted confocal microscope. Images were processed using GIMP 2.1. Confocal imaging was undertaken in conjunction with Mr. Joe Steele (PhD student, Stevens Group).

3.2.4 Assessment of antifouling ability of PCL-pOEGMA scaffolds

17% (w/w) PCL-pOEGMA scaffolds, having achieved >72% monomer to polymer conversion within the same reaction vessel were tested for antifouling ability and resistance to cellular adhesion.

3.2.4.1 Adsorption testing of PCL-pOEGMA scaffolds

In the literature there is no agreed protocol to test antifouling polymer brushes, so a panel of fluorescently labelled proteins and glycosaminoglycans (GAGs) was designed[285]. A group of compounds that are commonly found in either the ECM or blood were selected as they would interact with the scaffold *in vivo,* and are outlined in Table 3-1. I included several that are known to modulate the binding and activity of other biomolecules such as growth factors. All factors are negatively charged at pH 7. BSA, heparin, fibronectin, hyaluronic acid (HA), and chondroitin sulphate (CS) were selected. Adsorption of these biomolecules to a surface would likely lead to further biomolecule deposition and ultimately, to cell adhesion.

Table 3-1: The panel of biomolecules used to assess antifouling of the pOEGMA surface and their properties.

Compound	Type	M_w	Interaction with water	Where it is found	Function	Citations
BSA [286]	Protein (non glycosylated)	66 kDa	Hydrophilic	Serum	Colloidal osmotic pressure. Transport protein.	[287,288]
Heparin [289,290]	Sulfated GAG	3-30 kDa	Hydrophilic	Mast cells. Released into vasculature at injury sites.	Anticoagulant Binding of growth factors (e.g. basic FGF)	
Fibronectin [291]	Glycoprotein	440 kDa		Soluble: plasma Insoluble: ECM via integrin interaction.	Cell adhesion, growth, differentiation and migration.	[287,288,292]
HA [293]	Non sulfated GAG	5 kDa- 20 MDa	Hydrophilic	ECM, synovial fluid, cartilage	Broad. Structural role (cartilage, skin) lubrication (synovial fluid).	[294]
CS [295]	Sulfated GAG	50-100 kDa	Hydrophilic	ECM of connective tissues, cartilage	Resistance of compression in cartilage	

Notes: Fibroblast growth factor (FGF).

Stock solutions of labeled biomolecules of 50 µg/mL were made up in PBS with the exception of rhod-BSA which was 10 µg/mL in PBS. Circular PCL-Ini scaffolds, 6 mm in diameter, with and without pOEGMA brush functionalization were immersed in 70% (v/v) ethanol and washed with PBS three times to ensure uniform wetting. Excess liquid was blotted away and the scaffolds placed into individual high return 1.5 mL centrifuge tubes for incubation with 200 µL protein solution (test samples) or PBS (control) at 37^{o}C for 18 hours. Scaffolds were then washed in PBS in 28 mL light protected glass vials overnight to remove any unbound protein. The fluorescent signal on the scaffolds was then quantified using a plate reader (Perkin Elmer Envision Multimode Detector, Germany). An excitation wavelength of 550 nm and emission of 580 nm for rhodamine labeled biomolecules and 490 nm (excitation) and 520 nm (emission) for fluorescein labeled biomolecules was used. N = 4, with n = 3 technical internal replicates.

3.2.4.2 Cell binding assessment of PCL-pOEGMA scaffolds

Bovine tenocyte cultures were established and maintained in liquid nitrogen for long term storage until used for assessment of cell adhesion. Cell work was performed in a category II laminar flow cell culture hood and the cells stored in an O_2/CO_2 incubator at 37^{o}C, humidified with a CO_2 concentration of 5%. Cells were imaged using an Olympus DP70 digital camera mounted on a Leica inverted optical microscope.

3.2.4.2.1 Primary cell extraction

In brief, bovine lower leg joints from animals with a maximum of 2 years of age were refrigerated overnight on arrival before cleaning with soap and water, then 70% (v/v) ethanol. Tendon extraction was performed using an aseptic technique and sterile instruments; the dorsal skin over the surface of the shin was opened and a fascial flap was raised to expose the extensor tendons. Tendons were excised *en bloc* and placed in a sterile petri dish primed with 15 mL of warmed NGM. The tendon sections were then macerated and the media aspirated. The tissue pieces were immersed in 15 mL of 0.04% (w/v) collagenase type I in DMEM and 1% (v/v) anti/anti before being returned to the incubator. Every few hours the tissue pieces were agitated over a 24 hour period to encourage tissue digestion, following which the fluid was passed through sterile tea strainer to remove any large tissue pieces followed with a 70 μm cell strainer into sterile centrifuge tubes. The cells were pelleted through centrifugation at 300 rcf at 37^{o}C for 8 minutes following which they were re-suspended in media and counted using a haemocytometer and microscope. Cells were immediately seeded into a T25 cell culture flask primed with 5 mL of NGM at a density of 8.9x10^{4}/cm² (the equivalent of 2M cells for a T225 flask). The cells were expanded to 80-90% confluence with media being exchanged twice weekly and then cryopreserved at passage 1 in DMEM, 20% (v/v) FBS and 10% (v/v) sterile dimethyl sulfoxide (DMSO) hybrid-max at ~10^{7}/mL in liquid nitrogen.

Prior to use in scaffold experiments, cells from passage 1 that had been previously cryopreserved were removed from storage and seeded into T175 culture flasks primed with 25 mL NGM. Cells were expanded to 90% confluence before experimentation.

3.2.4.2.2 Cell adhesion assessment

Cell adhesion experiments were performed using a protocol modified from the literature[296]. In brief, 24-well plates were coated with a two-component silicone elastomer (Sygard 184, Dow Corning) prepared in a 10:1 ratio and cured for 48 hours on the bench at room temperature. Each independent experiment utilized seven PCL-pOEGMA scaffolds of 6 mm diameter, that had previously been functionalized with a pOEGMA brush and seven 6 mm diameter PCL scaffolds. Scaffolds and stainless steel insect pins (0.15 mm, Watkins and Doncaster, UK) were sterilized by immersion into 70% (v/v) ethanol for 15 minutes before washing in sterile PBS supplemented with 1% (w/v) anti/anti three times. The silicone-

coated well plate was thoroughly sprayed with 70% (v/v) ethanol before a scaffold was inserted into each well and fixed with an insect pin through the center of the scaffold using sterile instruments and aseptic technique. A row of vacant wells was left as a control. The plate and scaffolds were further sterilized under Ultra-violet (UV) light in the cell culture hood for 8 hours before being washed with sterile PBS immediately before cell seeding and the excess PBS blotted away.

Bovine tenocytes were prepared in a single cell suspension at a concentration of $5x10^5$ cells mL^{-1} from which 50 µL ($2.5x10^4$ cells) were seeded onto each scaffold. The cell-seeded scaffolds were returned to the incubator for 2 hours for cell attachment, following which a further 1 mL of normal growth media (NGM) was gently added to each well. Seeded scaffolds were cultured for 7 days, with the media exchanged on the 4^{th} day. On the 7^{th} day the media was aspirated from the wells and the scaffolds washed with sterile PBS. Two scaffolds of each type were prepared for SEM imaging and the remaining five scaffolds of each type were used for quantification of cellular metabolism using an MTT assay. This was compared to a calibration curve produced from a dilution series of a known cell number to allow for an estimate cell number from the experimentally measured absorbance.

3.2.4.2.3 MTT assay for cellular metabolism

A colorimetric assay for cellular metabolic activity based on the reduction of the tetrazolium dye 3-(4,5-dimethylthiazol-2-yl)-2,5-diphenyltetrazolium bromide (MTT) assay was used to approximate the relative number of cells[297].

A cell calibration ladder was first created in a tissue culture treated 24-well plate with cells from the same flask as those used for scaffold seeding. Serial dilutions were performed to give a ladder ranging from 100 000 cells to 3125 cells with cell free negative controls. Cells were cultured in the incubator for 2 hours until adhesion was observed, at which time a 3-(4,5-dimethylthiazol-2-yl)-2,5-diphenyltetrazolium bromide (MTT) cellular metabolism assay was performed. The cell calibration ladder was undertaken in triplicate to mirror the cell adhesion scaffold experiment with 3 different animals (N = 3), and three technical replicates (n = 3).

A stock solution of 5 mg mL^{-1} thiazolyl blue tetrazolium bromide (Sigma, UK) was prepared in sterile PBS and passed through a 0.22 µm syringe mounted filter. Cell culture media was

prepared using DMEM non-phenol red, low glucose media supplemented with 1% (m/v) L-glutamine and used to dilute the bromide salt to a concentration of 1 mg mL^{-1} (MTT solution). The MTT solution thoroughly mixed before adding to cells. The cell-seeded scaffolds were removed from the incubator, and the media was aspirated. The wells were gently washed three times with warm sterile PBS to remove any debris and non-adherent cells before 300 µL of the MTT solution added to each well. The plate was incubated at 37^{o}C for 2 hours after which point the MTT solution was aspirated and the plate put on ice. 500 µL IPA was added to each well and agitated to encourage mixing. The plate was sealed with plastic adhesive and refrigerated to limit any IPA evaporation whilst the purple formazan crystals were solubilized. 100 µL of the IPA was removed from each well after thorough mixing with a pipette to a new 96 well plate with three technical replicates being performed. The 96 well plate was sealed with plastic adhesive, kept on ice and protected from light before absorbance was read at 550 nm on a SpectraMax M5 plate reader.

When performed on scaffolds, the MTT assay was performed as above with minor modification. Following 7 days of culture, the scaffold containing well plate was removed from the incubator, the media aspirated, and the scaffolds washed in PBS. The scaffolds were then incubated with MTT solution as described above. After 2 hours, the scaffolds were gently removed from the well plate and introduced into 1.5 mL centrifuge tubes before 500 µL of IPA was added. Centrifuge tubes were thoroughly agitated using a vortex to facilitate the dissolution of all the formazan salt from any cells upon and within the scaffolds. The remainder of the assay was performed as described above.

3.2.4.2.4 Scaffold preparation for fluorescence imaging

Cell seeded scaffolds were fixed in 4% (w/v) paraformaldehyde (PFA) for 15 minutes, washed, and stored at 4°C in PBS until used. Immediately prior to imaging, scaffolds were blocked in 1% (w/v) BSA and 0.1% (w/v) tween 20 in PBS for 30 minutes. A solution of 5 µM draq5 (Thermo Scientific, UK) to stain cell nuclei and phalloidin (Alexa Fluor 488, diluted 1:400, Life Technologies) to stain actin was diluted in 1% (w/v) BSA in PBS and was incubated and light protected for 20 minutes before being washed with further PBS. Samples were imaged in PBS by inverted confocal microscopy as described in section 3.2.3.5 above.

3.2.5 Statistical Analysis

All experimental test groups had a sample size of at least n = 3 for biochemical analysis. All cell-related work was repeated with bovine tenocytes from three different animals. Data is presented as mean +/- standard deviation (SD). Statistical significance is determined using one-way ANOVA testing with an alpha value of 0.05 and post-hoc student's T-test. Excel software was used and a significance accepted where p-value < 0.05.

3.3 Results and Discussion

Surface-initiated ARGET ATRP of pOEGMA was successfully performed from 2D silicon surfaces, silicon wafers, and was optimized and characterized in Chapter two. This work was then expanded to surface initiated ARGET ATRP of pOEGMA from 3D electrospun scaffolds to form antifouling scaffolds.

3.3.1 Grafting pOEGMA from functionalised electrospun fibres

14 kDa PCL-diol was initially end-functionalised with the polymerisation initiating group BiBB to form PCL-Ini before electrospinning and undertaking surface initiated polymerisation to form the antifouling layer. A free sacrificial initiator, ethyl-α-bromoisobutyrate (EBiB), was used in solution to aid control of the polymerization and to allow analysis of the free polymer as a surrogate for the surface bound polymer; this has been shown to be a reliable tool for controlling the M_n and M_w/M_n for the polymers grown from surfaces within the same reaction vessel[298].

3.3.1.1 End functionalization of PCL with polymerisation initiator

In order to produce scaffolds with surface enrichment of initiating groups, PCL-diol (M_w 14000 Da), was modified with the initiating group (BiBB) to produce a polymerization initiating region at either end of the PCL polymer chain (PCL-Ini). PCL was selected to form the bulk of the scaffold due to its bioresorbability, good handling properties, electrospun fibre morphology, suitable degradation rate, ease of chemical modification and its current use in Food and Drug Administration (FDA) approved devices[299].

The successful conjugation of PCL-diol to BiBB was confirmed using ^{1}H-NMR (Figure 3-5) before processing the PCL-Ini to form scaffolds.

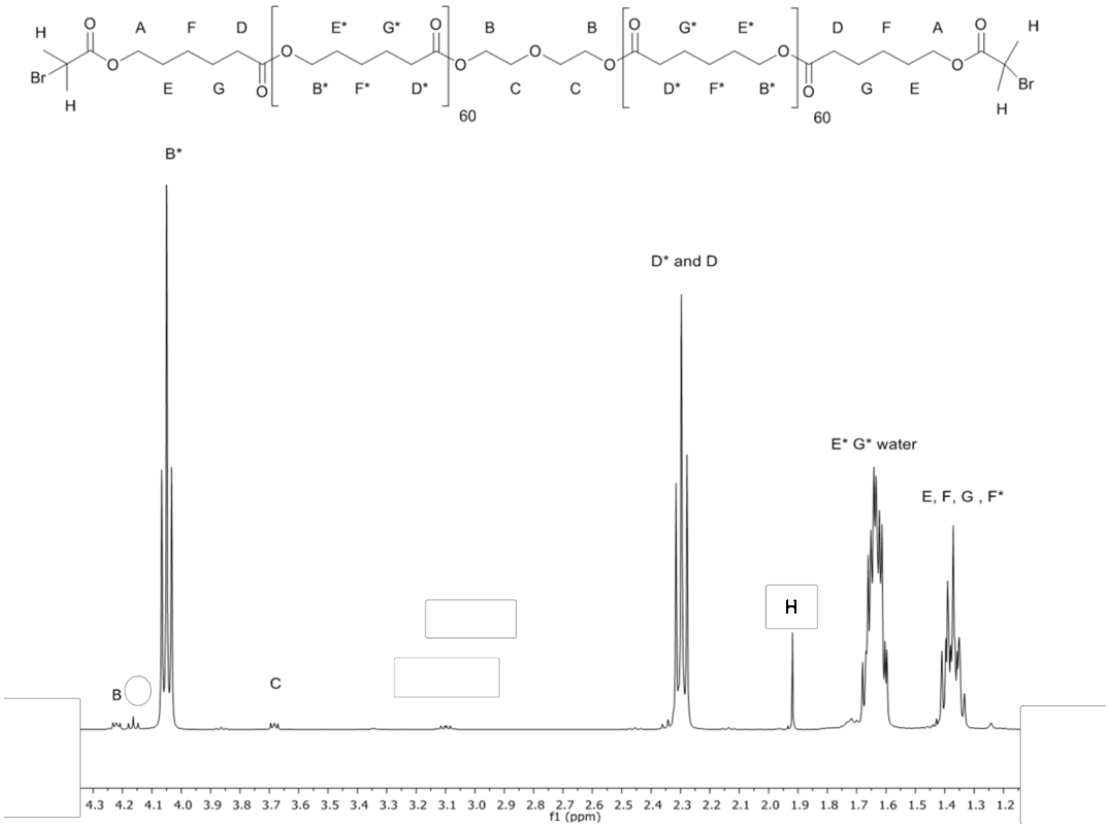

Figure 3-5: ^{1}H-NMR (400MHz, $CDCl_3$) of PCL-Ini

3.3.1.2 Electrospinning of scaffolds with end-functionalised PCL-Ini

To successfully establish surface enrichment of the polymerisation initiating group, we set up the electrospinner with the cathode at the spinneret to convey a positive charge to the surface of the polymer solution. The alkyl-bromide group present within BiBB compound can become electronegative due to its polarity[300], and through electrostatic attraction can migrate through the polymer solution and result in surface presentation of the initiating groups. The PCL-Ini was subsequently electrospun in combination with a high molecular weight PCL to form functionalized fibrous scaffolds which were then imaged by scanning electron microscopy (SEM) to validate consistent fibre morphology. Scaffolds with a high (17% w/w) and a low (9% w/w) concentration of PCL-Ini were electrospun. The addition of up to 17 % (w/w) of the PCL-Ini did not significantly alter the electrospinning process or fibre morphology as imaged on SEM (Figure 3-6).

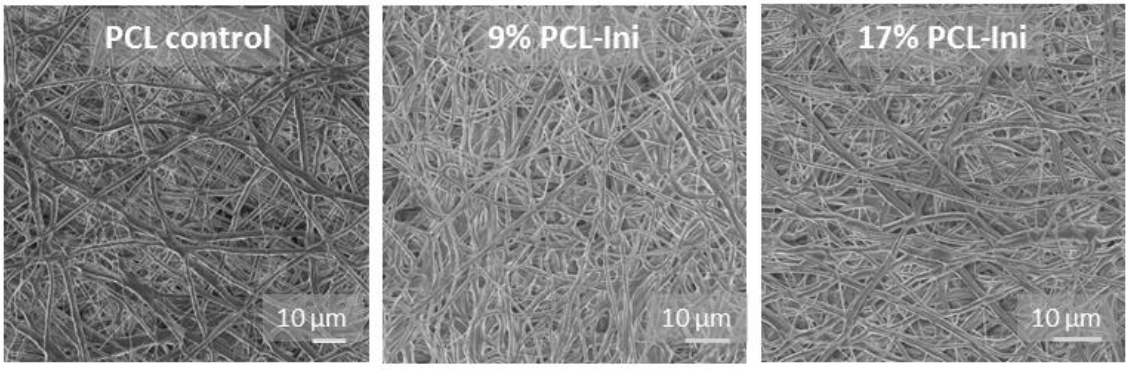

Figure 3-6: SEM images of control PCL scaffolds and modified PCL scaffolds (PCL-Ini) with 9% (w/w) and 17% (w/w).

3.3.1.3 Polymer brush grafting from electrospun fibres

pOEGMA bottlebrushes were grafted from the 3D electrospun scaffolds using the optimised reaction conditions. As with the 2D silicon surfaces, a sacrificial initiator was used in solution in order to target a degree of polymerisation of 150. A typical polymerization achieved a ~75% conversion (by ^{1}H-NMR) and M_n = 45000, M_w 53000 with a dispersity (M_w/M_n) of 1.18 (from size exclusion chromatography, SEC, analysis of the free polymer).

XPS confirmed successful surface initiated grafting of pOEGMA from functionalised electrospun scaffolds as a large increase in the core spectra of the C-O signal is observed following ARGET ATRP for both the 17% (w/w) and 9% (w/w) PCL-Ini scaffolds (Figure 3-7, A). Control scaffolds of unmodified PCL, with no initiating group, were included within the reaction vessel in which the ARGET ATRP of pOEGMA was performed. Following washing and drying, these were also assessed with XPS and demonstrate minimal increase in the C-O signal, thus confirming successful covalent attachment of the polymer to the fibres through the BiBB initiating groups, and the success of the washing steps (ultrasonication in ethanol) for removing any contaminant, unbound polymer. Please see Appendix F for discussion regarding the removal of adsorbed polymer.

The C-O signal intensity as measured by XPS for the 3D electrospun scaffolds (Table 3-2) and the C 1*s* signal breakdown for the 3D electrospun scaffolds (Table 3-3, and Figure 3-7, A) shows that the percentage of carbon within an ether state increases on pOEGMA grafting to PCL. Two independent replicates of each PCL-Ini concentration demonstrate the same trends supporting reproducible results. As shown in the 2D silicon wafers, the XPS data

clearly demonstrates the success of the PCL-pOEGMA functionalization. This success is also supported through the change in water contact angle following pOEGMA polymerisation. Furthermore, these data also supports the successful surface enrichment of the fibres with the alkyl-bromide initiating group following electrospinning as a random distribution amongst within the bulk of the fibres would not have led to a reasonable grafting density of pOEGMA. This conclusion is supported by similar work published from the group demonstrating over-representation of charged polymer-peptide conjugates following electrospinning[301].

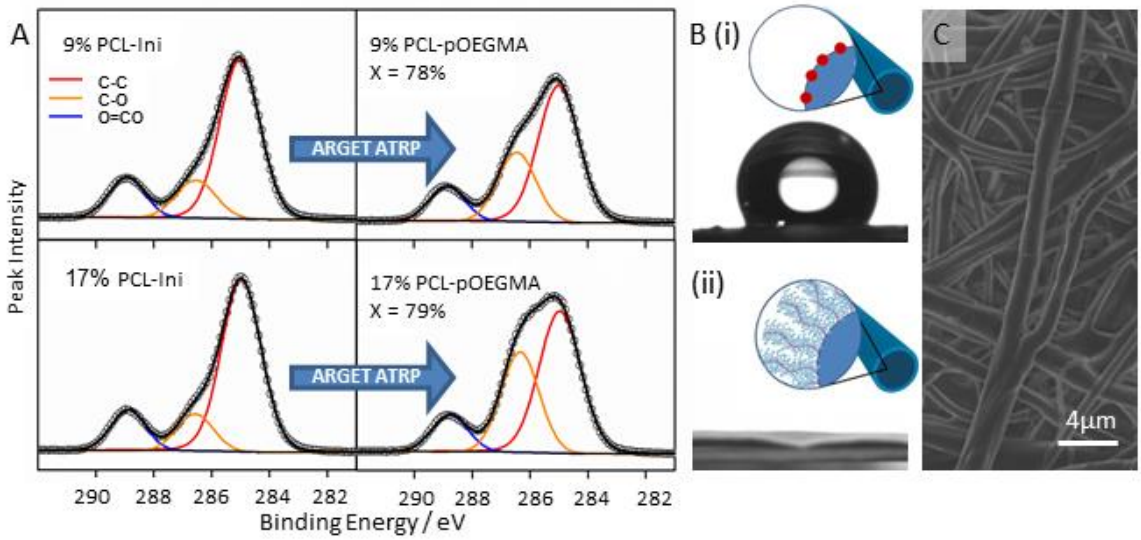

Figure 3-7: Demonstration and characterization of surface initiated polymer brush growth from functionalized 3D electrospun scaffolds, initially published in Harrison *et al.*[282] (A) High resolution C 1*s* core-level spectra of pOEGMA grafting from electrospun scaffolds with 9% and 17% (w/w) PCL-Ini before (left) and after (right) grafting of pOEGMA. Conversion by ^{1}H-NMR (X) is inset. (B) Water contact angle measurement of (i) electrospun PCL/PCL-Ini and (ii) PCL-pOEGMA with inset schematics. (C) Representative SEM micrograph of electrospun PCL-pOEGMA fibres.

Table 3-2: C-O signal intensity of 3D electrospun scaffolds as measured by XPS and the corresponding polymer M_n and $Đ$.

Repeat	+/- ATRP	3D electrospun scaffolds			Polymer characteristics			
		17% PCL[a]	9% PCL-Ini[b]	17% PCL-Ini[b]	X (%)	M_n (theo)[c]	M_n (SEC)[d]	$Đ$ (SEC)
1	-	12.0	15.5	12.9	-	-	-	-
2	-	15.9	9.5	13.6	-	-	-	-
1	+	19.6	27.3	38.2	78	56,200	44,800	1.12
2	+	8.4	34.5	33.9	79	56,900	45,000	1.13

Notes: [a] 17% (w/w) unfunctionalised PCL-diol is used as a control lacking in the polymerisation initiating group (BiBB). [b] Duplicate mats were electrospun at each concentration of PCL and PCL-Ini. [c] Theoretical M_n calculated by ^{1}H-NMR. [d] SEC molecular weight estimated relative to polystyrene standards in DMF without correction to a universal calibration.

Table 3-3: C 1*s* signal breakdown for the 3D electrospun scaffolds as measured by XPS.

		C-C		C-O		O=CO	
Scaffold replicate:	**+/- ATRP**	**1**	**2**	**1**	**2**	**1**	**2**
17% PCL	-	75.5	71.1	12.0	15.9	12.5	13.0
17% PCL-Ini	-	72.2	72.4	12.9	13.6	14.9	14.1
9% PCL-Ini	-	69.5	77.0	15.5	9.5	15.0	13.5
17% PCL	+	65.8	79.9	19.6	8.4	14.6	11.7
17% PCL-Ini	+	52.1	54.5	38.2	33.9	9.7	11.7
9% PCL-Ini	+	60.0	52.9	27.3	34.5	12.7	12.6

Notes: 1 and 2 refer to the replicates used and are the same samples as included in Table 3-2.

A dramatic change in water contact angle following pOEGMA grafting adds further evidence for successful surface grafting of polymer. Hydrophobic electrospun PCL/PCL-Ini scaffold surfaces typically exhibit a contact angle of 113.5° +/- 7.8°. This is completely reversed following pOEGMA grafting with the surface becoming hydrophilic; water droplets immediately wet the surface (Figure 3-7, B).

SEM images were taken of the PCL-pOEGMA functionalised scaffolds to establish whether the surface grafting had resulted in any disruption of fibre morphology. No such change was anticipated due to the expected length of the polymer brush as demonstrated in the 2D system (theoretical polymer length of 24.7 nm and a measured dry thickness of 6.2 nm [+/- 0.038 nm]). SEM imaging confirmed that no demonstrable changes had occurred in the fibre morphology following pOEGMA grafting (Figure 3-7, C).

3.3.1.4 Development of a biotinylated monomer for versatile functionalization of the polymer brush

A biotinylated PEG monomer was designed to allow the confirmation of the density of the polymer brush surface functionalization and to allow the analysis of its distribution through the thickness of the scaffold using fluorescent labelling. The biotinylated PEG monomer was successful synthesised and characterised with ^{1}H-NMR and ESI-MS (Appendix G, Figure 7-2 and 7-3). This monomer unit was also successfully polymerised with pOEGMA to produce p(OEGMA-*co*-biotin) that allowed versatile post-polymerisation functionalization of the polymer brush. I have utilised this for the conjugation of fluorescein-streptavidin allowing for fluorescence visualisation of the polymer brush. The biotin however could be used for the coupling of any streptavidin-coupled moiety, which gives significant flexibility to the system for the addition of further and varied functionality.

3D electrospun scaffolds underwent surface grafting of p(OEGMA-*co*-biotin) and were subsequently labelled, embedded in wax, histologically sectioned and imaged using fluorescent microscopy. These scaffolds, when compared to controls, which here are PCL-pOEGMA functionalised scaffolds (lacking the biotinylated monomer) show clear fluorescein conjugation (Figure 3-8).

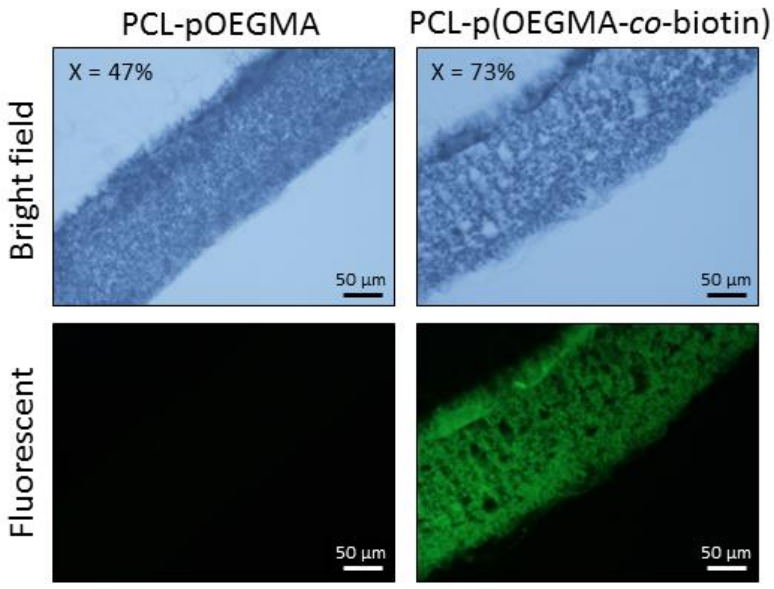

Figure 3-8 Fluorescent labelling and histological sectioning of PCL-pOEGMA and PCL-p(OEGMA-*co*-biotin) scaffolds following incubation with streptavidin-fluorescein, demonstrating even distribution of polymer across the scaffold cross section. Electrospun scaffolds of PCL-Ini 9% (w/w) underwent polymerisation with OEGMA (left) and OEGMA in conjunction with the biotinylated monomer (right) and were both subsequently labelled with streptavidin-fluorescein. Following which, the scaffolds were embedded and histologically sectioned. Bright field images (upper) and fluorescence images (lower) show clear signal on the PCL-p(OEGMA-*co*-biotin) fibres. Conversion of the sacrificial initiator by ^{1}H-NMR in included (X). Initially published in Harrison *et al.*[282].

Bright field images (upper) demonstrate the cross section of the 3D electrospun scaffolds, revealing the internal fibrous structure. Fluorescence imaging reveals clear staining of the PCL-p(OEGMA-*co*-biotin) functionalised scaffolds (lower, right) with minimal signal from the control scaffold (lower, left).

Scaffolds were intentionally stained with streptavidin-fluorescein before being embedded in wax and sectioned for histological analysis. This was done to indirectly assess the permeability and porosity of the scaffold to large molecules as other methods to establish this had been unsuccessful. These representative images demonstrate that the fluorescein signal appears uniform across the thickness of the scaffold and therefore provide evidence that not only is the polymer brush is present throughout scaffolds but there was also no impedance to diffusion of the streptavidin-fluorescein across the scaffold. Together with the histological appearance demonstrating an open porous structure, this result is encouraging that gas and nutrient exchange through the scaffold should be possible.

We further used the biotinylated monomer to further demonstrate that the polymer was indeed covalently bound as opposed to adsorbed onto the PCL fibre surface. 3D electrospun scaffolds, 17% (w/w) PCL-Ini and 17% (w/w) unmodified PCL-diol controls underwent polymerisation within the same reaction vessel to produce pOEGMA-*co*-biotin. The success of the polymerisation was confirmed with ^{1}H-NMR from the sacrificial initiator in solution. Following which, scaffolds were washed with ethanol and dried before being assessed with water contact angle measurements and imaging with fluorescence microscopy following staining with streptavidin-fluorescein. Water contact angle measurements for the control scaffolds remain hydrophobic (Figure 3-9, A) whilst PCL-Ini scaffolds exhibit complete surface wettability. Furthermore, following staining and fluorescent imaging using identical exposure times, the control scaffold demonstrates little signal when compared to the PCL-Ini scaffold. This corroborates the XPS data that the pOEGMA is indeed covalently bound to the 3D electrospun scaffolds through the initiating group.

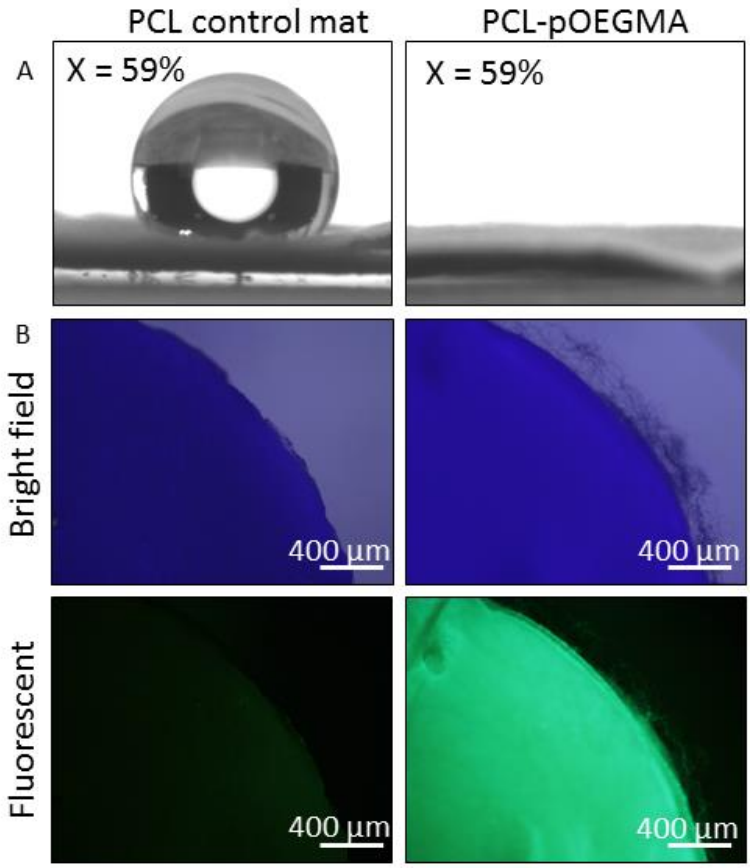

Figure 3-9: Confirmation of covalent attachment of pOEMGA to 3D electrospun scaffolds. (A) Water contact angle images of a control scaffold (with no initiating group) and 17% (w/w) PCL-Ini following polymerisation with OEGMA and the biotinylated monomer. The control scaffold remains hydrophobic after washing, suggesting little remaining surface pOEGMA (A). (B) Electrospun scaffolds of 17% (w/w) PCL-diol (control) and 17% (w/w) PCL-Ini underwent polymerisation with the biotninylated monomer and subsequent streptavidin-fluorescein labelling. Bright field images (upper) and fluorescence images (lower) show minimal signal on control fibres and labelling of pOEGMA-*co*-biotin. Conversion of the sacrificial initiator by ^{1}H-NMR is included (X). Adapted from Harrison *et al.*[282] .

3.3.2 Assessment of the antifouling ability of PCL-pOEGMA scaffolds

Poly (ethylene glycol), and thus, pOEGMA, is known to have antifouling properties and this was a key aspect of the design for this scaffold[302]. 17% (w/w) PCL-pOEGMA scaffolds having achieved a monomer to polymer conversion (X%) of >72% as calculated by ^{1}H-NMR, within the same reaction vessel, were assessed for antifouling ability and resistance to cell adhesion.

3.3.2.1 Adsorption testing of PCL-pOEGMA scaffolds

A panel of biologically relevant fluorescently labelled proteins and GAGs were used to assess the antifouling ability of the pOEGMA surface coating. A panel of biomolecules commonly found either within the ECM, or associated with the musculoskeletal system, was designed to mimic some of the compounds the scaffold would be exposed to *in vivo*. Several, including heparin and BSA, are known to bind and regulate the release of other biomolecules and growth factors. Adsorption of such molecules to a scaffold surface would likely lead to increased biomolecule deposition and ultimately cell adhesion. It is important to note that due to the differences in fluorescent labelling of the molecules the results cannot be compared between compounds, but only within each experiment (PCL control and PCL-pOEGMA scaffold).

pOEGMA scaffolds outperformed 17% (w/w) PCL-diol control scaffolds for both BSA and fibronectin binding, demonstrating a 3.6 fold decrease in binding for BSA, and greater than 10 fold decrease for fibronectin (Figure 3-10). Both CS and heparin had no difference in binding to control and functionalised scaffolds, with both showing a low level of adsorption. Interestingly, HA showed significant preferential adsorption onto the pOEGMA functionalised scaffolds compared to PCL controls ($p < 0.005$, Figure 3-10). HA is commonly combined with various PEG systems in tissue engineered constructs[301,303,304]. HA, a natural lubricant that is found within synovial fluid within the body has desirable properties for scaffolds particularly aimed at cartilage regeneration. Typically scaffolds or hydrogels utilising a HA binding peptide to enhance the HA binding[301,303,304]. Here I have found that the pOEGMA surface functionalization has preferentially bound HA, an unexpected result. Preferential binding of HA could however be advantageous in a scaffold designed for gliding tissue interfaces.

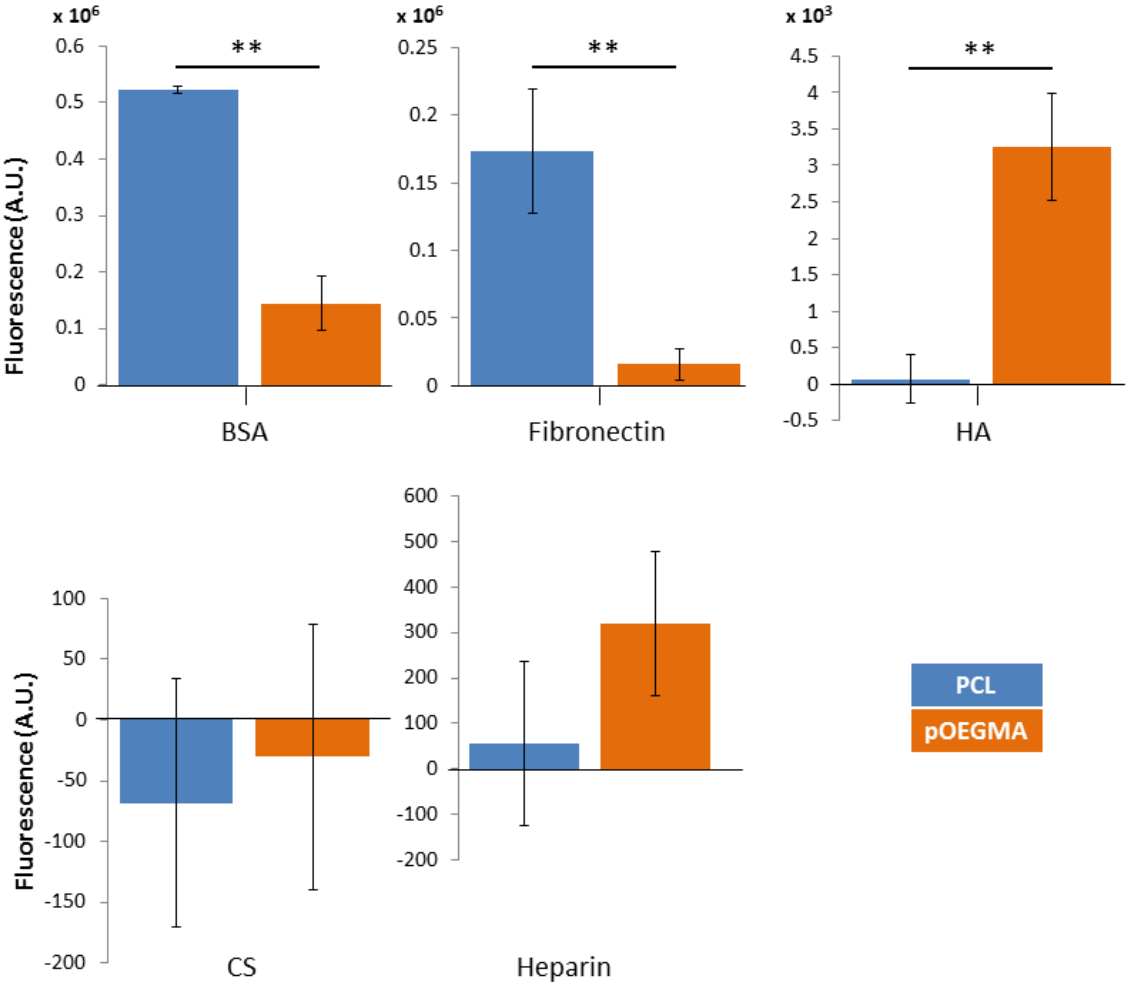

Figure 3-10: Antifouling ability of 17% (w/w) PCL-diol control scaffolds and 17% (w/w) PCL-pOEGMA scaffolds when incubated with a panel of fluorescently bound biomolecules. BSA, fibronectin, HA, CS and heparin were incubated with scaffolds for 18 hours before being washed. Fluorescence from absorbed biomolecules was read using a plate reader. **$p < 0.005$, N = 4 with 3 technical replicates. Error bars show standard deviation.

3.3.2.2 Cell binding assessment of PCL-pOEGMA scaffolds

To successfully create an antifouling scaffold for gliding tissue interfaces it is key that the scaffold can not only resist binding of proteins and GAGs, but also of cells themselves. A cellular adhesion assay was thus performed. Bovine tenocytes, isolated from juvenile animals were isolated and prepared in single cell culture.

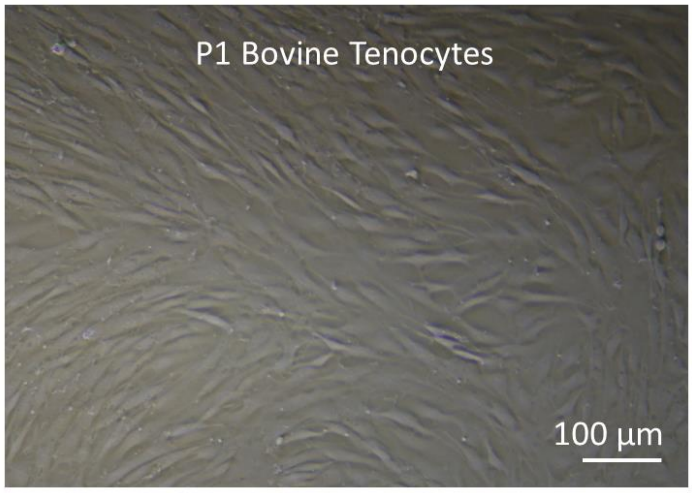

Figure 3-11 P1 bovine tenoytes in culture flasks before seeding on scaffolds.

Scaffolds, both 17% (w/w) PCL-diol control scaffolds and 17% (w/w) PCL-pOEGMA scaffolds were thoroughly washed, and incubated with heavy metal chelating beads to remove any potential copper contamination before use, as this could have led to spurious results. The cells were seeded onto the scaffolds and cultured for 7 days before being assessed to establish how the different surfaces supported cell adhesion and survival.

Fluorescent staining of the cells was used to study their appearance on the scaffolds using confocal microscopy. Tenocytes seeded onto PCL control scaffolds appeared to adhere reasonably well but did not appear to form confluent cell layers which are later seen with cell adhesive groups (Chapter four). Cells appeared to have adhered and spread, but not divided on control PCL scaffolds. In contrast, cells seeded on the PCL-pOEGMA scaffolds were very few in number, and those found exhibited a rounded morphology, indicating poor cell attachment (Figure 3-14). Some of the cells identified also appeared to be within the substance of the scaffold as opposed to the PCL control scaffolds where all cells were visualised on the scaffold surface. The lack of robust attachment to the scaffold, seen on the PCL-pOEGMA scaffolds, as indicated by the rounded cell morphology may have resulted in

the surface cells being washed away while the remaining cells were trapped within the fibrous structure. These observations were compared for the whole scaffolds using an MTT assay to approximate the relative number of cells using a calibration curve (Figure 3-12).

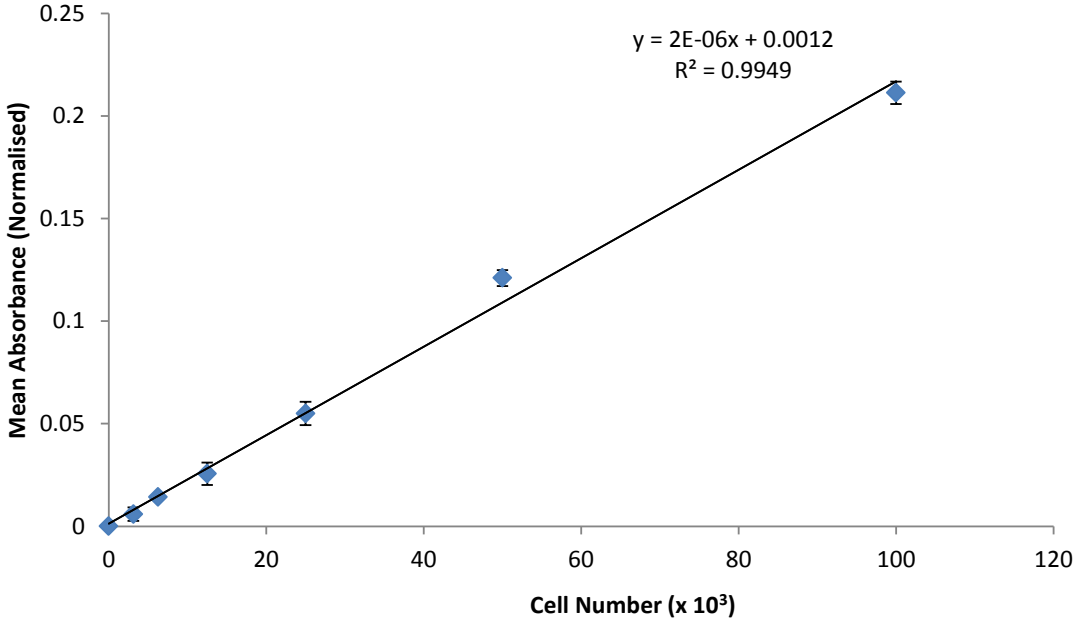

Figure 3-12: An MTT calibration curve was performed to allow the estimation of cell numbers from absorbance signal. Serial dilutions were performed on a single cell suspension of bovine tenocytes to give a series of known cell numbers ranging from 100 000 to 3125 cells. N = 3 with 3 technical replicates using 3 different animals. Normalised means are displayed with error bars showing the standard deviation.

Using the line of best fit, the estimated cell number (x) was calculated from the experimentally derived absorbance (y).

An MTT assay was performed to corroborate the confocal microscopy images and estimate cell number on the scaffolds at 7 days. A DNA assay was attempted to give absolute cell numbers, rather than relying on the MTT assay which measures cellular metabolism rather absolute numbers. This was unsuccessful due to the inability to reliably extract the DNA from the highly binding hydrophobic PCL control scaffolds, thus the MTT assay was used.

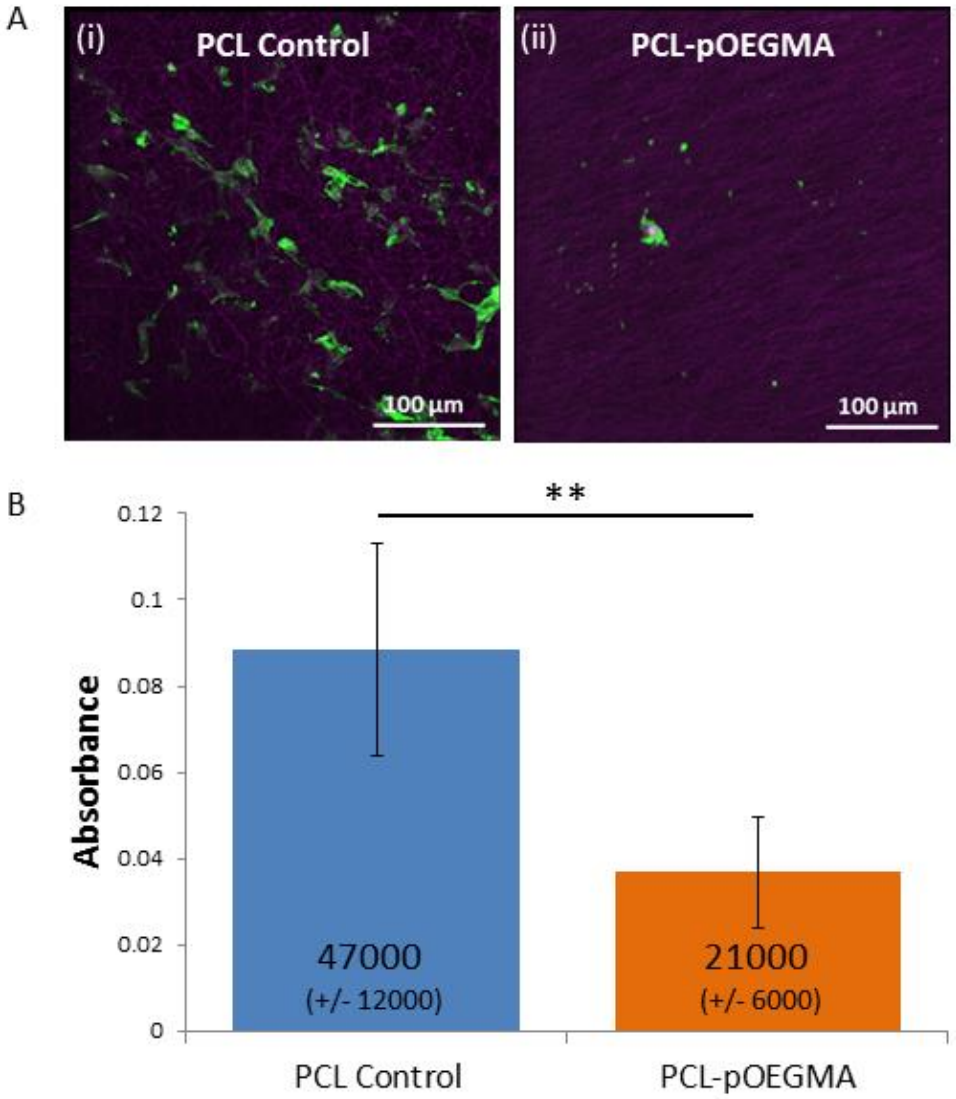

Figure 3-13: Assessment of cell adhesion to antifouling pOEGMA scaffolds and PCL control scaffolds. (A) Representative confocal microscopy images of bovine tenocytes cultured for 7 days on electrospun 17% (w/w) PCL-diol control scaffolds (i) and PCL-pOEGMA scaffolds (ii). Cell nuclei stained with draq5 (purple) and actin with phalloidin (green). (B) Metabolic activity of bovine tenocytes cultured on scaffolds for 7 days was assessed by MTT assay. Estimated cell numbers are stated for each bar. Significant difference ** $p < 0.01$, error bars represent standard deviation. N = 3, with a minimum of 3 internal replicates.

A significant reduction ($p < 0.01$) in the metabolic activity, and estimated number of cells, is seen between the PCL control scaffolds and the PCL-pOEGMA functionalised scaffolds, supporting the confocal microscopy findings. The PCL control scaffolds showed some variability between samples resulting in a wider standard deviation (error bars). The sample number however of a minimum of 3 internal replicates (n = 3), and 3 independent

experimental replicates (N = 3) result in a significant difference between PCL and PCL-pOEGMA being established using both a one-way ANOVA and post-hoc T-test.

The estimated cell numbers by MTT for the PCL-pOEGMA scaffolds are somewhat higher than the appearance of the scaffolds by confocal microscopy would suggest. This reflects the presence of a small number of rounded cellular aggregates seen on the PCL-pOEGMA scaffold surface (Figure 3-14). This indicates preferential cell-cell interactions over cell-surface interactions and is on contrast to the more spread morphology seen on the cells imaged on the control PCL scaffolds, on which no such aggregates were seen.

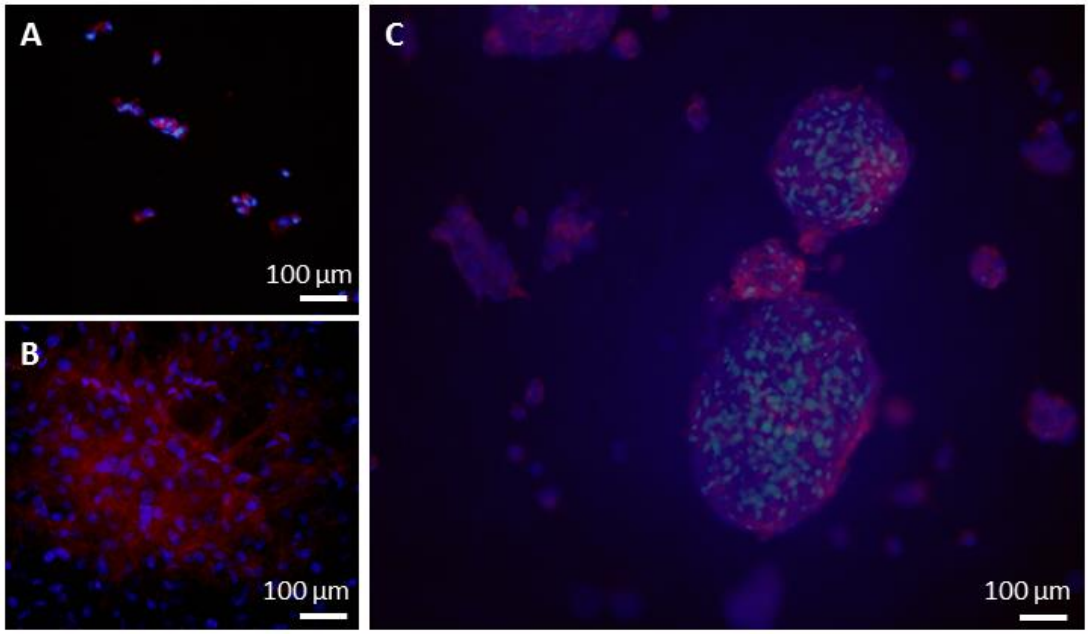

Figure 3-14: Fluorescence microscopy images showing cell morphology on PCL control and PCL-pOEGMA scaffolds after 24 hours in culture. (A) Representative image of bovine tenocytes on PCL-pOEGMA scaffolds (A) and PCL control scaffolds (B). (C) Cellular aggregates were occasionally seen on PCL-pOEGMA scaffolds indicating preferential cell-cell adhesion rather than cell-surface adhesion. Cellular nuclei stained with DAPI (blue) and actin with phalloidin (red).

Through the use of both cell binding and protein/biomolecule binding assays, the PCL-pOEGMA surface functionalization demonstrates superior antifouling ability when compared to PCL scaffolds.

Antifouling OEGMA surfaces from electrospun fibres are not found in the literature beyond this work currently. When compared to similar work using electrospun fibres of with either mixed PCL and PEG, or based on PCL and PEG coupled with ureido-pyr-imidinone (UPy)

units, the antifouling surface presented here exhibits superior resistance to cell attachment[305,306]. This is likely to be due to the high density of PEG presented from the surface presented in this work being much greater than those in the literature. The combination of a surface initiated, grafting from approach, coupled with the use of the OEGMA oligomer leads to the production of an extremely high density bottlebrush coating of PEG.

3.4 Conclusions

Surface initiated grafting of pOEGMA has been reproducibly and reliably achieved using ARGET ATRP from both 2D silicon wafer surfaces, and 3D electrospun fibres. Using a sacrificial initiator in solution the surface polymer properties have been estimated and further explored with state-of-the-art characterisation techniques such as XPS. Functional assays exploring the antifouling properties have demonstrated this to be effective in the reduction of protein, GAG and cell binding to PCL-pOEGMA surfaces. This system will now be exploited to provide an antifouling surface in a spatially controlled manner in a bi-functional scaffold.

References: Chapter 3

282 Harrison, R. H. *et al.* Modular and Versatile Spatial Functionalization of Tissue Engineering Scaffolds through Fiber-Initiated Controlled Radical Polymerization. *Advanced Functional Materials* **25**, 5748-5757, doi:10.1002/adfm.201501277 (2015).

283 Brandl, C., Greiner, A. & Agarwal, S. Quick Polymerization from Electrospun Macroinitiators for Making Thermoresponsive Nanofibers. *Macromolecular Materials and Engineering* **296**, 858-864, doi:10.1002/mame.201100031 (2011).

284 Steedman, H. F. Polyester wax; a new ribboning embedding medium for histology. *Nature* **179**, 1345-1345, doi:10.1038/1791345a0 (1957).

285 Barbey, R., Lavanant, L., Paripovic, D., Schu¨wer, N., Sugnaux C., Tugulu, S., Klok, H. Polymer Brushes via Surface-Initiated Controlled Radical Polymerization: Synthesis, Characterization, Properties, and Applications. *Chem. Rev.* **109**, 5437-5527 (2009).

286 Quinlan, G. J., Martin, G. S. & Evans, T. W. Albumin: Biochemical properties and therapeutic potential. *Hepatology* **41**, 1211-1219, doi:10.1002/hep.20720 (2005).

287 Telford, A. M. *et al.* Micropatterning of Polymer Brushes: Grafting from Dewetting Polymer Films for Biological Applications. *Biomacromolecules* **13**, 2989-2996, doi:10.1021/bm3010534 (2012).

288 Ma, H. W., Li, D. J., Sheng, X., Zhao, B. & Chilkoti, A. Protein-resistant polymer coatings on silicon oxide by surface-initiated atom transfer radical polymerization. *Langmuir* **22**, 3751-3756, doi:10.1021/la052796r (2006).

289 Folkman, J. & Klagsbrun, M. ANGIOGENIC FACTORS. *Science* **235**, 442-447, doi:10.1126/science.2432664 (1987).

290 Norris, D. A., Puri, N. & Sinko, P. J. The effect of physical barriers and properties on the oral absorption of particulates. *Advanced drug delivery reviews* **34**, 135-154, doi:10.1016/s0169-409x(98)00037-4 (1998).

291 Heath, M. D., Henderson, B. & Perkin, S. Ion-Specific Effects on the Interaction between Fibronectin and Negatively Charged Mica Surfaces. *Langmuir* **26**, 5304-5308, doi:10.1021/la100678n (2010).

292 Ma, H. W., Hyun, J. H., Stiller, P. & Chilkoti, A. "Non-fouling" oligo(ethylene glycol)-functionalized polymer brushes synthesized by surface-initiated atom transfer radical polymerization. *Advanced Materials* **16**, 338-+, doi:10.1002/adma.200305830 (2004).

293 Laurent, T. C. & Fraser, J. R. E. HYALURONAN. *Faseb Journal* **6**, 2397-2404 (1992).

294 Arnal-Pastor, M., Martinez Ramos, C., Perez Garnes, M., Monleon Pradas, M. & Valles Lluch, A. Electrospun adherent-antiadherent bilayered membranes based on cross-linked hyaluronic acid for advanced tissue engineering applications. *Mater. Sci. Eng., C* **33**, 4086-4093, doi:10.1016/j.msec.2013.05.058 (2013).

295 Henrotin, Y., Mathy, M., Sanchez, C. & Lambert, C. Chondroitin sulfate in the treatment of osteoarthritis: from in vitro studies to clinical recommendations. *Therapeutic advances in musculoskeletal disease* **2**, 335-348, doi:10.1177/1759720x10383076 (2010).

296 Guex, A. G., Fortunato, G., Hegemann, D., Tevaearai, H. T. & Giraud, M.-N. General protocol for the culture of cells on plasma-coated electrospun scaffolds. *Methods in molecular biology (Clifton, N.J.)* **1058**, 119-131, doi:10.1007/7651_2013_8 (2013).

297 Berridge, M. V. & Tan, A. S. CHARACTERIZATION OF THE CELLULAR REDUCTION OF 3-(4,5-DIMETHYLTHIAZOL-2-YL)-2,5-DIPHENYLTETRAZOLIUM BROMIDE (MTT) - SUBCELLULAR-LOCALIZATION, SUBSTRATE DEPENDENCE, AND INVOLVEMENT OF

MITOCHONDRIAL ELECTRON-TRANSPORT IN MTT REDUCTION. *Archives of Biochemistry and Biophysics* **303**, 474-482, doi:10.1006/abbi.1993.1311 (1993).

298 Yoshikawa, C., Zhang, K., Zawadzak, E. & Kobayashi, H. A novel shortened electrospun nanofiber modified with a "concentrated" polymer brush. *Sci. Technol. Adv. Mater.* **12**, 015003/015001-015003/015007, doi:10.1088/1468-6996/12/1/015003 (2011).

299 Woodruff, M. A. & Hutmacher, D. W. The return of a forgotten polymer-Polycaprolactone in the 21st century. *Prog Polym Sci* **35**, 1217-1256, doi:10.1016/j.progpolymsci.2010.04.002 (2010).

300 Fu, G. D. *et al.* Core-sheath nanofibers from combined atom transfer radical polymerization and electrospinning. *Macromolecules* **41**, 6854-6858, doi:10.1021/ma800499h (2008).

301 Chow, L. W. *et al.* Peptide-Directed Spatial Organization of Biomolecules in Dynamic Gradient Scaffolds. *Advanced Healthcare Materials* **3**, 1381-1386, doi:10.1002/adhm.201400032 (2014).

302 Tugulu, S., Klok, H. Stability and Nonfouling properties of Poly(poly(ethylene glycol) methacrylate) Brushes under Cell Culture Condtions. *Biomacromolecules* **9**, 906-912 (2008).

303 Unterman, S. A. *et al.* Hyaluronic Acid-Binding Scaffold for Articular Cartilage Repair. *Tissue Eng. Part A* **18**, 2497-2506, doi:10.1089/ten.tea.2011.0711 (2012).

304 Singh, A. *et al.* Enhanced lubrication on tissue and biomaterial surfaces through peptide-mediated binding of hyaluronic acid. *Nature Materials* **13**, 988-995, doi:10.1038/nmat4048 (2014).

305 Mollet, B. B. *et al.* A modular approach to easily processable supramolecular bilayered scaffolds with tailorable properties. *J. Mater. Chem. B* **2**, 2483-2493, doi:10.1039/C3TB21516D (2014).

306 Chen, C.-H., Chen, S.-H., Shalumon, K. T. & Chen, J.-P. Prevention of peritendinous adhesions with electrospun polyethylene glycol/polycaprolactone nanofibrous membranes. *Colloids and Surfaces B-Biointerfaces* **133**, 221-230, doi:10.1016/j.colsurfb.2015.06.012 (2015).

Chapter 4: Bilayer scaffolds

Some of the work in this chapter has been previously prepared for publication. The work in this chapter has been previously prepared for publication in "Modular and Versatile Spatial Functionalization of Tissue Engineering Scaffolds through Fiber-Initiated Controlled Radical Polymerization" by **Harrison RH**, Steele JAM, Chapman R, Gormley AJ, Chow LW, Mahat MM, *et al.* published in Advanced Functional Materials in September 2015[308].

4.1 Spatial control of functional groups and bilayer scaffold generation

Native tissues are typically heterogeneous and often exhibit hierarchical organisation. The generation of scaffolds that can mimic such properties is critical for tissue engineering applications and relies on the ability to spatially control functional groups. The ability to produce changing functionality across a scaffold provides differing cues to cells at the cell-scaffold interface and may provide optimised signalling to the cells and ultimately lead to desirable cell behaviour and outcomes. Gliding tissue interfaces, such as the surface of a tendon, ligament or muscle are examples of locations where a scaffold with an antifouling surface and an opposing cell-binding surface may be advantageous, which is discussed fully in chapter one.

Building from the antifouling scaffold presented within this thesis (Chapter 3), a bilayer system was designed and proposed for use at tissue interfaces (Figure 4-1). This was designed initially as a flat sheet with the two faces having opposing bio-functionality, but the flexibility of the design and synthesis steps will provide the ability to produce other architectures in the future. For example, this would include the possibility of a tube with an antifouling inner surface, and a cell binding outer surface which could potentially be used as an artificial blood vessel.

Within this chapter, PCL is firstly end functionalized in separate batches, with the polymerisation initiator (Chapter 3, 3.2.2.1) and the cRGDS peptide. These are then sequentially electrospun into a continuous layered scaffold. Surface initiated polymerisation of pOEGMA is then polymerised within the PCL-Ini layer of the scaffold to produce a spatially defined antifouling surface of the scaffold. Coupled with the PCL-cRGDS layer, this produces a scaffold with opposing antifouling and cell adhesive surfaces.

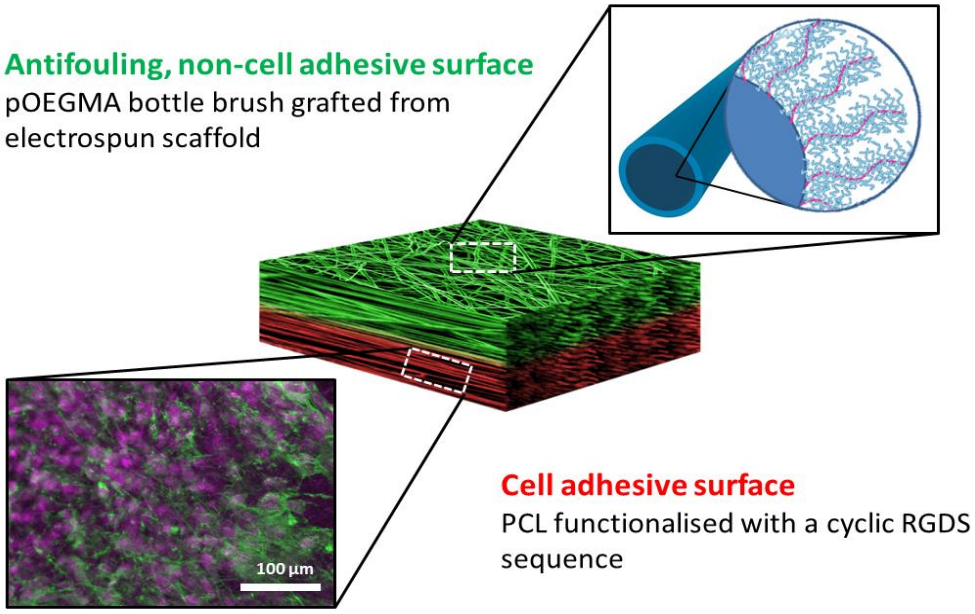

Figure 4-1: The bilayer scaffold design with an antifouling surface and a cell adhesive surface.

4.2 Materials and Methods

4.2.1 Materials

In addition to materials outlined in Chapters 2 and 3, P-maleimidophenyl isocyanate was purchased from (PMPI) Chem-Impex International Inc.

The amino-Cy5 dye used for labelling the cRGDS peptide was kindly synthesised and prepared by Dr Chris Spicer, and is outlined in Appendix H.

All other reagents were supplied from Sigma-Aldrich and were used as received unless specified. Deuterated solvents were used for ^{1}H-NMR and purchased from Merck, (Darmstadt, Germany).

4.2.2 End functionalization of PCL with cyclised RGDS peptide motif

PCL-cRGDS peptide was synthesized using a protocol adapted from the literature[307,309,310]. Dr Lesley Chow kindly performed the synthesis of the cRGDS peptide and coupled the cRGDS to the PCL- maleimide, and the PCL to PCL- maleimide step was performed by myself.

4.2.2.1 Synthesis of cRGDS peptide

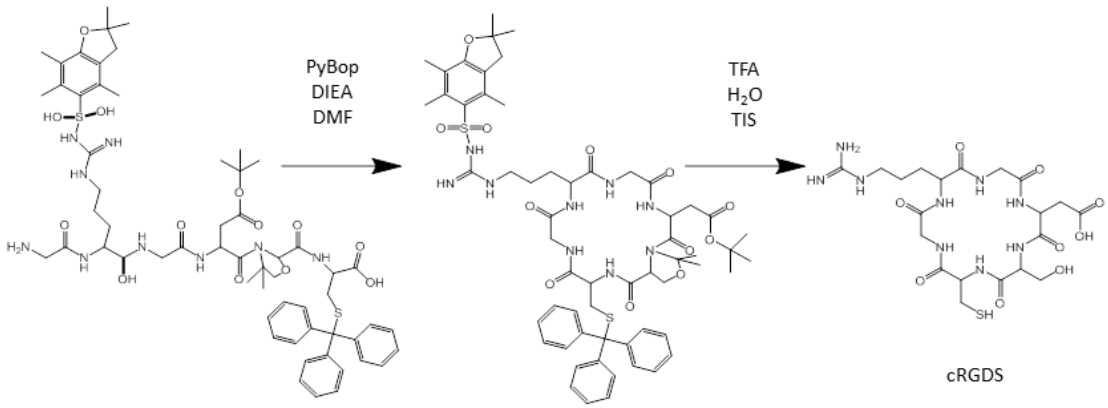

Figure 4-2: Synthesis scheme of cRGDS, adapted from Parmar *et al.* and initially published in Harrison *et al.*[308,309]

In brief, a 2-chlorotrityl chloride resin (100-200 mesh size, VWR) was used to synthesize the cRGDS peptide on a 1 mmol scale. Fmoc-Cys(Trt)-OH (Novabiochem) was dissolved in DCM

at 1M before DMF was added until fully solubilized. Half this solution was mixed with the resin and 500 µL of *N,N*-diisopropylethylamine (DIEA) and the mixture was shaken on a wrist action shaker for 15 minutes. This was repeated with the remaining solution before washing with DMF and DCM. The coupling reaction was tested using a ninhydrin test to detect free amines. Any remaining free amines were capped through the addition of 5% (v/v) acetic anhydride with 2.5% (v/v) DIEA in DMF for 10 minutes with shaking. This was repeated two further times following which the resin was washed with DCM and DMF before a further ninhydrin test was performed. Once no further free amines were identified 20% (v/v) piperidine in DMF was used to remove the Fmoc protecting group. DCM and DMF were then used to wash the resin and Fmoc-Asp(Otbu)-Ser(psiMe, Mepro)-OH (Merck) was coupled at molar ratios of 2:1.95:3 [amino acid]:[HBTU]:[DIEA] in DMF. Any free amines remaining were capped and all other amino acids were coupled using the previously described steps[1,3]. Once completed, the protected peptide was cleaved from the resin using 10 mL of 5% (v/v) trifluoroacetic acid in DCM for 10 minutes with shaking. The solution containing the cleaved peptide was then drained into a round bottom flask and the resin within the peptide vessel washed with further DCM until the solution became clear. The excess solvents were removed with rotary evaporation until approximate 40 mL of solution remained. 10 mL ammonium hydroxide was added to the mixture to neutralize the TFA followed with acetonitrile (ACN) to increase the peptide solubility.

Purification of the protected peptide was undertaken using reverse phase preparative high performance liquid chromatography (HPLC) running a mobile phase gradient of 80% ultrapure H_2O, 20% (v/v) ACN, and 0.1% (v/v) TFA. Rotary evaporation was then used to dry the solution to completeness and the product was then re-dissolved in DMF at 1 1mg mL^{-1}. The peptide was cyclized through the addition of 2 equivalents of benzotriazol-1-yl-oxytripyrrolidinophosphonium hexafluorophosphate (PyBop; AGTC Bioproducts) with 3 equivalents of DIEA overnight. Rotary evaporation was then used to remove the excess solvent and the remaining product dissolved in ACN/H_2O until solubilized. HPLC was then used to purify the cyclized peptide as previously described. The remaining protecting groups were removed using 95% (v/v) TFA with 2.5% (v/v) H_2O and 2.5% (v/v) triisopropylsilane (TIS). The de-protected peptide was precipitated in cold diethyl ether (DEE) and purified again with HPLC. The mass of the final, purified product was confirmed using Liquid

chromatography-mass spectrometry (LC-MS). An Agilent 6130 Quadrupole LC-MS coupled to an Agilent 1260 Infinity LC using a 150 x 4.6 mm Phenomenex Gemini NX C18 column with a 5 µm particle size and 110 Å pore size was used. The mobile phase consisted of ultrapure H_2O and ACN each supplemented with 0.1% (v/v) formic acid (VWR) by volume at a flow rate of 1 ml.min^{-1}. The electrospray source was operated with a capillary voltage of 3.2 kV and a cone voltage of 25 V with nitrogen used as the nebulizer and desolvation gas at a total flow of 600 L/h. The peptide was eluted with a gradient of 95% (v/v) H_2O to 95% (v/v) ACN over 11 minutes. The cRGDS unfortunately did not stick to the column, however electrospray ionization (ESI) of an early elution confirmed the correct mass.

4.2.2.2 Synthesis of end functionalised PCL-cRGDS

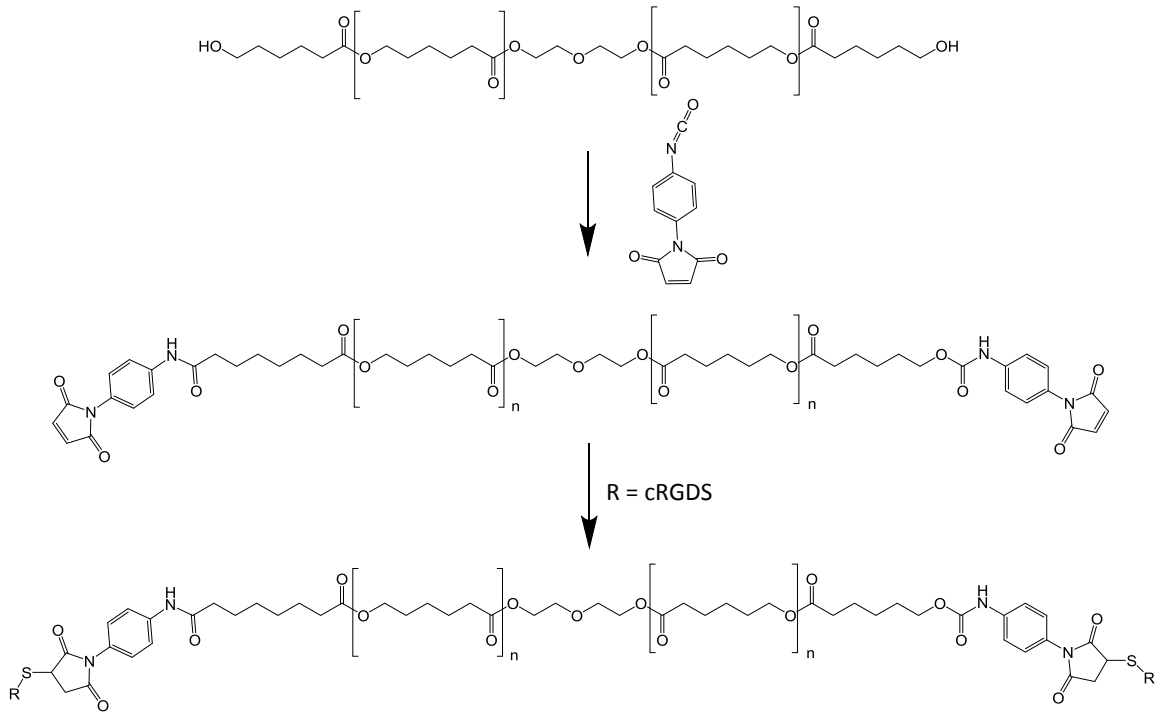

Figure 4-3: Synthesis scheme of the PCL-cRGDS end-functionalised polymer, adapted from Chow *et al.* and initially published in Harrison *et al*[307,308].

The purified cRGDS was conjugated to the PCL using a protocol adapted from the literature[307]. PCL (M_w 14 000, M_n 10 000) was dissolved in anhydrous n-methyl pyrrolidone (NMP) under a nitrogen atmosphere. PMPI was dissolved in further anhydrous NMP in a 15 molar excess and added drop-wise to the PCL solution while stirring and maintaining the

nitrogen atmosphere. The reaction was allowed to progress overnight and the product, PCL-maleimide, was purified through precipitation into cold DEE and washing with H_2O to remove any unbound PMPI before drying *in vacuo.* The PCL-maleimide was dissolved in anhydrous NMP and the cRGDS peptide in DMSO in separate vessels. A 4 fold molar excess of the cRGDS peptide was added dropwise to the PCL-maleimide and allowed to react overnight under a nitrogen atmosphere with stirring. The resultant product, PCL-cRGDS, was purified through precipitation into cold DEE, washed with H_2O to remove any unreacted cRGDS and dried *in vacuo* prior to use. Successful synthesis steps of the solid product were confirmed by ^{1}H-NMR and the final conjugation to form PCL-cRGDS was confirmed by Fourier transform infrared spectroscopy (FTIR) to evaluate the conjugation of the linker and the cRGDS peptide to PCL. FTIR was undertaken with a Perkin Elmer Spectrum One Spectrometer. The spectra were taken with a scanning wavenumber range from 4000 to 650 cm^{-1} and peaks were analysed. FTIR measurements were taken in collaboration with Mr Paresh Parmar who kindly interpreted the data.

4.2.2.3 Electrospinning of PCL-cRGDS

PCL-cRGDS was prepared for electrospinning by preparing a high (3 $mg.mL^{-1}$) and a low (1 $mg.mL^{-1}$) concentration added to two 12% (w/v) PCL (M_n 70,000-90,000 Da) solutions in HFIP and mixed overnight on rollers. The remaining procedure was undertaken using the protocol outlined in Chapter 3 (3.2.3.2). Scaffolds were stored until used in a vacuum dessicator in a centrifuge tube.

4.2.3 Assessment of cell binding of PCL-cRGDS scaffold

PCL-cRGDS (1 $mg.mL^{-1}$ and 3 $mg.mL^{-1}$) scaffolds were assessed for their cell-binding affinity. Cell binding was assessed using the protocol outlined in Chapter 3 (section 3.2.4.2), with some minor modifications.

An initial pilot study was performed that assessed the cell binding using fluorescence microscopy at 24 hours before to select which concentration of PCL-cRGDS provided the optimal cell binding. PCL controls, PCL-pOEGMA and PCL-cRGDS scaffolds were prepared with plates and seeded with cells as outlined in Chapter 2. After 24 hours the scaffolds were removed from the incubator, the media aspirated, and the scaffolds washed with sterile

PBS. The scaffolds were then fixed in 4% (w/v) paraformaldehyde (PFA) for 15 minutes, washed, and stored at 4°C in PBS until used. Immediately prior to imaging, scaffolds were blocked in 1% (w/v) BSA and 0.1% (w/v) tween 20 in PBS for 60 minutes. 4',6-diamidino-2-phenylindole (DAPI, diluted 1:5000, Sigma) and phalloidin (diluted 1:200, Alexa Fluor® 568, Invitrogen) were diluted in 1% (w/v) BSA solution and incubated with the scaffolds for 15 minutes. After washing in PBS the scaffolds were mounted on glass slides before imaging on the inverted optical microscope.

The PCL-cRGDS at 1 $mg.mL^{-1}$ was found to support the most cell attachment and so was used from this point forward for the PCL-cRGDS scaffold. A full cell adhesion study was performed with the 1 $mg.mL^{-1}$ PCL-RGDS scaffolds as outlined in Chapter 3 (section 3.2.4.2).

4.2.4 Layered electrospinning for the production of bilayer scaffolds

The bilayer scaffold was produced from the end-functionalised PCLs (PCL-Ini and PCL-cRGDS) before undergoing assessment to establish whether the advantageous properties of the different polymers had been maintained following the processing steps.

4.2.4.1 Electrospinning bilayer scaffolds

Dual functionality scaffolds were fabricated as a continuous scaffold using a layered electrospinning technique. Two separate solutions of functionalized PCL were prepared in HFIP as above with the addition of 1 mg.mL-1 PCL-cRGDS to one, and 17% (w/w) PCL-Ini to the other. These were sequentially electrospun in accordance with the protocol outlined in Chapter 3 (section 3.2.3.2). The PCL-cRGDS solution (2 mL) was electrospun first before the syringes were rapidly switched over and the PCL-Ini solution was then electrospun onto the fibres already formed (of PCL-cRGDS). This was allowed to run for a further 30 minutes to ensure coverage of the scaffold of both layers.

4.2.4.2 Spatially controlled polymerisation to produce dual functional scaffold

The scaffolds prepared through layered electrospinning underwent surface initiated polymerisation of pOEGMA in a spatially controlled manner. Scaffolds were polymerised using the standardised protocol outlined in Chapter 3 (section 3.2.3.3), with a minor change to the protocol; the reaction was allowed to proceed overnight to mitigate any alteration to the reaction kinetics as a result of the PCL-cRGDS presence in the reaction mixture. Layered scaffolds were prepared with both PCL-pOEGMA and PCL-p(OEGMA-*co*-biotin) for imaging.

4.2.5 Characterisation of bilayered scaffold

Bilayer scaffolds were characterised to ensure that the additional processing steps not performed for the individual polymer scaffolds had not had a detrimental effect on the desirable functional properties seen.

4.2.5.1 Histological cross sections of scaffolds to demonstrate spatial control of functional groups

Bilayer scaffolds were embedded in waxed, sectioned in wax, stained and imaged to demonstrate the spatial control of the functional groups within the electropsun scaffold. Bilayer scaffolds functionalised with a PCL-p(OEGMA-*co*-biotin) surface, as described in Chapter 3 (section 3.2.3.4), were taken and embedded in polyester wax and sectioned at 10 µm onto glass slides and dewaxed as described in Chapter 3 (section 3.2.3.5). Sections were immobilised onto glass coverslips with an inert adhesive at either end (Aquarium Sealant, King British^{TM}, Gainsborough, UK) that was allowed to cure overnight on the bench.

The sectioned scaffolds were incubated the following day in 0.2% (w/v) tween 20 / 0.2% (w/v) triton X in PBS for 1 hour before being washing in UHQ water and the excess blotted away with filter paper. The cRGDS moiety was labelled first using the amino-Cy5 dye (synthesis outlined in Appendix H). The pure dye was taken and diluted to 0.1 mM in 20 mM sodium borate buffer solution at pH 9, and combined with 1-ethyl-3(3-dimethylaminopropyl)carbodiimide (EDC) (2 mM) and *N*-hydroxysuccinimide (NHS, 2 mM). This solution, when thoroughly mixed, was then applied to the immobilized scaffolds and the reaction allowed to proceed on the bench at room temperature for 30 minutes, protected from light, following which the scaffolds were washed with 20 mM sodium borate buffer, UHQ H_2O, 0.2% (w/v) tween 20 / 0.2% (w/v) triton X solution, UHQ H_2O, 50% (v/v) IPA, 100% IPA, 50% (v/v) IPA and further UHQ H_2O. The scaffolds were then blocked and labelled with fluorescein-streptavidin as previously described in Chapter 3 (section 3.2.3.5). Sections were imaged on an upright Olympus BX51 epifluorescence microscope equipped with an Olympus DP70 camera. Images were obtained in three channels: Bright field, FITC to image the fluorescent brushes, and TxRed to image the Cy5 labelling of cRGDS. Images were processed and overlaid using ImageJ software.

4.2.5.2 Cell binding assay for assessment of dual functionality of the bilayer scaffold

Cell binding assays were performed on the PCL-cRGDS and bilayer scaffolds using a similar protocol to that used to assess the PCL and PCL-pOEGMA functionalised scaffolds. This was undertaken to firstly assess the cell binding affinity of the PCL-cRGDS scaffold and secondly to establish whether the properties of the constituent parts had been retained following the layered electrospinning and polymerisation process, namely the antifouling aspect of the pOEGMA surface and the cell-binding cRGDS surface.

Using the protocol outlined in Chapter 3 (section 3.2.4.2.2) 24-well plates were prepared with a two-component silicone elastomer and cured. From the PCL-cRGDS master electrospun scaffold, seven individual scaffolds were made using a 6 mm biopsy punch. Three bilayer scaffolds that had previously undergone ARGET ATRP polymerisation, and had been thoroughly washed and dried, were taken. The well plates, scaffolds and pins were prepared and sterilized using ethanol and UV light as previously described.

Bovine tenocytes were prepared as previously described prepared in a single cell suspension at a concentration of $5x10^5$ cells mL^{-1} from which 50 µL ($2.5x10^4$ cells) were seeded onto each scaffold. The plates were returned to the incubator to allow cell attachment. After 30 minutes the bilayer scaffold was removed from the incubator, and using sterile instruments and an aseptic technique, the scaffold was gently turned over and a further $2.5x10^4$ cells were seeded on the opposite surface. The scaffold was then re-immobilised in the silicone-coated well plate and positioned to ensure that there was free space for media below the scaffold (between the scaffold and the silicone elastomer base of the well plate). The plate was returned to the incubator and a further 2 hours allowed for cell attachment before NGM was added as per protocol. The PCL-cRGDS scaffold was managed as previously outlined with NGM being added after 2 hours.

The scaffolds remained in culture for 7 days with NGM being refreshed after 4 days. At this point, the PCL-cRGDS scaffolds were removed and subjected to the same assessment as previously outlined in Chapter 3, namely MTT assay for the assessment of cellular metabolism and an estimation of cell number, and imaging with fluorescence and confocal microscopy.

The bilayer scaffolds were fixed and stained before imaging with fluorescence and confocal microscopy. Scaffolds were immersed in 4% (w/v) PFA and blocked in 1% (w/v) BSA and 0.1% (w/v) tween 20 as previously described. The scaffolds were then stained with DAPI (diluted to 1:5000, Sigma) and phalloidin (diluted 1:200, Alexa Fluor® 568, Vector Laboratories) in PBS at pH 8.4 for a further 15 minutes. After washing in PBS the scaffolds were mounted on glass slides with Fluorosave™ mounting media and coverslipped. Slides were protected from light before being imaged on both surfaces.

4.2.6 Statistical Analysis

All experimental test groups had a sample size of at least N = 3 for biochemical analysis. All cell-related work was repeated with bovine tenocytes from three different animals. Data is presented as mean +/- standard deviation (SD). Statistical significance is determined using a one-way ANOVA with an alpha value of 0.05 and a post-hoc student's T-tests using Excel software with a significance accepted where p-value < 0.05.

4.3 Results and Discussion

In order to maintain the precise spatial control of cell binding we elected to use techniques that allowed the coupling of functional groups to PCL prior to electrospinning. This is in contrast to a number of approaches in the literature where bulk functionalization of scaffolds has been achieved either after electrospinning[311-317], during the electrospinning process[318] or with multiple functional groups mixed within the bulk scaffold[319]. As discussed in section 1.3.3, the approach presented in this work provides considerable control over the spatial location of the groups and the advantage that the production of bi- or multi-layered constructs is possible.

4.3.1 End functionalization of PCL with cyclised RGDS peptide motif

A cell adhesive PCL, PCL-cRGDS, was designed, synthesised and characterised to provide the cell adhesive layer of the planned bilayer scaffold. In order for the bilayer scaffold to be successful it was essential that the PCL-cRGDS scaffold was possible to electrospun with fibres morphologically similar to the PCL-Ini fibres. Furthermore, the surface presentation of the cRGDS peptide motif following the electrospinning process would be essential to their functioning as cell-adhesive fibres.

The canonical peptide sequence Arg-Gly-Asp-Ser (RGDS) was selected as a model cell-adhesive biomolecule that is known to promote cell-adhesion through integrin binding[320]. Fibroblasts, of which tenocytes are a specialised form, are also known to bind well to RGDS giving support to the choice of biomolecule[319]. The cyclised form of the RGDS ligand (cRGDS) was chosen specifically to be coupled to PCL as it provides the native presentation of the ligand, as found in fibronectin[321].

PCL was conjugated to cRGDS and was electrospun into scaffolds using the standard procedure. SEM was performed on a Phenom FEI (Phenom-World B.V., Netherlands) with a 10 nm chromium sputter coating to confirm no alterations to fibre morphology. Following which, the cell-adhesive properties of the PCL-cRGDS were assessed and compared to the PCL-pOEGMA scaffolds discussed at length in Chapter 3, section 3.3.2.2.

4.3.1.1 Synthesis of cRGDS peptide

The cRGDS product was synthesised and characterised with ESI, producing a dominant peak of 576.2, expected MW 577 (Figure 4-4).

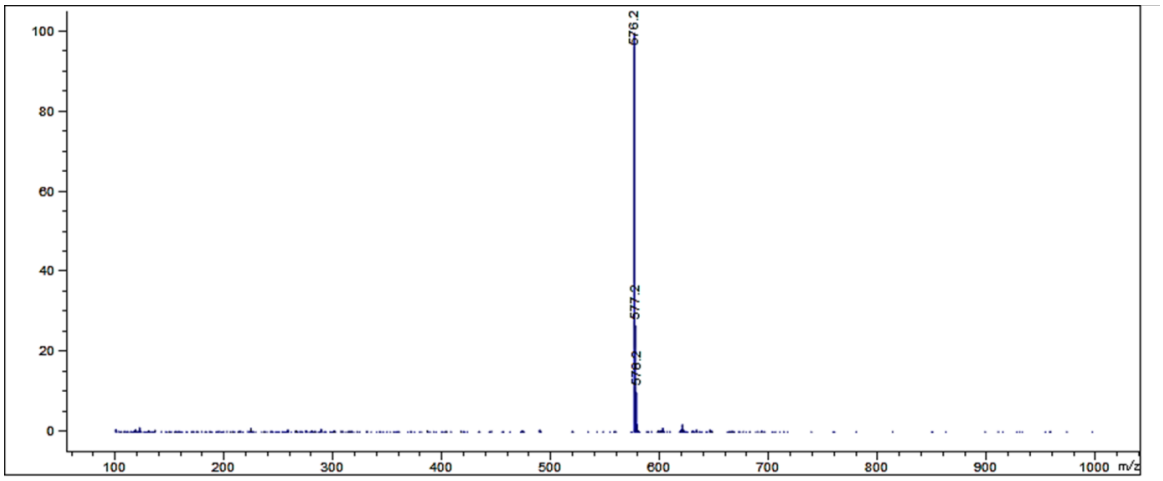

Figure 4-4: ESI of the cRGDS peptide confirming the correct mass of the product (MW 577) which is from the same batch previously published in Parmar *et al.*, Figure S3[309] and in Harrison *et al.*, Figure S8[308].

Following the confirmation of the product, the cRGDS was then coupled to PCL-diol to produce end-functionalised PCL-cRGDS.

4.3.1.2 Synthesis of end functionalised PCL-cRGDS

Synthesis steps of the solid product were confirmed by ^{1}H-NMR with the final conjugation to the PCL confirmed with Fourier transform infrared spectroscopy (FTIR). The FTIR spectra were taken with a scanning wavenumber range from 4000 to 650 cm^{-1} and peaks were analysed. The IR transmittance peaks at 3250 cm^{-1} and at 1630 cm^{-1} (the amide bonds C=O, boxed) are present in the cRGDS purified peptide and the PCL-cRGDS, but not the control PCL-diol and demonstrate successful conjugation (Figure 4-5).

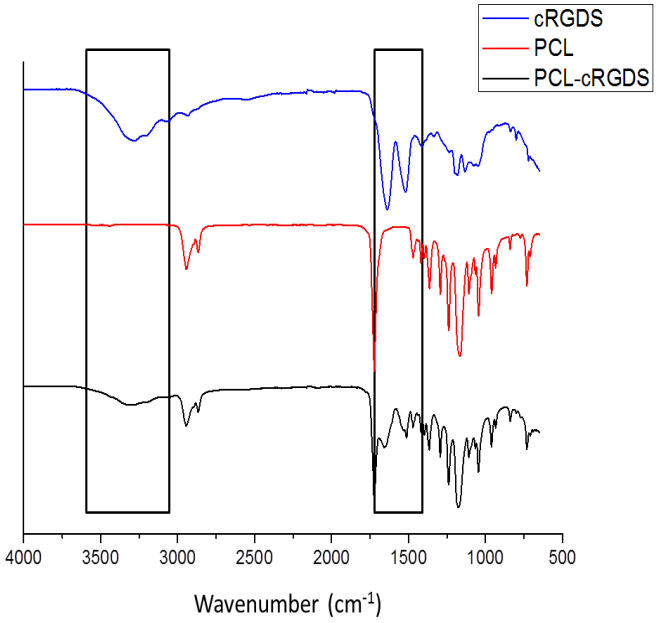

Figure 4-5: FTIR of the solid PCL-cRGDS, cRGDS, and control PCL-diol demonstrating successful coupling of the cRGDS to the PCL through the demonstration of the amide (C=O) bonds (boxed). Initially published in Harrison *et al.*[308].

4.3.1.3 Electrospinning of PCL-cRGDS

The PCL-cRGDS was electrospun using the same procedure for the PCL-Ini scaffolds. Importantly, the resultant fibres were imaged using SEM and demonstrate no difference in the fibre morphology following the addition of the cRGDS moiety when compared to controls (Figure 4-6). The addition of the PCL-cRGDS, as for the PCL-Ini appears to make no difference to the fibre formation during electrospinning (Figure 3-6). This allows for the same operating procedure to be carried out for all the electrospinning presented in this thesis. This is particularly important for the layered electrospinning when the syringes need to be swapped rapidly to ensure good fusion of the layers. Changes in topography are known to provide cues for cell behaviour[322,323]. The elimination of this variable allows for a fair comparison of cell behaviour between the PCL-pOEGMA and PCL-cRGDS surfaces.

Previous work by Gentsch *et al.* demonstrated surface enrichment of the RGDS motif when the spinneret is positive, which reflects the polarity of the electrospinning set up used in this work[324]. Gentsch *et al.* electrospun polymer-peptide conjugates of poly(lactic-*co*-glycolic acid) and a poly(L-lactic acid)-*block*-CGGRGDS peptide, the linear version of the cRGDS used in this work, leads to a surface enrichment of the peptide as shown by XPS. It is therefore expected that the cRGDS peptide would be similarly surface enriched in this work.

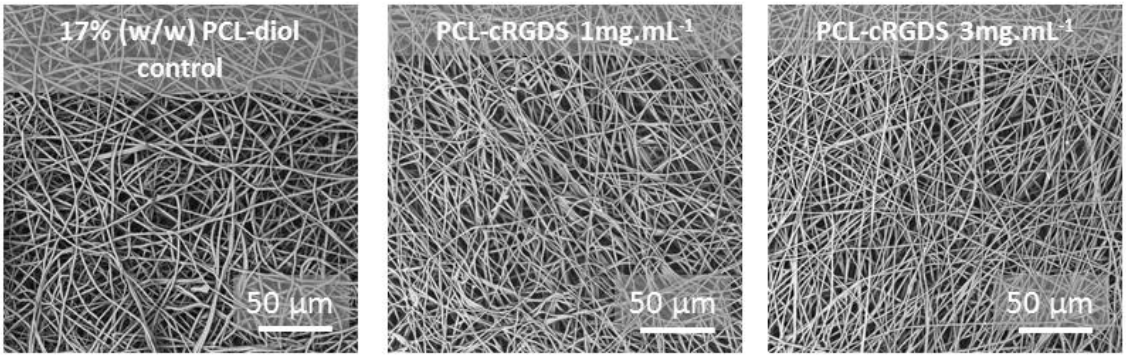

Figure 4-6: Representative SEM images of a control PCL scaffold (PCL-diol, left), and scaffolds modified with PCL-cRGDS in a low (middle) and high (right) concentration demonstrating no difference in fibre morphology following the addition of the cRGDS moiety.

4.3.2 PCL-cRGDS scaffolds promote cell adhesion of tenocytes

A pilot study was performed to assess the cell binding affinity with bovine tenocytes to the electrospun PCL-cRGDS scaffolds. A high (3 mg.mL^{-1}) and low (1 mg.mL^{-1}) concentration of PCL-cRGDS peptide were compared for cell binding affinity before one was selected and taken forward to produce the bilayered scaffold system.

The PCL-cRGDS end-functionalised polymer was electropsun in a high (3 mg.mL^{-1}) and a low (1 mg.mL^{-1}) concentration with a high MW PCL. Bovine tenocytes were seeded on sterile PCL-cRGDS scaffolds and cultured for 24 hours before undergoing fixation, staining, and imaging with fluorescence microscopy. The low (1 mg.mL^{-1}) concentration PCL-cRGDS scaffolds exhibited superior cell binding in line with previous findings in our research group and from this point forward were used for the PCL-cRGDS scaffolds (Figure 4-7).

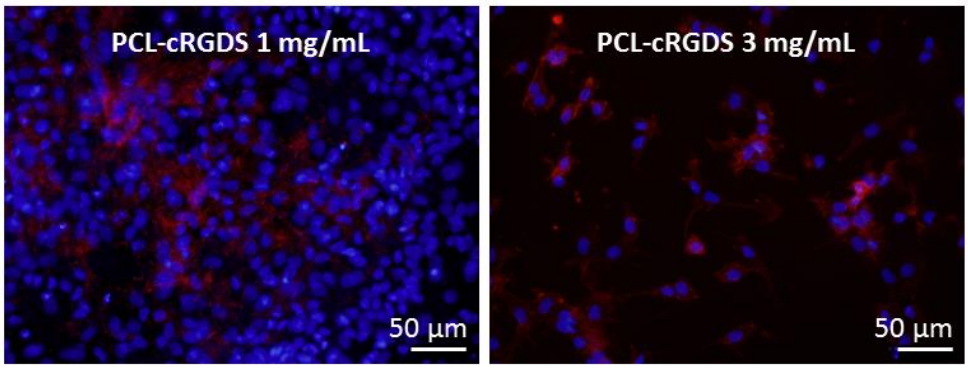

Figure 4-7: Representative fluorescence microscopy images of bovine tenocytes seeded on PCL-cRGDS electrospun scaffolds at a high (3 mg.mL-1) and a low (1 mg.mL-1) PCL-cRGDS concentration. Bovine tenocytes were seeded onto scaffolds and cultured for 24 hours before assessment. Cells were stained with DAPI (blue, cell nuclei) and phalloidin (red, cell actin) and imaged on a fluorescence microscope.

Having established an effective concentration of PCL-cRGDS to use, the full cell-adhesion assay was performed and compared to the PCL-pOEGMA scaffolds, the results of which are discussed in Chapter 3 (section 3.3.2.2). The PCL-pOEGMA results from that experiment are included here for comparison to the PCL-cRGDS scaffolds. Bovine tenocytes were seeded and cultured on scaffolds for 7 days before fixing, staining and imaging with confocal microscopy and assessment of cell metabolism with the MTT assay.

A significant difference is demonstrated between the PCL-cRGDS and PCL-pOEGMA scaffolds. Tenocytes seeded onto the PCL-cRGDS scaffolds adhered well, forming a confluent layer on the scaffold surface and exhibiting a spread morphology indicating good cell-scaffold adhesion (Figure 4-8). In contrast, as previously discussed in 3.3.2.2, the cells seeded on the PCL-pOEGMA scaffolds are few in number, tend to be within the scaffolds rather than on the surface, and are of a rounded appearance indicating a poor cell-scaffold adhesion.

A highly significant different is also seen in the MTT assay assessing the metabolic activity of the cells supported by the PCL-cRGDS and PCL-pOEGMA scaffolds using both a one-way ANOVA and *post hoc* T-test (p value < 0.0001) at 7 days, supporting the confocal microscopy findings. Using the cell calibration curve (Chapter 3, Figure 3-12), the number of cells supported by the scaffolds is estimated. The PCL-cRGDS scaffold is estimated to support approximately double the number of cells compared to the PCL-pOEGMA scaffold. As discussed in Chapter 3 (3.3.2.2), the PCL-pOEGMA cell number is predicted to be higher than

expected from the images due to the presence of infrequent, cell aggregates that were identified. For our anticipated use of this scaffold, at a gliding tissue interface, these aggregates are unlikely to be found due to the movement across the surface due to the gliding action, which would likely result in any loosely bound cells becoming detached.

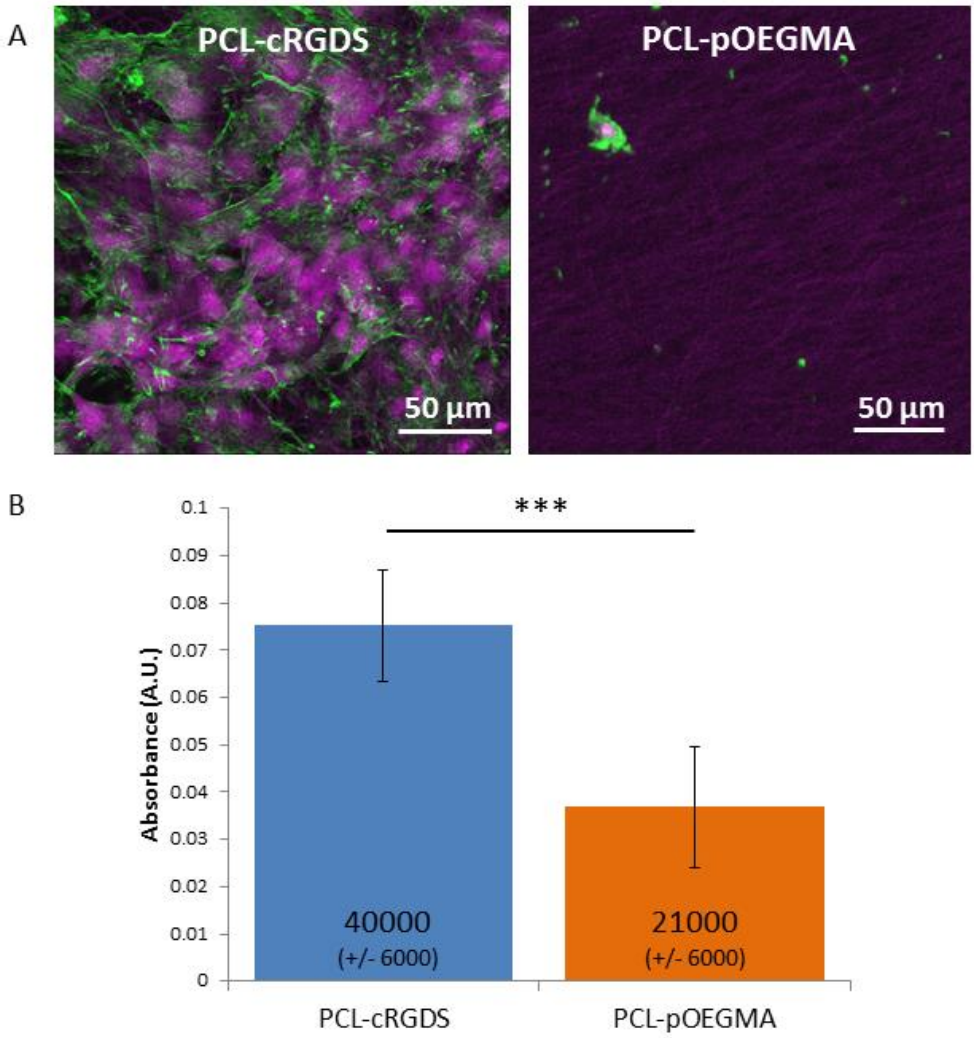

Figure 4-8: Cell-adhesive and non cell-adhesive properties of functionalised electrospun scaffolds, initially published in Harrison *et al.*[308] (A) Representative images of bovine tenocytes cultured on electropsun PCL-cRGDS and PCL-pOEGMA scaffolds for 7 days. Cell nuclei stained with draq5 (purple) and cell actin with phalloidin (green). (B) Metabolic activity of bovine tenocytes cultured on scaffolds for 7 days is assessed by MTT assay. Estimated cell numbers are stated for each bar. * Significant difference (p <0.0001), N = 3 with 5 internal replicates.**

4.3.3 Spatially controlled polymerisation within electrospun scaffolds

In order to create a bilayered scaffold with a cell adhesive surface and an opposing antifouling, non-cell adhesive surface, PCL was initially end functionalised with either a polymerisation initiator (Ini) or a cell adhesive peptide (cRGDS). These functional groups were then sequentially electrospun in layers within a continuous construct to produce scaffolds with opposing surface functionalities.

Through the control of the spatial location of the PCL-Ini polymer, it is hoped that the location of the antifouling polymer brush will be controlled within the scaffold structure. pOEGMA bottlebrushes were then grafted from the PCL-Ini layer of the bilayer scaffolds with no apparent detriment to the control of the polymerisation or the monomer to polymer conversion of the reaction when the reaction was allowed to proceed overnight. A conversion (X) as calculated by ^{1}H-NMR was 78%. The bilayer scaffolds were then characterised to establish whether spatial control of the functional groups had been achieved, and whether the material characteristics of the layers had been maintained following the processing steps.

4.3.4 Characterisation of bilayered scaffold

Bilayer scaffolds were interrogated and characterised. Firstly, histological sectioning, staining, and imaging were used to label the functional groups to demonstrate their spatially discrete locations within the scaffold structure. Then cell binding was assessed with a cell binding assay to ensure the functionality of the individual layers of the scaffold had been preserved.

4.3.4.1 Histological cross sections of scaffolds to demonstrate spatial control of functional groups

To confirm the spatial location of the functional groups two specific fluorescent tags were used to demonstrate the locations of the different moieties. To label the pOEGMA antifouling layer, the biotin PEG monomer was used to produce a p(OEGMA-*co*-biotin) bottlebrush that would allow labelling with streptavidin-fluorescein. To visualise the PCL-cRGDS, a Cy5 dye was modified with an amine to give amino-Cy5 that would allow a reaction onto a carboxylic acid. The only carboxylic acid found within this system is on the aspartic acid (D) residue side chains exposed on the PCL-cRGDS fibres.

Histological sections of the bilayer scaffolds were labelled to illustrate the discrete functional group locations and decisively and clearly demonstrate successful spatial control of the different functionalities within the substance of a single construct when imaged using fluorescence microscopy (Figure 4-9). Furthermore, the amino-Cy5 dye provides clear labelling of the cRGDS moiety within the scaffold.

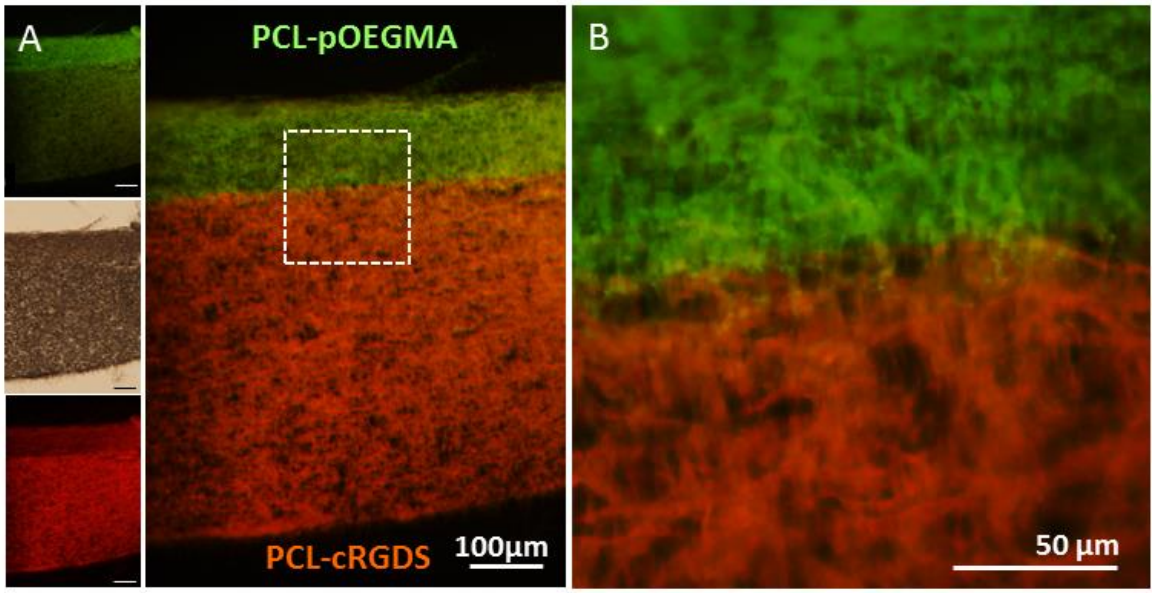

Figure 4-9: Dual functionality scaffolds demonstrated by fluorescent labelling of functional groups, adapted from Harrison *et al.*[308]. Fluorescence microscopy images of cross sections of bilayered scaffolds formed with opposing PCL-Ini and PCL-cRGDS electrospun fibre layers. Post-processing polymerisation was used to produce a PCL-p(OEGMA-*co*-biotin) surface (A-B). Overlaid fluorescence images of histological cross sections labelled with streptavidin-fluorescein (green) on the p(OEGMA-*co*-biotin) and with Cy5 (red) for the PCL-cRGDS show well defined spatial resolution of the moieties. Insets (left) show the bright field and single channel fluorescence images with 100 µm scale bars.

4.3.4.2 Cell binding assay for assessment of dual functionality of the bilayer scaffold

To ensure that the biofunctionality of the opposing surfaces was preserved through the processing and polymerisation steps, the cell binding assay that had previously been used to characterise the PCL-pOEGMA and PCL-cRGDS scaffolds was applied to the bilayer scaffolds. Bovine tenocytes were seeded on both sides of the bilayer scaffolds and cultured for 7 days. The scaffolds were then stained with DAPI to label the cell nuclei (blue) on both sides of the scaffold and fluorescent imaging was performed on one side of the scaffold, before gently turning it over and imaging the opposite side (Figure 4-10). The resultant images clearly demonstrate the maintained biofunctionality that was intended, with a cell adhesive surface and an opposing antifouling surface.

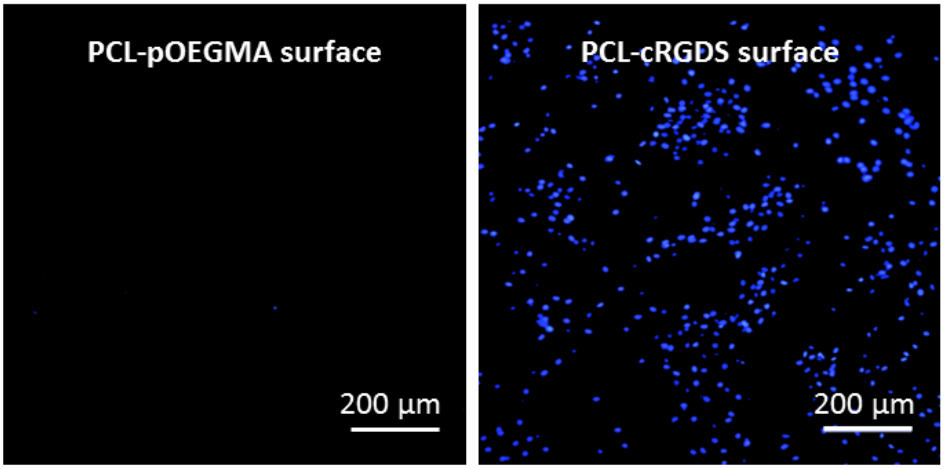

Figure 4-10: Representative images of bovine tenocytes seeded on bilayer scaffolds following post-processing polymerisation and 7 days of tissue culture before being stained with DAPI (blue) for cell nuclei and imaged with fluorescence microscopy. Cell adhesion is supported by the PCL-cRGDS surface and only minimally by the PCL-pOEGMA surface of the scaffold.

This work demonstrates superior results when compared to previous cell adhesive and non-cell adhesive bilayer scaffolds presented in the literature; a more pronounced difference is seen between the cell binding and antifouling surfaces with regard to their cell binding affinity. The antifouling face of the scaffold in particular outperforms previously published work, such as that by Mollet *et al.*[325]. This is likely due to a number of key factors incorporated into this design. Mollet *et al*. used a linear PEG-diol, with UPy end groups, that was mixed into PCL prior to electrospinning for the antifouling surface. Our approach likely results in a superior antifouling performance due to a number of factors that result in a higher concentration of PEG being present on the scaffold surface. By electing to electrospun PCL-Ini, we firstly have maximised the surface enrichment of the initiating group due to the polarity of the end group and set up of the electrospinning apparatus (discussed fully in Chapter 3, 3.3.1.2). Secondly, our use of the PEG methacrylate monomer unit (OEGMA), rather than a linear PEG, produces a bottle brush structure giving rise to a considerable increase in concentration of PEG presented at the surface. Coupled with the employment of a post-electrospinning *grafting from* approach, whereby steric hindrance is avoided, a high density of polymer brushes results with the presence of no further end groups that may hinder the action of the PEG for antifouling.

4.4 Conclusions

Excellent spatial control of functionalised polymer has been produced through layered electrospinning and post-processing with the grafting of pOEGMA bottlebrushes. This has generated a scaffold with an antifouling surface and an opposing cell adhesive surface. This has been clearly demonstrated through fluorescence microscopy with the sharp transition between fibres clearly visible with fluorescent labelling and furthermore, the functionality of the opposing surfaces with regard to cell adhesion has been maintained. This technique of sequential electrospinning of end-functionalised polymers is shown to be a highly effective method for providing spatial control within a single construct. This could be used to generate more complex architecture of spatially controlled functional groups within a tissue scaffold.

References: Chapter 4

307 Chow, L. W. *et al.* Peptide-Directed Spatial Organization of Biomolecules in Dynamic Gradient Scaffolds. *Advanced Healthcare Materials* **3**, 1381-1386, doi:10.1002/adhm.201400032 (2014).

308 Harrison, R. H. *et al.* Modular and Versatile Spatial Functionalization of Tissue Engineering Scaffolds through Fiber-Initiated Controlled Radical Polymerization. *Advanced Functional Materials* **25**, 5748-5757, doi:10.1002/adfm.201501277 (2015).

309 Parmar, P. A. *et al.* Collagen-mimetic peptide-modifiable hydrogels for articular cartilage regeneration. *Biomaterials* **54**, 213-225, doi:10.1016/j.biomaterials.2015.02.079 (2015).

310 Davies, J. S. The cyclization of peptides and depsipeptides. *Journal of Peptide Science* **9**, 471-501, doi:10.1002/psc.491 (2003).

311 Yuan, W. *et al.* Hemocompatible surface of electrospun nanofibrous scaffolds by ATRP modification. *Mater. Sci. Eng., C* **33**, 3644-3651, doi:10.1016/j.msec.2013.04.048 (2013).

312 Agarwal, S., Wendorff, J. H. & Greiner, A. Chemistry on Electrospun Polymeric Nanofibers: Merely Routine Chemistry or a Real Challenge? *Macromolecular Rapid Communications* **31**, 1317-1331, doi:10.1002/marc.201000021 (2010).

313 Ozcam, A. E., Roskov, K. E., Genzer, J. & Spontak, R. J. Responsive PET Nano/Microfibers via Surface-Initiated Polymerization. *ACS Appl. Mater. Interfaces* **4**, 59-64, doi:10.1021/am201559f (2012).

314 Fu, G. D. *et al.* Smart Nanofibers from Combined Living Radical Polymerization, "Click Chemistry" and Electrospinning. *Acs Applied Materials & Interfaces* **1**, 239-243, doi:10.1021/am800143u (2009).

315 Menkhaus, T. J. *et al.* Electrospun nanofiber membranes surface functionalized with 3-dimensional nanolayers as an innovative adsorption medium with ultra-high capacity and throughput. *Chemical Communications* **46**, 3720-3722, doi:10.1039/c001802c (2010).

316 Feng, Q. *et al.* Electrospun Regenerated Cellulose Nanofibrous Membranes Surface-Grafted with Polymer Chains/Brushes via the Atom Transfer Radical Polymerization Method for Catalase Immobilization. *ACS Appl Mater Interfaces* **6**, 20958-20967 (2014).

317 Gualandi, C. *et al.* Advantages of Surface-Initiated ATRP (SI-ATRP) for the Functionalization of Electrospun Materials. *Macromolecular Rapid Communications* **34**, 51-56, doi:10.1002/marc.201200648 (2013).

318 Wang, H. Y. *et al.* Fabrication of PU/PEGMA crosslinked hybrid scaffolds by in situ UV photopolymerization favoring human endothelial cells growth for vascular tissue engineering. *Journal of Materials Science-Materials in Medicine* **23**, 1499-1510, doi:10.1007/s10856-012-4613-7 (2012).

319 Grafahrend, D. *et al.* Biofunctionalized poly(ethylene glycol)-block-poly(ε-caprolactone) nanofibers for tissue engineering. *J. Mater. Sci.: Mater. Med.* **19**, 1479-1484, doi:10.1007/s10856-007-3299-8 (2008).

320 Hersel, U., Dahmen, C. & Kessler, H. RGD modified polymers: biomaterials for stimulated cell adhesion and beyond. *Biomaterials* **24**, 4385-4415, doi:10.1016/s0142-9612(03)00343-0 (2003).

321 Xu, F. J., Wang, Z. H. & Yang, W. T. Surface functionalization of polycaprolactone films via surface-initiated atom transfer radical polymerization for covalently

coupling cell-adhesive biomolecules. *Biomaterials* **31**, 3139-3147, doi:10.1016/j.biomaterials.2010.01.032 (2010).

322 Harrison, R. H., St-Pierre, J.-P. & Stevens, M. M. Tissue Engineering and Regenerative Medicine: A Year in Review. *Tissue Eng. Part B-Rev.* **20**, 1-16 (2014).

323 Downing, T., Soto, J.,Morez, C., Houssin, T., Fritz, A., Yuan, F., Chu, J., Patel, S., Schaffer, D., Li, S. Biophysical regulation of epigenetic state and cell reprogramming. *Nature Materials*, doi:doi:10.1038/nmat3777 (2013).

324 Gentsch, R. *et al.* Single-Step Electrospinning to Bioactive Polymer Nanofibers. *Macromolecules* **44**, 453-461, doi:10.1021/ma102847a (2011).

325 Mollet, B. B. *et al.* A modular approach to easily processable supramolecular bilayered scaffolds with tailorable properties. *J. Mater. Chem. B* **2**, 2483-2493, doi:10.1039/C3TB21516D (2014).

Chapter 5: Scaffold stability

5.1 Assessing scaffold integrity *in vitro* for a demanding *in vivo* environment

Tissue engineered scaffolds are often designed for demanding environments such as within joints or other moving surfaces. It is essential they are able to successfully withstand and maintain their desired function for the longevity required in order to be successful in their therapeutic aim. In this Chapter assessment is made of the stability of the antifouling surface for prolonged periods *in vitro*.

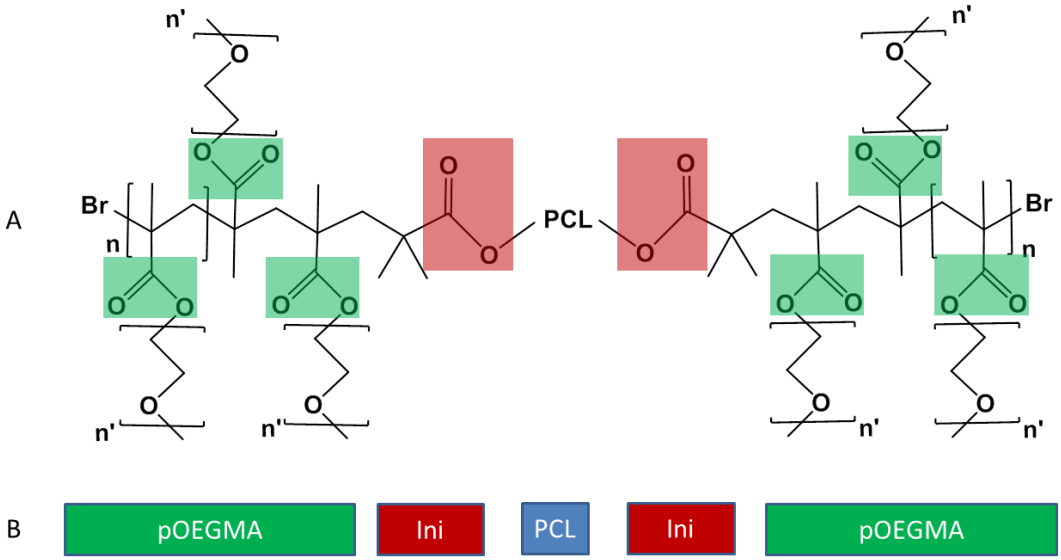

Figure 5-1: Chemical structure and schematic of modified 14 kDa PCL-ini with pOEGMA polymer brush grafted from either end. (A) Chemical structure with the ester bonds identified where hydrolysis may occur. Red shaded regions indicate the ester linkages binding a whole polymer bottlebrush to the PCL, originating from the initiator group, and green shaded regions indicating the ester bond binding a "branch" or single OEGMA unit to the bottlebrush backbone. (B) Schematic representation of the polymer structure with the PCL (blue, 1) portion, the structural contribution of the BiBB initiator (red, 2), and the pOEGMA bottlebrush (green, 3).

5.1.1 Stability and degradation of the pOEGMA surface

In order to create a tissue engineered scaffold that is useful as a surgical implant it is essential that the functionalised surface is stable for the required length of time. Ultimately it is generally desirable that the scaffold will be completely eliminated from the body but only after the required outcome has been achieved. With a primary tendon repair in mind, the desired functional life span of the implant would be ideally up to approximately 8 weeks with the first 2-4 weeks being the most critical time for patients as they build up their

movement with hand physiotherapy. There are two chemical mechanisms through which the functionalised pOEGMA surface coating may be lost from the scaffold. The first being the degradation of the pOEGMA chains themselves, and the second being the loss of the polymer brushes from their anchoring points on the PCL. This is outlined in Figure 5-1.

5.1.1.1 Monomer stability

Degradation of polymers and monomers can and does occur *in vitro* and *in vivo* depending on the characteristics of the polymer involved. PEG is a widely studied polymer that has been used extensively in the drug release field[1]. It is in clinical use in FDA approved drugs and devices and is generally very well tolerated in the body[326]. PEG is not biodegradable but may be renally excreted easily if below 20 kDa in size, above this threshold clearance is achieved through the liver[327]. PEG is subject to oxidative degradation and chain scission like other polyethers when exposed to aqueous environments[328]. It is of note that small PEG oligomers with molar masses of less than 400 Da have previously been shown to be toxic in humans due to the action of alcohol and aldehyde dehydrogenases leading to the formation of diacid and hydroxyacid metabolites[326,329]. This is not expected to be problematic in the system presented in this thesis as the expected degradation products would be larger than this size, although within the threshold of renal excretion.

OEGMA is an oligomer of PEG. This means that an OEGMA monomer is made up of several repeated units of PEG with a vinyl group at one end, so it acts as a single monomer unit. When polymerised to form pOEGMA, a backbone is formed with OEGMA branches linked to the polymer backbone through hydrolysable ester groups. These ester groups, and the resultant loss of the OEGMA side groups (or bottlebrush "branches"), have been posed as potential causes of reduced antifouling behaviours *in vitro* from surface bound polymer surfaces in the literature[330].

5.1.1.2 Polymer brush stability

The loss of the polymer brush *en bloc* through degradation of cleavage from the PCL fibre surface poses a higher risk for the short term stability of the functionalised surface. Investigation in the literature by Gautrot *et al.* has demonstrated that pOEGMA brushes grafted from gold surfaces showed excellent stability at ambient conditions and minimal brush cleavage when incubated for up to two months in PBS at room temperature[331]. This

is in comparison to Klok *et al.* who grafted poly(poly(ethylene glycol) methacrylate) brushes from glass and silicon substrates[332]. Klok *et al.* incubated polymer brushes in cell culture medium at 37^{o}C for 7 days and show clear delamination of polymer layers by 7 days by SEM.

PCL, the polymer that makes up the bulk of the scaffold, has been widely studied and is used in clinical devices such as absorbable sutures[333]. The degradation of PCL is discussed fully in Chapter one; in brief PCL is broken down initially through the action of random non-enzymatic surface hydrolysis leading to schism of the polymer through the ester linkages which may be observed at a similar rate *in vitro* and *in* vivo[334,335]. Once the M_n falls to < 5000 it is thought that enzymatic and phagocytic degradation will play a role in the final clearance of the material and the rate increases *in vivo*[336]. This mechanism of action means that PCL bioresorbs relatively slowly (months to years). The increased surface area seen when electrospun fibres are used, rather than larger (1.7 mm Ø diameter) struts used by Hutmacher *et al.*[334,336], increases the rate of bioresorption but this still falls in the region of many months. Bolgen *et al.* studied electrospun fibres for 6 months in various conditions *in vitro* and *in vivo* and demonstrated that the degradation profile of PCL still took many months[335]. The presence of the highly hydrated pOEGMA polymer brush layer surrounding the PCL fibres may accelerate the degradation of the PCL through hydrolysis due to the availability of water so close to the PCL surface, which is seen in other surface functionalization techniques[333]. The effect of PEG on the degradation of PCL has been assessed previously in the literature and shown to increase the rate of degradation[337]. The presence of the PEG did appear to increase the rate of PCL degradation but the results of this work are not directly comparable to the system presented here as they studied a PCL-PEG block copolymer that had been processed into films for hydrolysis assessment and using large diameter struts for *in vivo* work. Both the interaction between the PEG and the PCL, and the surface areas of the materials used are quite different. Whilst the functional pOEGMA layer remains the focus of this assessment, the gross morphology of the PCL fibres will be assessed at 10 weeks to see whether any clear differences can be seen between pOEGMA functionalised scaffolds and controls. This is not expected to be seen.

5.2 Materials and Methods

5.2.1 Materials

In addition to materials outlined in the previous chapters, additional materials were used for the experiments outlined here, and is detailed below.

Electrospun scaffolds of were manufactured using the methods outlined in Chapters 2 and 3 and were used in the experimentation outlined here.

A two component silicone elastomer, Sygard 184 was purchased from Dow Corning and was used during the mechanical testing to protect the instruments as a backing for the scaffolds. This was made up according to the manufacturer's instructions in ratios of 1:3 of curing agent to polymer in a plastic petri dish. This was well mixed before being allowed to cure standing on a warmed hot plate at 40^{o}C overnight. The required sizes of material were cut out.

Poly(ethylene glycol) mono methyl ether methacrylate (OEGMA, Sigma, UK) was initially purified into fractions using a silica column to give specific numbers of PEG units, and confirmed on ^{1}H-NMR. For the monomer degradation experiments, OEGMA with 3 PEG units was selected and used throughout the experiment and referred to as peg3ma.

5.2.2 Assessment of degradation and stability of pOEGMA in solution and from scaffolds

In order to establish the potential functional longevity of the PCL-pOEGMA polymer brush scaffolds *in vivo* their stability was assessed *in vitro*. The stability of the brushes was assessed in a 2 fold manner; firstly, the degradation of the monomer was observed by ^{1}H-NMR, and secondly, the degradation and changes in the bulk properties of the PCL-pOEGMA scaffold system were assessed.

5.2.2.1 OEGMA monomer degradation by ^{1}H-NMR

15 mg of mono-disperse peg3ma was dissolved in 80 µL of deuterium oxide (D_2O). The solution was divided between four newly purchased glass NMR tubes to give 20 µL and 5 mg of monomer per tube.

Deuterated phosphate buffered saline (dPBS) was made up using 10 x concentrated PBS solution diluted using D_2O to a standard concentration. From this dPBS solution buffers at pH 6.0, 7.4 and 8.1 were made in addition to a 0.1M sodium hydroxide (NaOH) solution in D_2O.

To each of the NMR tubes containing the monomer solution, 710 µL of one of the solutions was added. The tubes were immediately sealed with a stopper and parafilm, and labelled. The samples were immediately assessed using ^{1}H-NMR as a time 0 before being introduced to a water bath where they were maintained at 37^{o}C for 10 weeks, during which time ^{1}H-NMRs were regularly taken to assess the monomer.

5.2.2.2 Assessment of PCL-pOEGMA scaffold stability

17% (w/w) PCL-Ini scaffolds, 9% (w/w) PCL-Ini scaffolds and their matched controls were polymerised within a single polymerisation, washed and dried as outlined in Chapter 3 until ready to be used. A second set of scaffolds underwent polymerisation with the biotinylated monomer unit to form pOEGMA-*co*-biotin functionalization on the scaffolds and allow for fluorescent labelling.

Scaffolds were initially sterilised in 70 % (v/v) ethanol for 30 minutes in 15 mL centrifuge tubes on rollers before being washed three times in sterile PBS. Using aseptic technique, scaffolds were introduced into sterile PBS within 50 mL centrifuge tubes and maintained at 37^{o}C within an incubator. The tubes were agitated with continuous gentle rocking and the PBS changed every 2 weeks. Scaffolds were incubated up to a maximum of 10 weeks before being removed from the system, ultrasonicated in ethanol to remove any unbound polymer, rinsed in water three times, and dried before undergoing characterisation.

17% (w/w) PCL-pOEGMA scaffolds and their matched controls were characterised to assess whether the pOEGMA brushes remained present with water contact angle, as described in Chapter 2 (section 2.2.4.2.1), and SEM using the Phenom FEI SEM with a 10 nm chromium sputter coating. To assess whether the antifouling function had been maintained, the ability to withstand protein adhesion with fluorescein-BSA and cell adhesion were performed in an identical manner to the previous assessment outlined in detail in Chapter 3 (section 3.2.4.1). 17% (w/w) PCL-p(OEGMA-*co*-bioin) scaffolds were fluorescently labelled and imaged using fluorescence microscopy as outlined in Chapter 3.

The surface of the 17% (w/w) PCL-pOEGMA scaffolds and their matched controls that had been incubated in PBS for 0, 2, 4, 6, 8 and 10 weeks were characterised using XPS. The spectra were recorded on a Thermo Scientific K-Alpha^{+} X-ray Photoelectron Spectrometer (XPS) system operating at $2x10^{-9}$ mbar base pressure. This system incorporates a monochromated, microfocused Al Kα X-ray source (hν = 1486.6 eV) and a 180° double focusing hemispherical analyser with a two-dimensional detector. The X-ray source was operated a 6 mA emission current and 12 kV anode bias. Data were collected at 150 eV pass energy for survey and 20 eV pass energy for core level spectra using an X-ray spot size of 400 μm^2. A flood gun was used to minimize sample charging. All data were analysed using the Avantage software package.

5.2.3 Statistical Analysis

All experimental groups with reported statistical analysis had a sample size of at least N = 3. Data is presented as mean +/- standard deviation (SD). Statistically significance is determined using a student's T-test using Excel software with a significance accepted where *p*-value < 0.05.

5.3 Results and Discussion

Tissue engineered scaffolds may be designed with specific material properties in mind to compliment the intended use. The surface anchored pOEGMA bottlebrush system has considerable advantageous properties with regards to protein and cell antifouling. This property would ideally be stable and maintain a good level of function over a period of several weeks *in vivo*.

5.3.1 Degradation and stability of pOEGMA in solution and on scaffolds

The bulk of the scaffold, PCL, and the polymer brush functionalization with pOEGMA are known to undergo hydrolysis in aqueous environments[330,333]. In order to undertake an initial assessment of the scaffold stability a simplified system in PBS was used. PBS was used for the initial experimentation as the ester groups are vulnerable to hydrolysis in hydrated systems. This may be at a lower rate than would be found in physiological fluids due to the presence of enzymes. More complex media, such as serum or synovial fluid used *ex vivo,* was not chosen for use in this chapter as it was felt that this also may also not behave in a truly physiological manner as the enzymatic action may have been lost in the fluid treatment. The use is also complicated by the risk of bacterial contamination when maintained at physiological temperatures for prolonged periods, and there are inherent difficulties in measuring degradation products within them.

It was therefore decided that the hydrolysis of the polymer would be initially explored in PBS. The stability of the scaffolds will be tested *in vivo*, which falls beyond the scope of this thesis.

5.3.1.1 OEGMA monomer degradation by ^{1}H-NMR

The stability of a mono-disperse peg3ma monomer was assessed by ^{1}H-NMR in dPBS at a range of pHs whilst being maintained at 37^{o}C. An identical tube was also incubated with a 0.1M NaOH solution in D_2O to establish a complete degradation of the monomer as a comparison (Figure 5-2).

As expected, the 0.1M NaOH added to the peg3ma resulted in 100% degradation of the monomer instantaneously (not included in the Figure). Degradation of the monomer occurred most rapidly in the more basic solution (pH 8.0) with 19% degraded at 10 weeks, and 17% of the monomer at a physiological pH of 7.4. No degradation of the monomer in

the most acidic pH of 6.0 was seen up to 10 weeks. It was expected that the more basic solution would result in the most rapid hydrolysis of the ester. The pHs of the solutions were tested when the experiment was terminated at 10 weeks and they were found to be stable and unchanged from the starting pHs. This result is promising for the longevity of the system, although it would be expected to be faster *in vivo* due to the action of potential enzymatic breakdown.

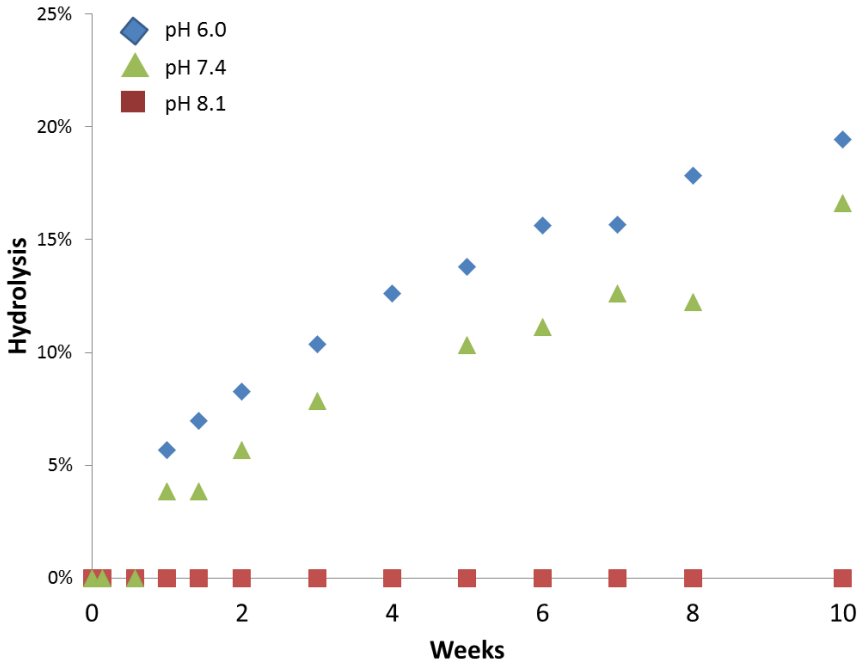

Figure 5-2: Peg3ma mono-disperse monomer degradation by ^{1}H-NMR in dPBS at pH 6.0, 7.4 and 8.1 over 10 weeks

5.3.1.2 PCL-pOEGMA scaffold stability in vitro

Scaffolds of both PCL-pOEGMA and PCL-p(OEGMA-*co*-biotin) and their matched controls were incubated at 37°C in PBS with continuous gentle agitation for a period of up to 10 weeks. PBS was deemed a reasonable fluid for initial testing *in vitro*, although it is acknowledged that this is a simplistic model and for a true representation of stability these or similar experiments would need to be undertaken following implantation *in vivo* in an animal model.

5.3.1.2.1 Material characterisation following prolonged incubation

Material characterisation was undertaken to establish whether the pOEGMA bottlebrush remained in situ following 10 weeks of incubation in PBS using XPS, fluorescent labelling,

water contact angle measurements and SEM. XPS measurements were taken by Dr Anna Regoutz by samples made by me. Data interpretation was done in collaboration with Dr Regoutz and me.

5.3.1.2.1.1 XPS characterisation

*X*PS characterisation was undertaken on 17% (w/w) PCL-pOEGMA scaffolds and their matched controls, 17% (w/w) PCL-diol that had been incubated in PBS at 37°C and with

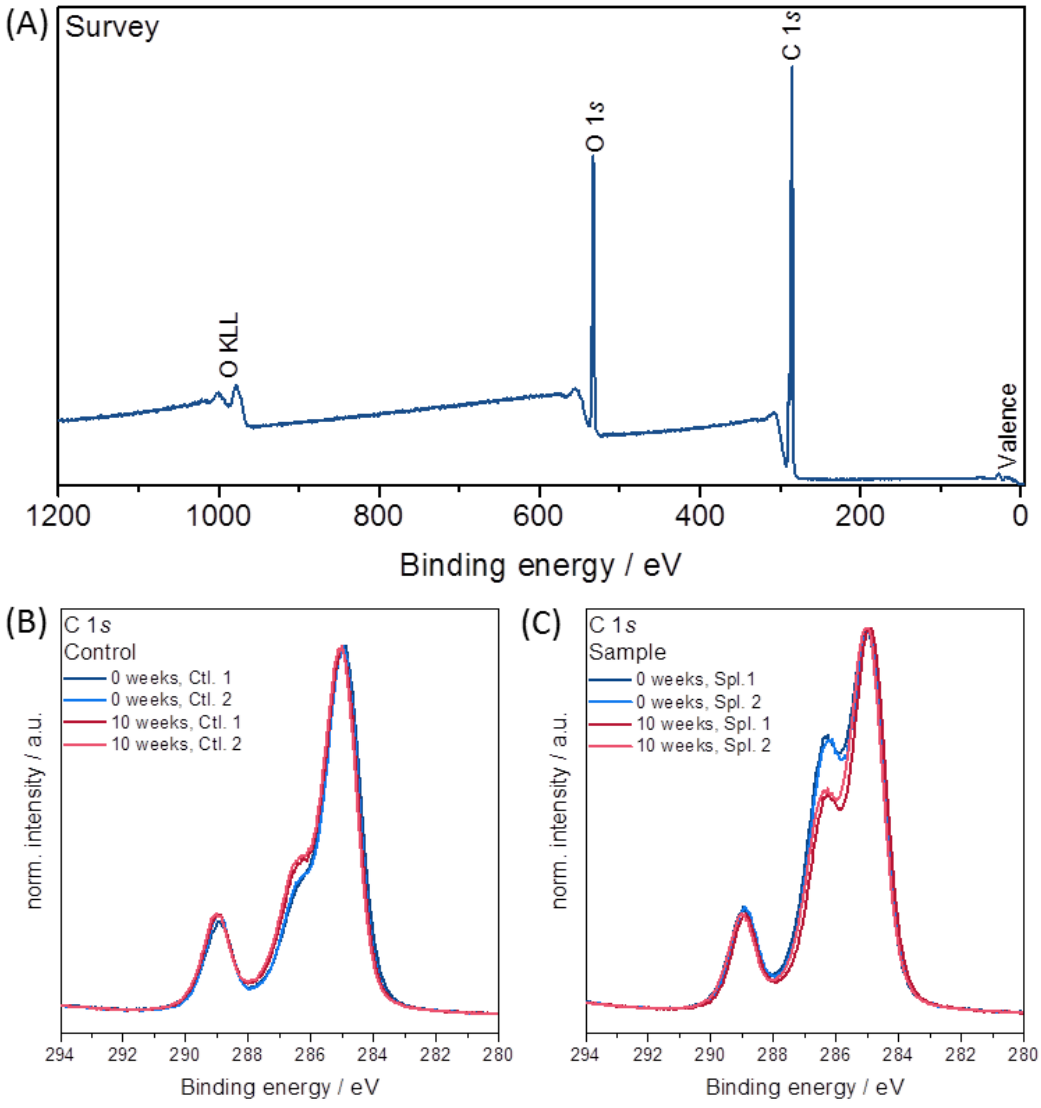

Figure 5-3: Normalised C 1*s* XPS characterisation of the 17% (w/w) PCL-pOEGMA scaffolds and the 17% (w/w) PCL-diol matched controls before (0 weeks) and following 10 weeks incubation in PBS. (A) Representative survey spectra of a control scaffold following 0 weeks incubation demonstrating no observable scaffold contamination and clean samples. C 1*s* spectra of the control 17% (w/w) PCL-diol scaffolds (B) and the 17% PCL-pOEGMA scaffolds (C) before (0 weeks), and following 10 week incubation in PBS. (N = 2)

agitation. Scaffolds that had been incubated for 0, 2, 4, 6, 8, and 10 weeks were analysed with XPS. The XPS C 1*s* spectra (Figure 5-3) were normalised to the maximum signal intensity and survey scans (Figure 5-3, A) indicate that the samples were clean with no additional elements found, such as sodium, on any sample.

As anticipated, the C 1*s* spectra for the 17% (w/w) PCL-diol control samples represent the base line of the PCL backbone with peaks corresponding to the ether (-CH_2-O-CH_2-), hydroxyl (-OH) and ester (-CH_2-COO-CH_2-) groups. These groups are identified through their characteristic reference energies and correspond well to those published in the literature (Table 5-1)[338]. It is noteworthy that the hydroxyl and ether peaks are indistinguishable from one another in these samples as the peaks fall closely together and cannot be accurately resolved. The 17% (w/w) PCL-pOEGMA scaffolds however are markedly different to controls at time 0. Within this dataset, the atomic percentage of hydroxyl/ether peak is seen to be 28% in controls in contrast to 40% seen in the 17% (w/w) PCL-pOEGMA samples at 0 weeks prior to incubation. This represents the presence of the pOEGMA bottlebrush and successful surface functionalization, as discussed in Chapter 3.

The control samples demonstrate relative stability following 10 week incubation in PBS with only a small increase in the hydroxyl/ether groups present. This could be as a result of the prolonged incubation in PBS resulting in an increase in hydroxyl groups. However, the 17% (w/w) PCL-pOEGMA samples show a marked reduction in the hydroxyl/ether peak signal following 10 week incubation in PBS. This demonstrates that whilst there is some reduction in the presence of the polymer brush, the stability is excellent over a 10 week incubation in PBS. The reduction in the hydroxyl/ether peak signal is likely to be due to the hydrolysis of some of the ether bonds stemming from some degradation of the pOEGMA brush. However, the strong signal remaining at 10 weeks demonstrates that the polymer brush is still present, albeit reduced, supporting the stability of the pOEGMA functionalization (Figure 5-3 and 5-4). This is further reflected in the atomic percentages seen with the peak fit results for both the controls and samples (Table 5-1).

Table 5-1: XPS C 1*s* peak fit results for the 17% (w/w) PCL-diol control scaffolds and the 17% (w/w) PCL-pOEGMA scaffolds following 0 and 10 weeks incubation in PBS. The published binding energies are included.

	C-C	C-O (ether)	O=C-O (ester)
Published BE (eV)[13]	285.0	286.2 (-OH) 286.5 (-CH_2-O-CH_2-)	289
0 weeks			
Control / BE (eV)	285.0	286.4	289.0
Sample / BE (eV)	284.9	286.3	288.9
Control / at%	59	28	13
Sample / at%	48	40	12
10 weeks			
Control / BE (eV)	285.0	286.4	289.0
Sample / BE (eV)	285.0	286.4	289.0
Control / at%	58	27	15
Sample / at%	55	33	12

Notes: Binding energy (BE). Atomic percentage (at%)

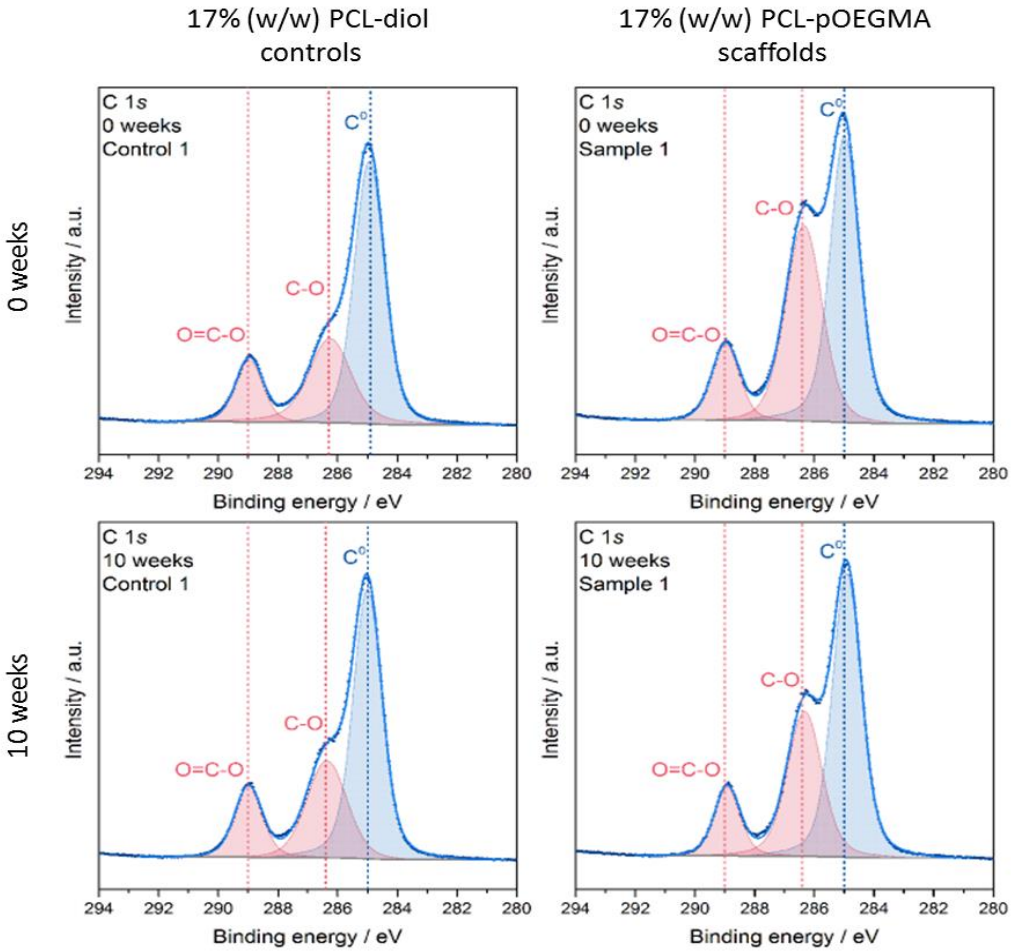

Figure 5-4: XPS peak fits for the C 1*s* spectra for the 17% (w/w) PCL-diol controls (left) and the 17% (w/w) PCL-pOEGMA scaffolds (right) following 0 (upper) and 10 weeks (lower) incubation in PBS demonstrating the relative contributions of the different groups to the shape of the spectra.

17% (w/w) PCL-diol controls and 17% (w/w) PCL-pOEGMA samples were measured with XPS at 0, 2, 4, 6, 8 and 10 weeks incubation. The relative change in the atomic percentages over this period demonstrates the progressive loss of the hydroxyl/ether groups from the 17% (w/w) PCl-pOEGMA samples and the relative stability of the ester groups over the incubation period (Figure 5-5). The lines of best fit are based on the average reading from 2 points on a single scaffold.

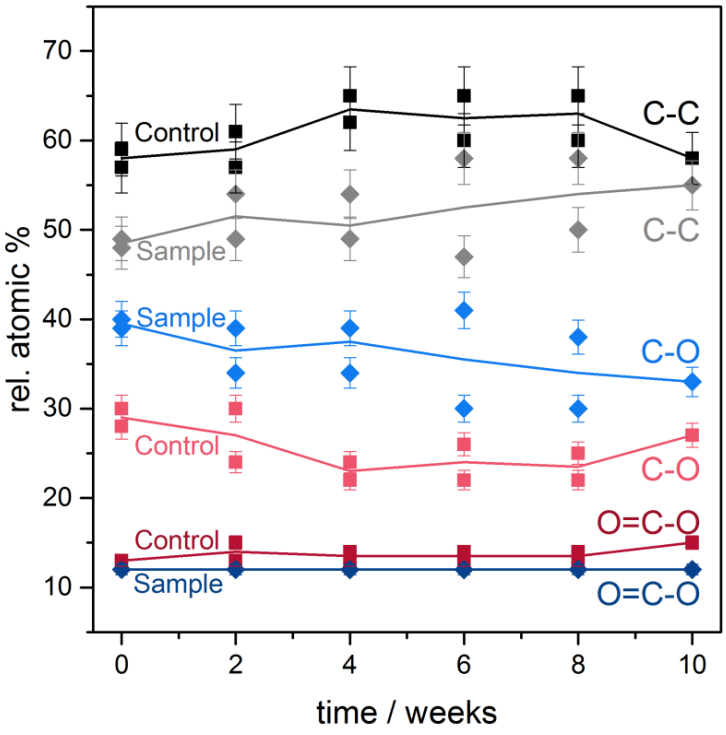

Figure 5-5: C 1*s* components quantified using peak fits from the 17% (w/w) PCL-diol controls and 17% (w/w) PCL-pOEGMA samples over 10 weeks of incubation in PBS. The relative atomic percentages demonstrate the progressive loss of the C-O ether signal from the 17% (w/w) PCL-pOEGMA samples indicating some loss of the polymer brush. Two scaffolds (N = 2) were analysed for time 0 and 10 weeks, otherwise single scaffolds were analysed (N = 1). 2 points were measured from each scaffold and the guidelines are based on the average values from these points. Error bars demonstrate an assumed error of 5%.

5.3.1.2.1.2 Further characterisation of incubated scaffolds

Scaffolds polymerised with pOEGMA-*co*-biotin were labelled with streptavidin-fluorescein as a qualitative assessment of the presence of the polymer brush as this has been shown to be an effective method for displaying the presence of the brush (Chapter 3, Figure 3-9). Scaffolds were imaged using fluorescence microscopy and demonstrate that a clear fluorescein signal remains present on scaffolds incubated for 10 weeks in PBS (Figure 5-6). To ensure that this was indeed due to the presence of the covalently bound polymer brush, the 17% (w/w) PCL-pOEGMA-*co*-biotin scaffold that was labelled with fluorescein-

streptavidin underwent hydrolysis of the polymer brushes. The polymer brushes were removed using NaOH in a protocol previously established by ^{1}H-NMR to produce complete hydrolysis of the pOEGMA polymer. The scaffolds were incubated with 2 µM NaOH at 40^{o}C for 2 h before being thoroughly washed in UHQ water at pH 7.4. The fluorescein signal is lost (Figure 5-6, right), suggesting that the polymer brushes have been completely hydrolysed from the scaffold.

Figure 5-6: Representative fluorescence microscopy images of PCL-pOEGMA-*co*-biotin scaffolds incubated for 10 weeks in PBS at 37^{o}C. Scaffolds were labelled with streptavidin-fluorescein before imaging.

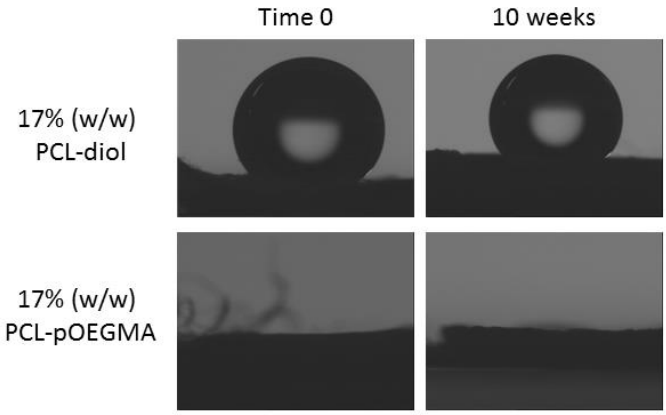

Figure 5-7: Water contact angle measurements for 17% (w/w) PCL-diol (control) and 17% (w/w) PCL-pOEGMA scaffolds before (time 0) and after incubation in PBS for 10 weeks.

Water contact angle measurements were taken from 17% (w/w) PCL-diol control and 17% (w/w) PCL-pOEGMA scaffolds before (time 0) and after incubation in PBS for 10 weeks (Figure 5-7). A contact angle of zero is maintained for the 17% (w/w) PCL-pOEGMA scaffolds

at 10 weeks indicating that there is some pOEGMA brush functionalization remaining on the scaffold. The 17% (w/w) PCL-diol control scaffolds remain unchanged also (134.5^{o}, time 0, 133.3^{o}, 10 weeks).

SEM images were taken of the scaffolds before and after incubation in PBS for 10 weeks. As expected from the literature discussed above, no morphological differences are seen in the scaffolds following 10 weeks incubation in PBS (Figure 5-8).

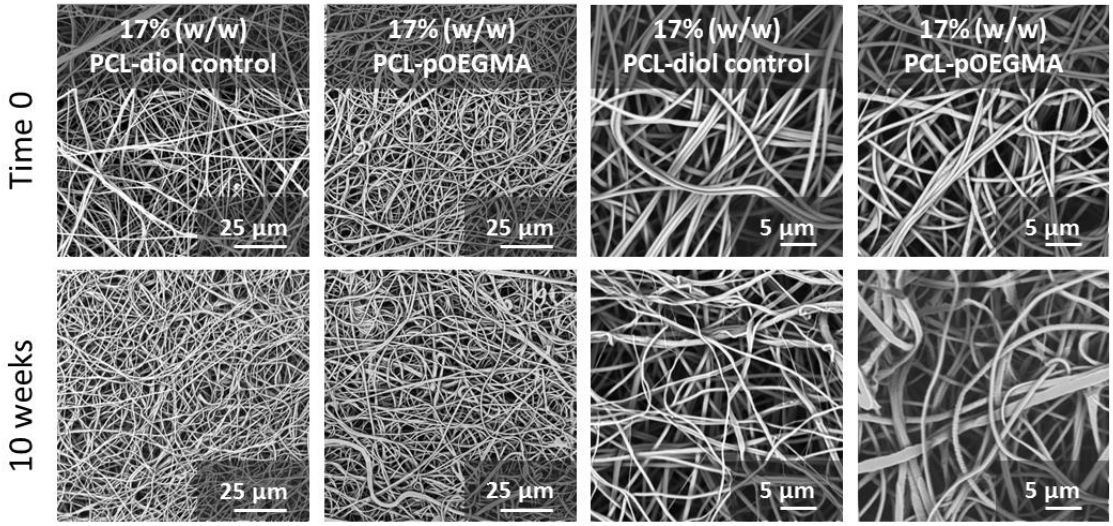

Figure 5-8: Representative SEM images of scaffolds before (time 0) and after 10 week incubation in PBS at 37^{o}C. 17% (w/w) PCL-pOEGMA and matched control scaffolds show no difference in fibre morphology before and after incubation.

All the data presented supports the excellent stability of the pOEGMA surface functionalization following incubation for 10 weeks in PBS. The XPS measurements on samples over the 10 week period suggest that whilst some of the pOEGMA is lost over this period (Figure 5-5, the reduction in the C-O, ether signal), following 10 weeks incubation a good amount of the pOEGMA brush is maintained. This is encouraging that the functional characteristics may also be maintained following this time.

5.3.1.2.2 Functional characterisation following prolonged incubation

pOEGMA functionalised scaffolds significantly resist BSA binding when compared to PCL scaffolds when they are newly made (Chapter 3, Figure 3-10). In order for this material to be useful clinically, it is essential that this functional behaviour is stable and is maintained. PCL-pOEGMA and PCL control scaffolds that had been incubated for 10 weeks in PBS in

physiological conditions were assessed for fluorescent BSA binding and compared to scaffolds from the same polymerisation that had been maintained *in vacuo* and protected from light. Scaffolds were incubated with fluorescein labelled BSA for 18 hours before being washed, and the intensity of the absorbed protein assessed (Figure 5-9).

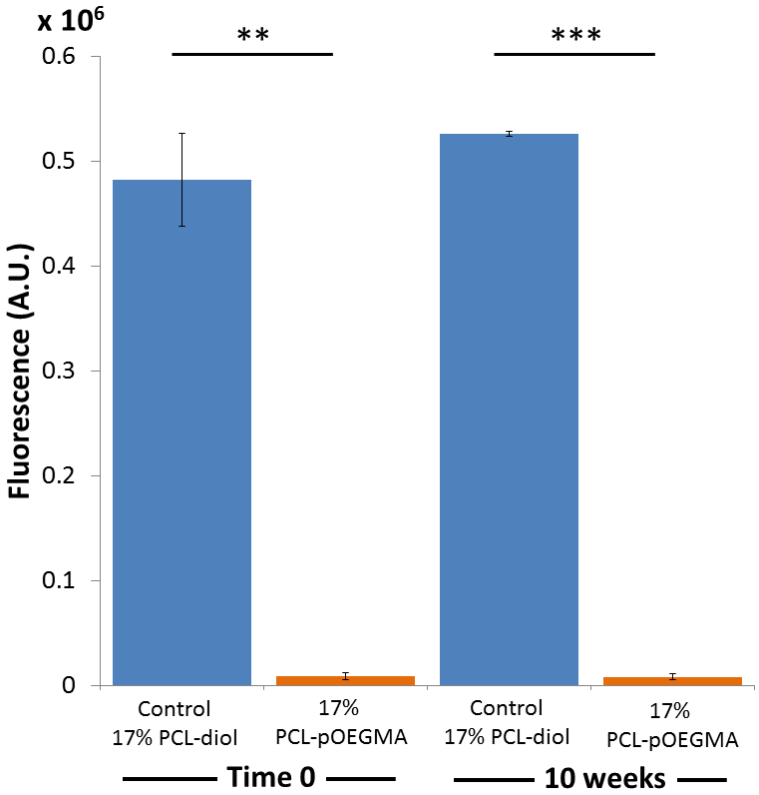

Figure 5-9: Antifouling ability of 17% (w/w) PCL-diol control scaffolds and 17% (w/w) PCL-pOEGMA scaffolds when incubated with fluorescently labelled BSA. Scaffolds from the same polymerisation were maintained *in vacuo* or incubation in PBS at physiological conditions for 10 weeks before assessment. The polymerisation had a conversion (X) of 73% by ^{1}H-NMR and MW 19000. ($p < 0.005$, *** $p < 0.001$). N = 4. Error bars show standard deviation.**

The antifouling ability of the pOEGMA functionalization is highly effective for the scaffolds that had been maintained *in vacuo* when compared to the 17% (w/w) PCL-diol control scaffolds that had been maintained within an identical manner. The signal from the fluorescent BSA read from the 17% (w/w) PCL-pOEGMA scaffolds is significantly below that of the 17% (w/w) PCL-diol scaffolds ($p < 0.005$). Furthermore, the antifouling ability is maintained following 10 weeks incubation in PBS at physiological conditions with the 17% (w/w) PCL-pOEGMA scaffolds again significantly outperforming the 17% (w/w) PCL-diol

control scaffolds ($p < 0.001$). The ability of the pOEGMA bottlebrush to effectively resist protein binding appears unaffected by 10 weeks incubation in PBS at physiological conditions. Scaffolds were further tested with cells for their antifouling properties.

25 000 bovine tenocytes were seeded onto 17% PCL-pOEGMA and 17% PCL-diol control scaffolds from the same polymerisation that had been incubated in PBS for 10 weeks, and those that had been maintained in a vacuum dessicator and assumed to be equivalent to a time 0. These were cultured for 7 days, at which time an estimation of cell number was established using an MTT assay. This was performed in an identical manner to that described in Chapter 3 3.3.2.2 except that the scaffolds were blocked, the cell nuclei stained with DAPI and imaged using fluorescence microscopy to visualise the distribution of the cells. A cell calibration curve was produced at the time of cell seeding to allow for estimation of the cell number on completion of the experiment (Figure 5-10).

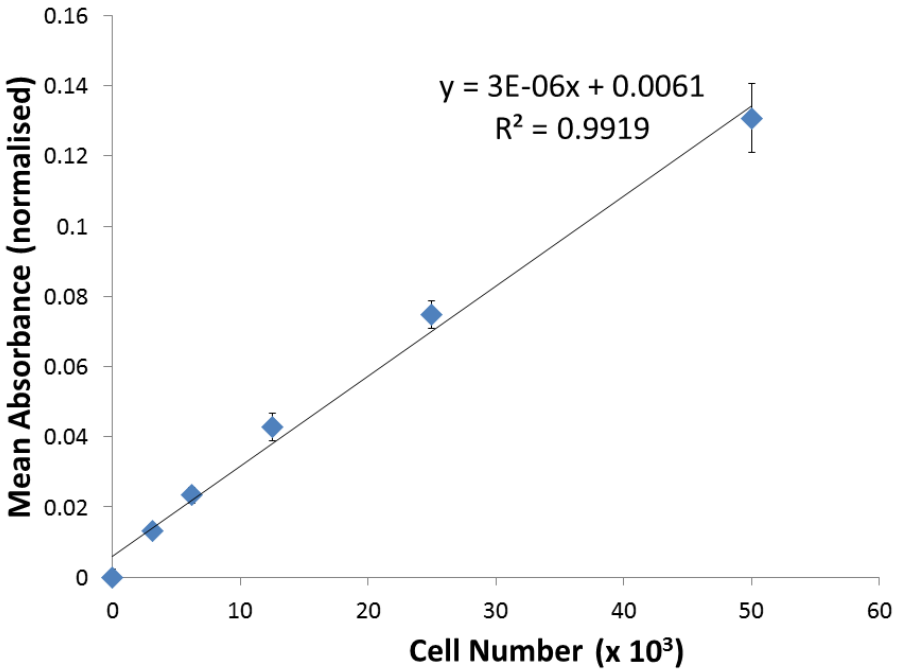

Figure 5-10: An MTT calibration curve was performed to allow for the estimation of cell numbers from absorbance readings. Serial dilutions were performed on a single cell suspension of bovine tenocytes to give a series of known cell numbers ranging from 100 000 to 3125 cells. Using a single animal donor, 3 independent ladders were produced and read in triplicate. Normalised means are displayed with error bars showing standard deviation.

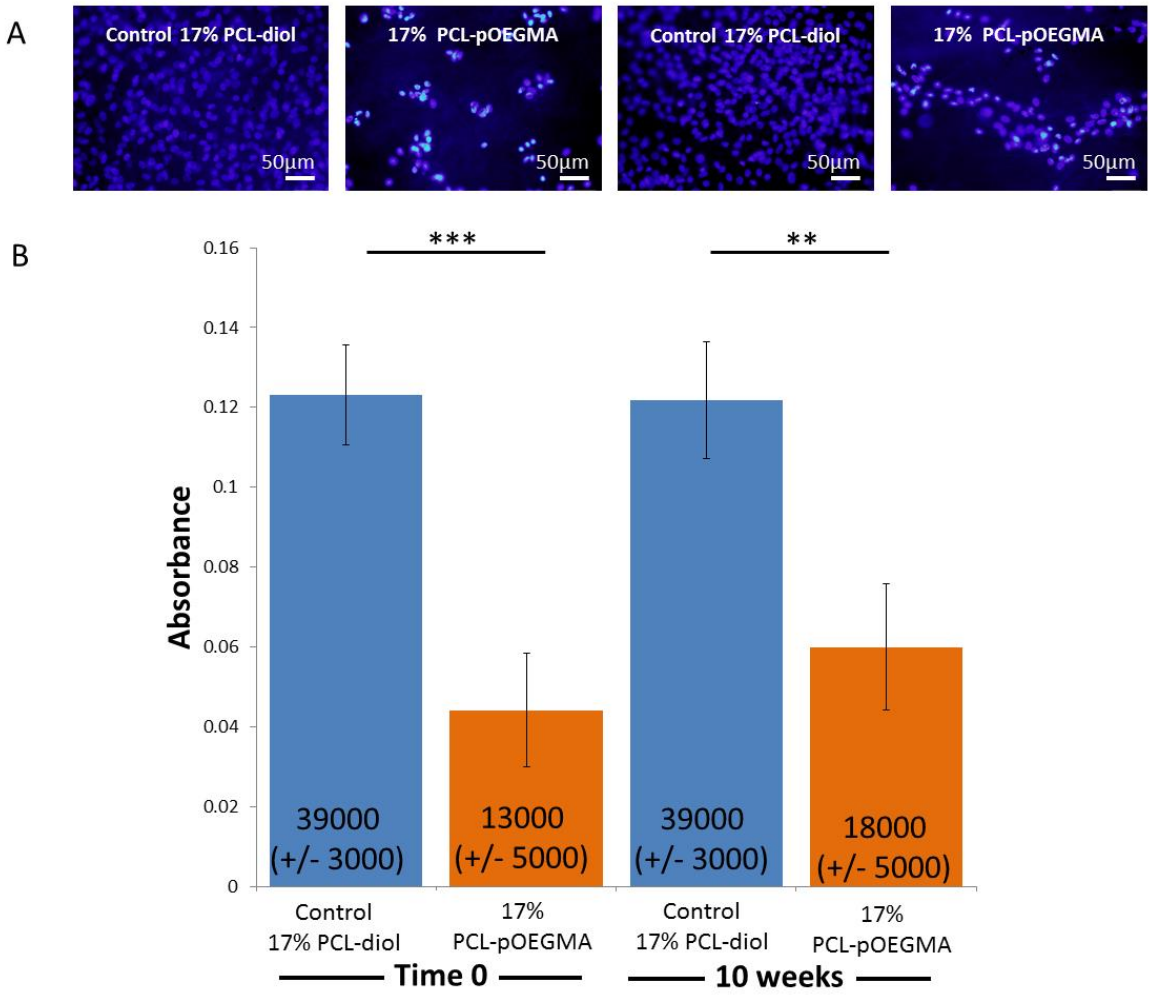

Figure 5-11: Assessment of cell adhesion to antifouling pOEGMA scaffolds and PCL control scaffolds before and after incubation in PBS for 10 weeks to assess potential loss of antifouling function. Cells cultured on scaffolds for 7 days. (A) Representative fluorescence microscopy images of bovine tenocytes seeded on scaffolds having been stained with DAPI (blue) for cell nuclei. (B) Metabolic activity of bovine tenocytes cultured on scaffolds for 7 days was assessed by MTT assay. Estimated cell numbers are started for each bar. Significant difference ** $p < 0.01$, *** $p < 0.001$. Single animal cell line with N = 5 scaffolds read in technical triplicates. Error bars represent standard deviation (SD) and error in cell number is SD in calculated cell number.

Fluorescence microscopy reveals clear differences in cell numbers between 17% PCL-diol controls and 17% PCL-pOEGMA scaffolds before (Figure 5-11, A, left) and after (right) incubation in PBS for 10 weeks. The DAPI nuclear stain demonstrates a high number of cells on the 17% PCL-diol control scaffolds and a reduced number on the 17% PCL-pOEGMA scaffolds. The images also suggest that an increase in cell number is seen on 17% PCL-

pOEGMA scaffolds following scaffold incubation in PBS for 10 weeks. This is further explored with the cell metabolic assay MTT to estimate cell number.

A significant difference is expected, and seen, between the cell binding affinity for 17% PCL-diol controls and 17% PCL-pOEGMA scaffolds that did not undergo incubation in PBS for 10 weeks ($p < 0.001$, Figure 5-11). This is similar to results reported in Chapter 3 section 3.3.2.2. The difference in cell binding affinity is maintained in scaffolds following 10 week incubation in PBS ($p < 0.01$, Figure 5-11). Interestingly, the imaging suggests an increase between cell numbers seen on 17% PCL-pOEGMA scaffolds before and after 10 week incubation in PBS, with a trend to a higher number of cells being supported following incubation. This, however, is not statically significant.

The data presented indicates that the pOEGMA bottlebrushes are stable and remain bound to the functionalised scaffolds, retaining their material and functional features following 10 weeks incubation in PBS. The XPS and cell data however do indicate that there is some reduction of pOEGMA functionalization, but at this point enough remains to maintain an antifouling surface. In line with the literature, there also appears to be no bulk changes to the PCL fibres, which is known to degrade slowly through hydrolysis[334].

This data is in contrast to that presented by Klok *et al.*[332], and offers some support to that presented by Gautrout *et al*.[331]. Klok *et al.* grafted poly(poly(ethylene glycol) methacrylate) brushes from glass and silicon substrates and incubated them in cell culture medium at 37^{o}C for 7 days. Clear delamination of polymer layers is seen by 7 days on SEM. Gautrot *et al.* however demonstrated that pOEGMA brushes grafted from gold surfaces showed excellent stability at ambient conditions and minimal brush cleavage when incubated for up to two months in PBS at room temperature[331]. There are several important differences to note between this work; firstly, Klok *et al.* used hydroxyl-terminated monomers which are known to contain di-methacrylates in comparison to oligo(ethylene glycol methyl ether methacrylate) used by Gautrout *et al*. and in this work. This will lead to the formation of cross-linkages between polymer chains and increase the chances of the polymer layer being removed as a sheet. Klok *et al.* hypothesise that the detachment of the polymer coating from the surface may be due to osmotic stress being exerted on the polymer as a result of hydration, leading to cleavage of the Si-O bond anchoring the polymer backbone to the

surface[332]. Whilst the same osmotic stress may be experienced by the system presented in this thesis, the Si-O bond is not present, so direct comparison cannot be made. Furthermore, the 3D scaffold presented in this thesis, whereby the hydrated polymer brush layer is presented circumferentially around a fibre, in contrast to from a planar 2D surface, may give the polymer layer more room to swell. This may result in a lower level of osmotic pressure within the 3D system presented here and reduce the risk of this leading to polymer brush cleavage.

Klok *et al.* also propose that the PEG side chains may also have further bound alkali and alkali earth metal ions within the culture medium. They suggest that this may lead to further swelling of the polymer layer with water and further promoting the detachment of the polymer brush layer to alleviate the entropically unfavourable stretched chain confirmation. Gautrout *et al.* did however use pOEGMA functionalised surfaces successfully for up to 7 days in cell culture conditions to prevent cell spreading. Their results suggest that the pOEGMA brush layer is stable at this time as the cells are limited in their movement. Further work by Klok *et al.* added a hydrophobic spacer between the Si-O anchoring bond and hydrophilic polymer brushes[339]. This successfully improved the stability of polymer brushes from silicon surfaces.

Long term stability of pOEGMA brushes in cell culture conditions were further investigated by Fan *et al.* who grafted pOEGMA from titanium surfaces using a catechol initiator[330]. Cells were seeded onto pOEGMA functionalised surfaces twice weekly for 2.5 months. No differences were seen in surfaces up to 3 weeks with all pOEGMA surfaces maintaining an effective antifouling coating. After this time however, a trend between polymer chain length and antifouling ability emerges with shorter chain lengths progressively losing their antifouling ability. The authors hypothesise that this is due to the hydrolysis of the PEG side chains from the polymer backbone as their previous work has shown the anchoring covalent bond to be stable in long term cell culture conditions (> 5 months). Fan *et al.* demonstrate that through their system pOEGMA functionalised surfaces become support fully confluent cell layers at 7, 10 and 11 weeks for oligomers of 4, 9 and 23 repeated PEG units respectively. This work utilises an oligomer of 9 repeated PEG units, and through the use of a 3D scaffold structure will have a higher density of PEG presented than in a 2D system, as used by Fan *et al.* which may confer a slightly increased longevity.

5.4 Conclusions

Scaffolds developed for implantation into the body must be able to withstand their biochemical environment whilst maintaining their desired function for as long as required. The stability of the pOEGMA bottlebrush layer grafted from electrospun PCL fibres has been investigated following prolonged incubation in PBS in physiological conditions. XPS, fluorescent labelling and water contact angle measurements presented demonstrate that the pOEGMA layer remains present following 10 weeks incubation. Furthermore, the pOEGMA layer also maintains its antifouling ability following 10 weeks incubation as demonstrated using a protein adhesion assay and a cell adhesion assay.

These data are extremely encouraging that the system presented within this thesis is relatively stable *in vitro* to both degradation. These samples now need to be incubated *in vivo* to assess their chemical stability in the physiological environment, which falls beyond the scope of this work.

References: Chapter 5

326 Knop, K., Hoogenboom, R., Fischer, D. & Schubert, U. S. Poly(ethylene glycol) in Drug Delivery: Pros and Cons as Well as Potential Alternatives. *Angewandte Chemie-International Edition* **49**, 6288-6308, doi:10.1002/anie.200902672 (2010).

327 Pasut, G. & Veronese, F. M. Polymer-drug conjugation, recent achievements and general strategies. *Progress in Polymer Science* **32**, 933-961, doi:10.1016/j.progpolymsci.2007.05.008 (2007).

328 Sharma, S., Johnson, R. W. & Desai, T. A. Evaluation of the stability of nonfouling ultrathin poly(ethylene glycol) films for silicon-based microdevices. *Langmuir* **20**, 348-356, doi:10.1021/la0347531 (2004).

329 Herold, D. A., Keil, K. & Bruns, D. E. OXIDATION OF POLYETHYLENE GLYCOLS BY ALCOHOL-DEHYDROGENASE. *Biochemical Pharmacology* **38**, 73-76, doi:10.1016/0006-2952(89)90151-2 (1989).

330 Fan, X., Lin, L. & Messersmith, P. B. Cell fouling resistance of polymer brushes grafted from Ti substrates by surface-initiated polymerization: Effect of ethylene glycol side chain length. *Biomacromolecules* **7**, 2443-2448, doi:10.1021/bm060276k (2006).

331 Gautrot, J. E. *et al.* Exploiting the superior protein resistance of polymer brushes to control single cell adhesion and polarisation at the micron scale. *Biomaterials* **31**, 5030-5041, doi:10.1016/j.biomaterials.2010.02.066 (2010).

332 Tugulu, S., Klok, H. Stability and Nonfouling properties of Poly(poly(ethylene glycol) methacrylate) Brushes under Cell Culture Condtions. *Biomacromolecules* **9**, 906-912 (2008).

333 Woodruff, M. A. & Hutmacher, D. W. The return of a forgotten polymer-Polycaprolactone in the 21st century. *Prog Polym Sci* **35**, 1217-1256, doi:10.1016/j.progpolymsci.2010.04.002 (2010).

334 Lam, C. X. F., Savalani, M. M., Teoh, S.-H. & Hutmacher, D. W. Dynamics of in vitro polymer degradation of polycaprolactone-based scaffolds: accelerated versus simulated physiological conditions. *Biomedical Materials* **3**, doi:10.1088/1748-6041/3/3/034108 (2008).

335 Bolgen, N., Menceloglu, Y. Z., Acatay, K., Vargel, I. & Piskin, E. In vitro and in vivo degradation of non-woven materials made of poly(epsilon-caprolactone) nanofibers prepared by electrospinning under different conditions. *Journal of Biomaterials Science-Polymer Edition* **16**, 1537-1555, doi:10.1163/156856205774576655 (2005).

336 Lam, C. X. F., Hutmacher, D. W., Schantz, J.-T., Woodruff, M. A. & Teoh, S. H. Evaluation of polycaprolactone scaffold degradation for 6 months in vitro and in vivo. *Journal of Biomedical Materials Research Part A* **90A**, 906-919, doi:10.1002/jbm.a.32052 (2009).

337 Huang, M. H. *et al.* Degradation and cell culture studies on block copolymers prepared by ring opening polymerization of epsilon-caprolactone in the presence of poly(ethylene glycol). *Journal of Biomedical Materials Research Part A* **69A**, 417-427, doi:10.1002/jbm.a.30008 (2004).

338 Giesbers, M., Marcelis, A. T. M. & Zuilhof, H. Simulation of XPS C1s Spectra of Organic Monolayers by Quantum Chemical Methods. *Langmuir* **29**, 4782-4788, doi:10.1021/la400445s (2013).

339 Paripovic, D. & Klok, H.-A. Improving the Stability in Aqueous Media of Polymer Brushes Grafted from Silicon Oxide Substrates by Surface-Initiated Atom Transfer Radical Polymerization. *Macromolecular Chemistry and Physics* **212**, 950-958, doi:10.1002/macp.201000729 (2011).

Chapter 6 : Conclusions and Future Directions

6.1 Conclusions

Involvement of clinicians and surgeons in basic science research is essential as they are in a unique position to undertake research that can lead to surgical innovation and improvement in patient care, an area of focus for the Royal College of Surgeons of England and supported in their recent publication of professional standards in "Good Surgical Practice" (2014)[1]. Furthermore, the field of tissue engineering and regenerative medicine has caught the attention of the British Association of Plastic, Reconstructive and Aesthetic Surgeons (BAPRAS) and European Association of Plastic Surgeons (EURAPS) and featured heavily in the national and international meetings of 2015 as an area to focus upon with expected significant impact in the future for the speciality.

The work presented within this thesis began as a clinical question in a hand trauma clinic; "how can adhesions at gliding tissue interfaces, particularly in the hand, be reduced?" Adhesions in the hand, and elsewhere in the body, arise through the migration of cells following an injury as part of the healing response. Through the collaborative working that is present within the tissue engineering and regenerative medicine field, some underpinning technology that could one day develop into a potential solution to this clinical question is presented in this work. The experience and expertise from individuals trained in material science, engineering, chemistry and clinical surgery allowed the development of a scaffold that extends beyond a single functional use. An innovative and rationally designed scaffold is presented that could be adapted in a facile way for use at sites of injury for any gliding tissue interface, and beyond.

In the process of designing a scaffold that could be used to reduce adhesion formation in the hand, a modular and versatile approach was proposed to expand the potential applications for such a scaffold. Although not yet tested in a hand model, the work presented in this thesis theoretically could reduce adhesion formation following primary tendon repair. This is as a result of the pOEGMA antifouling polymer coating which has been shown to effectively reduce both protein and cell binding, outperforming similar work in the literature. This should result in the reduction in cell migration onto the tendon surface and

into the space adjacent to the tendon surface that results in scarring adhesion formation. Furthermore, the longevity of the pOEGMA functionalization was explored *in vitro* and demonstrated to have excellent stability following 10 week incubation in PBS in physiological conditions. Both the chemical and material properties, the antifouling actions, of pOEGMA are maintained to both cell and protein binding. Whilst this needs to be further assessed *in vivo*, it is encouraging that the lifespan of the antifouling action may indeed be satisfactory for controlling cell migration in the body over prolonged periods. This is essential for a surgical implant of this type. To establish whether this scaffold would indeed be effective following a primary tendon repair, a focused *in vivo* test would need to be undertaken in the future.

A bilayered scaffold with an antifouling surface and an opposing cell adhesive surface was further produced. Using a sequential electrospinning technique, excellent spatial control over functional groups was achieved. Through the use of end-functionalised polymers, this allowed the production of the pOEGMA antifouling bottlebrush and the placement of the cell adhesive cRGDS peptide in spatially discrete locations within the scaffold. This spatial control over a thickness of several hundred microns is particularly useful for the production of implants where a bi-functional scaffold could be useful in an anatomically narrow space. The space surrounding a tendon and within a tendon sheath is such an example where this narrow bilayer scaffold could be employed. The spatial control of such groups using the versatile electrospinning technique also allows the expansion of this scaffold to different architectures and different clinical applications for the future.

The work presented within the thesis has expanded the field of surface functionalization, particularly from electrospun fibres. The grafting of OEGMA from a PCL surface using controlled radical polymerisation was a first in field when published in Harrison *et al.*[2]. The combination of this approach and layered electrospinning of end-functionalised polymers gives excellent spatial resolution of cell adhesive and antifouling surfaces with a level of performance not yet seen in the literature. The versatile design outlined in this work has not yet been fully explored, for example the expansion of the work exploring novel monomer units for drug release. Furthermore, the biotiylated monomer also provides a facile method for the non-covalent incorporation of biological cues through the streptavidin-biotin interaction, not yet explored in this work.

6.2 Future directions

The scaffold design presented in this thesis was designed to be deliberately versatile and modular. This work has laid the foundation to explore this system further and to produce scaffolds with specific clinical aims to be taken forward into *in vivo* models, of which there are two that will be outlined below. There are also some further explorations of the properties of the design that could be explored for interesting and novel materials.

6.2.1 Exploring and expanding the mechanical properties

Mechanical testing of the scaffold demonstrated some interesting properties that have not yet been fully characterised by this work. Appendix I demonstrates that relatively thin scaffolds of electrospun scaffolds are able to withstand quite considerable normal forces. Further investigation into the mechanical properties, such as the frictional properties, would be of interest for a lubricating surface. Furthermore, the use of alternative monomers, such as 2-methacryloyloxyethyl phosphorylchloride (MPC) an antifouling monomer that appears to be more potent that PEG, which may provide a surface coating with a higher performance with regard to antifouling and gliding friction.

6.2.1.1 Creating a fibre-reinforced hydrogel

Through the facile modification of the polymerisation it should be possible to make the polymer brushes effectively create a hydrogel that is covalently bound to the fibres. This could be achieved through modifying the monomer to initiator ratio, or through reactivating the polymerisation reaction, to create much longer polymer chains. A cross-linking monomer unit could also be incorporated to form covalent bridges between polymer brushes to stabilise the gel layer.

The formation of a fibre-reinforced hydrogel may have advantageous mechanical properties for musculoskeletal tissue engineering, such as for cartilage regeneration in loaded joints. Investigating the impact of cross-linking on the antifouling behaviour of the pOEGMA would be essential as it may impact this important aspect of the surface functionalization.

6.2.2 Drug releasing polymer brushes

Pilot investigation into drug releasing monomers was investigated and has been included within the appendix of this work (Appendix K). Ibuprofen was used as a drug candidate for release by hydrolysis from the polymer brush. This proved to be quite challenging as the

ester linkage used appear very stable within this system and little drug release was seen. This system needs considerable further investigation and optimisation, but a drug releasing monomer may be possible from the polymer brush system. Initial work would focus on using a more labile linker, such as a thioester, to establish whether this would lead to an increased rate of hydrolysis.

6.2.3 In vivo testing

In vivo models are extremely useful for both investigating fundamental properties of scaffolds and for testing their designed function; both are required in this case.

6.2.3.1 Establishing the stability of the pOEGMA functionalization *in vivo*

The formation of a scaffold functionalization that is stable for the required length of time to perform its function is essential for a useful product. Within this thesis *in vitro* stability of the pOEGMA surface functionalization is explored in PBS and in physiological conditions (Chapter 5). It is highly likely that the presence of enzymes within tissue fluids would lead to the degradation of the pOEGMA brush more rapidly than in PBS. Due to the inherent difficulties of maintaining a sterile environment that would be an accurate representation of the *in vivo* situation, a formal assessment of the stability of the pOEGMA functionalization *in vivo* is planned.

Scaffolds functionalised with a pOEGMA antifouling surface will be implanted into a subcutaneous pocket in a mouse model with matched controls. These will be removed periodically over several weeks and analysed with XPS to characterise the breakdown of the polymer brush layer to accurately demonstrate the stability *in vivo*.

6.2.2.2 *In vivo* testing of the scaffold for flexor tendon repair

The scaffold in its current form with an antifouling surface and an opposing cell adhesive surface was designed with the test case of a flexor tendon primary repair in mind. This would be the first clinical application to test this scaffold against *in vivo* once the remaining tests detailed above were completed.

There are several ways that this scaffold could be further optimised with a primary tendon repair in mind. The use of orientated fibre electrospinning could be used to form a scaffold

with fibres that orientate to along the axis of the tendon. This may confer additional mechanical strength to the design. The scaffold could also be used as a cell donor to improve the healing of the injured tendon; a recent paper has demonstrated improved strength of repair when adipocyte derived stem cells (ASCs) were applied to a healing tendon[3]. The scaffold could be used as a cell donor vehicle whereby the ASCs could be applied to the cell-adhesive PCL-cRGDS surface and applied to the healing surface of the tendon with the antifouling face of the scaffold facing outwards.

6.2.3 Applying the versatile design for a different application: an engineered blood vessel

The scaffold was specifically designed to facilitate the facile modification to alternative applications; one such application a bioengineered blood vessel. Engineered blood vessels of less than 6 mm diameter are challenging to produce as they tend to thrombose, and are fully discussed in this recent review[4].

pOEGMA, in association with its antifouling properties, is known to be non-thrombogenic and could be used to generate a non-thrombogenic vascular interface[5]. Through the modification of the scaffold design in this thesis, a layered tubular scaffold could be produced by electrospinning with the inner surface functionalised with PCL-Ini. Following which, in line with this work, a pOEGMA bottlebrush could be produced from the inner surface to generate a non-thrombogenic lining for a tissue engineered vessel. With the versatility of the electrospinning processing, other layers of polymer could be used to generate the required mechanical properties. This could pose an exciting new direction for this work, and demonstrate the versatility of this system to the field of tissue engineering.

References: Chapter 6

1 (ed Professional Standards) (Royal College of Surgeons of England, London, 2014).

2 Harrison, R. H. *et al.* Modular and Versatile Spatial Functionalization of Tissue Engineering Scaffolds through Fiber-Initiated Controlled Radical Polymerization. *Advanced Functional Materials* **25**, 5748-5757, doi:10.1002/adfm.201501277 (2015).

3 Uysal C, T. M., Hyakusoku H, Mizuno H. Adipose-derived stem cells enhance primary tendon repair: Biomechanical and immunohistochemical evaluation. *Journal of Plastic, Reconstructive & Aesthetic Surgery* **65**, 1712-1719 (2012).

4 Thottappillil, N. & Nair, P. D. Scaffolds in vascular regeneration: current status. *Vascular health and risk management* **11**, 79-91, doi:10.2147/vhrm.s50536 (2015).

5 Hahn, M. S., McHale, M. K., Wang, E., Schmedlen, R. H. & West, J. L. Physiologic pulsatile flow bioreactor conditioning of poly(ethylene glycol)-based tissue engineered vascular grafts. *Annals of biomedical engineering* **35**, 190-200, doi:10.1007/s10439-006-9099-3 (2007).

Chapter 7 : List of appendices

A **Harrison RH** *et al*. "Tissue Engineering and Regenerative Medicine: a Year in Review" Tissue Engineering Part B: Reviews. February 2014, 20(1):1-16. Impact factor 4.254. Reprinted with permission from TISSUE ENGINEERING, Part B, February 2014, Volume 20, Issue 1, pp. 1-16, published by Mary Ann Liebert, Inc., New Rochelle, NY.

B **Harrison RH** *et al.* "Modular and Versatile Spatial Functionalization of Tissue Engineering Scaffolds through Fiber-Initiated Controlled Radical Polymerisation" Advanced Functional Materials (Volume 25, Issue 36 p5748-5757). 2015. Impact factor 10.8. This is reproduced under a Creative Commons Attribution License (CC BY).

C Purification of Cu(I)Br

D SOP for ARGET ATRP in solution

E Tof-SIMS assessment of silicon surfaces

F Method and assessment of adsorbed polymer removal from scaffolds

G Characterisation of the biotin monomer

H Synthesis of the amino-cy5 dye and characterization

I Mechanical testing of scaffolds

J Calculating the contact pressure on scaffolds exerted by mechanical testing

K Chapter: Drug Releasing Scaffolds

L Permission for reproduction of Figure 7-12 from Ricciotti *et al.*[340]

M List of publications

Appendix A

TISSUE ENGINEERING: Part B
Volume 20, Number 1, 2014

DOI: 10.1089/ten.teb.2013.0668

Year in Review

Tissue Engineering and Regenerative Medicine: A Year in Review

Rachael H. Harrison, MBBS, BSc,[1–3,*] Jean-Philippe St-Pierre, PhD,[1–3,*] and Molly M. Stevens, PhD[1–3]

It is an exciting time to be involved in tissue engineering and regenerative medicine (TERM) research. Despite its relative youth, the field is expanding fast and breaking new ground in both the laboratory and clinically. In this ''Year in Review,'' we highlight some of the high-impact advances in the field. Building upon last year's article, we have identified the recent ''hot topics'' and the key publications pertaining to these themes as well as ideas that have high potential to direct the field. Based on a modified methodology grounded on last year's approach, we have identified and summarized some of the most impactful publications in five main themes: (1) pluripotent stem cells: efforts and hurdles to translation, (2) tissue engineering: complex scaffolds and advanced materials, (3) directing the cell phenotype: growth factor and biomolecule presentation, (4) characterization: imaging and beyond, and (5) translation: preclinical to clinical. We have complemented our review of the research directions highlighted within these trend-setting studies with a discussion of additional articles along the same themes that have recently been published and have yet to surface in citation analyses. We conclude with a discussion of some really interesting studies that provide a glimpse of the high potential for innovation of TERM research.

The Aim, Scope, and Methods of This Review

Last year's ''Year in Review'' article,[1] the first in this journal, provided a solid starting point for this year's examination of the literature. We adapted the method described by Fisher and Mauck to identify the highly cited publications. Here, we will only give a brief outline of this methodology and discuss the modifications that were necessary to adapt to a more restrained time frame encompassing the period after last year's review. The modified method looks to identify publications primarily based on the number of times each one has been cited in the literature (an unbiased criterion). However, we have also had to rely on our own appreciation of the field to identify publications that we believe are likely to impact tissue engineering and regenerative medicine (TERM) but have been published too recently to be identified based on the citation number alone. We used the Web of Knowledge[SM] database to search for original articles on the topics of ''tissue engineering'' and ''regenerative medicine'' published between January 2012 and September 2013 inclusively. While this exhibits some overlap with the previous review, we believe that the increased lead-time for citation may reveal some interesting articles that may have escaped the net in the previous year. In much the same way, we expect next year's review to highlight some key publications that we may have overlooked in this work. Our search revealed over 8000 original publications for tissue engineering or regenerative medicine since January 2012. We found that in particular the articles published in 2013 had low levels of citation. This is not surprising as it is likely to take several years before the true impact of a publication can really be revealed with its citation number.

We will caveat our review in that while we have endeavored to identify exciting new developments, the sheer number of publications in the field is staggering and cannot be condensed into this work. As indicated in the previous review, very often the most important articles that change the course of a field arise from the pool of knowledge and can require time to take hold in the field. Furthermore, TERM research is diverse and continues to expand into uncharted waters. Areas such as state-of-the-art chemistry, imaging, computational design, engineering, and the importance of close clinical collaboration are becoming increasingly relevant as the field matures. There are therefore vast areas of the field that we have not been able to cover, but we hope to give you a flavor of some of the exciting developments in the TERM field in the last year.

Pluripotent Stem Cells: Efforts and Hurdles to Translation

Primary cells and adult stem cells remain often-used cell sources in a number of TERM applications and have been

Departments of [1]Materials and [2]Bioengineering, Imperial College London, London, United Kingdom.
[3]Institute of Biomedical Engineering, Imperial College London, London, United Kingdom.
*These authors contributed equally to this work.

applied with a range of success in clinical settings.[2] Nevertheless, growing interest in the potential of pluripotent stem cells and specifically induced pluripotent stem cells (iPSCs) for disease modeling and drug discovery as well as therapeutic applications has led to major breakthroughs in the last year or so. These new developments in our understanding of pluripotent stem cells, as well as the unmet challenges toward clinical translation will be the focus of this section.

The work by Takahashi and Yamanaka to demonstrate that mouse somatic cells can be reprogrammed into pluripotent stem cells by forcing the expression of four transcription factors (*Oct4*, *Sox2*, *Klf4*, and *c-Myc*; Yamanaka factors) published in 2006[3] and later adapted to human cells[4,5] has had a tremendous impact on our field. This is best evidenced by the attribution of the 2012 Nobel Prize in Medicine to Dr. Shinya Yamanaka jointly with Sir. John Gurdon ''for the discovery that mature cells can be reprogrammed to become pluripotent.'' First and foremost, this technique is proving to be powerful research tools in disease modeling, as well as drug discovery and screening because of the ability to generate patient-specific cells. For those interested in the progress made along those lines of investigation, a number of reviews are suggested.[6,7] The potential for the generation of patient-specific stem cells with the ability to differentiate into any cell type in the body unveiled by this discovery has also led to the rapid adoption of the technology in TERM research and has fueled efforts to attempt to address its limitations. Key issues with the original protocol for the generation of these iPSCs that have been the source of many concerns with regard to their clinical translation pertain to the random genomic integrations of the transgenes and the tumorigenic risks associated with the use of *C-MYC*, an oncogenic factor.[8] While numerous strides have been accomplished in addressing these issues, an approach whereby only small chemical molecules could be used to generate iPSCs remained elusive. Recently, Hou *et al.* were able to generate these chemically induced pluripotent stem cells (CiPSCs) without the need for viral transfection[9]; building on previous work in which the authors identified a combination of four small molecules that enabled the reprogramming of somatic cells to iPSCs with the transfection of a single gene (*Oct4*).[10] Further improvements focused on the identification of molecules that drive late reprogramming and increase the efficiency of the process to match that obtained with the Yamanaka approach. Another interesting advance in the field of iPSCs research that was published in the last year was the demonstration that the depletion of a single protein, the epigenetic repressor factor *Mbd3*, was sufficient to increase the iPSCs reprogramming efficiency with the transfection of the Yamanaka factors to nearly 100%.[11]

Another concern associated with the clinical translation of iPSCs is the potential immunogenicity of autologous cell-derived iPSCs due to the potential for incomplete reprogramming and genetic instabilities. The previous ''Year in Review'' publication highlighted an article by Zhao *et al.* in which it was reported that the transplantation of undifferentiated iPSCs resulted in an important immune reaction in syngenic mice compared to embryonic stem cells (ESCs).[12] These findings have sparked a debate in the field as to the immunogenicity of iPSCs and their potential for regenerative medicine applications.[13] In a recent study, Araki *et al.* addressed what they perceived as limitations of this previous study by evaluating the immunogenicity of terminally differentiated cells obtained from chimeric mice developed from integration-free iPSCs and ESCs with germ line transmission capabilities in transplantation experiments.[14] Through this approach, they observed limited or no immune response to the transplantation of dermal and bone marrow tissues originating from either cell source in syngeneic conditions. This line of investigation is much more relevant to TERM applications in which cells would be fully differentiated *in vitro* before transplantation. Another study by Guha *et al.* corroborates these observations with *in vitro* and transplantation data on the immunogenicity of syngeneic iPSCs-derived embryoid bodies, as well as endothelial cells, hepatocytes, and neuronal cells (representing the three embryonic germ layers).[15] While the authors found that these iPSCs-derived cells expressed low levels of CD80, CD86, and CD40 that have been associated with the stimulation of T-cell proliferation, further characterization demonstrated that these cells exhibited negligible effects on T-cell proliferation *in vitro* in a syngeneic context. Furthermore, iPSCs- and ESCs-derived differentiated cells transplanted in the subcapsular renal space of mice were shown to survive in 100% of the syngeneic recipients and did not exhibit $CD4^+$ and $CD8^+$ T-cell infiltration up to 3 months post-transplantation. In another study, Liu *et al.* compared the immunogenicity of neural progenitor cells differentiated from iPSCs derived from skin fibroblasts and umbilical cord mesenchymal cells, known to be less immunogenic than other cell types.[16] They were able to show that the low immunogenic state of the cells of origin could be retained following reprogramming. Further to this discussion, mounting evidence accumulates to support the view that the reprogramming process and *in vitro* culture protocols may affect the genetic, epigenetic, and transcriptional make-up of a cell. Nazor *et al.* identified such aberrations in a large number of iPSCs lines by comparing their epigenetic patterns with that of cells found in 17 distinct tissues from multiple individuals and primary cell lines.[17] Of importance, these aberrations were maintained following spontaneous and directed differentiation. Hence, it is becoming clear that despite the encouraging reports on the low immunogenicity of differentiated cells derived from iPSCs of a syngeneic source, immunogenicity must be examined for each individual protocol toward clinical translation.

One recent article tackled the need for a quick and reliable screening protocol to assess the tumorigenic potential of individual iPSCs lines.[18] In this work, the authors demonstrated that the chondrogenic differentiation of iPSCs in micro-mass cultures allows the identification of cell lines that display abnormalities. While the majority of human iPSCs tested formed cartilage similar to that obtained with ESCs, some lines led to glandular epithelial cysts with columnar epithelium together with the expression of specific tumor markers. Implantation of these tissues subcutaneously in immune-compromised mice led to the generation of tumors despite these iPSCs lines appearing normal in their undifferentiated state. However, it must be stated that some cell lines with tumorigenic potential could only be identified after long *in vitro* incubation periods of more than 8 weeks. Such protocols will become essential to screen iPSCs lines in clinical translation efforts.

While these safety concerns are being investigated, research to demonstrate the potential of iPSCs in different TERM applications continues apace. In a highly cited study, the transplantation of long-term self-renewing neuroepithelial stem cells derived *in vitro* from human iPSCs promoted the recovery of hind limb motor function in a mouse spinal cord injury model, which also allows control mice to recover some of their hind limb mobility.[19] The functional recovery was comparable to that observed following the injection of human fetal spinal cord-derived neural stem cells, and it was shown that neurons differentiating from the transplanted cells participated in this recovery. In another study that highlights the potential of iPSCs for clinical interventions, Tedesco *et al.* generated autologous mesoangioblast-like cells from iPSCs derived from patients with limb-girdle muscular dystrophy type 2D and corrected the genetic disorder via lentiviral transfection of the gene for human α-sarcoglycan.[20] The potential of mesoangioblasts for the treatment of muscular dystrophy had previously been demonstrated, but these cells are depleted in patients with limb-girdle muscular dystrophy type 2D. In this study, the potential clinical benefits of corrected iPSCs-derived mesoangioblasts were demonstrated by transplantation in α-sarcoglycan-null immunodeficient mice, which led to the formation of new muscle fibers positive for α-sarcoglycan.

Our citation analysis has highlighted the fact that increasing efforts are being focused on the development of reprogramming protocols to transdifferentiate cells to other lineages while bypassing the pluripotency step. Advantages of this approach include lowered risks of tumor development compared to the use of pluripotent stem cells in TERM applications and simplified differentiation protocols. In one such study, Margariti *et al.* transfected human fibroblasts with the Yamanaka factors by nucleofection for only 4 days to generate partial iPSCs with altered phenotypes.[21] Importantly, these cells did not form tumors up to 2 months after transplantation in immunodeficient mice. The cells were directed to differentiate into endothelial-like cells with the ability to form vascular-like tubes both *in vitro* and *in vivo* in Matrigel® plugs. These promoted increased blood flow compared to fibroblasts when injected into mice with an ischemic hind limb. In a similar study, Meng *et al.* generated induced mesenchymal stem cells (MSCs) with the potential to differentiate into osteoblasts, chondrocytes, or adipocytes from cord blood $CD34^+$ cells and adult peripheral blood $CD34^+$ cells by forced overexpression of OCT4 (human) with the MSCs phenotype stabilizing over a period of approximately 4 weeks.[22] Again, these induced MSCs did not form tumors up to 3 months after transplantation into immunodeficient mice. Interestingly, the authors selected blood cells as the source for induced MSCs because these cells are likely to contain fewer acquired genetic mutations than dermal fibroblasts and their collection is minimally invasive. Another study accomplished the reprogramming of astrocytes to neuroblasts with the ability to differentiate into neurons *in vivo* via lentiviral delivery of *Sox2* in mouse brains.[23] Taking it a step further, Abad *et al.* published a first report of the generation of iPSCs *in vivo* with teratoma-forming capability via reprogrammable mice modified to express the Yamanaka factors when induced by doxycycline.[24]

While the proportion of publications on pluripotent stem cells for TERM applications that focus on iPSCs has increased constantly since their discovery, a large body of work published every year still involves ESCs. Of major significance, one recent study by Tachibana *et al.* made the first demonstration of an approach to generate patient-matched human ESCs lines by somatic cell nuclear transfer (NT-ESCs) through a systematic evaluation of factors that may work to retain meiosis factors within oocytes during their enucleation and subsequent somatic cell nucleus introduction.[25,26] NT-ESCs lines expressed the major pluripotency genes, displayed a normal diploid karyotype with a nuclear genome matched to the nuclear donor cells, and were shown to differentiate into cells from the three germ layers when injected into immunodeficient mice. As the mitochondrial DNA of NT-ESCs originated in large part from the oocytes, the authors also suggested that such cells may offer a strategy to correct mutations in patients with inherited or acquired mitochondrial DNA diseases.

A trend in pluripotent stem cell research toward an increased proportion of studies on the combined topics of iPSCs and ESCs highlights a discussion in the field as to the optimal cell source for TERM applications. Some of these comparative studies have been discussed in detail here. In light of the major developments in the field of pluripotent stem cell research that have occurred in the last year with regard to both iPSCs and ESCs (particularly the generation of CiPSCs and NT-ESCs), it will be exciting to see how the field evolves in the coming years and if one of these two cell sources will gain clinical traction and impact in TERM or if indeed adult progenitor and primary cells will remain the most applied cell sources.

Tissue Engineering: Complex Scaffolds and Advanced Materials

While materials have been implanted in humans for more than 3000 years,[27] the period that spans the 1960s and 1970s is generally considered the beginning of the modern era of biomaterials design. During that period, researchers aimed to develop implants that performed mainly mechanical functions while eliciting minimal host response. The ''bioinert'' materials developed during this period have had, and still have, a major impact on the treatment of a number of diseases. In the 1980s, a natural transition occurred toward the design of biomaterials with a controlled biological activity. The advent of TERM has fueled another paradigm shift in our approach to biomaterials design toward complex and smart materials that interact with cells to direct their biological response and can even be responsive to cells. In this section, we will review some of the interesting advances of the last year or so toward the development of these smart biomaterials. Scaffold engineering incorporating both base material synthesis and design considerations is a field that is rapidly growing to become increasingly multidisciplinary. In this section, we will cover scaffold design, both using natural and artificial base materials, and the importance of the cell–surface interface.

Decellularized scaffolds

Decellularization is an approach that removes the resident cells and a large proportion of the major histocompatibility complex (MHC) from a tissue or whole organ through optimized protocols that rely considerably on perfusion with

detergents.[28] The extracellular matrix (ECM) can be preserved complete with native geometry and anatomical features, including perfusable vasculature. These scaffolds can then be seeded with cells to repopulate the matrix and ensure a degree of functionality before implantation. This approach offers an attractive option for tissue scaffolds in a number of applications as it provides macro- and micro-environmental cues at both the compositional and structural levels that are likely to direct cellular phenotype.

Song *et al.* decellularized cadaveric rat kidneys via detergent perfusion through the renal artery.[29] The optimization of the process ensured that the intricate structures of the renal glomerular and tubular compartments, essential for renal function, were preserved. Recellularization using human umbilical venous endothelial cells also via the renal artery and rat neonatal kidney cells through the ureter was achieved with the assistance of a vacuum. After seeding, organs were transferred into a perfusion bioreactor to provide whole organ culture conditions. Filtrate (''urine'') was produced from the recellularized kidney both *in vitro* and *in vivo* (Fig. 1). While it would be premature to herald this as the replacement for traditional renal transplantation, it is an exciting proof-of-concept study that emphasizes a real potential for renal scaffolds. Like conventional renal transplantation (allogenic renal transplantation), whole organ decellularization requires one organ to be sourced per intervention and thus may not address the imbalance between supply and demand for organ transplantation. This process,

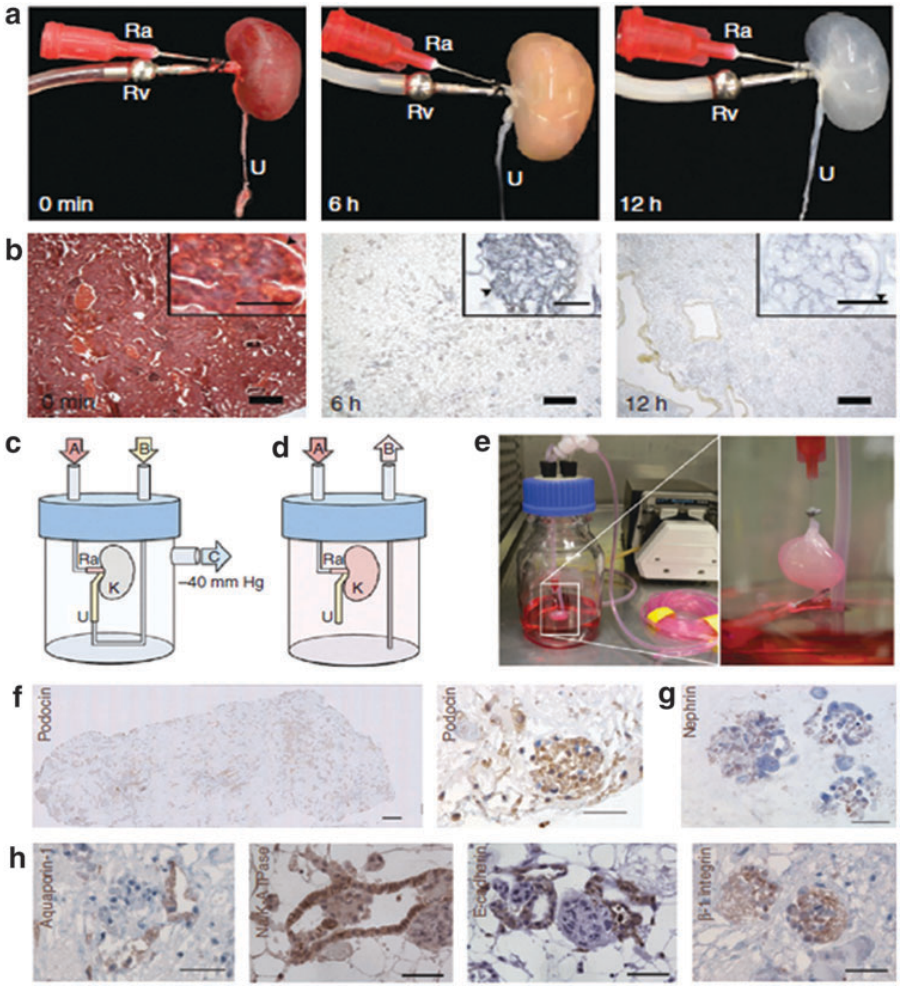

FIG. 1. Perfusion decellularization of whole rat kidneys (adapted with permission from Macmillan Publishers Ltd: *Nature Medicine*,[29] copyright 2014). **(a)** Time lapse photographs of a cadaveric rat kidney undergoing antegrade renal arterial perfusion decellularization. Ra refers to renal artery, Rv to renal vein, and U to ureter. **(b)** Associated Movat's pentachrome-stained sections. Black arrowheads indicate the Bowman's capsule. Scale bars 250 μm (main images); 50 μm (insets). **(c)** Cell seeding and **(d** and **e)** whole-organ culture set-up for decellularized rat kidneys. **(f–h)** Immunohistochemical images of **(f)** an entire graft cross section confirming engraftment of podocin-expressing epithelial cells (left) and of a reseeded glomerulus showing podocin expression (right) [scale bars, 500 μm (left); 50 μm (right)], **(g)** Nephrin expression in regenerated glomeruli (scale bar, 50 μm), and **(h)** Aquaporin-I expression in regenerated proximal tubular structures (left); Na/K-ATPase expression in regenerated proximal tubular epithelium (middle left); E-cadherin expression in regenerated distal tubular epithelium (middle right); and β-1 integrin expression in a regenerated glomerulus (right) (scale bars, 50 μm).

while not eliminating the need for donor kidneys, has two potential principle advantages based on their immunogenicity (which should be low due to the few MHC remaining). First, it is likely that organs would not need to be matched for human leukocyte antigens (HLA), and second, that the patients will not require lifelong treatment with immunosuppressant therapy, drugs that have considerable side effects and high medical costs. These conclusions are drawn from successful implantation (into human patients) of decellularized scaffolds for other purposes that have been re-seeded with autologous cells.[30–31] The kidney decellularization study comes on the heels of two other major accomplishments by the same group in the field of whole organ decellularization with methodologies tailored for the heart[32] and lung.[33]

A significant disadvantage of decellularization protocols is the reduction in the material integrity of the tissue as it tends to leave a soft and compliant scaffold. For some structures such as the airway, this is especially problematic. To withstand the rigors of respiration, the trachea must have longitudinal flexibility and lateral rigidity. This is achieved through C-shaped cartilage rings found along its length. Decellularized tracheal scaffolds have been successfully used in patients, but processing renders the cartilage very lax and the scaffolds tend to collapse inward on inspiration and may ultimately lead to stenosis. This is prevented with the use of a stent either on a temporary or permanent basis. This issue has been examined by Partington *et al.*, who have proposed that the loss of glycosaminoglycan (GAG) content from the cartilage may cause this loss of strength.[34] An interesting alternative to the use of stents has been proposed by Ma *et al.* who devised a decellularization protocol for the larynx that allows for improved preservation of the cartilage ECM and resident chondrocytes.[35] Previous work by the same group had demonstrated that this protocol maintained the mechanical properties of the laryngeal framework in a canine model.[36] The examination of the cadaveric human larynx for the distribution of HLA has demonstrated differences between HLA I and II distribution. HLA II (found on highly immunogenic antigen presenting cells and a key initiator in transplant rejection) was not expressed by chondrocytes or found within the cartilage ECM but was strongly expressed by the epithelium, submucosal glands, and perichondrium. HLA I was identified on chondrocytes, but the antigens are protected from exposure to lymphocytes as they are held within a dense avascular matrix.[37] This infers an immune-privileged characteristic to cartilage, and allografts have been used clinically without rejection.[38] Ma *et al.* demonstrated that after 12 weeks *in vivo* scaffolds showed no sign of collapse or T-cell-mediated immune rejection.[35]

Clinical successes with decellularized tissue/organ scaffolds will be discussed later in this review and reinforce how important the cellular environment is for supporting tissue regeneration. However, decellularized ECM does not need to be isolated from an organ or tissue biopsy. A recent article highlighted in our citation analysis used ECM deposited *in vitro* by adipocyte-derived stem cells (ASCs) or synovium-derived stem cells (SDSCs) to enhance the chondrogenic differentiation of ASCs.[39] The ASCs were expanded on either of these deposited ECMs or on culture plastic. Cells cultured on both ASC- and SDSC-derived ECM had enhanced chondrogenic differentiation capacity when compared to cells grown on culture plastic. Interestingly, there was no significant difference between cells grown on ASC- or SDSC-derived ECM. The authors emphasize the tremendous potential of ASCs as a source of autologous cells for a number of clinical applications as they can be isolated in high numbers by simple procedures in an average patient with minimal morbidity. This work builds upon previous efforts from our group demonstrating similar findings when differentiating ESCs into the osteogenic lineage using ECM.[40] Another interesting article highlighted by our citation analysis challenges the conception that tissue reconstruction using a decellularized scaffold requires replacement on a like-for-like basis. Wolf *et al.* suggested that this may not always be the case.[41] In this article, the authors compared the remodeling outcome in a rat abdominal wall injury model following the implantation of decellularized skeletal muscle tissue (similar to the native injured tissue) and decellularized small intestine mucosa (different to native injured tissue). To their surprise, both scaffolds induced a similar positive healing response with evidence of scaffold degradation and myogenesis. In fact, they could not identify any histological difference in the repair tissues formed with the two scaffold types at 35 days.

While current advances in the area of tissue and organ decellularization are exciting, they do not address the potential Achilles heel of the process, which is the one-for-one need for a tissue or organ to become the scaffold. Further challenges to clinical translation include sterilization procedures for scaffolds (without compromise to the protein framework), sufficient cell numbers, the need for clinical grade bioreactors, and the clinical logistics of this approach. A more detailed discussion is contained in a review by Song *et al.*[42] Artificial scaffolds are not held back by many of these constraints, and while considerable challenges remain to be addressed to envelop the innate complexity of natural tissue and organs, a number of very interesting advances over the last year suggest that we are gaining ground in replicating the structures present in native tissues within these artificial scaffold designs.

Artificial scaffolds and materials

A number of artificial scaffold designs have become integral parts of the clinical tool box with which practitioners treat patients with skin,[43] bladder,[44] cartilage,[45] and bone[46] damage. As the first-generation designs are making a clinical impact, increasing complexity is being incorporated into new scaffold designs. These strides forward stem from an improved integration of the different fields that form the multidisciplinary environment required for advances in the design of truly biomimetic ''smart'' scaffolds. Collaboration between chemists, material scientists, and cell and molecular biologists has been coupled with important advances in our understanding of the structural and compositional organization of tissues and organs and the cell–material interface. It must be emphasized, however, that it may not always be necessary to replicate the complexity of the native environment to generate functional tissue. This was demonstrated previously with a successful bone tissue engineering approach in a simple system, the use of an ''*in vivo* bioreactor.''[47] This study created a subperiosteal space through hydrostatic dissection of the tibial periosteum in

New Zealand white rabbits (the ''*in vivo bioreactor*''). A calcium-alginate hydrogel was injected into this space, and led to woven bone formation at 2 weeks maturing to fully mineralized compact bone by 6 weeks. This simple system harnesses the body's own healing mechanism and can generate large amounts of bone without involving the implantation of cells or growth factors.

A traditional challenge in the design of scaffolds for tissue engineering applications is the lack of a perfusing blood supply to nourish the resident cells upon implantation. This impacts upon scale-up to sizes relevant to human applications, the ability to preseed the scaffolds, cell survival, and subsequent construct function. Angiogenesis and the control thereof is a field in its own right, but the consideration of vasculature and perfusion in scaffold design is essential to many TERM applications and a topic that has seen interesting developments in the last year or so. Miller *et al.* proposed an interesting approach to this problem by generating a perfusable vascular network via a three-dimensional (3D) printed network of carbohydrate glass.[48] This sacrificial mould was coated by a thin layer of poly(D-lactide-co-gylcolide) (PLGA) before being encapsulated within a suspension of cells in a range of hydrogels, including agarose, alginate, poly(ethylene glycol) (PEG) hydrogels, and Matrigel®. These were then cross-linked before the glass filaments were dissolved away to reveal patent fluidic PLGA channels. The approach was successful using a variety of ECM prepolymers, natural and synthetic, differing in both bulk material properties and means of cross-linking. This technique is advantageous over other channel-forming techniques previously proposed as the carbohydrate glass mould can be removed without the use of cytotoxic organic solvents and can be accomplished in aqueous conditions in the presence of living cells.[49,50] An alternative approach to vascularization was proposed by Jiang *et al.* who loaded a salt-leached porous PEG hydrogels with different concentrations of fibrin. *In vivo* studies showed that increased cellular penetration and vascularization were seen in scaffolds containing fibrin, but interestingly, the effect was not concentration dependent.[51]

Another area highlighted by our search featured the employment and advancements in computational design for scaffolds. As the need for scaffold complexity increases, this technique has allowed for greater control over topographical features. Gauvin *et al.* used a versatile layer-by-layer approach to build a porous scaffold of photocrosslinkable gelatin methacrylate using projection stereolithography based on computer-aided design.[52] The structural properties of a scaffold are known to be very important in the provision of cellular cues, so using a technique that allows fine-tuning of features such as pore size has a direct impact on cell migration and fluid diffusion through the scaffold. Such computational design also allows for high-throughput production and the possibility of patient-specific scaffold fabrication through the combination with patient imaging and data.

Our citation analysis pointed out some interesting articles demonstrating the advances in materials synthesis and design that can be used for improved scaffolds and are hence relevant to the field. Of particular note is the article by Sun *et al.* on hydrogels, which are commonly used scaffolds in the field, but their indications are often limited by their mechanical properties. In this study, the authors synthesized a hydrogel capable of stretching to 20 times its initial length. This was achieved by mixing two cross-linked polymers: ionically cross-linked alginate and covalently cross-linked polyacrylamide. The hydrogel also exhibited a fracture energy of $\sim$9000 Jm^{-2}, which is very favorable when compared to other gels and was relatively unaffected by notching (holes).[53] It will be interesting to see if this design of hydrogel will find a niche in TERM applications requiring high elasticity materials.

Tissue regeneration can be achieved with scaffold-free systems. Advances in fabrication of functional 3D tissues through stacking of cell sheets can lead to the formation of tissue or organ models. Coined ''cell-sheet engineering,'' a temperature-responsive surface, is used to culture cells. Upon reaching confluency, the surface can be cooled to 20°C to reduce its hydrophobicity, and the intact cell sheet can be removed easily. Cell–cell junctions, ECM, and cell surface proteins are preserved with this process. Cell sheets can be stacked to generate cell-dense tissues. It is also possible to include prevascular networks within the stack providing a possible connection to host vessels on transplantation and another approach to the problem of perfusion. Stacked layers of cardiomyocytes that beat simultaneously without the use of a formal scaffold are a powerful example of the strength of this method.[54]

Controlled or uniform cell seeding of scaffolds is a complex endeavor that has limited the successful implementation of a number of scaffold designs. Recent articles by Sampson *et al.*[55] and Wang *et al.*[56] have proposed interesting approaches to address this limitation. Sampson *et al.* have found a clever methodology to incorporate cells within electrospun scaffolds that typically exhibit poor cell infiltration capabilities. In this process, a biopolymer (modified Matrigel®) was used to form fibers, and the cells were incorporated in the polymer solution so that they were entrapped within the fibrous network. The group accomplished this with the typical voltage-driven electrospinning process and aerodynamically assisted bio-threading, which utilizes a pressure differential to produce the fibers. The fabrication process constructs supported cell viability and demonstrated no changes in cell phenotype when compared to controls following fiber formation and *in vivo* implantation.

The cell–substrate interface

One of the key features of a smart material is the surface with which the cell interacts. The importance of controlling the biophysical cues presented by materials to direct cell response has been central to TERM efforts for some time. This was demonstrated by Engler *et al.*, who showed that the elasticity of the matrix microenvironment can direct the differentiation of MSCs to different lineages.[57] The importance of biophysical cues has been exemplified in a recent study by Downing *et al.* who investigated the effects of cues in the form of parallel grooves and aligned nanofibers on the epigenetic state of adult fibroblasts.[58] With such an approach, they observed up to fourfold increase in Nanog-positive colonies in cells that had been transduced with the four Yamanaka factors or with only three factors (*Oct4*, *Sox2*, and *Klf4*). The authors attributed this increased reprogramming efficiency to decreased histone deacetylase 2 activity and the upregulation of WDR5 (a subunit of H3

methyltranferase) accompanied by increased histone H3 acetylation and trimethylation of histone H3 lysine 4. They proposed that these changes were linked to changes in the cell and nucleus shape as well as the cytoskeletal organization resulting from culture on microgrooved surfaces. In another article, Wang *et al.* demonstrated the regulation of cell behavior, including locomotion, proliferation, and differentiation, using stiffness gradients prepared with polydimethylsiloxane.[59] The effect of tissue elasticity on cell phenotype continues to be the subject of detailed investigations as in a recent publication by Swift *et al.*[60] Nevertheless, incorporation of such biophysical cues within scaffold designs remains a challenging endeavor.

Directing the Cell Phenotype: Growth Factor and Biomolecule Presentation

Beyond the cellular signals provided by a scaffold's chemistry, structure and mechanical cues, the delivery of growth factors can instruct cellular response and favorably impact tissue and/or organ regeneration. Traditionally, growth factors and other bioactive molecules have been administered either in solution or via controlled delivery systems. These approaches have been essential parts in a number of successful TERM applications, and defined media supplemented with key growth factors and biomolecules are essential components of *in vitro* cell differentiation and culture protocols. However, optimized growth factor combinations to instruct specific cell responses, such as adhesion, proliferation, migration, differentiation, and eventually tissue regeneration simultaneously or in a relevant sequence, often remain to be revealed by fundamental studies. Not only is the optimal concoction specific to the target tissue or organ, but it can also depend on the cell source, scaffold, and patient-specific factors, such as age and comorbidity.

Gene therapy has emerged as an interesting tool for the delivery of growth factors to encourage tissue regeneration in TERM applications. It has been proposed as a means to circumvent the limitations associated with growth factor delivery, such as high costs, the limited stability of these biomolecules, and the ability to localize the expression of these factors by harnessing the cells involved in the regenerative process as factories for growth factor production and release (or alternatively as a means to inhibit the expression of a specific protein through the delivery of siRNA or shRNA). Readers who would like more information on recent advances in gene therapy for specific TERM applications are referred to the following review.[61] Here, we will focus on a few recent studies that exemplify efforts in the field to integrate gene therapy with TERM approaches. A highly cited study published in the last year illustrates the advantageous combination of gene therapy and scaffold design. Human MSCs were encapsulated within fibrin, alginate, or agarose hydrogels along with nonintegrating adenoviral vectors containing the cDNA for bone morphogenetic protein-2 (BMP-2) or insulin growth factor-1.[62] This approach allowed transfection to occur *in situ*, bypassing the need for additional *in vitro* culture steps and increasing transfection efficiency compared with cells cultured in two dimensional (2D). Interestingly, high levels of transgene expression could be obtained with a much lower multiplicity of infection than in 2D systems. This approach may minimize the concentration of viral vectors required to induce the release of a therapeutic concentration of growth factors and therefore improve the safety profile. Other studies reported on scaffold modifications to extend the duration of transduction activity. One such study showed that the conjugation of polysaccharides (such as chitosan and heparin) onto the surfaces of porous PLGA scaffolds increased the incorporation and retention of lentiviral vectors onto the scaffolds, as well as the transgene expression by cells seeded within the porous structure.[63] The authors demonstrated that such surface modification of scaffolds also led to increased and sustained transgene expression in a mouse spinal cord injury model. Similarly, another study demonstrated that the incorporation of hydroxyapatite nanoparticles within fibrin hydrogels led to prolonged lentivirus-driven expression of GFP by cells migrating within the scaffold and in the surrounding tissue following subcutaneous implantation.[64] Using a microinfusion approach, Zou *et al.* were able to generate gradients of hydroxyapatite via amino groups generated on the surface of electrospun mats by an aminolysis process.[65] This was accomplished by sequential incubations of the mats in glutaraldehyde, gelatin, and simulated body fluid and allowed spatially controlled loading of the mats with plasmid DNA for cell transfection and associated control over the ability to transfect cells. Aside from the spatial control over transfection, the gradients of gelatin and hydroxyapatite on the surface of the mats were shown to impact viability and alkaline phosphatase (ALP) activity in preosteoblastic cells.

Alternatively, elegantly designed and increasingly complex biomimetic matrices incorporating peptide sequences specifically chosen to retain biomolecules such as growth factors in a biologically relevant manner (controlling their half-life and activity) have been developed. A recent study by Martino *et al.* perfectly exemplifies the principles behind this novel approach to the presentation of growth factors in TERM systems.[66] In this work, the authors demonstrated and characterized the specific binding of a range of growth factors to the heparin-binding domain of fibrinogen (Fg $\beta 15\text{-}66_{(2)}$) in a manner that does not influence their activity. The heparin-binding domain was then conjugated within a PEG hydrogel in combination with a cell adhesion peptide. The synthetic matrix, intended to mimic fibrin, was then loaded with fibroblast growth factor-2, placenta growth factor-2, or a combination of the two. This was implanted in full thickness skin defects in a genetic mouse model of diabetes characterized by impaired wound healing. Those scaffolds incorporating the heparin-binding domain and growth factors led to significantly faster wound healing when compared to controls (synthetic matrices loaded with growth factors, but without the heparin-binding domain). In fact, the results were comparable to those observed when the growth factors were delivered within a natural fibrin matrix.

Another study in a similar vein was highlighted in our literature analysis. Lee *et al.* used heparin-binding peptide amphiphiles to form nanofiber gel networks within the pores of a collagen sponge with the ability to bind BMP-2 and regulate its activity.[67] The addition of heparin sulfate during the gelation process led to a more gradual release of the BMP-2 bound within the nanofiber gel. When implanted within 5 mm (critical size) femoral defect in rats, collagen foams filled with heparin-binding peptide amphiphile gels (containing both heparin sulfate and BMP-2) led to

significantly more new bone formation than controls in which one or more of the components were absent. Furthermore, bridges had been achieved in greater than 50% of the defects in animals treated with this construct after 6 weeks. This is a significant result given that the concentration of BMP-2 added to the system was one order of magnitude lower than the required dose in other systems tested with the same animal model. This is especially pertinent since questions are being raised in regard to the potential negative effects associated with the administration of large quantities of growth factors such as BMP-2 including those resulting from significant off-label administration.[68]

As discussed in the section pertaining to advances in the design of complex scaffolds, the formation of a competent vascular network within regenerating tissues is essential to the survival of tissue-engineered constructs and/or the retention of cells at the site of injured tissues for many applications. The delivery of angiogenic factors to the site of injury or in scaffold systems has been used extensively to instruct vascular invasion. One recent article by Lin *et al.* demonstrates the benefits of injecting vascular endothelial growth factor (VEGF) mixed with peptides that self-assemble into nanofibrous gels into the myocardium following infarction in both rat and pig models.[69] VEGF release was sustained for more than 14 days *in vitro* and retained for at least the same period *in vivo* when injected with the self-assembling peptides into rat myocardium. Significant improvements of the cardiac systolic function and reduced infarct size were seen after 28 days compared to the treatment with the hydrogel or VEGF alone. While all three treatments led to equivalent increases in capillary density, the combination treatment with both the growth factor and the nanofibrous environment led to significant increases in both arteriole and artery densities compared to individual treatments alone. The results highlight the importance of the microenvironment created by the nanofibers in the recruitment of myofibroblasts to the injury site independent of the administration of VEGF but suggest that the growth factor ensures the long-term maintenance of the local cell density.

Similarly, a functional vascular network is essential to the success of bone tissue engineering. A study identified with our analysis tackles this problem with an alternative method to growth factors delivery. Wu *et al.* developed a bioactive glass scaffold with controllable cobalt ion release as it is known to induce a hypoxia-like response involving the increased cellular expression of hypoxia-inducing factor-1α transcription factor.[70] In this study based on work by Azevedo *et al.*,[71] the authors demonstrate that the cobalt substituted bioactive glasses cause an increased VEGF gene expression. However, only the glasses with a low percentage of calcium substitution by cobalt caused an increase in VEGF protein expression by bone marrow stromal cells.

Peptides with binding affinities for specific biomolecules have also been used for other purposes than growth factor sequestration with promising results. In a recent study, a PEG hydrogel was designed to exhibit specific hyaluronic acid (HA) binding capabilities through a peptide identified for this purpose by phage display.[72] Goat MSCs encapsulated within these HA-binding hydrogels containing different concentrations of exogenous HA were cultured in chondrogenic conditions for up to 6 weeks and formed significantly more cartilage-like matrix as determined by the GAG content than cells cultured in hydrogels without HA-binding capabilities. Implantation of acellular HA-binding hydrogels and hydrogels with a scrambled peptide sequence within osteochondral defects in rat knees led to improved cartilage repair compared to untreated defects at 6 weeks. HA has been used as a base material in a number of scaffold systems, but this approach is interesting as it takes advantage of the increased control capabilities of synthetic base materials in building scaffolds while still benefiting from the bioactivity of biomolecules, such as HA. Furthermore, the authors emphasize that the noncovalent binding of the HA to the hydrogel may allow for improved preservation of its bioactivity compared to fabrication techniques that require its cross-linking or chemical modifications.

Our citation analysis brought forward another study on this theme that takes advantage of a relatively novel approach based on the application of a polydopamine coating to immobilize neurotrophic growth factors and adhesion peptides on the surface of commonly used synthetic polymers in the TERM field.[73,74] Dopamine is a structural mimic of the amino acid, 3,4-dihydroxy-L-phenylalanine, which is found in high concentrations in the adhesive plaque of the *Mytilus edulis* foot protein-5, thought to be responsible for their adhesion to surfaces. This can be easily coated as polydopamine on many natural or synthetic surfaces, thereby providing sites for the covalent conjugation of amine and thiol groups. In this study, Yang *et al.* used this approach to conjugate adhesion peptides from the fibronectin and laminin proteins, as well as nerve growth factor and glial cell line-derived neurotrophic factor to polystyrene and PLGA surfaces in a facile, stable, and reproducible manner. These functionalized surfaces were then used to control the differentiation of mouse and human neural stem cells, as well as iPSCs-derived human neural stem cells. Other groups have used similar techniques to immobilize other factors such as combinations of the cell adhesive Arg-Gly-Asp sequence, BMP-2 and HA to synthetic scaffolds to enhance osteogenic differentiation of both adipocyte-derived[75] and bone marrow-derived stem cells.[76] Owing to its ease of application on a wide range of natural and synthetic substrates, this surface functionalization approach has already been used in a broad range of applications in the TERM field in recent years.

Our understanding of the optimal environment and spatiotemporal sequence of signals required for tissue regeneration in a number of systems continues to expand. As new discoveries are made in the fields of stem cell and developmental biology, TERM investigators will be able to apply this knowledge to the design of increasingly elegant and intricate cellular microenvironments to induce tissue regeneration. A number of approaches have been published in the last year or so to control the spatial and temporal presentation of growth factors and other biomolecules. In one such study, PLGA microspheres containing cartilage-promoting transforming growth factor-β1 or bone-promoting BMP-2 were prepared, stacked with an infusion syringe pump according to the desired gradient and ''sintered'' in ethanol to create an osteochondral scaffold with a continuous gradient transition.[77] Others have designed sequential compositional electrospinning regimens to create spatial and temporal gradients with multiple biomolecules.[78] Another strategy that has previously been used requires the incorporation of multiple growth factor reservoirs with tailored

release profiles. Nelson *et al.* have used this approach and developed thermoresponsive hydrogels incorporating protein conjugation sites as well as PLGA microspheres leading to two distinct release profiles.[79]

Characterization: Imaging and Beyond

Cutting edge characterization and imaging methods are an essential adjunct to TERM research efforts. The proper evaluation of the composition and structure of tissue-engineered constructs compared to the native tissue they aim to replace, repair, or regenerate and *in vivo* tracking of transplanted cells are often challenging. This can limit our understanding of the hurdles that need to be overcome in our attempts to recreate fully functional tissues and organs or treat disease. Keeping updated with novel characterization and imaging techniques is essential to allow us to gain an improved understanding of the systems we aim to regenerate and to probe the quality of bioengineered tissues and the success of our cell- and tissue-based approaches.

The past year has seen some high profile publications that may supplement our armamentarium of imaging techniques. Chung *et al.*'s *Nature* publication of the method termed CLARITY is a powerful demonstration of a novel way to obtain high-resolution images from complex 3D tissue systems without the requirement for sequential sectioning and reconstruction.[80] In this study, the authors demonstrated imaging of whole brains in 3D. To achieve this, the tissue was infused with hydrogel monomers that were then cross-linked to the tissue proteins via treatment with formaldehyde. Thermally triggered polymerization of the hydrogel secured the tissue architecture by holding the proteins in place. The key step of this procedure involved the removal of unbound materials (such as lipids) with an ionic detergent extraction step using active transport organ-electrophoresis (Fig. 2). This method revolved around the idea that lipids are responsible for much of the light scattering encountered when imaging tissues. This was demonstrated by immersing the remaining hydrogel-tissue hybrid in a liquid with a refractive index matching the structure, thereby making it appear uniformly transparent. Of importance for the field of TERM, it was suggested that this approach could be applied to other tissues.

Harnessing the properties of nanomaterials for applications as delivery vehicles, cell tracking, and cell homing has

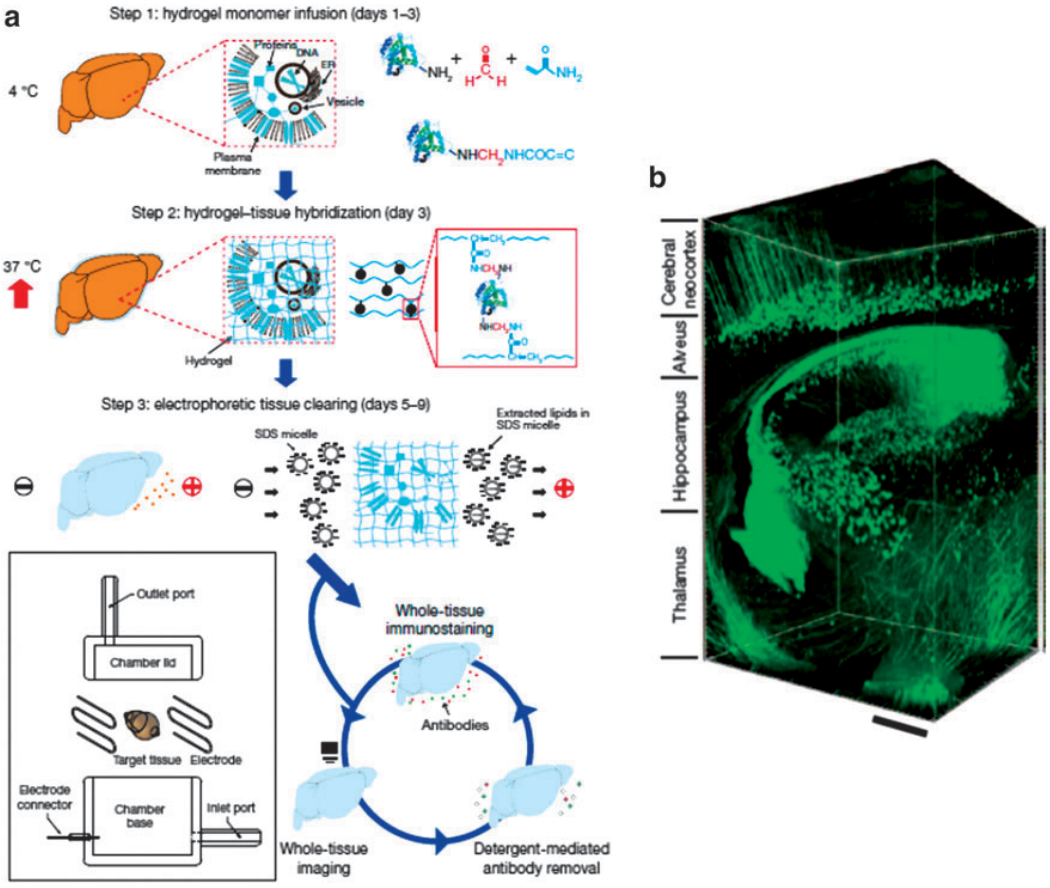

FIG. 2. An overview of the CLARITY procedure (adapted with permission from Macmillan Publishers Ltd: *Nature*,[73] copyright 2014). **(a)** The tissue is cross-linked with formaldehyde (red) in the presence of hydrogel monomers (blue), covalently linking the tissue to a hydrogel mesh. Following a washing step, an electric field is applied across the sample in ionic detergent that actively transports lipids out of the tissue leaving fine structure and cross-linked biomolecules in place. The electrophoretic tissue-clearing chamber is depicted in the boxed region. **(b)** Non-sectioned mouse brain tissue demonstrating cortex, hippocampus, and thalamus (×10 objective; stack size, 3,400 μm; step size, 2 μm). Scale bar, 400 μm.

featured in some high-impact publications in the last year or so. One study demonstrates the preparation of highly fluorescent water-soluble graphene quantum dots with suitable properties for cell labeling.[81] When incubated with progenitor cells, these quantum dots were internalized in the cytoplasm where they only minimally affected cell viability over a period of 3 days. Moreover, the high photostability of these nanoparticles allowed repeated cell imaging without the loss of fluorescence intensity. An alternative approach to achieve cell labeling uses upconversion nanoparticles coated with PEG modified with oligo-arginine to improve cell uptake.[82] Upconversion particles exhibit a number of features that are beneficial for cell imaging applications, including photostability, low autofluorescence, and large anti-Stokes shift. The authors demonstrated that the nanoparticles did not undergo exocytosis over a period of up to 10 days *in vitro*. Cytoplasmic uptake of the nanoparticles did not impact mouse MSCs viability, proliferation, lactate dehydrogenase, or reactive oxygen species release. Similarly, labeling did not affect the differentiation potential of MSCs. Interestingly, labeled MSCs injected intravenously could be tracked by whole-body imaging in mice. The same group was able to combine the features of core upconversion nanoparticles with magnetic properties by depositing a layer of iron oxide particles and a thin layer of gold.[83] The benefits of this system were illustrated by the ability to direct labeled MSCs to a remote injury site using a magnetic field following intraperitoneal injection. What is more, these cells were retained at the injury site for up to 2 weeks and the mice exhibited significantly improved tissue repair.

In a recent example of high-quality tissue imaging, Bertazzo *et al.* used focused ion beam (FIB) milling combined with transmission electron microscopy to identify and characterize calcified spherical particles present in cardiovascular tissues.[84] Correlation between the topographical and compositional information gathered from secondary electron and backscattering signals with a scanning electron microscope (SEM) by color-coding and overlapping the information produced maps that highlight the location of nanoscale calcified features within organic matrix. Utilizing the FIB milling and SEM approach, Al-Abboodi *et al.* examined a cell-seeded hydrogel scaffold at the microscale in a study that is directly relevant to TERM research.[85]

Spectroscopy techniques, such as Raman microspectroscopy and Fourier transform infrared spectroscopy, are also powerful approaches for the characterization of tissue-engineered constructs and their validation against the native tissues they aim to replace. These techniques can be coupled with light microscopy to produce maps of the molecular vibrations measured in tissues and cells with a relatively high resolution. Through interpretation of these molecular vibrations, a molecular fingerprint of the sample can be obtained that provides valuable information on the composition of a tissue or cell. Both these methods are finding increasing applications in TERM studies. One such study made use of Raman microspectroscopy for ECM analysis of chondrocyte-seeded scaffolds.[86] In a seminal study in the field, Raman microspectroscopy was also used to characterize the bone nodules formed by ESCs, MSCs, and osteoblasts and highlighted cell-specific differences.[87]

Translation: Preclinical and Clinical

TERM technologies are translating into more ''routine'' clinical practice. Over the last year, there have been an interesting series of developments: treatments becoming more established, the use of experimental tissue-engineered constructs that have been given emergency approval for implantation, and an increase in clinical trial activity in the field (both in publication and in registration). As predicted in the Year in Review article for 2012,[1] the number of clinical trials within the field is increasing. Since January 2012, there have been 29 further clinical trials registered with the global database in the USA (www.clinicaltrials.gov) and a further 2 within the European Union (www.clinicaltrialsregister.eu). When search terms are extended to include ''stem cells'' rather than just ''tissue engineering'' or ''regenerative medicine,'' a further 389 studies have been registered with the global database since January 2013 alone! There is a natural delay in the translation of TERM strategies into clinical trial, but as momentum builds in the field, further research that is currently laboratory based will progress into the preclinical and clinical arena. As further interest and acceptance in the medical community builds, greater collaboration between scientists and clinicians will allow for more rapid and efficacious translated therapies. We cannot stress enough the benefits that can be reaped in the field from continued efforts to increase the lines of communication between the two communities.

Preclinical translation

In the final hurdles before reaching clinical trial, TERM efforts undergo preclinical trials in animal models. We have included some of these here as they are likely to represent the next wave of advancements to make the jump between the laboratory- and human-based trials, and potentially, into more conventional clinical practice. Several preclinical articles using *in vivo* models have caught the attention of the international press over the last year. Whole-tooth replacement typically uses an implant-based approach and often leads to bone resorption around the base of the implant due to the lack of a root structure. Angelova-Volponi *et al.* have successfully produced bioengineered teeth with a root structure.[88] This was accomplished with a combination of adult human gingival epithelial cells and mouse embryonic tooth mesenchymal cells cultured within a porcine collagen solution, implanted into the renal capsules of immune-compromised mice. This is an extension of the work published by the same group in 2004, which demonstrated that the reciprocal inductive interaction between adult nondental mesenchymal cells (isolated from bone marrow) and mouse embryonic gingival epithelium will also produce teeth.[89] While clearly stating that the clinical translation of such a procedure is a distant reality, it is nonetheless an important step toward tooth regeneration.

Singhal *et al.* differentiated human Müller stem cells into retinal ganglion cell precursors *in vitro* before implanting them into a rat model.[90] When combined with adjuvant anti-inflammatory and matrix degradation agents, the cells contributed to an improvement in retinal ganglion cell function. Cells were injected into the intravitreal space adjacent to the inner retinal surface and then seen to migrate into the retinal

ganglion cell layer. The results suggest that the implanted cells may be either establishing local interneuron synapses and/or releasing neurotropic factors facilitating the recovery of cellular function.

Clinical translation

The last year has seen some, literally lifesaving, use of TERM technologies, and the medical community is really starting to engage more closely with the field. The use of decellularized scaffolds for implantation in human patients has been established for some time; the first decellularized trachea (allogenic cadaveric donor) having been implanted in 2008.[28] The first synthetic tissue-engineered organ (also a trachea) soon followed in 2011.[91] This was a synthetic polymer scaffold seeded with bone marrow-derived MSCs. Since that time, there has been clinical success in this area as the procedure has increasingly become more accepted. There are now nine further patients who have benefited from this or similar approaches, including two children, the youngest of whom is a 2 year old who underwent the procedure in April 2013.[31]

Another case, this time regarding the pathology in the lower airway, saw the use of a purely synthetic poly-ε-caprolactone implant custom-made using computer-aided design and generated using laser-based 3D printing (Fig. 3).[92] This was used as a novel extra-bronchial splint in a 2 month old with critical bronchomalacia. This procedure was approved under the emergency-use exemption from the Food and Drug Administration (FDA). This case exemplifies how quickly an anatomically specific implant can be produced using a material-only scaffold with life-saving results.

A decellularized scaffold has also recently been used with clinical success. An allogenic iliac vein scaffold, seeded with autologous endothelial and smooth muscle cells derived from bone marrow stromal cells, has been used as a conduit for a bypass procedure in a 10-year-old girl with extrahepatic

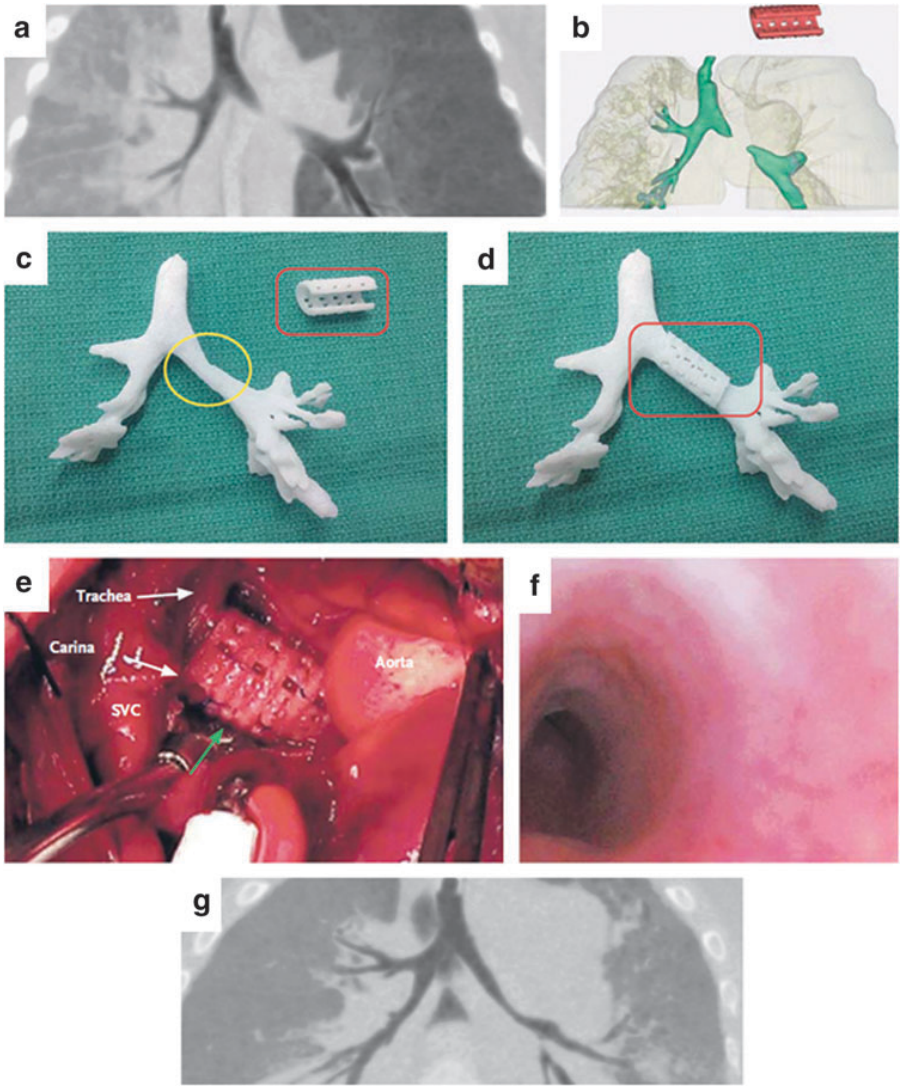

FIG. 3. A 3D printed bioresorbable airway (adapted from Schwartz *et al.*[93]© 2013 Massachusetts Medical Society. Reprinted with permission from Massachusetts Medical Society). **(a)** The airway in expiration before splint placement. **(b)** The patient-specific computed tomography-based design of the splint (red). **(c)** Image-based three-dimensional (3D) printed cast of the airway without the splint in place. **(d)** Image-based 3D-printed cast of the airway with the splint in place. **(e)** Intraoperative photograph of the splint *in situ* (green arrow) overlying the narrowed left mainstem bronchial segment. SVC denotes superior vena cava. **(f)** Bronchoscopic view of the left mainstem bronchus following splint placement. **(g)** The patent airway in expiration 1 year after the placement of the splint.

portal vein obstruction.[30] Despite some extrinsic compression at 1 year requiring a further length of graft to restore adequate blood flow, the child has improved in physical and cognitive function, as well as growth. She has also avoided liver transplantation. Children are good candidates for tissue-engineered therapies due to their higher capacity for healing and tissue regeneration, but their growth following the intervention poses a potential challenge that must be addressed in the design of tissue-engineered constructs.

Another area that has seen interesting clinical success over the last year is that focused on cell-based therapies to treat retinal degenerative diseases of the eye. A preliminary report of two clinical trials into the use of ESC therapies for Stargardt's macular dystrophy and dry age-related macular degeneration (the leading cause of blindness in the developed world) was published in the *Lancet* and claims to be the first description of human embryonic-derived stem cells transplanted into human patients.[93] This report primarily assesses the safety of the procedure and at date of publication has been performed in only two patients, one with each of the conditions described. At 4 months of follow-up, no evidence of complication (such as teratoma formation, rejection, or inflammation) was identified. While there is significant disagreement in how best to assess patients with low vision, it is interesting that both patients report an apparent improvement.

Some of the other clinical trials reported this year include the use of biomaterials for cartilage and bone regeneration, an area of popular focus within the field. Early results have been published from a photoreactive adhesive PEG-based hydrogel used in a large animal model and human patients combined with conventional microfracture treatment for cartilage defects. The treatment arm demonstrating improved tissue fill on magnetic resonance imaging and reduced pain scores compared to standard treatment alone (namely debridement and microfracture).[94] Results from a longer term follow-up are awaited. An alternative approach is offered by Crawford *et al.* who used a natural scaffold employing a type 1 collagen matrix seeded with autologous chondrocytes (NeoCart®) in a phase II randomized control trial.[95] Patient outcomes were assessed using validated subjective questionnaires on the outcomes including pain and ability to perform the activities of daily living. An objective assessment of short- and long-term knee function was carried out by a blinded clinician as part of the International Knee Documentation Committee (IKDC) tool. The results at 2 years are suggestive that the scaffold is beneficial for treatment response. Bone regeneration through TERM efforts aims to address or reduce the use of traditional autologous bone grafting. Autologous osteoblasts cultured on demineralized bone matrix (Osteovit®) have been employed in craniofacial reconstruction in children with complete cleft palates in a report published in the last year or so.[96]

Concluding Remarks and Discussion

In writing the 2013 Year in Review article, we were faced with a slightly different challenge from Fisher and Mauck in the inaugural review, namely to highlight some of the key advances in the TERM field in the relatively short period of just over a year. Given this limited time frame, we were able to identify ''hot topics'' during that period in TERM with an objective evaluation of the citation records, but we could not rely solely on this criterion because of the bias against more recent studies resulting from ''citation lag time.'' We have therefore relied substantially on our own assessment of the TERM literature to identify studies with a high potential to impact the field within the themes highlighted by our analysis of highly cited articles. We hope that the resulting review represents an exciting portrait of the diversity of advances over the last year and a bit in TERM.

We would like to conclude this year's review of TERM research with a quick mention of some inspiring and imaginative studies that have emerged during this process that clearly demonstrate the breadth of the field and the high potential for building complex functional systems. This year has seen the birth of two independently mobile synthetic part biological machines: one swimming and one walking, both harnessing the contraction and pacemaking ability of cardiomyocytes. Nawroth *et al.* have developed a freely swimming jellyfish (''medusoid'') based on the juvenile *Aurelia aurita* scyphozoan jellyfish (Fig. 4).[97] Chan *et al.* have forward engineered a locomotive ''bio-bot'' by using 3D stereo-lithographic printing to construct a cantilever and base structure made up of layered hydrogel polymers with specifically chosen properties. Cardiomyocytes were seeded to form a sheet on the cantilever that performed synchronous contraction resulting in deformation. This deformation combined with friction on the ''ground'' surface allowed for forward propulsion.[98]

In this review, we have highlighted some major advances in the field of pluripotent stem cell research including studies that attempted to address undergoing debates as to the clinical potential of iPSCs. The excitement around iPSCs and its rapid integration within the TERM field over the past 7 years has led to a tremendous pace of discoveries to clarify issues such as their immunogenicity and the risks of tumor development. Given the high costs associated with patient-specific medicine, the use of iPSCs from allogenic sources and the development of nuclear transfer-derived ESCs will undoubtedly fuel the debate as to the optimal cell source for TERM applications. We have also discussed at length efforts in the field over the last year or so to develop increasingly complex scaffolds and growth factor presentation schemes reminiscent of (and often inspired by) the intricate biological organization of tissues and organs. Notably, we have attempted to convey the broad spectrum of approaches that are being proposed from materials, cellular and molecular biology standpoints to address the critical issues associated with the need to generate vascularized and/or angiogenic TERM constructs. We also believe that it was an opportune time to discuss some of the approaches that have emerged in the last year or so to image and characterize cells and tissues both *in situ* and *ex vivo*. We believe that such research avenues that enable a better understanding of the systems that we aim to regenerate and to better characterize the tissue repair obtained through our efforts go hand in hand with innovation in the field. The last year has also seen continued translation of ideas emerging from TERM research into the clinical arena. The accelerated pace at which TERM ideas benefit the patient combined with

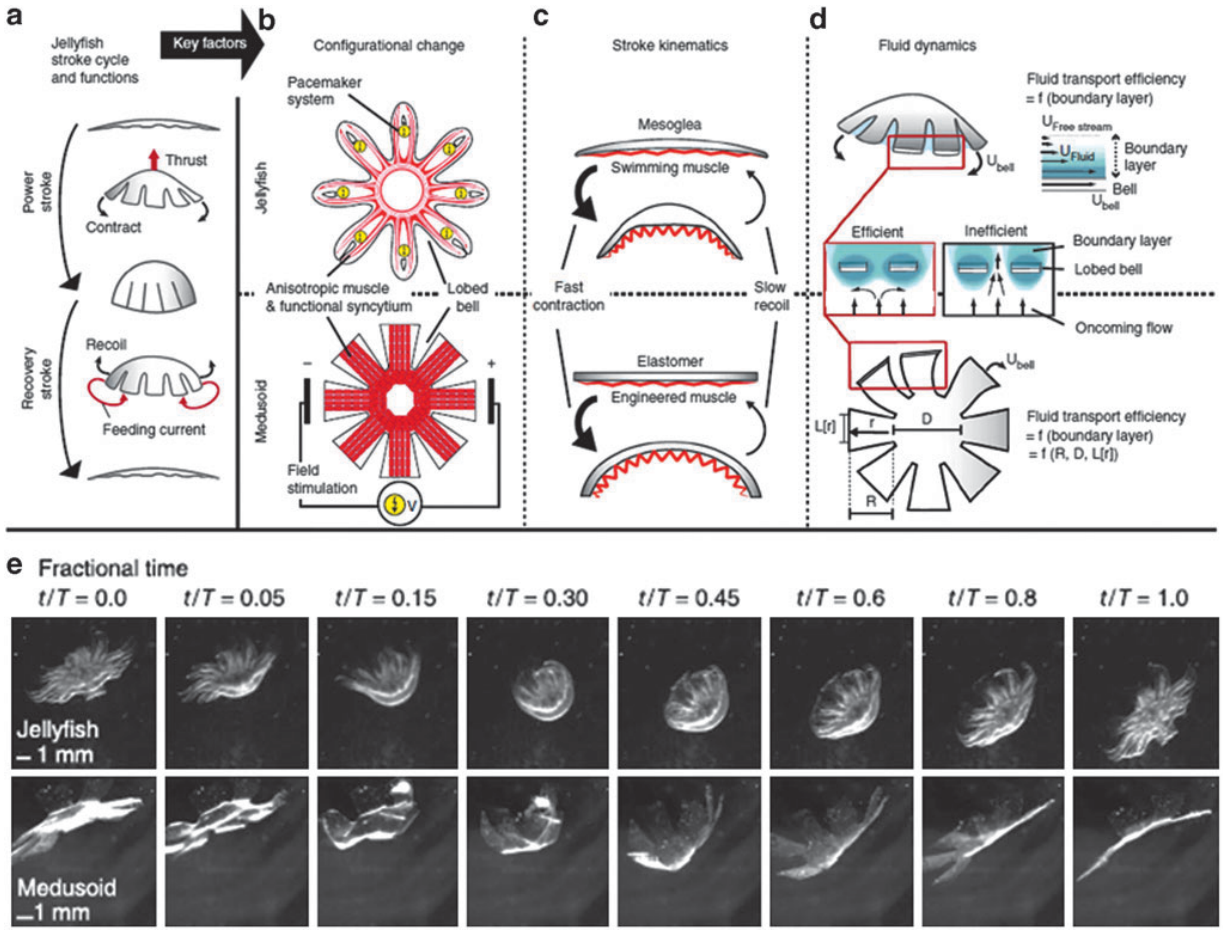

FIG. 4. The key concepts of the design of the biomimetic jellyfish (adapted with permission from Macmillan Publishers Ltd: *Nature Biotechnology*,[98] copyright 2014). **(a)** Schematic representation of jellyfish stroke cycle generating thrust during the power stroke and feeding currents during recovery stroke. **(b)** Controlled configuration change in the medusoid. Where the jellyfish (top) exhibits symmetric complete bell contraction medicated by anisotropic striated muscle tissue, the medusoid (bottom) approximates this mechanism by electrical field stimulation of electromechanically coupled anisotropic cardiac muscle. **(c)** Stroke kinematics is approximated by a flexible elastomer that opposes an actuator promoting asymmetric strokes: active fast contraction with passive slow recoil. **(d)** Fluid dynamics. **(e)** Time lapse photography of the stroke cycle in the jellyfish (top) and the medusoid paced at 1 Hz (bottom); t, time (sec) elapsed since start of stroke cycle; T, duration of stroke cycle; here: jellyfish, $T = 0.3$ s: medusoid, $T = 1.0$ s.

increased visibility for the field with a general audience from features in global news outlets, as well as inclusion in high-level political debate,[99] suggests a continued and growing impact on the quality of life of the global population.

The future of our field is bright and we are looking forward to seeing the advances to come in the next year, just like we hope that the next Year in Review will look back on 2013 with some retrospect and highlight some of the studies that will have taken hold of the field, expectedly as highlighted here, or in an unexpected leap forward.

Acknowledgments

R.H.H. gratefully acknowledges funding from the bursary scheme at the Imperial College London. J.P.S. and M.M.S. thank the Medical Engineering Solutions in Osteoarthritis Centre of Excellence funded by the Wellcome Trust and the Engineering and Physical Sciences Research Council. M.M.S. gratefully acknowledges the financial support from the Rosetrees Trust.

Disclosure statement

No competing financial interests exist.

References

1. Fisher, M.B., and Mauck, R.L. Tissue engineering and regenerative medicine: recent innovations and the transition to translation. Tissue Eng Part B Rev **19,** 1, 2013.
2. Baiguera, S., Jungebluth, P., Mazzanti, B., and Macchiarini, P. Mesenchymal stromal cells for tissue engineered tissue and organ replacements. Transplant Int **25,** 369, 2012.

3. Takahashi, K., and Yamanaka, S. Induction of pluripotent stem cells from mouse embryonic and adult fibroblast cultures by defined factors. Cell **126,** 663, 2006.
4. Yu, J., Vodyanik, M.A., Smuga-Otto, K., Antosiewicz-Bourget, J., Frane, J.L., Tian, S., *et al.* Induced pluripotent stem cell lines derived from human somatic cells. Science **318,** 1917, 2007.
5. Takahashi, K., Tanabe, K., Ohnuki, M., Narita, M., Ichisaka, T., Tomoda, K., *et al.* Induction of pluripotent stem cells from adult human fibroblasts by defined factors. Cell **131,** 861, 2007.
6. Brock, A., Goh, H.T., Yang, B., Lu, Y., Li, H., and Loh, Y.H. Cellular reprogramming: a new technology frontier in pharmaceutical research. Pharm Res **29,** 35, 2012.
7. Bellin, M., Marchetto, M.C., Gage, F.H., and Mummery, C.L. Induced pluripotent stem cells: the new patient? Nat Rev Mol Cell Biol **13,** 713, 2012.
8. Hussein, S.M.I., Nagy, K., and Nagy, A. Human induced pluripotent stem cells: the past, present, and future. Clin Pharm Ther **89,** 741, 2011.
9. Hou, P., Li, Y., Zhang, X., Liu, C., Guan, J., Li, H., *et al.* Pluripotent stem cells induced from mouse somatic cells by small-molecule compounds. Science **341,** 651, 2013.
10. Li, Y., Zhang, Q., Yin, X., Yang, W., Du, Y., Hou, P., *et al.* Generation of iPSCs from mouse fibroblasts with a single gene, Oct4, and small molecules. Cell Res **21,** 196, 2011.
11. Rais, Y., Zviran, A., Geula, S., Gafni, O., Chomsky, E., Viukov, S., *et al.* Deterministic direct reprogramming of somatic cells to pluripotency. Nature **502,** 65, 2013.
12. Zhao, T., Zhang, Z-N., Rong, Z., and Xu, Y. Immunogenicity of induced pluripotent stem cells. Nature **474,** 212, 2011.
13. Okita, K., Nagata, N., and Yamanaka, S. Immunogenicity of induced pluripotent stem cells. Circ Res **109,** 720, 2011.
14. Araki, R., Uda, M., Hoki, Y., Sunayama, M., Nakamura, M., Ando, S., *et al.* Negligible immunogenicity of terminally differentiated cells derived from induced pluripotent or embryonic stem cells. Nature **494,** 100, 2013.
15. Guha, P., Morgan, J.W., Mostoslavsky, G., Rodrigues, N.P., and Boyd, A.S. Lack of immune response to differentiated cells derived from syngeneic induced pluripotent stem cells. Cell Stem Cell **12,** 407, 2013.
16. Liu, P., Chen, S., Li, X., Qin, L., Huang, K., Wang, L., *et al.* Low immunogenicity of neural progenitor cells differentiated from induced pluripotent stem cells derived from less immunogenic somatic cells. PloS One **8,** e69617, 2013.
17. Nazor, K.L., Altun, G., Lynch, C., Tran, H., Harness, J.V., Slavin, I., *et al.* Recurrent variations in DNA methylation in human pluripotent stem cells and their differentiated derivatives. Cell Stem Cell **10,** 620, 2012.
18. Yamashita, A., Liu, S., Woltjen, K., Thomas, B., Meng, G., Hotta, A., *et al.* Cartilage tissue engineering identifies abnormal human induced pluripotent stem cells. Sci Rep **3,** 1978, 2013.
19. Fujimoto, Y., Abematsu, M., Falk, A., Tsujimura, K., Sanosaka, T., Juliandi, B., *et al.* Treatment of a mouse model of spinal cord injury by transplantation of human induced pluripotent stem cell-derived long-term self-renewing neuroepithelial-like stem cells. Stem Cells **30,** 1163, 2012.
20. Tedesco, F.S., Gerli, M.F.M., Perani, L., Benedetti, S., Ungaro, F., Cassano, M., *et al.* Transplantation of genetically corrected human iPSC-derived progenitors in mice with limb-girdle muscular dystrophy. Sci Transl Med **4,** 140ra89, 2012.
21. Margariti, A., Winkler, B., Karamariti, E., Zampetaki, A., Tsai T-n, Baban, D., *et al.* Direct reprogramming of fibroblasts into endothelial cells capable of angiogenesis and reendothelialization in tissue-engineered vessels. Proc Natl Acad Sci U S A **109,** 13793, 2012.
22. Meng, X., Su, R.J., Baylink, D.J., Neises, A., Kiroyan, J.B., Lee, W.Y.W., *et al.* Rapid and efficient reprogramming of human fetal and adult blood CD34(+) cells into mesenchymal stem cells with a single factor. Cell Res **23,** 658, 2013.
23. Niu, W., Zang, T., Zou, Y., Fang, S., Smith, D.K., Bachoo, R., *et al. In vivo* reprogramming of astrocytes to neuroblasts in the adult brain. Nat Cell Biol **15,** 1164, 2013.
24. Abad, M., Mosteiro, L., Pantoja, C., Canamero, M., Rayon, T., Ors, I., Grana, O., Megias, D., Dominguez, O., Martinez, D., Manzanares, M., Ortega, S., and Serrano, M. Reprogramming *in vivo* produces teratomas and iPS cells with totipotency features. Nature **502,** 340, 2013.
25. Tachibana, M., Amato, P., Sparman, M., Gutierrez, N.M., Tippner-Hedges, R., and Ma, H., *et al.* Human embryonic stem cells derived by somatic cell nuclear transfer. Cell **153,** 1228, 2013.
26. Tachibana, M., Amato, P., Sparman, M., Gutierrez, N.M., Tippner-Hedges, R., Ma, H., *et al.* Human Embryonic Stem Cells Derived by Somatic Cell Nuclear Transfer (vol 153, pg 1228, 2013). Cell **154,** 465, 2013.
27. Irish, J.D. A 5,500-year-old artificial human tooth from Egypt: a historical note. Int J Oral Maxillofac Implants **19,** 645, 2004.
28. Macchiarini, P., Jungebluth, P., Go, T., Asnaghi, M.A., Rees, L.E., Cogan, T.A., *et al.* Clinical transplantation of a tissue-engineered airway. Lancet **372,** 2023, 2008.
29. Song, J.J., Guyette, J.P., Gilpin, S.E., Gonzalez, G., Vacanti, J.P., and Ott, H.C. Regeneration and experimental orthotopic transplantation of a bioengineered kidney. Nat Med **19,** 646, 2013.
30. Olausson, M., Patil, P.B., Kuna, V.K., Chougule, P., Hernandez, N., Methe, K., *et al.* Transplantation of an allogeneic vein bioengineered with autologous stem cells: a proof-of-concept study. Lancet **380,** 230, 2012.
31. Haag, J.C., Jungebluth, P., and Macchiarini, P. Tracheal replacement for primary tracheal cancer. Curr Opin Otolaryngol Head Neck Surg **21,**171, 2013.
32. Ott, H.C., Matthiesen, T.S., Goh, S.K., Black, L.D., Kren, S.M., Netoff, T.I., *et al.* Perfusion-decellularized matrix: using nature's platform to engineer a bioartificial heart. Nat Med **14,** 213, 2008.
33. Ott, H.C., Clippinger, B., Conrad, C., Schuetz, C., Pomerantseva, I., Ikonomou, L., *et al.* Regeneration and orthotopic transplantation of a bioartificial lung. Nat Med **16,** 927, 2010.
34. Partington, L., Mordan, N.J., Mason, C., Knowles, J.C., Kim, H.W., Lowdell, M.W., *et al.* Biochemical changes caused by decellularization may compromise mechanical integrity of tracheal scaffolds. Acta Biomater **9,** 5251, 2013.
35. Ma, R.N., Li, M., Luo, J.S., Yu, H.T., Sun, Y.Z., Cheng, S.Y., *et al.* Structural integrity, ECM components and immunogenicity of decellularized laryngeal scaffold with preserved cartilage. Biomaterials **34,** 1790, 2013.
36. Xu, L., Cui, P.C., Chen, Z.F., and Ma, R.N. Biomechanical study on decellularized laryngeal scaffold in dogs. Chin J Otorhinolaryngol Head Neck Surg **46,** 331, 2011.
37. Wang, E.C., Damrose, E.J., Mendelsohn, A.H., Nelson, S.D., Shintaku, I.P., Ye, M., *et al.* Distribution of class I

and II human leukocyte antigens in the larynx. Otolaryngol Head Neck Surg **134,** 280, 2006.
38. Adkisson, H.D., Milliman, C., Zhang, X., Mauch, K., Maziarz, R.T., and Streeter, P.R. Immune evasion by neocartilage-derived chondrocytes: implications for biologic repair of joint articular cartilage. Stem Cell Res **4,** 57, 2010.
39. He, F., and Pei, M. Extracellular matrix enhances differentiation of adipose stem cells from infrapatellar fat pad toward chondrogenesis. J Tissue Eng Regen Med **7,** 73, 2013.
40. Evans, N.D., Gentleman, E., Chen, X.Y., Roberts, C.J., Polak, J.M., and Stevens, M.M. Extracellular matrix-mediated osteogenic differentiation of murine embryonic stem cells. Biomaterials **31,** 3244, 2010.
41. Wolf, M.T., Daly, K.A., Reing, J.E., and Badylak, S.F. Biologic scaffold composed of skeletal muscle extracellular matrix. Biomaterials **33,** 2916, 2012.
42. Song, J.J., and Ott, H.C. Organ engineering based on decellularized matrix scaffolds. Trends Mol Med **17,** 424, 2011.
43. Supp, D.M., and Boyce, S.T. Engineered skin substitutes: practices and potentials. Clin Dermatol **23,** 403, 2005.
44. Oberpenning, F., Meng, J., Yoo, J.J., and Atala, A. *De novo* reconstitution of a functional mammalian urinary bladder by tissue engineering. Nat Biotechnol **17,** 149, 1999.
45. Freed, L.E., Langer, R., Martin, I., Pellis, N.R., and VunjakNovakovic, G. Tissue engineering of cartilage in space. Proc Natl Acad Sci U S A **94,** 13885, 1997.
46. Thesleff, T., Lehtimaki, K., Niskakangas, T., Mannerstrom, B., Miettinen, S., Suuronen, R., *et al.* Cranioplasty with adipose-derived stem cells and biomaterial: a novel method for cranial reconstruction. Neurosurgery **68,** 1535, 2011.
47. Stevens, M.M., Marini, R.P., Schaefer, D., Aronson, J., Langer, R., and Shastri, V.P. *In vivo* engineering of organs: the bone bioreactor. Proc Natl Acad Sci U S A **102,** 11450, 2005.
48. Miller, J.S., Stevens, K.R., Yang, M.T., Baker, B.M., Nguyen D-HT, Cohen, D.M., *et al.* Rapid casting of patterned vascular networks for perfusable engineered three-dimensional tissues. Nat Mater **11,** 768, 2012.
49. Therriault, D., White, S.R., and Lewis, J.A. Chaotic mixing in three-dimensional microvascular networks fabricated by direct-write assembly. Nat Mater **2,** 265, 2003.
50. Wu, W., Hansen, C.J., Aragon, A.M., Geubelle, P.H., White, S.R., and Lewis, J.A. Direct-write assembly of biomimetic microvascular networks for efficient fluid transport. Soft Matter **6,** 739, 2010.
51. Jiang, B., Waller, T.M., Larson, J.C., Appel, A.A., and Brey, E.M. Fibrin-loaded porous poly(ethylene glycol) hydrogels as scaffold materials for vascularized tissue formation. Tissue Eng Part A **19,** 224, 2013.
52. Gauvin, R., Chen, Y.C., Lee, J.W., Soman, P., Zorlutuna, P., Nichol, J.W., *et al.* Microfabrication of complex porous tissue engineering scaffolds using 3D projection stereolithography. Biomaterials **33,** 3824, 2012.
53. Sun, J.Y., Zhao, X.H., Illeperuma, W.R.K., Chaudhuri, O., Oh, K.H., Mooney, D.J., *et al.* Highly stretchable and tough hydrogels. Nature **489,** 133, 2012.
54. Haraguchi, Y., Shimizu, T., Sasagawa, T., Sekine, H., Sakaguchi, K., Kikuchi, T., *et al.* Fabrication of functional three-dimensional tissues by stacking cell sheets *in vitro*. Nat Protoc **7,** 850, 2012.
55. Sampson, S.L., Saraiva, L., Gustafsson, K., Jayasinghe, S.N., and Robertson, B.D. Cell electrospinning: an in vitro and in vivo study. Small **10,** 78, 2014.
56. Wang, H.B., Liu, Z.Q., Li, D.X., Guo, X., Kasper, F.K., Duan, C.M., *et al.* Injectable biodegradable hydrogels for embryonic stem cell transplantation: improved cardiac remodelling and function of myocardial infarction. J Cell Mol Med **16,** 1310, 2012.
57. Engler, A.J., Sen, S., Sweeney, H.L., and Discher, D.E. Matrix elasticity directs stem cell lineage specification. Cell **126,** 677, 2006.
58. Downing, T., Soto, J.,Morez, C., Houssin, T., Fritz, A., Yuan, F., Chu, J., Patel, S., Schaffer, D., and Li, S. Biophysical regulation of epigenetic state and cell reprogramming. Nat Mater **12,** 1154, 2013.
59. Wang, P.Y., Tsai, W.B., and Voelcker, N.H. Screening of rat mesenchymal stem cell behaviour on polydimethylsiloxane stiffness gradients. Acta Biomater **8,** 519, 2012.
60. Swift, J., Ivanovska, I.L., Buxboim, A., Harada, T., Dingal. P.C.D.P., Pinter, J., *et al.* Nuclear lamin-A scales with tissue stiffness and enhances matrix-directed differentiation. Science **341,** 1240104, 2013.
61. Giatsidis, G., Dalla Venezia, E., and Bassetto, F. The role of gene therapy in regenerative surgery: updated insights. Plast Reconstr Surg **131,** 1425, 2013.
62. Neumann, A.J., Schroeder, J., Alini, M., Archer, C.W., and Stoddart, M.J. Enhanced adenovirus transduction of hMSCs using 3D hydrogel cell carriers. Mol Biotechnol **53,** 207, 2013.
63. Thomas, A.M., and Shea, L.D. Polysaccharide-modified scaffolds for controlled lentivirus delivery *in vitro* and after spinal cord injury. J Controlled Release **170,** 421, 2013.
64. Kidd, M.E., Shin, S., and Shea, L.D. Fibrin hydrogels for lentiviral gene delivery *in vitro* and *in vivo*. J Controlled Release **157,** 80, 2012.
65. Zou, B., Liu, Y., Luo, X., Chen, F., Guo, X., and Li, X. Electrospun fibrous scaffolds with continuous gradations in mineral contents and biological cues for manipulating cellular behaviors. Acta Biomater **8,** 1576, 2012.
66. Martino, M.M., Briquez, P.S., Ranga, A., Lutolf, M.P., and Hubbell, J.A. Heparin-binding domain of fibrin(ogen) binds growth factors and promotes tissue repair when incorporated within a synthetic matrix. Proc Natl Acad Sci U S A **110,** 4563, 2013.
67. Lee, S.S., Huang, B.J., Kaltz, S.R., Sur, S., Newcomb, C.J., Stock, S.R., *et al.* Bone regeneration with low dose BMP-2 amplified by biomimetic supramolecular nanofibers within collagen scaffolds. Biomaterials **34,** 452, 2013.
68. Epstein, N.E. Complications due to the use of BMP/INFUSE in spine surgery: the evidence continues to mount. Surg Neurol Int **4,** S343, 2013.
69. Lin, Y.D., Luo, C.Y., Hu, Y.N., Yeh, M.L., Hsueh, Y.C., Chang, M.Y., *et al.* Instructive nanofiber scaffolds with VEGF create a microenvironment for arteriogenesis and cardiac repair. Sci Transl Med **4,** 146ra109, 2012.
70. Wu, C., Zhou, Y., Fan, W., Han, P., Chang, J., Yuen, J., *et al.* Hypoxia-mimicking mesoporous bioactive glass scaffolds with controllable cobalt ion release for bone tissue engineering. Biomaterials **33,** 2076, 2012.
71. Azevedo, M.M., Jell, G., O'Donnell, M.D., Law, R.V., Hill, R.G., and Stevens, M.M. Synthesis and characterization of hypoxia-mimicking bioactive glasses for skeletal regeneration. J Mater Chem **20,** 8854, 2010.
72. Unterman, S.A., Gibson, M., Lee, J.H., Crist, J., Chansakul, T., Yang, E.C., *et al.* Hyaluronic acid-binding scaffold for articular cartilage repair. Tissue Eng Part A **18,** 2497, 2012.

73. Yang, K., Lee, J.S., Kim, J., Lee, Y.B., Shin, H., Um, S.H., *et al.* Polydopamine-mediated surface modification of scaffold materials for human neural stem cell engineering. Biomaterials **33,** 6952, 2012.
74. Yang, K., Lee, J.S., Kim, J., Lee, Y.B., Shin, H., Um, S.H., *et al.* Polydopamine-mediated surface modification of scaffold materials for human neural stem cell engineering (vol 33, pg 6952, 2012). Biomaterials **33,** 8186, 2012.
75. Ko, E., Yang, K., Shin, J., and Cho, S-W. Polydopamine-assisted osteoinductive Peptide immobilization of polymer scaffolds for enhanced bone regeneration by human adipose-derived stem cells. Biomacromolecules **14,** 3202, 2013.
76. Chien, C.Y., and Tsai, W.B. Poly(dopamine)-assisted immobilization of Arg-Gly-Asp peptides, hydroxyapatite, and bone morphogenic protein-2 on titanium to improve the osteogenesis of bone marrow stem cells. Acs Appl Mater Interfaces **5,** 6975, 2013.
77. Dormer, N.H., Singh, M., Zhao, L., Mohan, N., Berkland, C.J., and Detamore, M.S. Osteochondral interface regeneration of the rabbit knee with macroscopic gradients of bioactive signals. J Biomed Mater Res Part A **100A,** 162, 2012.
78. Bonani, W., Motta, A., Migliaresi, C., and Tan, W. Biomolecule gradient in micropatterned nanofibrous scaffold for spatiotemporal release. Langmuir **28,** 13675, 2012.
79. Nelson, D.M., Ma, Z., Leeson, C.E., and Wagner, W.R. Extended and sequential delivery of protein from injectable thermoresponsive hydrogels. J Biomed Mater Res Part A **100A,** 776, 2012.
80. Chung, K., Wallace, J., Kim, S.Y., Kalyanasundaram, S., Andalman, A.S., Davidson, T.J., *et al.* Structural and molecular interrogation of intact biological systems. Nature **497,** 332, 2013.
81. Zhang, M., Bai, L.L., Shang, W.H., Xie, W.J., Ma, H., Fu, Y.Y., *et al.* Facile synthesis of water-soluble, highly fluorescent graphene quantum dots as a robust biological label for stem cells. J Mater Chem **22,** 7461, 2012.
82. Wang, C., Cheng, L., Xu, H., and Liu, Z. Towards whole-body imaging at the single cell level using ultra-sensitive stem cell labeling with oligo-arginine modified upconversion nanoparticles. Biomaterials **33,** 4872, 2012.
83. Cheng, L., Wang, C., Ma, X.X., Wang, Q.L., Cheng, Y., Wang, H., *et al.* Multifunctional upconversion nanoparticles for dual-modal imaging-guided stem cell therapy under remote magnetic control. Adv Funct Mater **23,** 272, 2013.
84. Bertazzo, S., Gentleman, E., Cloyd, K.L., Chester, A.H., Yacoub, M.H., and Stevens, M.M. Nano-analytical electron microscopy reveals fundamental insights into human cardiovascular tissue calcification. Nat Mater **12,** 576, 2013.
85. Al-Abboodi, A., Fu, J., Doran, P.M., and Chan, P.P.Y. Three-dimensional nanocharacterization of porous hydrogel with ion and electron beams. Biotechnol Bioeng **110,** 318, 2013.
86. Kunstar, A., Leferink, A.M., Okagbare, P.I., Morris, M.D., Roessler, B.J., Otto, C., *et al.* Label-free Raman monitoring of extracellular matrix formation in three-dimensional polymeric scaffolds. J R Soc Interface **10,** 20130464, 2013.
87. Gentleman, E., Swain, R.J., Evans, N.D., Boonrungsiman, S., Jell, G., Ball, M.D., *et al.* Comparative materials differences revealed in engineered bone as a function of cell-specific differentiation. Nat Mater **8,** 763, 2009.
88. Angelova Volponi, A., Kawasaki, M., and Sharpe, P.T. Adult human gingival epithelial cells as a source for whole-tooth bioengineering. J Dental Res **92,** 329, 2013.
89. Ohazama, A., Modino, S.A.C., Miletich, I., and Sharpe, P.T. Stem-cell-based tissue engineering of murine teeth. J Dental Res **83,** 518, 2004.
90. Singhal, S., Bhatia, B., Jayaram, H., Becker, S., Jones, M.F., Cottrill, P.B., *et al.* Human muller glia with stem cell characteristics differentiate into retinal ganglion cell (RGC) precursors in vitro and partially restore rgc function in vivo following transplantation. Stem Cells Transl Med **1,** 188, 2012.
91. Jungebluth, P., Alici, E., Baiguera, S., Le Blanc, K., Blomberg, P., Bozoky, B., *et al.* Tracheobronchial transplantation with a stem-cell-seeded bioartificial nanocomposite: a proof-of-concept study. Lancet **378,** 1997–2004, 2011.
92. Zopf, D.A., Hollister, S.J., Nelson, M.E., Ohye, R.G., and Green, G.E. Bioresorbable airway splint created with a three-dimensional printer. N Engl J Med **368,** 2043, 2013.
93. Schwartz, S.D., Hubschman, J.P., Heilwell, G., Franco-Cardenas, V., Pan, C.K., Ostrick, R.M., *et al.* Embryonic stem cell trials for macular degeneration: a preliminary report. Lancet **379,** 713, 2012.
94. Sharma, B., Fermanian, S., Gibson, M., Unterman, S., Herzka, D.A., Cascio, B., *et al.* Human cartilage repair with a photoreactive adhesive-hydrogel composite. Sci Transl Med **5,**167ra6, 2013.
95. Crawford, D.C., DeBerardino, T.M., and Williams, R.J. NeoCart, an autologous cartilage tissue implant, compared with microfracture for treatment of distal femoral cartilage lesions an FDA phase-II prospective, randomized clinical trial after two years. J Bone Joint Surg-Am **94A,** 979, 2012.
96. Pradel, W., and Lauer, G. Tissue-engineered bone grafts for osteoplasty in patients with cleft alveolus. Ann Anat-Anat Anz **194,** 545, 2012.
97. Nawroth, J.C., Lee, H., Feinberg, A.W., Ripplinger, C.M., McCain, M.L., Grosberg, A., *et al.* A tissue-engineered jellyfish with biomimetic propulsion. Nat Biotechnol **30,** 792, 2012.
98. Chan, V., Park, K., Collens, M.B., Kong, H., Saif, T.A., and Bashir, R. Development of miniaturized walking biological machines. Sci Rep **2,** 857, 2012.
99. Science and Technology Committee HoL. Science and Technology Commitee 1st Report of Session 2013–2014: Regenerative Medicine Report. House of Lords Paper 23, 2013.

Address correspondence to:
Molly M. Stevens, PhD
Department of Materials
Imperial College London
London SW7 2AZ
United Kingdom

E-mail: m.stevens@imperial.ac.uk

Received: October 29, 2013
Accepted: December 16, 2013
Online Publication Date: January 29, 2014

Appendix B

Materials Views
www.MaterialsViews.com

ADVANCED FUNCTIONAL MATERIALS
www.afm-journal.de

Modular and Versatile Spatial Functionalization of Tissue Engineering Scaffolds through Fiber-Initiated Controlled Radical Polymerization

*Rachael H. Harrison, Joseph A. M. Steele, Robert Chapman, Adam J. Gormley, Lesley W. Chow, Muzamir M. Mahat, Lucia Podhorska, Robert G. Palgrave, David J. Payne, Shehan P. Hettiaratchy, Iain E. Dunlop, and Molly M. Stevens**

Native tissues are typically heterogeneous and hierarchically organized, and generating scaffolds that can mimic these properties is critical for tissue engineering applications. By uniquely combining controlled radical polymerization (CRP), end-functionalization of polymers, and advanced electrospinning techniques, a modular and versatile approach is introduced to generate scaffolds with spatially organized functionality. Poly-ε-caprolactone is end functionalized with either a polymerization-initiating group or a cell-binding peptide motif cyclic Arg-Gly-Asp-Ser (cRGDS), and are each sequentially electrospun to produce zonally discrete bilayers within a continuous fiber scaffold. The polymerization-initiating group is then used to graft an antifouling polymer bottlebrush based on poly(ethylene glycol) from the fiber surface using CRP exclusively within one bilayer of the scaffold. The ability to include additional multifunctionality during CRP is showcased by integrating a biotinylated monomer unit into the polymerization step allowing postmodification of the scaffold with streptavidin-coupled moieties. These combined processing techniques result in an effective bilayered and dual-functionality scaffold with a cell-adhesive surface and an opposing antifouling non-cell-adhesive surface in zonally specific regions across the thickness of the scaffold, demonstrated through fluorescent labelling and cell adhesion studies. This modular and versatile approach combines strategies to produce scaffolds with tailorable properties for many applications in tissue engineering and regenerative medicine.

1. Introduction

The ability to design surface properties of scaffolds to direct cell and protein binding is key in tissue engineering (TE) and regenerative medicine. Following injury or scaffold implantation there are many scenarios where cell ingrowth or protein fouling onto a tissue or scaffold surface may lead to undesirable outcomes such as problematic scar tissue. This is particularly key at gliding tissue interfaces. Scaffolds that exhibit effective opposing cell-adhesive and antifouling sides would revolutionize the outcome of injuries and operations at such biological interfaces through their ability to support tissue healing (cell-adhesive surface) and to reduce cell-ingrowth and protein adsorption (antifouling surface) in a spatially controlled manner. Injuries or operations to gliding surfaces such as musculoskeletal tissues or involving the peritoneal tissues of the abdomen or pelvis are often complicated with undesirable adhesions. These adhesions are bands of scar tissue that directly result from cellular ingrowth

R. H. Harrison, J. A. M. Steele, Dr. R. Chapman, Dr. A. J. Gormley, Dr. L. W. Chow, M. M. Mahat, L. Podhorska, Dr. D. J. Payne, Dr. I. E. Dunlop, Prof. M. M. Stevens
Department of Materials
Imperial College London
London SW7 2AZ, UK
E-mail: m.stevens@imperial.ac.uk

R. H. Harrison, J. A. M. Steele, Dr. R. Chapman, Dr. A. J. Gormley, Dr. L. W. Chow, M. M. Mahat, L. Podhorska, Prof. M. M. Stevens
Institute of Biomedical Engineering
Imperial College London
London SW7 2AZ, UK

R. H. Harrison, J. A. M. Steele, Dr. R. Chapman, Dr. A. J. Gormley, Dr. L. W. Chow, M. M. Mahat, L. Podhorska, Prof. M. M. Stevens
Department of Bioengineering
Imperial College London
London SW7 2AZ, UK

R. H. Harrison, S. P. Hettiaratchy
Department of Plastic and Reconstructive Surgery
Imperial College Healthcare NHS Trust
Charing Cross Campus
Fulham Palace Road, London W6 8RF, UK

Dr. R. G. Palgrave
Department of Chemistry
University College London
20 Gordon Street, London WC1H 0AJ, UK

DOI: 10.1002/adfm.201501277

and bridging between previously gliding surfaces resulting in restriction of movement that causes pain and compromised function. Similarly, protein deposition at vascular interfaces such as on artificial blood vessels or at sites of injury can lead to blood clotting that can cause disastrous consequences.

This work presents a modular and versatile scaffold system that has been specifically designed to allow facile modification for specific application. A porous structure manufactured with a processing technique that can add to this versatility is required; this can be achieved with electrospinning. Electrospinning is an ideal technique for producing 3D networks of fibers of tunable size, orientation, composition, and density that mimic the properties of native extracellular matrix (ECM)[1–3] and can generate scaffolds with spatially arranged functionalization through layering of various polymers during electrospinning.[4–9] Developing a controlled method that allows multiple zonally arranged functional groups within a continuous scaffold allows for the production of a hierarchical structure that can modulate cell behavior within each functional zone. Electrospinning and the use of fibers also allows for high density surface functionalization that can dramatically change the surface properties whilst maintaining the spatial control of presentation and fiber morphology.

Controlled radical polymerization (CRP) techniques are facile and versatile methods for providing surface functionalization with a wide range of monomers. These have not been fully exploited in scaffold functionalization and yet are extremely powerful methods for preparing antifouling surfaces. Atom transfer radical polymerization (ATRP) and reversible addition-fragmentation chain transfer (RAFT) have been used to attach polymers to a variety of surfaces to generate surface-derived functionality.[10–13] These polymerization methods are versatile and offer excellent control of chain length, architecture, reaction kinetics, and they can add a vast array of functionality as a large number of monomers may be incorporated, which dictates the final material properties.[10,14] In this work we have employed the versatility of surface-initiated CRP to create an antifouling polymer bottlebrush on one side of an electrospun poly-ε-caprolactone (PCL) scaffold with a cell-adhesive peptide on the opposing surface across a diameter of a few hundred micrometers.

The antifouling surface is generated by grafting a high density, antifouling, biocompatible polymer bottlebrush based on poly(ethylene glycol) (PEG) from initiators presented on the PCL scaffold surface. PEG is an antifouling polymer that has been used to mediate cell and protein adhesion to surfaces and has been used in devices approved for implantation into the body.[15] The ability to incorporate additional (bio)functionalities within the antifouling brushes is showcased with the addition of a biotinylated monomer, which can provide a versatile handle for the *post hoc* addition of various streptavidin-coupled moieties. To maximize the antifouling ability by creating a dense hydrated polymer layer, we elected to use the "grafting from" approach, whereby the initiating group is attached to the surface and the polymer grows out from it. This avoids the steric hindrance and resultant low density that is found in a "grafting to" approach.[16] Second, we selected the oligomeric monomer of PEG, poly(ethylene glycol) methyl ether methacrylate (OEGMA) to generate a pOEGMA bottlebrush structure that leads to a vastly higher density of PEG being displayed on the surface for superior performance. Polymer brush growth from electrospun fibers has typically been achieved using ATRP polymerization of a variety of different monomers. In most approaches that are directed towards biomedical applications, the initiating group is incorporated as a post electrospinning modification before polymerization has been undertaken.[17–22] Our strategy offers significant advantages to this by incorporating the initiator as an end-group to the polymer prior to electrospinning to allow precise control over the spatial position of the functional groups without disrupting the fiber architecture. This approach has been used previously for the polymerization of styrene,[23] 2-hydroxyethyl methacrylate,[16] and *N,N*-isopropylacrylamide,[24] but not in a biomedical application. The selection of the initiating group and electrospinning arrangement further allows surface enrichment of the fibers with initiating groups through electrostatic attraction.[23] Second, a modified form of ATRP, namely, activators regenerated by electron transfer atom transfer radical polymerization (ARGET ATRP), was employed that avoids the high concentrations of potentially toxic transition metal catalyst and organic solvents used in conventional ATRP.[25] This is critical for scaffolds designed for biomedical use as high levels of contamination can be difficult to thoroughly remove from a bulk scaffold. Finally, in contrast to conventional ATRP, ARGET is less sensitive to small amounts of oxygen contamination, offering increased ease of use.[26] To our knowledge this is the first use of controlled radical polymerization to polymerize pOEGMA from a PCL surface.

Our approach of pre-functionalizing PCL with end-functional groups before electrospinning offers a facile and versatile method for maintaining scaffold architecture, functionality, and material properties whilst having precise control over the spatial location and molecular weight of the grafted polymer. It also allows control over the density of functional groups by simply changing the concentration of the PCL conjugates. Specifically, we modified one batch of PCL with the initiating group for polymerization and a separate batch with the canonical adhesion peptide sequence Arg-Gly-Asp-Ser (RGDS). The polymer conjugates were sequentially electrospun as a bilayer to achieve spatial control of the functionality and surface properties. This work builds from our recent work using sequential electrospinning to form opposing gradients of two different peptides in a PCL scaffold, which directed the specific binding and spatial organization of biopolymers (glycosaminoglycans, GAG) within the scaffold.[27] These techniques provide a new and versatile platform for the preparation of multi-functional TE scaffolds to address unmet clinical need in orthopedic, plastic, reconstructive, and general surgery.

2. Results and Discussion

2.1. Production of Polymer Bottlebrush through Surface-Initiated Polymerization

ARGET ATRP reaction kinetics were first established and optimized in solution; polymerizations were conducted in water/IPA (1:1 v/v) in order to prevent dissolution of the PCL. A molar ratio of 150:1:1:0.15 OEGMA : initiator : $Cu(II)Cl_2$: sodium ascorbate at 30°C resulted in reproducible >70% conversion

within 2 h. Good control was achieved as evidenced by pseudo first-order kinetics and the low molecular weight dispersity of the polymers ($M_w/M_n < 1.3$).

Surface-initiated ARGET ATRP of pOEGMA was successfully performed from 2D silicon surfaces, silicon wafers, optimized and characterized, before progressing to 3D electrospun scaffolds to ensure reproducible results. The initiating group α-bromoisobutyryl bromide (BiBB) was attached to the surfaces using 3-(aminopropyl)triethoxysilane (APTES) before pOEGMA was grafted from the wafer. A free sacrificial initiator, ethyl-α-bromoisobutyrate (EBiB), was used in solution to aid control of the polymerization and to allow analysis of the free polymer as a surrogate for the surface bound polymer; this has been shown to be a reliable tool for controlling the M_n and M_w/M_n for the polymers grown from surfaces within the same reaction vessel.[28] Ellipsometry and atomic force microscopy (AFM) confirmed the presence of a polymer brush layer with a dry thickness of ≈6.2 nm (±0.038 nm, MSE 3.548) (**Figure 1**B,C and Figure S1, Supporting Information), and X-ray photoelectron spectroscopy (XPS) confirmed this layer to be organic with the expected changes in the ratio of the C–O bond (Table S1, Supporting Information). Further evidence for the successful polymerization of OEGMA from the surface is given by the increased wettability after polymerization with a change in water contact angle from 63.6° ± 2.3° on Si-APTES-Ini functionalized wafers to 36.3° ± 5.9° (Figure 1D).

2.2. Surface-Initiated Polymerization from 3D Electrospun Fibers

To undertake surface-initiated polymerization from 3D electrospun fibrous scaffolds we commenced by modifying a PCL-diol (M_w 14 000 Da) with the initiating group (BiBB) to produce a polymerization initiating region at either end of the PCL

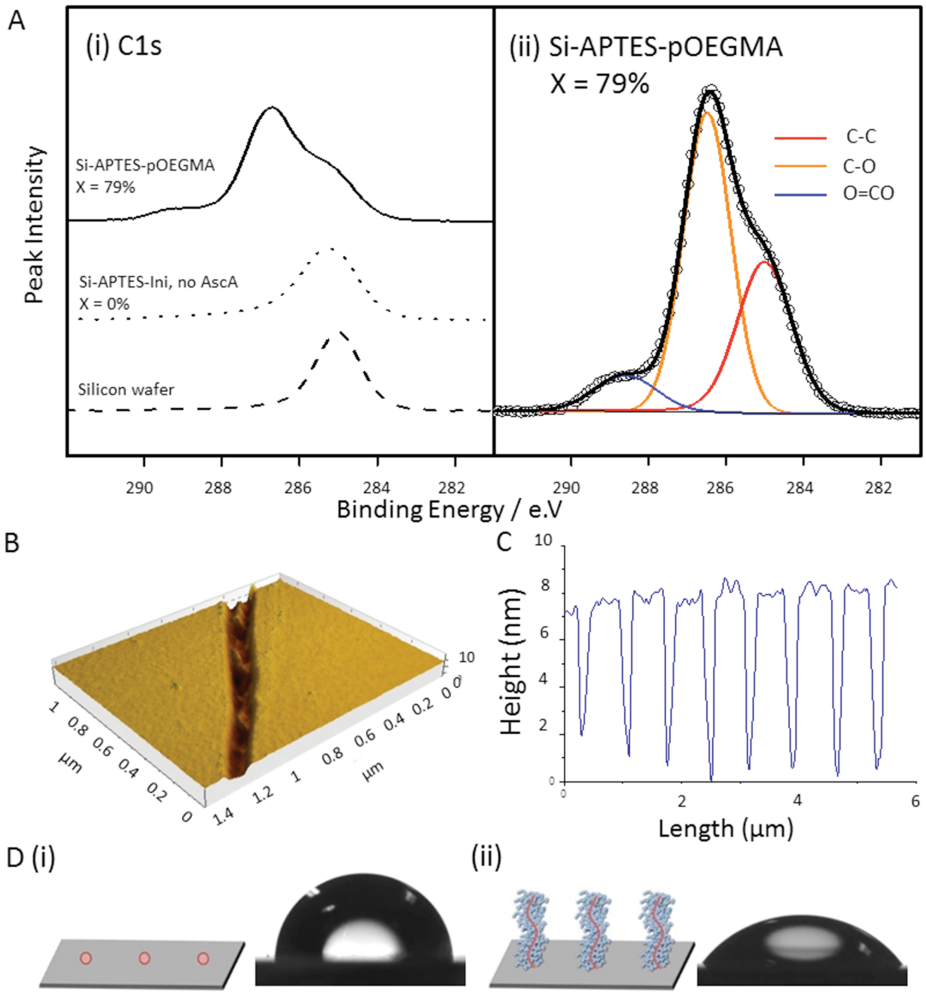

Figure 1. Demonstration and characterization of surface-initiated polymer brush growth from functionalized 2D silicon surfaces. A) XPS analysis of pOEGMA grafting from a silicon wafer functionalized with APTES-Ini with controls (dashed bottom trace), silicon functionalized with APTES-Ini that underwent polymerization with no reducing agent, ascorbic acid (AScA, dotted middle trace), and pOEMGA grafting from a silicon wafer (top trace, left). Conversion by ^{1}H-NMR (X) is included above each trace. Si-APTES-pOEGMA sample with the C1s peaks fitted (right). B) AFM scratch test and C) representative profile of pOEGMA grafted from silicon wafers. D) Water contact angle measurement of a silicon wafer functionalized with (i) APTES-Ini and (ii) following grafting of pOEGMA.

ADVANCED FUNCTIONAL MATERIALS
www.afm-journal.de

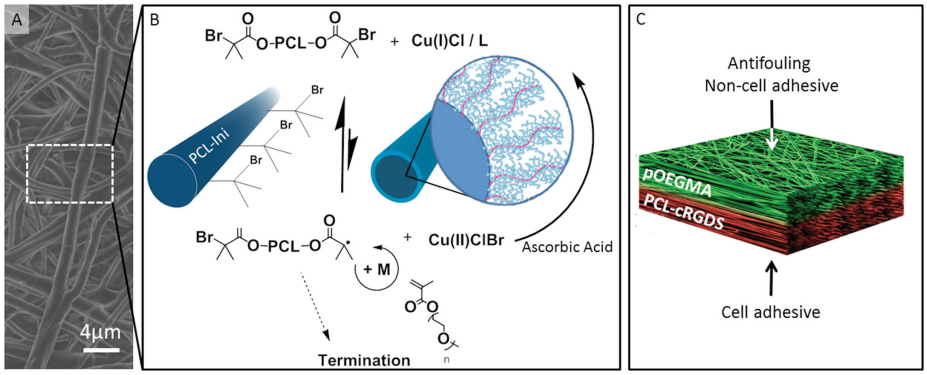

Figure 2. Grafting of pOEGMA bottlebrushes from prefunctionalized electrospun scaffolds to create an antifouling, non-cell-adhesive surface as part of a dual functional scaffold. A) Representative SEM micrograph of electrospun PCL-pOEGMA fibres. B) ARGET ATRP reaction scheme for polymerization of pOEGMA from the PCL-Ini fibers with inset schematic images of PCL-Ini following electrospinning (left) and following polymerization of pOEGMA from the fiber surface (right). C) Schematic outlining the bifunctional scaffold structure produced using layered electrospinning with postprocessing polymerization to create an antifouling PCL-pOEGMA surface with an opposing cell binding PCL-cRGDS surface.

polymer chain (PCL-Ini). PCL was selected to form the bulk of the scaffold due to its bioresorbability, good handling properties, electrospun fiber morphology, suitable degradation rate, ease of chemical modification, and its current use in Food and Drug Administration (FDA)-approved devices.[29] To ensure that the initiating region of the PCL conjugates was presented on the fiber surface, we set up the electrospinner with the cathode at the spinnerette to convey a positive charge to the surface of the polymer solution. The alkyl-bromide group present within BiBB can become electronegative due to its polarity,[23] dragging it electrostatically to the surface of the polymer solution stream and leading to surface enrichment of the initiating group on the fiber. The PCL-Ini was subsequently electrospun in combination with a high molecular weight PCL to form functionalized fibrous scaffolds which were then imaged by scanning electron microscopy (SEM) to validate consistent fiber morphology (**Figure 2**A). The addition of up to 17% (w/w) of the PCL-Ini did not significantly alter the electrospinning process or fiber formation (Figure S2, Supporting Information). pOEGMA bottlebrushes were grafted from the electrospun fibers using the parameters optimized in the 2D silicon system (Figure 2B). As with the 2D silicon surfaces, a sacrificial initiator was included in order to target a degree of polymerization (DP) of 150. A typical polymerization achieved a ≈75% conversion (by ^{1}H-NMR) and M_n 45 000, M_w 53 000 with a dispersity (M_w/M_n) of 1.18 (from size exclusion chromatography, SEC, analysis of the free polymer).

XPS confirmed successful grafting of pOEGMA from functionalized electrospun scaffolds as a large increase in C–O signal is observed following polymerization for both the 17% PCL-Ini (w/w) and the 9% PCL-Ini (w/w) (**Figure 3**A). This is in contrast to the control scaffold lacking in initiating groups that shows minimal increase in the C–O signal confirming successful covalent attachment of polymer to the scaffolds through the initiating groups (Table S1, Supporting Information). A dramatic change in the water contract angle adds further evidence for successful pOEGMA grafting. Hydrophobic electrospun PCL/PCL-Ini scaffold surfaces, with contact angles of 113.5° ± 7.8°, become hydrophilic after polymerization, with the water droplet immediately completely wetting the surface (Figure 3B).

To visualize the polymer brush and to demonstrate the versatility of the system we included a biotinylated monomer unit (biotinylated PEG monomer **3**, Supporting Information) that could be co-polymerized into the bottlebrush. The resultant random co-polymer of PCL-pOEGMA-*co*-biotinylated PEG (PCL-p(OEGMA-*co*-biotin)) allows labeling with streptavidin-conjugated probes. Following histological sectioning of the scaffolds, labelling with fluorescein-streptavidin, and imaging with confocal microscopy, the fluorescent signal was clearly visualized on the electrospun fibers demonstrating that the polymer brush is grafted from the fiber surface (Figure 3D). Histological sections of the scaffolds imaged with wide field fluorescent microscopy further demonstrated the polymer brush evenly distributed throughout the cross section of the scaffold (Figure S3, Supporting Information) and further imaging of electrospun scaffolds following grafting of PCL-p(OEGMA-*co*-biotin) confirmed the covalent attachment of the pOEGMA to the fiber surfaces. A control scaffold of electrospun PCL without the initiating group was present in the same reaction vessel as PCL-Ini (17% w/w) scaffolds and demonstrated no fluorescent signal following washing, and incubation with fluorescein-streptavidin. The successful surface grafting of pOEGMA is further supported by the difference observed in water contact angle between electrospun scaffolds with and without initiating groups that underwent polymerization. The control scaffolds remained hydrophobic while the pOEGMA functionalized scaffolds were highly hydrophilic (Figure S4, Supporting Information).

2.3. pOEGMA Surface Functionalization for Antifouling and Prevention of Cell Adhesion

pOEGMA is known to have antifouling properties and we looked to demonstrate this property from the functionalized scaffold.[30] 17% (w/w) PCL-pOEGMA scaffolds having achieved a conversion of >72% within the same reaction vessel were

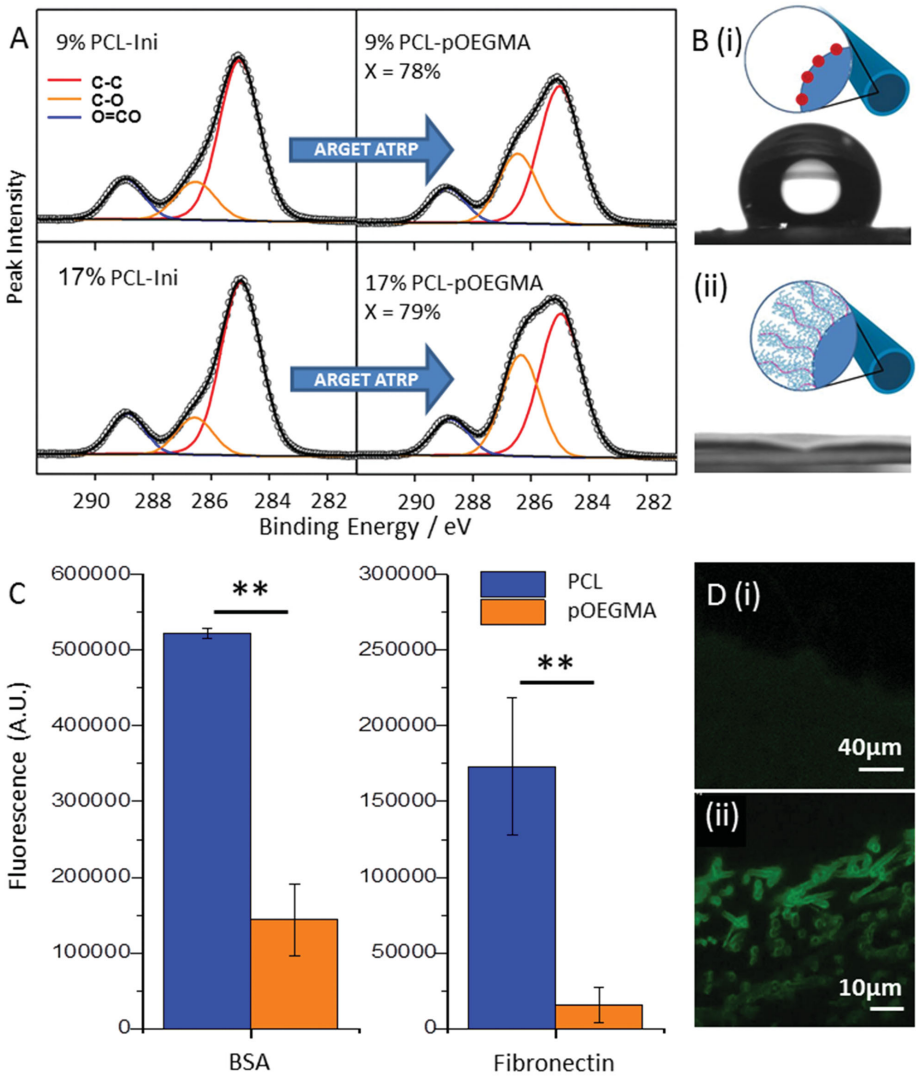

Figure 3. Demonstration and characterization of surface-initiated polymer brush growth from functionalized 3D electrospun scaffolds. A) High resolution C1s core-level spectra of pOEGMA grafting from electrospun scaffolds with 9% and 17% (w/w) PCL-Ini before (left) and after (right) grafting of pOEGMA. Conversion by ^{1}H-NMR (X) is inset. B) Water contact angle measurement of (i) electrospun PCL/PCL-Ini and (ii) PCL-pOEGMA with inset schematics. C) Antifouling ability of PCL and PCL-pOEGMA electrospun scaffolds was compared using fluorescently labelled proteins and GAGs, expressed as µg cm^{-2} of electrospun scaffold, $^{**}p < 0.005$. D) PCL (i) and PCL-p(OEGMA-*co*-biotin) (ii) fibers labeled with fluorescein-streptavidin and imaged using confocal microscopy.

tested for antifouling and resistance to cell adhesion. pOEGMA grafted scaffolds demonstrated excellent antifouling ability and resistance to common ECM protein absorption when compared to PCL scaffolds. This was established using a panel of fluorescently labelled proteins and GAGs. These biomolecules were chosen as they represent a range of molecular weights, charge, and hydrophilicity, and several are known to modulate the binding and activity of other biomolecules such as growth factors. Adsorption of these molecules to a surface would likely lead to increased biomolecule deposition and ultimately, cell adhesion. pOEGMA scaffolds dramatically outperformed native PCL for both bovine serum albumin (BSA) and fibronectin showing a 3.6 fold decrease in binding for BSA and greater than ten fold decrease for fibronectin (Figure 3C). Relative to BSA, adsorption of hyaluronic acid (HA), heparin, and chondroitin sulphate (CS) for both PCL and pOEGMA scaffolds was negligible.

In preparation for the creation of the dual functionality scaffold we prepared a cell adhesive PCL to compare to the PCL-pOEGMA. We selected the canonical peptide motif RGDS sequence as a model cell-adhesive biomolecule that promotes cell adhesion through integrin binding.[31] Fibroblasts, of which tenocytes are a specialized form, are known to bind to RGDS.[32] PCL was conjugated to a cyclized form of the RGDS (cRGDS), the natural presentation of the ligand in fibronectin.[33] PCL was conjugated with the cRGDS (Supporting Information) and electrospun into a scaffold using the standardized protocol. Bovine tenocytes were seeded onto both the PCL-cRGDS and

ADVANCED FUNCTIONAL MATERIALS
www.afm-journal.de

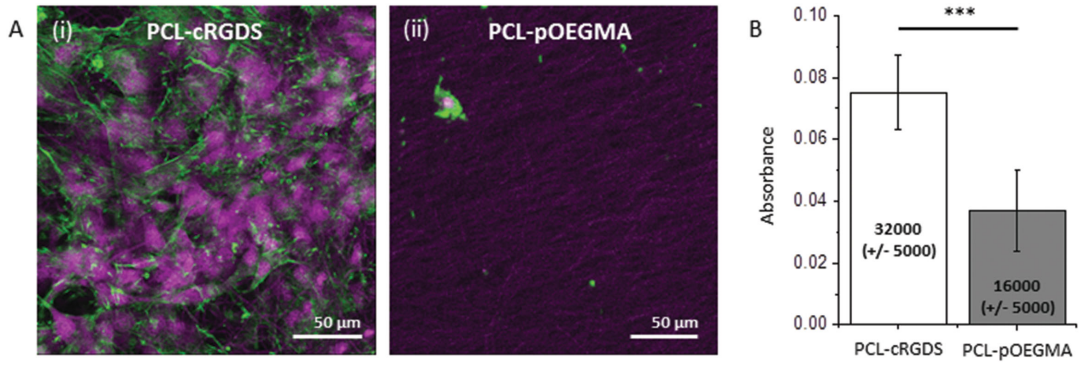

Figure 4. Cell-adhesive and non-cell-adhesive properties of functionalized electrospun scaffolds. A) Representative confocal microscopy images of bovine tenocytes cultured for 7 d on electropun PCL-cRGDS (i) and PCL-pOEGMA scaffolds (ii). Cell nuclei stained with draq5 (purple) and actin with phalloidin (green). B) Metabolic activity of bovine tenocytes cultured on scaffolds for 7 d was assessed by MTT assay. Estimated cell number is stated for each bar. *** Significant difference ($p < 0.0001$), error bars represent standard deviation.

PCL-pOEGMA scaffolds and cultured for 7 d to assess how the different surfaces supported cell adhesion and survival. Tenocytes seeded on the PCL-cRGDS scaffolds adhered well, formed a confluent cell layer, and exhibited spread morphology as demonstrated by confocal imaging of the scaffold surface. Conversely, the cells seeded on the PCL-pOEGMA scaffolds were few in number and those found were more rounded in morphology, indicating poor attachment (**Figure 4**A). The lack of robust attachment to the scaffold, as indicated by the rounded morphology, may have resulted in the surface cells being washed away while the remaining cells were trapped within the fibrous structure. These observations were compared for the whole scaffolds using a colorimetric assay for cellular metabolic activity based on the reduction of the tetrazolium dye 3-(4,5-dimethylthiazol-2-yl)-2,5-diphenyltetrazolium bromide (MTT) to approximate the relative number of cells (Supporting Information). A large reduction ($p < 0.0001$) in overall metabolic activity was observed at day 7 between PCL-cRGDS and PCL-pOEGMA scaffolds implying a reduced cell number on the PCL-pOEGMA scaffolds (Figure 4B). The estimated cell numbers are somewhat higher than the appearance of the scaffolds by confocal microscopy would suggest. This reflects the presence of a small number of rounded cellular aggregates on the PCL-pOEGMA surface, indicative of preferential cell–cell interactions over cell–surface interactions, in contrast to the densely populated spread cell morphology seen on the PCL-cRGDS surface. Together, the estimated cell numbers and confocal microscopy findings show consistently different cellular adhesion between the PCL-pOEGMA and PCL-cRGDS surfaces. This is preserved in the bi-functional scaffold, as evidenced by fluorescence microscopy, in accordance with our design (**Figure 5**C,D).

2.4. Spatial Control of Polymer Brush Leading to a Dual Functionality Scaffold

Having demonstrated the antifouling property of the PCL-pOEGMA surface and cell-adhesive property of the PCL-cRGDS surface, we progressed to immobilizing them within a single construct. We sequentially electrospun the two functionalized

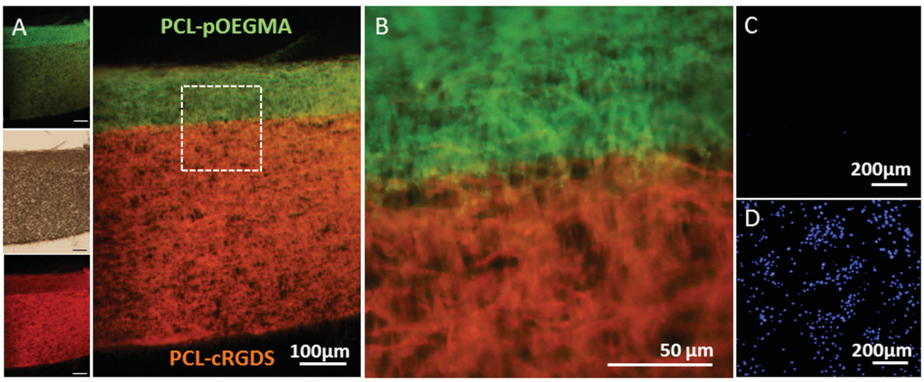

Figure 5. Dual functionality scaffolds demonstrated by fluorescent labelling of functionalities and cell adhesion. Fluorescence microscopy images of cross sections of bi-functional scaffolds formed with opposing PCL-Ini and PCL-cRGDS surfaces. Post-processing polymerization was used to produce a PCL-p(OEGMA-*co*-biotin) surface. A,B) Overlaid fluorescence images of histological cross-sections labelled with fluorescein-streptavidin (green) on the p(OEGMA-*co*-biotin) and with Cy5 (red) for the PCL-cRGDS showing well defined spatial resolution. Insets (left) show the brightfield and single channel fluorescence images with 100 µm scale bars. C,D) Bovine tenocytes were seeded on fresh scaffolds and cultured for 7 d before being stained with DAPI (blue) for cell nuclei and imaged with fluorescent microscopy. The PCL-pOEGMA surface is shown in the upper image (C) and the opposing PCL-cRGDS surface is shown in the lower image (D).

DOI: 10.1002/adfm.201501277

polymers, PCL-Ini and PCL-cRGDS, to produce discrete sections within the same electrospun construct. To confirm the presence and spatial location of the functionalized PCL, we used specific fluorescent labels to tag corresponding functional groups within the pOEGMA or cRGDS sections. The PCL-pOEGMA side included the biotinylated monomer previously described, to produce a PCL-p(OEGMA-*co*-biotin) brush that could be labeled with streptavidin-fluorescein. To visualize the cRGDS, we modified a Cy5 dye with an amine, which can react with the carboxylic acids found only on the aspartic acid (D) residue side chains exposed on the PCL-cRGDS fibers (Figure S13, Supporting Information). Histological sections of the dual functional scaffolds were labeled to illustrate these discrete fiber locations and show successful spatial control of the different functionalities within the substance of a single electrospun construct (Figure 5A,B).

To further interrogate the dual functionality scaffolds, bovine tenocytes were seeded on both surfaces of the scaffolds and cultured for 7 d. The scaffolds were then stained with 4′,6-diamidino-2-phenylindole (DAPI) to label the cell nuclei on both sides of each scaffold and fluorescent imaging was performed by imaging one side, before turning it over and imaging the opposite side. The desirable functionality of the opposing surfaces is preserved despite the bilayer processing. The PCL-cRGDS surface supports a high cell density whereas very few cells are seen on the opposing pOEGMA surface (Figure 5C,D). Excellent spatial control of functionalized polymers is demonstrated by the sharp transition of layers seen with fluorescent labelling. Sequential electrospinning of end-group functionalized polymers is shown to be a highly effective method for spatial control within a construct. This could be used to generate more complex architecture including multilayering.

3. Conclusion

In conclusion, an effective dual functionality scaffold with a cell adhesive surface and an opposing antifouling, non-cell adhesive surface has been successfully produced using a combination of end functionalization of PCL with a polymerization initiating group (BiBB) and a cell binding motif (cRGDS) that may be sequentially electrospun to produce a scaffold with zonally arranged functional groups. Post-processing with ARGET ATRP is a facile and highly versatile method to produce a surface-initiated pOEGMA bottlebrush that elicits a high performance antifouling and cell resistant coating. We have demonstrated the versatility of the polymerization for the addition of multifunctionality through the use of a biotinylated monomer unit in a single processing step. This modular and versatile approach could be used as a platform scaffold for multiple applications in tissue engineering.

4. Experimental Section

All chemical reagents were purchased from Sigma Aldrich (UK) and deuterated solvents for ^{1}H-NMR from Merck (Darmstadt, Germany) unless specifically noted.

ARGET ATRP of OEGMA in Solution and from Surfaces: pOEGMA bottlebrushes were produced in solution and from 2D silicon and 3D electrospun functionalized surfaces. When producing brushes from surfaces, a sacrificial initiator, ethyl 2-bromoisobutyrate (EBiB), was used in solution to enhance control of the polymerization and allow for surrogate characterization of the polymerization on the surface.[14,34] The amount of initiator present on the 2D silicon and 3D electrospun surfaces was estimated and if greater than 10% of the sacrificial initiator mass, the mass of sacrificial initiator was reduced proportionally to maintain the reaction conditions.

In a typical experiment OEGMA (340 mg, 0.7 mmol, with a M_w of the poly(ethylene glycol unit) of 400 Da, Polysciences, Germany), activated by the removal of inhibitors, was introduced into a round bottom flask with copper (II) chloride ($Cu(II)Cl_2$, 0.64 mg, 0.0047 mmol), tris[(2-pyridyl) methyl]amine (TPMA, 1.37 mg, 0.0047 mmol), and EBiB (0.92 mg, 0.0047 mmol) in 3 mL of 50:50 isopropyl alcohol (IPA)/H_2O. Following through mixing 2 mL was transferred to a test tube that was empty or containing functionalized 2D silicon or 3D electrospun surfaces. It was sealed, introduced into an ice bath, and degassed with argon for 20 min before ascorbic acid (AscA 0.08 mg, 0.00047 mmol) was added from a degassed solution using a gas tight syringe. The vessel was transferred to a pre-warmed heat block at 30 °C and allowed to react for 2 h at which time the reaction was quenched by bubbling oxygen through the reaction mixture. Conversion was calculated by ^{1}H-NMR (400 Hz, *d*4-MeOD) and molecular weights determined by SEC using a GPCMax VE 2001 (Viscotek). The SEC was run with an eluent of *N,N*-dimethylformamide (DMF) with 0.075% (w/v) at a flow rate of 0.7 mL min^{-1} over two Polymer Standards Service (PSS) Gram DMF columns at 35 °C. Molecular weights were determined relative to pMMA standards (Agilent Technologies, UK) without correction. Prior to the measurements the copper was removed using heavy metal chelating beads (Cuprisorb, Fish Fish Fish, UK) and filtered through a 0.22 µm syringe mounted polytetrafluoroethylene filter. Scaffolds and silicon wafers functionalized with polymer brushes were removed from solutions and thoroughly rinsed three times in 100% ethanol before washing in Milli-Q H_2O for 24 h with three intermittent water changes. Any remaining copper was removed through the addition of Cuprisorb heavy metal chelating beads in the final washing step before drying in a vacuum desiccator at room temperature.

Functionalization of Silicon Wafers with APTES and BiBB for 2D Silicon Polymerization: P-doped silicon wafers (University Wafer, Boston, USA) were prepared for functionalization with sonication in acetone for 3 min, rinsing with Milli-Q H_2O and immersion in piranha solution (1:3, hydrogen peroxide: concentrated sulfuric acid) for 1 h, rinsing twice with Milli-Q H_2O, and drying under a stream of nitrogen. APTES was deposited on the surface of the silicon wafers using vapor deposition using a modified protocol from the literature; cleaned silicon wafers were laid in a glass petri dish and a glass vial containing 10 mL of anhydrous hexane and 0.25 mL of APTES was placed in the center of the dish.[35] The petri dish was placed in a desiccator to which a vacuum was applied and maintained for 90 min. Wafers were subsequently removed and inserted into test tubes, sealed with septa and parafilm, degassed with nitrogen and to each a degassed solution of 5 mL of anhydrous hexane, 0.125 mL of BiBB, and 0.165 mL of anhydrous triethylamine (TEA) was introduced and allowed to react at room temperature for 1 h. Following this the wafers were removed and washed with hexane, ethanol and Milli-Q H_2O and then dried under a stream of nitrogen. Wafers were stored in a vacuum desiccator and protected from light until used.

Water Contact Angle Measurement: Water contact angles on 2D silicon wafer surfaces and electrospun scaffolds were measured with a Krüss Easy Drop DSA 100 (Hamburg, Germany) and the associated DSA1 v 1.9 software, a drop size of 7 µL, and at room temperature.

Brush Thickness Measurements with AFM and Spectroscopic Ellipsometry: Dry thickness measurements were undertaken with AFM and ellipsometry on the same 2D silicon samples to establish the thickness of the grafted pOEGMA layer. AFM measurements were taken using an Agilent Technologies 5500 atomic force microscope with a silicon probe, tip radius <10 nm, force constant 40 nN m^{-1}. A scratch test was performed whereby the AFM probe tip was moved towards the sample, contact was made, and the force increased until the underlying silicon wafer was contacted. The tip was then moved laterally to create a

full-thickness scratch. The AFM was then used in tapping mode to create a depth profile across the scratch area. Using the associated software (Pico Image) thickness measurements of the polymer layer were made.

Ellipsometry measurements were performed at room temperature using a SOPRA GESP 5 variable angle spectroscopic ellipsometer. The data were recorded through incidence angles of 65°–75° with respect to the substrate normal, across a wavelength range from 900–1600 nm (20 nm steps). Cauchy model fits were used to analyze the ellipsometric data. Good agreement was found between the ellipsometrically deduced brush thicknesses and AFM.

*Production of Functionalized Electrospun Scaffolds and Fiber-Initiated Controlled Radical Polymerization–Synthesis of PCL-Ini**1**:* PCL-diol (M_w 14 000 Da) was functionalized with 2-bromoisobutyryl bromide (BiBB) using a protocol adapted from the literature to produce PCL-Ini**1**.[24] In a typical run, 5 g of 14 kDa PCL-diol was introduced to 200 mL of anhydrous tetrahydrofuran in a round bottom flask and stirred at room temperature in a sealed nitrogen atmosphere. Following dissolution of the PCL, 2.9 mL TEA and 50 mg of 4-dimethylaminopyridine were added and the vessel immersed in an ice bath. After 15 min of cooling, 265 µL of BiBB was introduced dropwise, the ice bath removed, and the reaction stirred overnight at room temperature. The mixture was filtered, and the filtrate was collected, reduced through vacuum rotary evaporation, and precipitated into cold diethyl ether. The precipitate was isolated by vacuum filtration and dried. The product was confirmed using ^{1}H-NMR (400 MHz, deuterated $CDCl_3$) and was stored until needed in a vacuum desiccator, protected from light. ^{1}H NMR (400 MHz, $CDCl_3$) δ ppm: 4.24 – 4.20 (m, 4H) 4.05 (*t*, *J* = 6.7 Hz, 240H), 3.78 – 3.71 (m, 4H), 2.30 (*t*, *J* = 7.5 Hz, 244H), 1.92 (s, 0H), 1.73 – 1.55 (m, 480H), 1.46 – 1.32 (m, 252H) (see Figure S5, Supporting Information, for peak assignments).

Electrospinning PCL and PCL Conjugates: Two different PCL-Ini:PCL ratios were electrospun into scaffolds; 12 mg mL^{-1} (9% w/w) PCL-Ini or 24 mg mL^{-1} (17% w/w) PCL-Ini was added to 12% (w/v) PCL (M_n 70 000–90 000 Da) in 1,1,1,3,3,3-hexafluoro-2-propanol (HFIP) and mixed overnight. Solutions were transferred to plastic syringes, loaded onto a programmable syringe pump (Kd Scientific, UK) and extruded at a rate of 2 mL h^{-1} through a blunt 18-gauge stainless steel needle charged with +16 kV (Glassman, Bramley, Hampshire, UK). The needle was placed at distance of 11 cm from a grounded 10 × 10 cm plate for small master scaffolds or a mandrel rotating at 0.33 m s^{-1} for large master scaffolds, each coated with aluminum foil. No difference was seen in fiber alignment or morphology between collectors. All scaffolds were electrospun under the same conditions, stored in a vacuum desiccator, and protected from light until needed.

XPS Analysis of the 2D Silicon and 3D Electrospun Polymer Brush Functionalized Surfaces: XPS was used to characterize the surface of both the 2D silicon and 3D electrospun samples. The spectra were measured using a Thermo Fisher K-Alpha XPS System (Thermo Fisher Scientific Inc.) with a monochromatic Al-Kα (energy = 1486.71 eV) X-ray source. Samples were positioned at the electron take-off angle normal to the surface with respect to the analyzer. Survey spectra were measured over a range of 0–1400 eV and recorded for each sample, then followed by high resolution spectra for C1s and O1s. A low energy electron/ion flood gun was used to ensure effective surface charge compensation. XPS spectra were calibrated to the adventitious C1s signal (285.0 eV). Curve fitting was carried out using Thermo Avantage Software (v. 5.948) using a Shirley background. Peak areas were normalized within Thermo Avantage using atomic sensitivity factors for the Al Kα anode ("AlWagner" library)[36] and from these areas the carbon composition and elemental ratios were determined.

Modification of the Polymerization Protocol for Use with the Biotinoylated PEG Monomer 3: For samples requiring fluorescent labeling, minor modifications were needed to mitigate any possible chelation of the copper catalyst by additional groups in the reaction mixture. The reaction was prepared as previously outlined but with 5 mol% of the OEGMA replaced with biotinylated PEG monomer 3 (Supporting Information), and the reaction was left to proceed overnight. Samples were washed and prepared as previously described.

Histological Sectioning, Labeling, and Fluorescent Imaging of the Scaffolds: Scaffolds for histological section and analysis were embedded in polyester wax (VWR, UK) in a method modified from Steedman et al.[37] Scaffolds were embedded following incubation in a series of wax solutions maintained at 42 °C, first 30 min in 1:1 (v/v) polyester wax and ethanol, followed by two rounds of pure polyester wax for 30 min and 1 h, respectively. The scaffolds were then embedded vertically in polyester wax and allowed to set. Sections were cut at 10 µm onto untreated glass slides, dried, dewaxed with ethanol, and affixed at either end with a drop of inert adhesive. Sections were blocked with 1% (w/w) BSA and 0.1% (w/v) tween 30 in phosphate buffered saline (PBS) for 30 min, stained for 15 min with fluorescein-streptavidin (Vector Labs, UK) diluted to 1 µg mL^{-1} in 1% (w/w) BSA in PBS at pH 8.4, and washed three times in PBS. Slides were coverslipped for confocal microscopy with FluorSave fluorescent mounting media (Millipore, UK). Standard fluorescent imaging was performed on a Leica inverted optical microscope fitted with an Olympus DP70 digital camera. Confocal imaging was performed on a Leica SP5 inverted confocal microscope and images processed using GIMP 2.1.

Measurement of Protein Adsorption onto PCL and pOEGMA Scaffolds: Fluorescently labeled rhodamine-heparin (rhod-hep, M_W 18 kDa), rhodamine-CS (rhod-CS, M_W 50 kDa), and fluorescein-HA (fluor-HA, M_W 1500 kDa) were purchased (Creative PEGWorks, Winston Salem, USA). Rhodamine-fibronectin (rhod-fib) and rhotamine-BSA (rhod-BSA) were synthesized prior to experimentation (Supporting Information). Stock solutions of labeled protein were 50 µg mL^{-1} in PBS for all proteins with the exception of rhod-BSA which was 10 µg mL^{-1} in PBS. Circular PCL-Ini scaffolds, 6 mm in diameter, with and without pOEGMA brush functionalization were immersed in 70% (v/v) ethanol and washed with PBS three times to ensure uniform hydration. Excess liquid was removed and the scaffolds introduced into high return 1.5 mL centrifuge tubes for incubation with 200 µL protein solution (test samples) or PBS (control) at 37 °C for 18 h. Scaffolds were then washed in PBS in 28 mL light protected glass vials overnight to remove any unbound protein. The fluorescent signal in the scaffolds was then quantified on a Perkin Elmer Envision multimode detector (Germany) at an excitation wavelength of 550 nm and emission of 580 nm for rhodamine labeled proteins and at an excitation wavelength of 490 nm and emission of 520 nm for fluorescein labeled proteins.

Cell Adhesion Testing of PCL-cRGDS and PCL-pOEGMA Scaffolds: Bovine tenocytes were isolated through primary cell culture from three independent animals all of which were a maximum of 2 years in age (Supporting Information). Cell adhesion experiments were performed using a protocol modified from the literature.[38] In brief, 24-well plates were coated with two-component silicon elastomer (Sygard 184, Dow Corning) prepared in a 10:1 ratio and cured for 48 h. Each independent experiment utilized seven PCL-pOEGMA scaffolds of 6 mm diameter, that had previously been functionalized with a pOEGMA brush and seven 6 mm diameter PCL-cRGDS scaffolds. Scaffolds and stainless steel insect pins (0.15 mm, Watkins and Doncaster, UK) were immersed into 70% (v/v) ethanol for 15 min before washing in sterile PBS supplemented with 1% (w/v) anti/anti three times. The silicone-coated well plate was thoroughly sprayed with 70% (v/v) ethanol before a scaffold was inserted into each well and fixed with an insect pin through the center of the scaffold. A row of empty wells was left as a control. The plate and scaffolds were sterilized under UV light in the cell culture hood for 8 h. Scaffolds were washed with sterile PBS immediately before cell seeding.

Bovine tenocytes were prepared in a single cell suspension at a concentration of 5 × 10^5 cells mL^{-1} from which 50 µL (2.5 × 10^4 cells) were seeded onto each scaffold. After allowing 2 h for cell attachment at 37 °C, 5% CO_2, and 100% relative humidity, a further 1 mL of normal growth media (NGM) was gently added to each well. Seeded scaffolds were cultured for 7 d, with the media replaced after the fourth day. On the seventh day the media was aspirated from the wells and the scaffolds were washed with sterile PBS. Two scaffolds of each type were prepared for imaging, the remaining five scaffolds of each type were used for quantification of cellular metabolism using an MTT assay. This was compared to a standard curve produced from a cell ladder to estimate cell number.

Scaffolds reserved for imaging were fixed in 4% (w/v) paraformaldehyde (PFA) for 15 min, washed, and stored at 4 °C in PBS until used. Prior to imaging, scaffolds were blocked in 1% (w/v) BSA and 0.1% (w/v) tween 20 in PBS for 30 min. A solution of 5×10^{-6} M draq5 (Thermo Scientific, UK) to stain cell nuclei and phalloidin (Alexa Fluor 488, diluted 1:400, Life Technologies) to stain actin was diluted in 1% (w/v) BSA in PBS and was incubated with the scaffolds under light protection for 20 min before being washed with further PBS. Samples were imaged in PBS by inverted confocal microscopy as previously described.

Production of Dual Functionality Scaffolds and Characterization: Dual functionality scaffolds were fabricated as a continuous scaffold using layered electrospinning. Two separate solutions of functionalized PCL were prepared in HFIP as above with the addition of 1 mg mL^{-1} PCL-cRGDS to one, and 17% (w/w) PCL-Ini to the other. These were sequentially electrospun in accordance with the protocol described above. The PCL-cRGDS solution (2 mL) was electrospun first, followed by PCL-Ini solution. This was allowed to run for a further 30 min to ensure coverage of the scaffold. Post-processing polymerization of pOEGMA and pOEGMA-*co*-biotin was performed as described above.

Sectioning, Labeling, and Imaging of Dual Functionality Scaffolds: Dual functionality scaffolds with a PCL-p(OEGMA-*co*-biotin) surface were embedded in polyester wax and blocked out in a vertical orientation before sectioning at 10 µm onto glass slides, and dewaxed with ethanol as previously described. The scaffolds were immobilized onto glass coverslips with an inert adhesive (Aquarium Sealant, King British, Gainsbrough, UK) that was allowed to cure overnight on the bench. The scaffolds were then incubated in 0.2% (w/v) tween 20/0.2% (w/v) triton X in PBS for 60 min before being washed in Milli-Q H_2O and the excess blotted away with filter paper. To label the cRGDS moiety, an amino-Cy5 dye **7** was synthesized (Supporting Information), diluted to 0.1×10^{-3} M in 20×10^{-3} M sodium borate buffer solution at pH 9, and combined with 1-ethyl-3(3-dimethylaminopropyl)carbodiimide (EDC, 2×10^{-3} M) and *N*-hydroxysuccinimide (NHS, 2×10^{-3} M). This solution was applied to the immobilized scaffolds and the reaction proceeded on the bench at room temperature for 30 min before the immobilized scaffolds were washed with 20×10^{-3} M sodium borate buffer, Milli-Q H_2O, 0.2% (w/v) tween 20/0.2% (w/v) triton X solution, Milli-Q H_2O, 50% (v/v) IPA, 100% IPA, 50% (v/v) IPA, and further Milli-Q H_2O. The scaffolds were then blocked and labeled with fluorescein-streptavidin as previously described, light protected, and imaged immediately. Sections were imaged on an upright Olympus BX51 epifluorescent microscope equipped with an Olympus DP70 camera. Images were obtained in three channels: Bright field, FITC to image the fluorescent brushes, and TxRed to image the Cy5 labeling of cRGDS.

Cell Adhesion Assessment and Imaging of Dual Functionality Scaffolds: Cell adhesion was assessed on the dual functionality scaffolds using a minor variation to the above protocol. Scaffolds and cells were prepared in an identical manner. When seeded, 25 000 cells were seeded on one side of the scaffold, incubated for 30 min to allow for cell attachment, gently turned over with sterile forceps, and a further 25 000 cells were seeded on the opposing side. The scaffold was then immobilized in a silicone-coated well plate ensuring that there was free space for media below the scaffold (between the scaffold and the silicon coating). The plate was then returned to the incubator for 2 h for further cell attachment before NGM was gently added as per protocol. After 7 d the dual functional scaffolds were fixed in 4% (w/v) PFA and blocked in 1% (w/v) BSA and 0.1% (w/v) tween 20 as described above. 4′,6-diamidino-2-phenylindole (DAPI, diluted 1:5000, Sigma) and phalloidin (diluted 1:200, Alexa Fluor 568, Invitrogen) were diluted in 1% (w/v) BSA solution and incubated with the scaffolds for 15 min. After washing in PBS the scaffolds were incubated in fluorescein-streptavidin (diluted 1:500, Vector Laboratories) in PBS at pH 8.4 for a further 15 min. After washing in PBS the scaffolds were mounted on glass slides with Fluorosave mounting media (Calbiochem, VWR) and coverslipped. Slides were protected from light before being imaged on both the confocal and inverted optical microscopes as described above.

Statistical Analysis: All experimental test groups had a sample size of at least $n = 3$ for biochemical analysis. All cell-related work was repeated with bovine tenocytes from three different animals. Data are presented as mean +/− standard deviation (SD). Statistical significance was determined by students T-tests using Excel software, with a significance accepted where p-value < 0.05.

Supporting Information

Supporting Information is available from the Wiley Online Library or from the author.

Acknowledgements

The authors acknowledge Dr. Chris Spicer for synthesizing the Cy5 dye, Dr. Eugene Pashuck III for assistance with the PCL-cRGDS synthesis, Paresh Parmar for optimizing the cRGDS synthesis and FTIR, Dr. Nadav Amdursky for his assistance with the AFM measurements, Dr. Jean-Philippe St-Pierre for his help with the primary cell cultures, Dr. A. Géraldine Guex for her assistance with the XPS interpretation, Stephanie Maynard for her assistance with confocal microscopy, and Dr. Benjamin Pierce for his assistance in proof reading of this manuscript. The authors thank the Facility for Imaging by Light Microscopy Core Facility (FILM) at Imperial College London. R.H.H. gratefully acknowledges funding from the EPSRC-DTA bursary scheme at Imperial College London and the Blond One Year Research Fellowship through the Royal College of Surgeons of England. J.A.M.S. thanks the Natural Sciences and Engineering Research Council of Canada. A.J.G. thanks the support of the Whitaker International Program. M.M.M. would like to thank the Public Service Department of Malaysia for PhD scholarship via King of Malaysia scheme and University Teknologi MARA (UiTM) Malaysia for the lectureship. R.H.H., J.A.M.S., and M.M.S. thank the Rosetrees Trust for very generous support. L.W.C. and M.M.S were funded by the Medical Engineering Solutions in the Osteoarthritis Centre of Excellence, funded by the Wellcome Trust and the Engineering and Physical Sciences Research Council (EPSRC) [088844]. D.J.P. acknowledges support from the Royal Society [UF100105].

Received: March 30, 2015
Revised: June 19, 2015
Published online:

[1] S. D. McCullen, H. Autefage, A. Callanan, E. Gentleman, M. M. Stevens, *Tissue Eng. Part A* **2012**, *18*, 2073.
[2] Y. Zhang, F. Yang, K. Liu, H. Shen, Y. Zhu, W. Zhang, W. Liu, S. Wang, Y. Cao, G. Zhou, *Biomaterials* **2012**, *33*, 2926.
[3] S. Liu, M. Qin, C. Hu, F. Wu, W. Cui, T. Jin, C. Fan, *Biomaterials* **2013**, *34*, 4690.
[4] S. Liu, J. Zhao, H. Ruan, T. Tang, G. Liu, D. Yu, W. Cui, C. Fan, *Biomacromolecules* **2012**, *13*, 3611.
[5] M. Angarano, S. Schulz, M. Fabritius, R. Vogt, T. Steinberg, P. Tomakidi, C. Friedrich, R. Mulhaupt, *Adv. Funct. Mater.* **2013**, *23*, 3277.
[6] F. J. Bye, J. Bissoli, L. Black, A. J. Bullock, S. Puwanun, K. Moharamzadeh, G. C. Reilly, A. J. Ryan, S. MacNeil, *Biomater. Sci.* **2013**, *1*, 942.
[7] H. Wang, Y. Feng, H. Zhao, R. Xiao, J. Lu, L. Zhang, J. Guo, *Macromol. Res.* **2012**, *20*, 347.
[8] S. Kidoaki, I. K. Kwon, T. Matsuda, *Biomaterials* **2004**, *26*, 37.
[9] M. Arnal-Pastor, C. M. Ramos, M. P. Garnes, M. M. Pradas, A. V. Lluch, *Mater. Sci. Eng. C* **2013**, *33*, 4086.

[10] R. Barbey, L. Lavanant, D. Paripovic, N. Schüwer, C. Sugnaux, S. Tugulu, H. Klok, *Chem. Rev.* **2009**, *109*, 5437.
[11] T. Ameringer, F. Ercole, K. M. Tsang, B. R. Coad, X. Hou, A. Rodda, D. R. Nisbet, H. Thissen, R. A. Evans, L. Meagher, J. S. Forsythe, *Biointerphases* **2013**, *8*, 16.
[12] W. J. Yang, T. Cai, K. G. Neoh, E. T. Kang, G. H. Dickinson, S. L. M. Teo, D. Rittschof, *Langmuir* **2011**, *27*, 7065.
[13] C. Gao, D. Yan, *Prog. Polym. Sci.* **2004**, *29*, 183.
[14] A. M. Telford, L. Meagher, V. Glattauer, T. R. Gengenbach, C. D. Easton, C. Neto, *Biomacromolecules* **2012**, *13*, 2989.
[15] B. B. Mollet, M. Comellas-Aragones, A. J. H. Spiering, S. H. M. Soentjens, E. W. Meijer, P. Y. W. Dankers, *J. Mater. Chem. B* **2014**, *2*, 2483.
[16] T. Yano, W. O. Yah, H. Yamaguchi, Y. Terayama, M. Nishihara, M. Kobayashi, A. Takahara, *Polym. J.* **2011**, *43*, 838.
[17] A. E. Ozcam, K. E. Roskov, J. Genzer, R. J. Spontak, *ACS Appl. Mater. Interfaces* **2012**, *4*, 59.
[18] G. D. Fu, L. Q. Xu, F. Yao, K. Zhang, X. F. Wang, M. F. Zhu, S. Z. Nie, *ACS Appl. Mater. Interfaces* **2009**, *1*, 239.
[19] T. J. Menkhaus, H. Varadaraju, L. F. Zhang, S. Schneiderman, S. Bjustrom, L. Liu, H. Fong, *Chem. Commun.* **2010**, *46*, 3720.
[20] Q. Feng, D. Hou, Y. Zhao, T. Xu, T. J. Menkhaus, H. Fong, *ACS Appl. Mater. Interfaces* **2014**, *6*, 20958.
[21] C. Gualandi, C. D. Vo, M. L. Focarete, M. Scandola, A. Pollicino, G. Di Silvestro, N. Tirelli, *Macromol. Rapid Commun.* **2013**, *34*, 51.
[22] W. Yuan, Y. Feng, H. Wang, D. Yang, B. An, W. Zhang, M. Khan, J. Guo, *Mater. Sci. Eng. C* **2013**, *33*, 3644.
[23] G. D. Fu, J. Y. Lei, C. Yao, X. S. Li, F. Yao, S. Z. Nie, E. T. Kang, K. G. Neoh, *Macromolecules* **2008**, *41*, 6854.
[24] C. Brandl, A. Greiner, S. Agarwal, *Macromol. Mater. Eng.* **2011**, *296*, 858.
[25] W. Jakubowski, K. Matyjaszewski, *Macromolecules* **2005**, *38*, 4139.
[26] J. Miao, W. He, L. Zhang, Y. Wang, Z. Cheng, X. Zhu, *J. Polym. Sci., Part A-1: Polym. Chem.* **2012**, *50*, 2194.
[27] L. W. Chow, A. Armgarth, J.-P. St-Pierre, S. Bertazzo, C. Gentilini, C. Aurisicchio, S. D. McCullen, J. A. M. Steele, M. M. Stevens, *Adv. Healthcare Mater.* **2014**, *3*, 1381.
[28] C. Yoshikawa, K. Zhang, E. Zawadzak, H. Kobayashi, *Sci. Technol. Adv. Mater.* **2011**, *12*, 015003.
[29] M. A. Woodruff, D. Hutmacher, *Prog. Polym. Sci.* **2010**, *35*, 1217.
[30] S. Tugulu, H. Klok, *Biomacromolecules* **2008**, *9*, 906.
[31] U. Hersel, C. Dahmen, H. Kessler, *Biomaterials* **2003**, *24*, 4385.
[32] D. Grafahrend, J. Lleixa Calvet, J. Salber, P. D. Dalton, M. Moeller, D. Klee, *J. Mater. Sci.: Mater. Med.* **2008**, *19*, 1479.
[33] F. J. Xu, Z. H. Wang, W. T. Yang, *Biomaterials* **2010**, *31*, 3139.
[34] J. K. Oh, K. Min, K. Matyjaszewski, *Macromolecules* **2006**, *39*, 3161.
[35] I. E. Dunlop, R. K. Thomas, S. Titmus, V. Osborne, S. Edmondson, W. T. S. Huck, J. Klein, *Langmuir* **2012**, *28*, 3187.
[36] a) C. D. Wagner, L. E. Davis, M. V. Zeller, J. A. Taylor, R. M. Raymond, L. H. Gale, *Surf. Interface Anal.* **1981**, *3*, 211; b) C. D. Wagner, *Practical Surface Analysis* Vol. *1*, 2nd ed. (Eds: D. Briggs, M. P. Seah), John Wiley and Sons, New York **1990**.
[37] H. F. Steedman, *Nature* **1957**, *179*, 1345.
[38] A. G. Guex, G. Fortunato, D. Hegemann, H. T. Tevaearai, M.-N. Giraud, *Methods Mol. Biol.* **2013**, *1058*, 119.

Appendix C – Purification of Cu(I)Br

Cu(I)Br was purified to eliminate any Cu(II)Br using a protocol from the literature[341]. In brief, Cu(I)Br (2 g) was introduced into a 250ml conical flask. Glacial acetic acid (200 mL) was added and the flask sealed with a rubber septa and parafilm and stirred at room temperature (RT) for two hours. Under an argon atmosphere, the solution was passed through a size 3 pore glass frit under a vacuum. The solid was washed a two further times with acetic acid. Absolute ethanol was then used to wash the purified Cu(I)Br five times within the funnel of the glass frit whilst maintaining the argon atmosphere. A colour change from grey to near white was seen. The solid was collected and dried in a desiccator *in vacuo* before being stored at RT under argon. Samples were removed periodically for experimentation after which the storage vessel was again filled with argon and sealed.

Appendix D – SOP for ARGET ATRP in solution

STANDARD OPERATING PROCEDURE

File Reference:	

Document Title:	ARGET ATRP of OEGMA		
SOP Number:		Version #:	v1.0
Author:	Rachael Harrison	Prepared Date:	14/12/2015
Reviewed By:		Review Date:	
Approved By:		Approval Date:	

1. PURPOSE

To produce polymer bottlebrushes of OEGMA either in solution or from surface initiated polymerisation.

2. DEFINITIONS

PCL = poly(caprolactone)
OEGMA = oligomer of ethylene glycol – poly(ethylene glycol) monomethyl ether monomethacrylate.
Cu(II)Cl = copper (II) chloride
TPMA = tris[(2-pyridyl)methyl]amine
EBiB = ethyl-α-bromoisobutyrate
AScA = ascorbic acid
IPA = isopropyl alcohol

3. MATERIALS

EQUIPMENT

Balance
General Laboratory Glassware (graduated cylinders, beakers)
Hot plate, preheated to 31°C
Small glass test tubes (about 3 mL) or glass vials
New rubber (WHITE) septa that fit closely with the glassware
Plastic Transfer Pipettes – [VWR#612-1681]

REAGENTS

Basic activated aluminium oxide (Sigma, CAS 1344-28-1)
Inhibitor removal beads for removal of MEHQ (Sigma, 311332 aldrich)
OEGMA monomer (interchangeable with other monomers, but item used here: **Polysciences**, 26915-72-0 with a PEG unit of 400) – *NB – MUST be polysciences*.
Cu(II)Cl (Sigma, CAS 7447-39-4)
TPMA (Sigma, CAS 16858-01-8)
EBiB (Sigma, CAS 600-00-0)
AScA (Sigma, CAS 50-81-7)

SOLUTIONS

A. 50% (v/v) IPA
Distilled water – 14 mL
IPA – 14 mL

4. PROCEDURE

A. Removal of inhibitors from the OEGMA monomer

1. Take a 20 mL plastic syringe (the “column”)
2. Put a small amount of cotton wool in the bottom of the syringe to act as a filter
3. Add up to the 8 mL mark with basic aluminium oxide (CARE – fine particulate – do this in the hood).
4. Add on top of the aluminium oxide up to the 16 mL level with inhibitor removal beads.
5. Attach the column to a clamp stand.
6. Pour OEGMA monomer onto the column you have made and allow to filter through using gravity this process can be speeded up a bit using the syringe plunger to add some pressure to the top of the column.
7. Collect aliquots of monomer that drip out of the bottom of the column in 1.75 mL glass vials.
8. Freeze the monomer aliquots in the -20°C freezer until needed.

B. ARGET ATRP reaction [1]

1. Make up stock solutions of the reagents (Cu(II)Cl, TPMA and EBiB) in 1.5 mL epindorf tubes and dissolve in 1 mL of 50% (v/v) IPA. Take care to re-seal the Cu(II)Cl under inert gas after you have opened it.
2. Make up stock solution of the AScA in a 7 mL glass vial and dissolve in 7 mL of 50% (v/v) IPA, seal with a good septa.
3. Weigh out the monomer into the reaction vessel (small test tube for small reactions).
4. Calculate reagents for the volume you are using:
Molar ratios monomer**:**Cu(II)Cl:TPMA:EBiB:AScA are 150:1:1:1:0.15 and how much of the stock solutions you need to add, and how much extra solvent you need.
5. In a 2 mL volume of solvent :OEGMA (0.227 mg), Cu(II)Cl (0.42 mg), TPMA (0.91 mg), EBiB (0.61mg), AScA (0.08 mg).
6. Put the stock solutions on ice to cool.
7. Add the solvent to the OEGMA and dissolve and also put on ice.
8. You need to use argon degassing – at this point turn on the argon tank on the schlenk line to purge the line. *(NB – do not use the nitrogen line – it doesn't work!).*
9. Add the Cu(II)Cl, TPMA and EBiB to the reaction vessel.
10. Seal the vial of the reaction vessel and the AScA stock with septa and parafilm and allow to cool in the ice.
11. Into each septum place a long (approximately 5 inch) and short (2 inch) green needle – with the long needle going into the liquid and the short needle (the vent) being as far from the liquid as possible.
12. Attach the argon line to the long green needles of the reaction vessel(s) and the AScA stock solution. Make sure the needles are bubbling before pulling them out of the liquid to degass the headspace. *(Care: make sure the vent needle is not too close to the liquid otherwise you will loose it!).*
13. Degass the headspace for 5 minutes before pushing the needles back into the liquid and continue to degas the liquid for a further 15 minutes whilst the vessels remain on ice.
14. When the time is complete, take a gas tight syringe and green needle (short) of the appropriate size for the volume of AScA you need to transfer and remove the plunger
15. Apply the needle/syringe into the AScA vial and degas the syringe/needle for about a minute before applying the plunger and aspirating the required volume of AScA stock (*CARE: make sure the degassing needle is pulled back out of the liquid when you put the plunger in otherwise you will push the AScA up the schlenk line).*
16. Quickly transfer the AScA into the degassed reaction vessel. Once the AScA is in, allow the reaction vessel to continue to degas for a further 2 minutes.
17. Once the degassing is complete, remove the vent needle, then the degassing needle, and apply a small blob of silicone grease to the top of the vial.
18. Transfer the vessel to the prewarmed heat block.

C: Terminating the reaction

1. Allow the reaction to run for 2 hours.
2. Once the time is complete, open the vessel and bubble compressed air through to stop the reaction.

D: Characterising the results

1. ^{1}H-NMR – take a small amount of the solution (~20 µL) and put into a clean NMR tube. Using deuterated methanol run an NMR to calculate the monomer to polymer conversion.
2. GPC – Add a small volume (approximately 60 µL) of the solution to the GPC running solution. Copper was removed from the samples prior to running on the SEC using heavy metal chelating beads (Cuprisorb^{TM}, Fish Fish Fish, UK – incubate with the sample for 30 minutes) and filtered through a 0.22 µm syringe mounted polytetrafluoroethylene filter.

GPC was performed on a GPCMax VE 2001 (Viscotek) and was run with an eluent of *N,N*-Dimethylformamide (DMF) with 0.075% (w/v) at a flow rate of 0.7 mL.min^{-1} over two Polymer Standards Service (PSS^{TM}) Gram DMF columns at 35^{o}C. The molecular weights were determined using a conventional pMMA calibration without correction (Agilent Technologies, UK).

5 NOTES

1. Larger volumes can be polymerised – if using > 5mL then add a stir bar and undertake the reaction in a silicone oil bath.
2. Consider the headspace of the reaction vessel carefully – this needs to be minimised.
3. Performing surface initiated ARGET ATRP – if using functionalised scaffolds for example (e.g. PCL-BiBB) then if the molar ratio of the initiator on the surface you are putting in solution is > 10% of the molar mass of the EBiB initiator in solution, then you need to reduce the EBiB as needed.

If polymerising from surfaces, the sacrificial initiator in solution (EBiB) has been shown to be an effective way of both improving control and allowing characterisation of the surface bound polymer. This is discussed more fully in [1]. This SOP was adapted from methods used in the literature [2, 3].

This has been optimised for the OEGMA monomer – there are a large number of variables, including the glassware you use.

6 LIMITATIONS

The reaction proceeds more slowly when certain functional groups are within the solution, possibly due to chelation of the copper catalyst. If carboxylic acids or amides are in solution – perform the reaction overnight as it will proceed more slowly. The reaction may not work if primary amines are present within the solution.

7 REFERENCES

1. **RH Harrison**, JAM Steele, R Chapman, AJ Gormley, LW Chow, MM Mahat, L Podhorska, RG Palgrave, DJ Payne, SP Hettiaratchy, IE Dunlop, MM Stevens. “Modular and Versatile Spatial Functionalization of Tissue Engineering Scaffolds through Fiber-Initiated Controlled Radical Polymerisation” Advanced Functional Materials (Volume 25, Issue 36 p5748-5757). 2015.

2. Oh JK, Min K, Matyjaszewski K. Preparation of poly(oligo(ethylene glycol) monomethyl ether methacrylate) by homogeneous aqueous AGET ATRP. Macromolecules. 2006 May 2;39(9):3161-7. PubMed PMID: WOS:000237390100012.

3. Telford AM, Meagher L, Glattauer V, Gengenbach TR, Easton CD, Neto C. Micropatterning of Polymer Brushes: Grafting from Dewetting Polymer Films for Biological Applications. Biomacromolecules. 2012 Sep;13(9):2989-96. PubMed PMID: WOS:000308508500042.

Appendix E – ToF-SIMS analysis of silicon surfaces

Time-of-flight Secondary Ion Mass Spectrometry (Tof-SIMS) was performed by Dr Sarah Fern (Research Scientist at Imperial College) on a single set of silicon samples. This was done to assess whether an even surface coating of bromine had been produced prior to surface grafting of polymer brushes from functionalized surfaces and to establish whether an even coverage of pOEGMA brushes had been produced.

An IONTOF TOF.SIMS5 instrument was used and utilises a 25 keV Bi+ analytical ion beam, O2+, Ar, and Cs+ sputter guns and a 10keV C60+ source operating under ultra-high vacuum. Samples were prepared as outlined in Chapter 2, 2.2.4.1 then polymerised as outlined in 2.2.4.2. Wafers were washed in ethanol and dried before analysis.

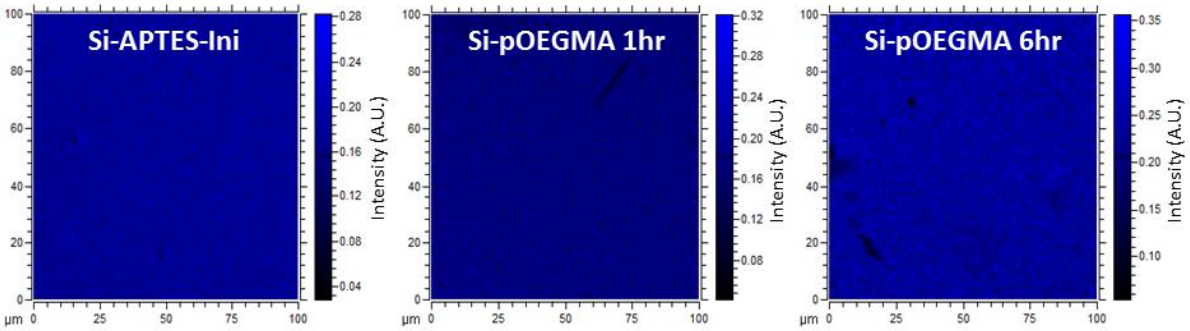

Figure 7-1: ToF-SIMS heat maps depicting the bromine coverage of silicon samples before and after polymerisation with OEGMA. Si-APTES-Ini (left) is a pre-polymerisation sample; a silicon wafer has been functionalized with APTES and the bromine containing initiating group has been reacted onto the surface. The Si-pOEGMA samples (middle and right) are post polymerisation samples.

Due to the anticipated surface chemistry of the samples it was expected that should the functionalization have been successful an even surface coating of bromine should be seen, and is demonstrated on the samples. The heat maps show that there is a relatively even coverage of bromine both before and after polymerisation, with some defects in the surface being present following grafting.

What this data is unable to demonstrate is whether the bromine signal seen following grafting is that from bromine groups at the superficial end of a polymer brush, or whether it is from an un-reacted initiating group remaining on the silicon surface. XPS analysis is however able to make this distinction though the analysis of different chemical bonds seen within the polymer brush; XPS surface analysis was therefore performed. XPS analysis of silicon wafers is outlined in Chapter 2.

Appendix F - Method and assessment of adsorbed polymer removal from scaffolds

Effective washing of the scaffolds following surface initiated polymerisation is essential to ensure that the polymer present is covalent bound to the fibre surfaces and not merely adsorbed. Any adsorbed polymer must be effectively removed to maintain ability to control the spatial location of the polymer within the scaffold.

The effectiveness of various washing steps were analysed and optimised. PCL-diol control and PCL-Ini scaffolds underwent a polymerisation with the biotin monomer within the same reaction vessel. Following which, the scaffolds were washed three times with either UHQ water, ethanol (100% or 50% v/v), or IPA (100% or 50% v/v), both with and without sonication for 30 seconds. Scaffolds were then dried and investigated with water contact angle measurements. Selected scaffolds were blocked and labelled with streptavidin-fluorescein as described in Chapter 3 (section 3.2.3.5).

Table 7-1: Contact angle and staining appearance of PCL-diol control and PCL-p(OEGMA-*co*-biotin) scaffolds following different washing regimes.

Scaffold replicate:	+/- ATRP	Wash	Contact angle			Staining appearance
			1	2	3	
17% PCL	-	-	128.5	129.5	134.7	-
17% PCL-Ini	-	-	109.5	108.4	122.5	-
17% PCL	+	H_2O	0	0	0	Green
17% PCL	+	IPA + S	121.6	140.7	118.6	-
17% PCL	+	IPA	59.0	119.0	127.8	-
17% PCL	+	50% (v/v) IPA	0	0	0	-
17% PCL	+	ETOH + S	125.5	117.4	120.0	Minimal
17% PCL	+	ETOH	128.7	113.0	130.2	-
17% PCL	+	50% (v/v) ETOH	112.3	119.5	122.0	-
17% PCL-p(OEGMA-*co*-biotin)	+	H_2O	0	0	0	Green
17% PCL-p(OEGMA-*co*-biotin)	+	IPA + S	0	0	0	-
17% PCL-p(OEGMA-*co*-biotin)	+	IPA	0	0	0	-
17% PCL-p(OEGMA-*co*-biotin)	+	50% (v/v) IPA	0	0	0	-
17% PCL-p(OEGMA-*co*-biotin)	+	ETOH + S	0	0	0	Green
17% PCL-p(OEGMA-*co*-biotin)	+	ETOH	0	0	0	-
17% PCL-p(OEGMA-*co*-biotin)	+	50% (v/v) ETOH	0	0	0	-

Notes: Ethanol (ETOH). Sonication for 30 seconds is indicated by "S".

The water contact angle measurements suggest that the bulk surface functionalization of the PCL-p(OEGMA-*co*-biotin) mats was not affected by the different washing regimes as they remained at 0^{o} throughout. The PCL control mats however present varied contact angle measurements depending on the washing steps used, suggesting that some methods do not effectively remove the adsorbed polymer as the surfaces remain hydrophilic. Electrospun PCL is hydrophobic in nature, and several of the washing steps returned the PCL control scaffold to the native hydrophobic state. Overall, ethanol appeared more effective at removing the adsorbed polymer than IPA. Fluorescence microscopy of scaffolds labelled with streptavidin-fluorescein revealed good staining of the PCL-p(OEGMA-*co*-biotin) scaffold and minimal staining of the PCL control scaffold that had both been washed three times in ethanol with ultrasonication (Figure 3-9). This technique was used as the washing step for all scaffolds presented in this thesis.

Appendix G – Characterisation of the biotin monomer

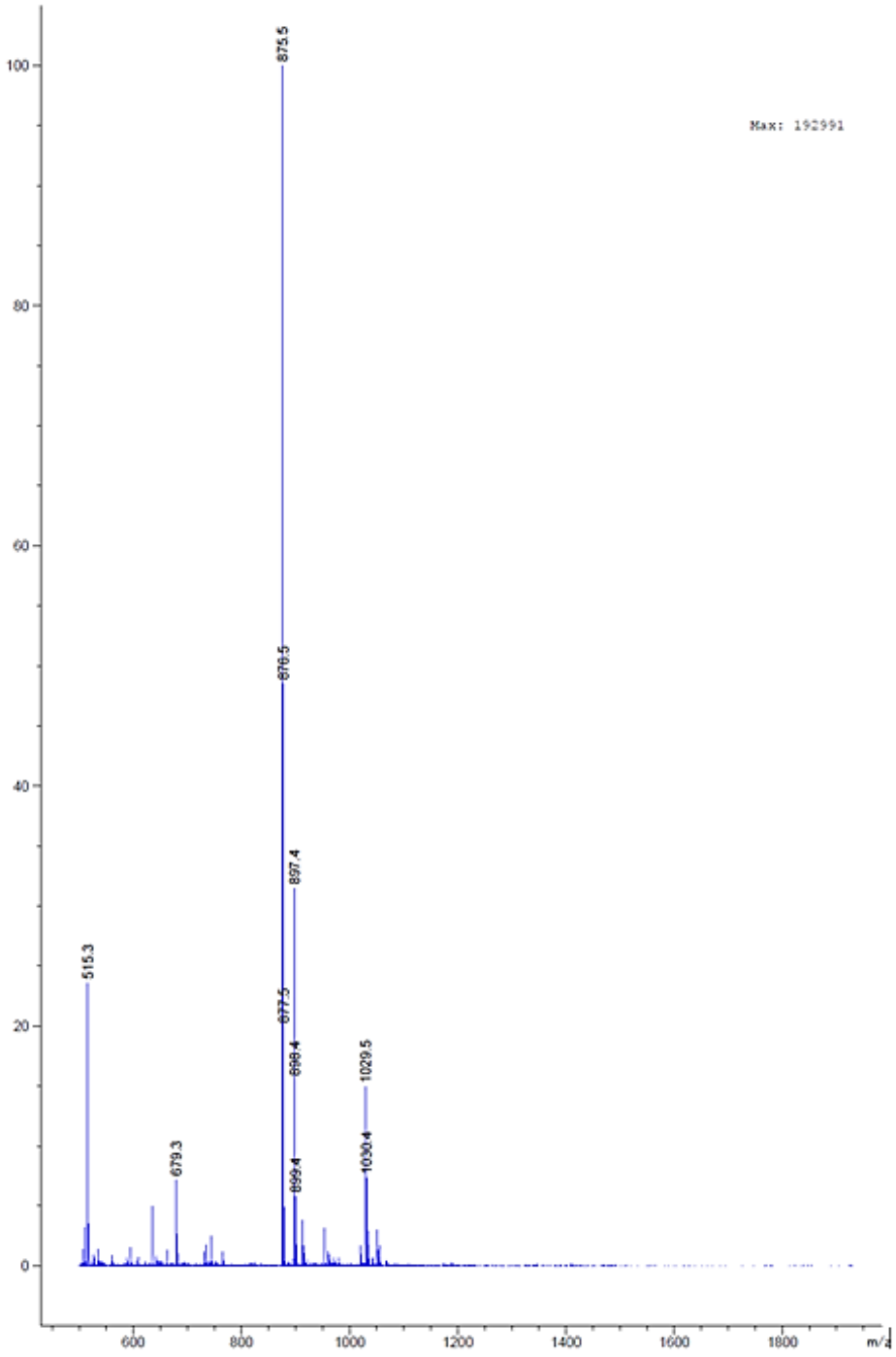

Figure 7-2: ESI-MS for the biotin-PEG monomer. Calculated 875.5 (M+H+), found 875.5.

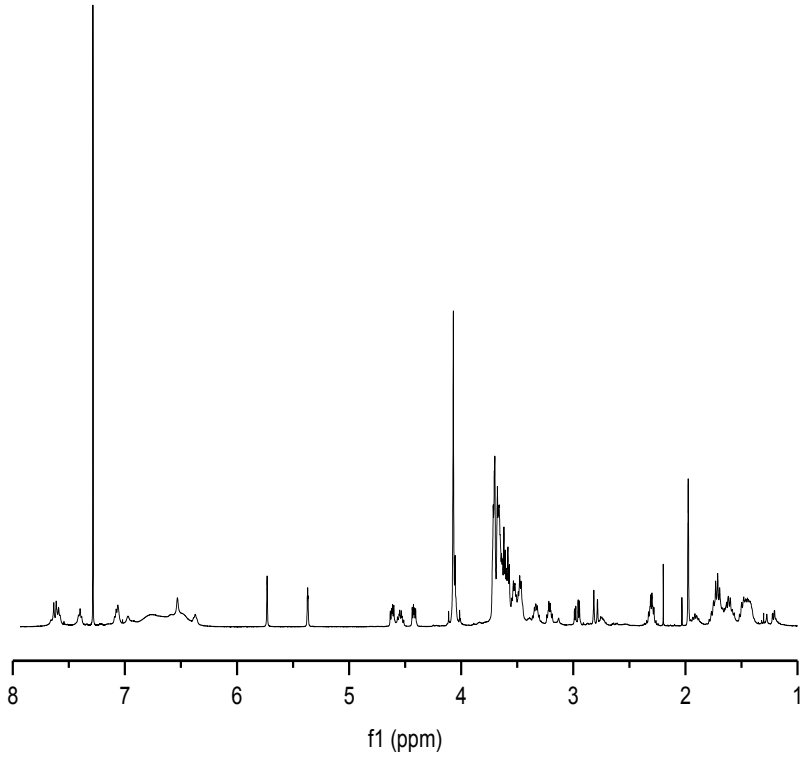

Figure 7-3: ^{1}H-NMR of biotin-PEG monomer.

Appendix H – Synthesis of amino-cy5 dye

The work in this appendix has been previously prepared for publication in "Modular and Versatile Spatial Functionalization of Tissue Engineering Scaffolds through Fiber-Initiated Controlled Radical Polymerization" by Harrison RH, Steele JAM, Chapman R, Gormley AJ, Chow LW, Mahat MM, *et al.* pblished in Advanced Functional Materials in September 2015[342].

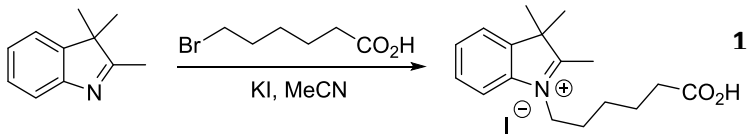

Figure 7-4: Synthesis scheme for compound 1.

In brief, the synthesis of compound 1 was adapted from Simmons *et al.*[343]. 2,3,3-Trimethylindolenine (2.5 g, 15.5 mmol), 6-bromohexanoic acid (3.9 g, 20.2 mmol) and potassium iodide (3.4 g, 20.2 mmol) were heated to 85˚C in acetonitrile (30 mL) for 30 hours. After cooling to room temperature, the mixture was filtered and concentrated using rotary evaporation. The residue was diluted with cold diethyl ether (300 mL) and left to precipitate at 4 ˚C overnight. The resultant solid was collected by filtration, washed with further diethyl ether (2 x 50 mL) and dried *in vacuo*. A yield of 4.8 g, 12.1 mmol (61 %) was obtained as a red solid. Spectroscopic data were consistent with those previously reported[292]. ^{1}H NMR (400 MHz, DMSO): δ = 7.96-8.00 (1H, m, H8), 7.85 (1H, dd, *J* = 5.9, 2.9 Hz, H5), 7.61-7.67 (2H, m, H6 and H7), 4.46 (2H, t, *J* = 7.7 Hz, -C$\underline{H}_2$Ar), 2.84 (3H, s, -C$\underline{H}_3$), 2.24 (2H, t, *J* = 7.2 Hz, -C$\underline{H}_2$CO$_2$H), 1.84 (2H, tt, J_1 = J_2 = 7.8 Hz, -C$\underline{H}_2$CH$_2$Ar), 1.49-1.63 (8H, m, -(C$\underline{H}_3$)$_2$ and –C$\underline{H}_2$CH$_2$CO$_2$H), 1.35-1.49 (2H, m, -C$\underline{H}_2$CH$_2$CH$_2$Ar) ppm.

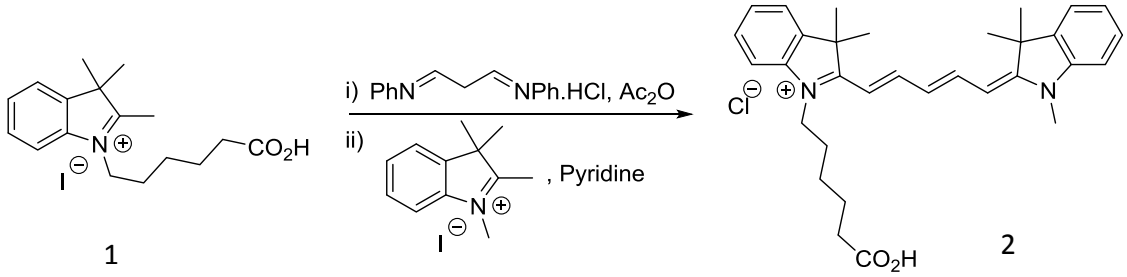

Figure 7-5: Synthesis of Cy5.HCL 2 from compound 2

Synthesis of Cy5.HCl **2** was adapted from Kvach *et al*.[344] Indole 1 (2.4 g, 6 mmol) and malonaldehyde bis(phenylimine) monohydrochloride (1.8 g, 7.2 mmol) were dissolved in acetic anhydride (15 mL) and heated to 120 ˚C for 30 minutes. After cooling to room and temperature 1,2,3,3-tetramethyl-3H-indolium iodide (2.5 g, 8.4 mmol) and pyridine (15 mL) were added and the reaction stirred for 18 hours during which time a colour change occurred and it turned dark blue. After concentration *in vacuo* at 80 ˚C, the residue was precipitated in hexane (100 mL), the solvent decanted and the procedure repeated twice. The resultant blue oil was dissolved in chloroform (100 mL), washed with H_2O (2 x 100 mL) and brine (100 mL), dried with $MgSO_4$, filtered and concentrated with rotary evaporation. The residue was purified by flash column chromatography, eluting with 10 % EtOH:$CHCl_3$. Pure fractions were concentrated *in vacuo* to give the DP as a purple foam. A yield of 2.5 g, 4.8 mmol (80 %) was obtained. Spectroscopic data were consistent with those previously reported[293]. ^{1}H NMR (400 MHz, DMSO): δ = 12.03 (1H, s, -COO<u>H</u>), 8.29-8.40 (2H, m, b-<u>H</u>), 7.52-7.67 (2H, m, <u>H</u>$5_{a/b}$), 7.36-7.53 (4H, m, <u>H</u>$7_{a/b}$ and <u>H</u>$8_{a/b}$), 7.20-7.34 (2H, m, <u>H</u>$6_{a/b}$), 6.51-6.63 (1H, m, c-<u>H</u>), 6.22-6.36 (2H, m, a-<u>H</u>), 4.09 (2H, t, *J* = 8.3 Hz, -C<u>H</u>$_2$Ar), 3.61 (3H, s, Ar<u>Me</u>), 2.29 (2H, m, -C<u>H</u>$_2$CO$_2$H), 1.64-1.74 (14 H, m, -C<u>H</u>$_2$CH$_2$Ar and Ar(C<u>H</u>$_3$)$_2$), 1.50-1.60 (2H, m, -C<u>H</u>$_2$CH$_2$CO$_2$H), 1.39 (2H, dt, *J* = 15.3, 6.4 Hz, -C<u>H</u>$_2$CH$_2$CH$_2$Ar) ppm.

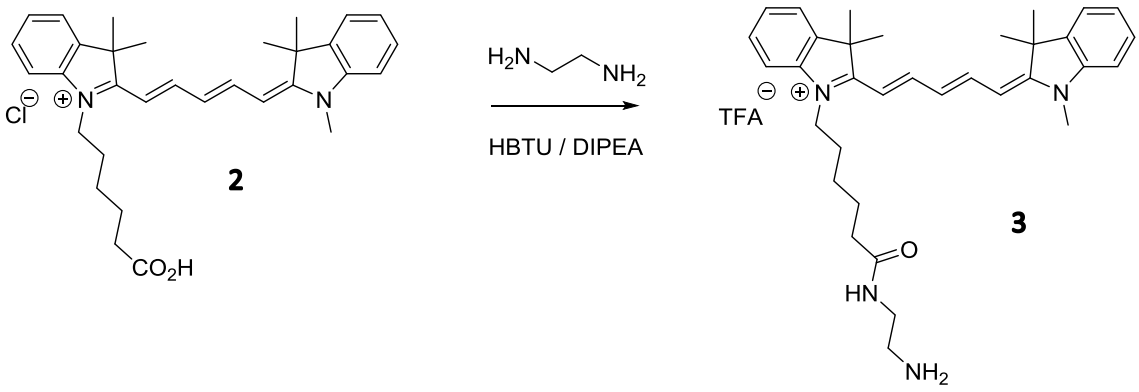

Figure 7-6: Synthesis of amino Cy5 3 from Cy5.HCL 2

Cy5.HCl **2** (65 mg, 0.12 mmol) and ethylene diamine (83 µl, 1.2 mmol) were then dissolved in dichloromethane (DCM, 8 ml) and 213rimethylamine (TEA, 125 mg, 1.2 mmol) and HBTU (93 mg, 0.24 mmol) were added in DCM (2 ml). The reaction was stirred overnight at room temperature, concentrated, and precipitated twice from ice cold diethyl ether. The precipitate was purified by HPLC over a C18 column (H_2O / acetonitrile gradient) and freeze dried to yield the product as a dark blue solid. ESI-MS for $C_{34}H_{45}N_4O^+$ Calcd. 525.4 M^+, Found 525.4 (Figure 7-7). ^{1}H-NMR (400 MHz, $CDCl_3$) δ ppm: 7.94 – 7.73 (td, *J* = 13.1, 4.8 Hz, 2H, b-H), 7.44 – 7.29 (m, 4H, H5$_{a/b}$ and H7$_{a/b}$), 7.29 – 7.17 (m, 2H, H8$_{a/b}$), 7.15 – 7.02 (d, *J* = 7.9 Hz, 2H, H6$_{a/b}$), 6.60 (t, *J* = 12.4 Hz, 1H, c-H), 6.36 – 6.02 (dd, *J* = 20.1, 13.4 Hz, 2H, a-H), 3.99 (t, *J* = 7.5 Hz, 2H, CH_2Ar), 3.57 (s, 3H, ArMe), 3.14 (s, 2H, -$CH_2CH_2NH_2$), 2.36 (m, 2H, -CH_2CO), 1.93 – 1.75 (m, 2H, -CH_2CH_2Ar), 1.51 – 1.36 (m, 2H, -$CH_2CH_2NH_2$), 1.68 (s, 12H, Ar(CH_3)$_2$), 1.59 – 1.53 (m, 2H, -CH_2CH_2CO-), 1.36 – 1.11 (s, 2H, $CH_2CH_2CH_2$Ar). Spectra displayed in Figure 7-8.

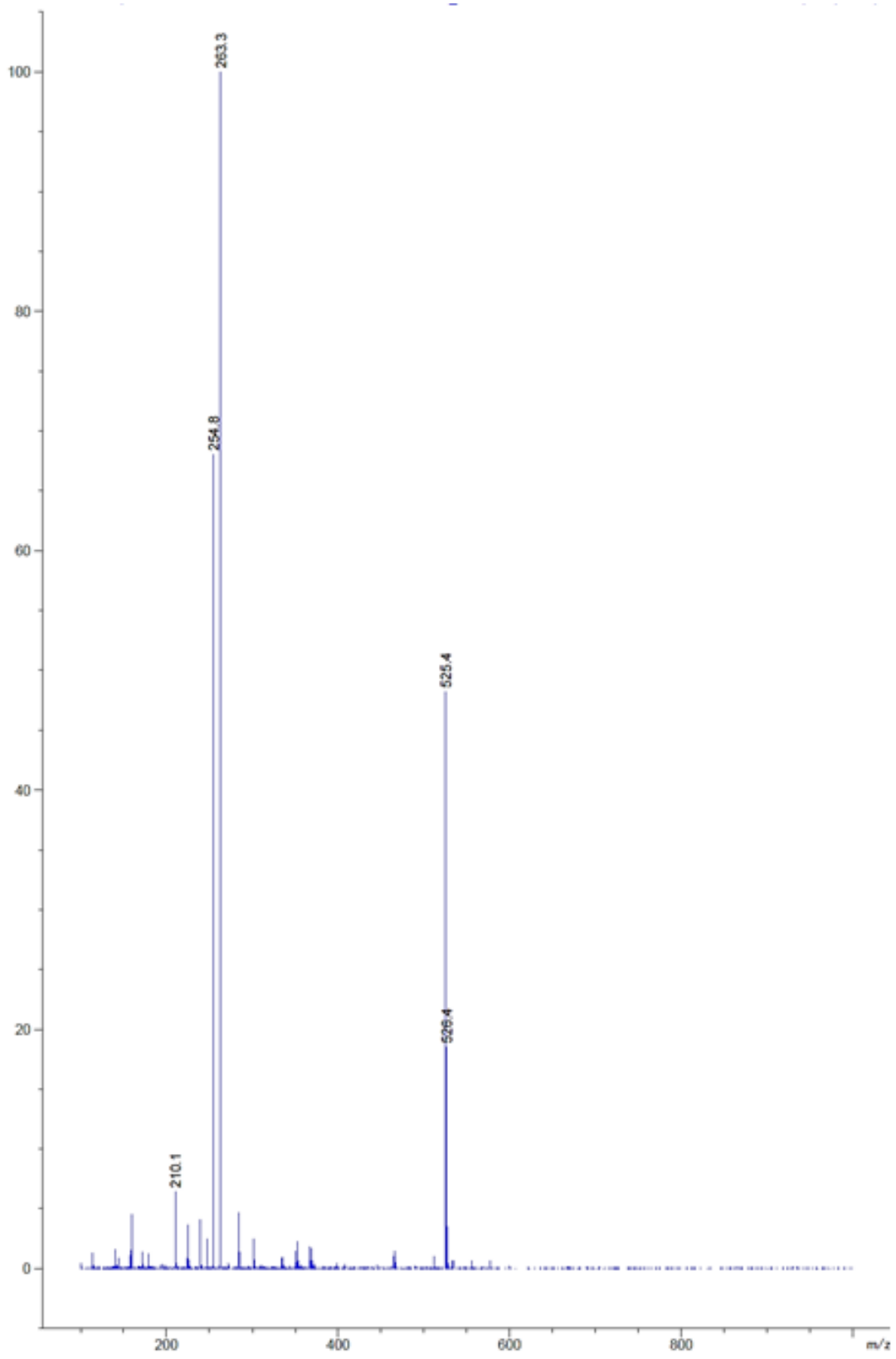

Figure 7-7 : ESI-MS for the amino Cy5 dye. Calculated 525.4 M+, Found 525.4.

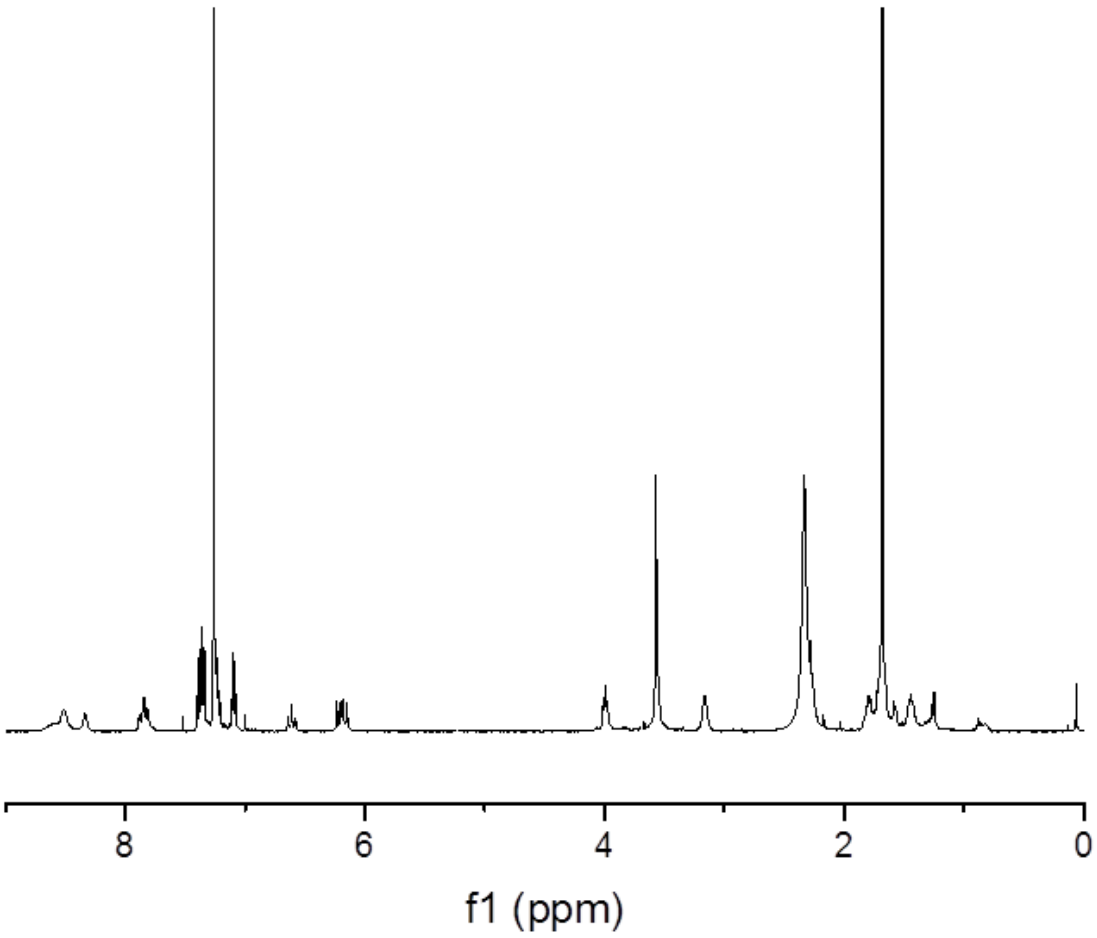

Figure 7-8: ^{1}H NMR characterisation of amino-Cy5. Please see above for peak assignments

Appendix I: Mechanical testing of scaffolds

I.1 Polymer brushes to protect surfaces subject to loading

Tissue engineered scaffolds are increasingly being proposed in the literature for the treatment, reconstruction or regeneration of various musculoskeletal tissues following injury, articular cartilage being such a target for the field. Electrospun scaffolds often form the bulk or part of these scaffolds due to their advantageous structure and versatility[345,346]. Such scaffolds, if to be placed into the demanding environment of a load bearing joint, need to be mechanically robust in order to withstand the loads upon them and maintain their integrity for the desired length of time *in vivo* to complete their function.

When a hydrophilic polymer brush functionalised surface becomes hydrated it may lead to a change in the load bearing properties of the material. Whilst investigating the frictional properties of polymer brush systems, several groups have reported an improved wear of materials that were functionalised with polymer brushes[347,348]. It is suggested that this is due to the water-swollen brush layer, when compressed by a normal force, giving a high resultant repulsive force. Authors suggest this would result from the osmotic pressure of the hydrated brushes combined with the steric repulsion increasing between brushes when compressed. It may be that such a hydrated polymer brush system could be used to protect the integrity of an electrospun scaffold during high loading. This is investigated in this Appendix.

I.2 Uniaxial, unconfined compression testing of scaffolds

Electrospun scaffolds of 17% (w/w) PCL-Ini and 17% (w/w) PCL-diol (control), and 9% (w/w) PCL-Ini and 9% (w/w) PCL-diol (control) firstly underwent polymerisation within the same reaction vessel for functionalization with pOEGMA brushes. Following which, scaffolds were thoroughly washed using ultrasonication in ethanol for 30 seconds three times, and rinsed three times with UHQ water, air dried and stored in a vacuum dessicator until needed. Before being used for vertical loading, scaffolds were dipped in ethanol before being rinsed in PBS three times to ensure uniform wetting. Samples were kept hydrated (immersed in PBS) using a custom built apparatus (Figure 7-9) and maintained in PBS throughout the experimentation. A silicone ring was made using the two part silicone elastomer and placed on the rubber mat backing to allow hydration of the sample.

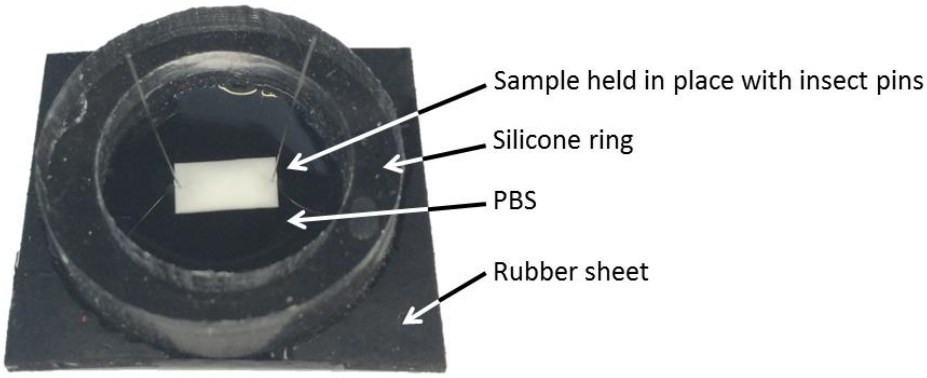

Figure 7-9: Custom built hydration chamber for the uniaxial compression testing of the scaffolds.

Mechanical loading was undertaken using a Bose ElectroForce 3200 Series III (TA Instruments, UK) equipped with a 50 lbf (220 N) load cell. The samples were placed on a 1.5 mm thick reinforced rubber sheet (RS Components, Corby, UK) and unconfined uniaxial compression testing was undertaken with the samples fully hydrated in PBS.

A period of optimisation was undertaken to establish the best protocol to load the samples. Final compression tests were carried out using a ramp to a pre-defined force (0.1, 1, 10, 20, 25, 30, 40, or 50 N) at a rate of 0.2 mm/s before undertaking a sinusoidal loading waveform to the desired normal force and unloading at a frequency of 10 Hz for 1000 cycles. A 6.5 mm diameter, hemispherical indentor probe was used to compress the samples.

Following testing, samples were washed with UHQ water after testing, dried and imaged using the Phenom FEI SEM with a 10 nm chromium sputter. A single set of samples was used for testing, N = 1.

I.3 Uniaxial, unconfined compression testing of scaffolds

Some preliminary work in mechanical testing, not included in this thesis, suggested that there may be a difference in the fibre morphology between scaffolds with and without pOEGMA functionalization following vertical loading. Using the Bose mechanical testing apparatus, a range of parameters were explored to load the scaffolds in a hydrated, uniaxial and unconfined condition. All the scaffolds were imaged using SEM following the loading to assess the damage done to the electrospun fibres. Initially, a flat headed indenter probe was used to load the samples. This was exchanged for a 6.5 mm diameter hemispherical probe as edge effects were seen with the flat probe. This gave the disadvantage that the

estimation for the stress (force per unit area) being experienced by the scaffolds would be more challenging to establish.

A range of forces, from 0.1 to 40 N was used which extends beyond forces used in similar work previously. McCullen *et al.* loaded samples with a flat indenter probe to 10 N (1.4 MPa)[345,346]. This was calculated to result in a range of stress from 0.83 MPa (1 N) to 2.85 MPa (40 N) for this indenter. This was calculated by measuring the Young's modulus of the rubber used the back the samples using the Hertz model to calculate the surface area of the sphere in contact with the sample (Appendix J)[349]. This range of stress falls just below the expected maximal stress of 3 MPa experienced in the human knee of a 70 kg person walking or running[350,351].

A systematic assessment exploring different testing parameters was undertaken in a scaffold system hydrated with PBS at RT. Once the parameters were established a full set 17% (w/w) PCL-pOEGMA scaffolds and their matched controls were tested and imaged using SEM (Figure 5-13). No difference is seen between 17% (w/w) PCL-pOEGMA scaffolds and matched controls with regard to changes in fibre morphology during uniaxial, unconfined compression testing at normal forces between 0.83 MPa (1 N) to 2.85 MPa (40 N) using these parameters. The samples tested at 0.1 N are not shown as the areas that underwent testing could not be reliably identified.

The stresses being applied to the samples at the point of contact between the spherical probe and the polymer interface may have led to the water molecules being pushed out from the polymer brush layer. This would remove any protective effect that may be experienced through a hydrated polymer brush and no difference being seen between PCL control scaffolds and PCL-pOEGMA scaffolds. The polymer brush layer resulting from the DP used in this work has been measured from 2D silicon wafers to be approximately 6 nm (Chapter 2). A longer and potentially cross-linked polymer brush may result in improved water trapping and result in advantageous mechanical properties of the scaffolds. Is it interesting to note however, that the fibres are relatively well preserved up to 2.43 MPa (25 N) with little loss of fibre integrity.

Few electrospun scaffolds with surface grafted polymer brushes are found in the literature and to the best of my knowledge this is the first time such a system has been systematically

uniaxially loaded to assess for any protective effect on the fibre morphology from a hydrated polymer brush layer. Theoretically it may be expected that a hydrated layer bound to the surface of the polymer fibres may provide some protection from uniaxial loading up to a critical point, at which the protective water layer would be lost. It may be that we have not been able to draw out this difference between the pOEGMA functionalised scaffolds and the controls with the experimental design used and that investigation on the nanoscale would be required. In future work, beyond the scope of this thesis, we hope to investigate cross-linking as a potential method for maintaining the water layer, which may reveal some interesting mechanical properties.

In the literature there is some interest in the production and mechanical testing of electrospun fibre reinforced hydrogels for tissue engineering which have shown that the combination of the electrospun fibres and hydrogel give advantageous mechanical properties to the scaffold[352,353]. Through modification of the polymerisation, this scaffold system could be modified to make a scaffold functionalised with a covalently bound hydrogel which may be of interest in the field of tissue engineering.

I.4 Conclusions

The mechanical stability of the electrospun scaffolds was also investigated using unconfined uniaxial compression testing. The integrity of the fibres is relatively well preserved in both the control and pOEGMA functionalised forms up to approximately 2.43 MPa. This falls marginally below the pressure experienced on the tibial plateaux of a 70 kg adult during walking or running[350,351]. This suggests that in its current form, the scaffold would not be robust enough to withstand the stresses experienced within a weight bearing, fully loaded joint. It is encouraging however that it may be robust enough to withstand stresses below this level, such as may be experienced in the hand, the test-case design focus of this work.

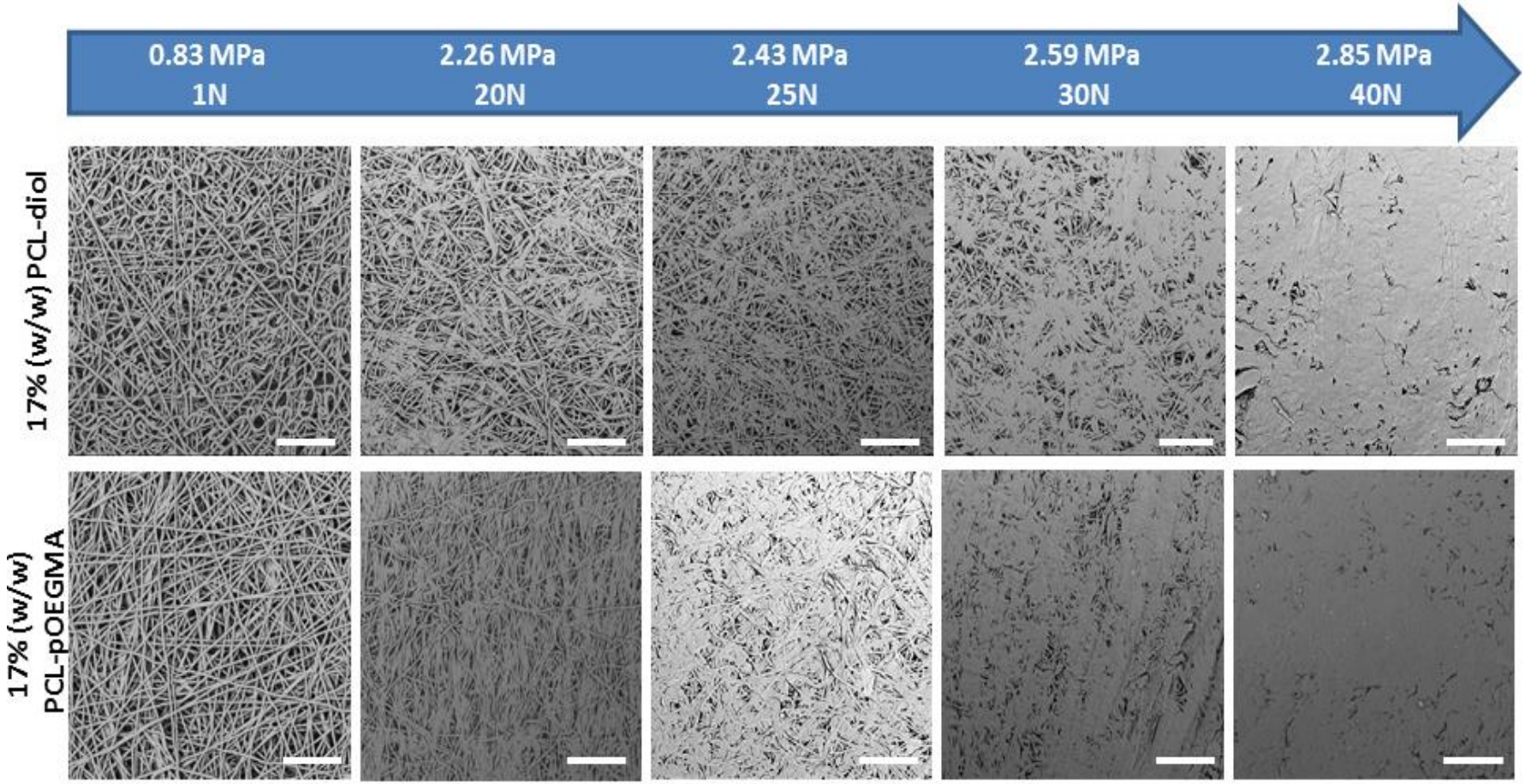

Figure 7-10: Uniaxial, unconfined load testing of matched electrospun 17% (w/w) PCL-diol scaffolds (A, upper) and 17% (w/w) PCL-pOEGMA scaffolds (B, lower) with a range of normal forces from 1 N to 40 N using a hemispherical indentor at a rate of 10 Hz for 1000 cycles. Representative SEM images showing the resultant change in fibre morphology at the central point of loading is shown. Scale bars 50 µm.

Appendix J: Calculating the contact pressure on scaffolds exerted by mechanical testing

The pressure exerted between the hemispherical indenter probe and the scaffold was calculated by Dr Joe Steele using the Hertz Model and has been included here for completeness. The Hertz Model (Formula 1A[349]) was rearranged (Formula 1B) to calculate the depth of indentation, *d*, for a known force between a sphere and a planar surface, taking into account elastic deformation and thus a changing contact area (Figure 7-11).

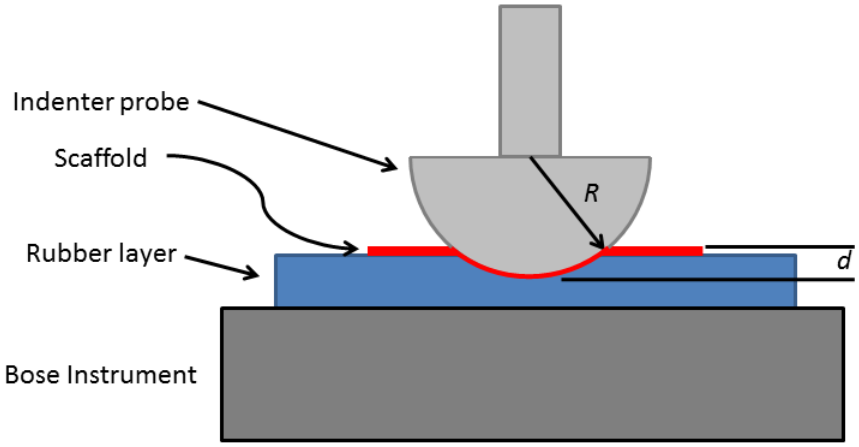

Figure 7-11: Schematic representation of the indenter probe striking the sample in the unconfined uniaxial compression testing.

Formula 1A

$$F = \frac{4}{3}\left(\frac{E}{[1-v^2]}\right)\sqrt{Rd^3}$$

Formula 1B

$$d = \sqrt[3]{\frac{\left[\frac{3}{4}F\left(\frac{[1-v^2]}{E}\right)\right]^2}{R}}$$

Notes: where *F* is the applied force, *d* is the depth of indentation of the sphere into the material, *E*, elastic modulus, *v*, Poisson's ratio of the material, and *R* is the radius of the indenter. This model assumes that the indenter is very stiff compared to the sample.

The modulus, *E*, of the rubber was calculated experimentally using the BOSE Electroforce 3200 (Bose, USA) mechanical testing machine by Dr Joe Steele. He performed three uniaxial compression tests using a 6.5 mm cylindrical probe at a speed of 0.2 mm/s over a range of 5-25% strain. The modulus was the mean of the three experimental findings. It is assumed that the scaffold modulus has a negligible impact on the displacement of the probe. The Poisson's ratio for rubber, 0.48, was taken from published tables (http://www.engineeringtoolbox.com/poissons-ratio-d_1224.html).

Using this data, the surface area of contact between the hemispherical indenter probe and the scaffold were calculated (Formula 2, http://mathworld.wolfram.com/SphericalCap.html). With a known force and surface area of contact as determined by the Hertz model, the pressure exerted on the scaffold was then calculated (Formula 3).

Formula 2

$$SA_{cap} = 2\pi Rd$$

Notes: where SA_{cap} refers to the surface area of the hemispherical indenter probe in contact with the scaffold/rubber. *R* is the radius of the probe and *d* is the depth to which the probe has indented the scaffold/rubber.

Formula 3

$$P = \frac{F}{SA_{cap}}$$

Notes: *P* is pressure, *F* is the normal force, and SA_{cap} is the surface area in contact.

Appendix K : Drug Releasing Scaffolds

K.1 Tissue Engineering and Drug Release

Smart scaffolds within the tissue engineering and regenerative medicine field may include a drug releasing moiety as part of their design and function[354-357]. Within the field, electrospinning in particular has received particular interest for scaffold processing for drug release[358,359]. In this Appendix the scaffold presented within this thesis (Chapter 1 to 6) is adapted for drug release of ibuprofen, a non-steroidal anti-inflammatory drug (NSAID). Ibuprofen was selected in line with tendon injury being used as a model system for the versatile scaffold design as NSAID drugs, and ibuprofen in particular, appears to reduce adhesion formation following tendon injury and repair.

K.1.1 Non-steroidal anti-inflammatory drugs

NSAIDs are a class of drugs that produce antipyretic, analgesic and anti-inflammatory effects. Their use spans millennia; the Ebers papyrus suggests the use of a decoction of dried leaves of myrtle for the alleviation of rheumatic pain from the womb in ancient Egypt some 3500 years ago[360]. Hippocrates, approximately 1000 years later, recommends the juice of the poplar tree for the treatment of eye complaints and the use of the willow bark to ease the pain of child birth and reduce fever[360]. The first closer examination, and perhaps clinical trial, was performed in 1763[361]. The Reverend Edward Stone of Chipping Norton in Oxfordshire was a believer in the "doctrine of signatures" whereby the cure for a disease would be found in the same location that the malady occurred[360]. Since the "willow delights in a moist and wet soil, where agues chiefly abound" he collected willow bark which he then dried in a bakers oven and ground to a powder. A range of dosages were tried and he showed most success with 1 dram (1.8 g) of powder. The safety and success of which was reported in 50 patients and was published in a paper at the Royal Society[361]. All of these early remedies contained salicylates.

Salicylic acid was chemically synthesised in 1860 in Germany and by 1899 acetylsalicylate, more commonly known as aspirin, had been produced by Bayer[360]. During the early 1900s the mechanism of actions of these drugs were explored and further therapeutics found that had similar actions, such as paracetamol, and more latterly the fenamates a group of drugs that include ibuprofen and indomethacin. As a result of their similar actions

such drugs were grouped together as “non-steroidal anti-inflammatory drugs” (NSAIDs).

The NSAID group of drugs are a chemically diverse group but share the same therapeutic actions and adverse effects. This led scientists to conclude that they shared a mechanism of action through a single biochemical intervention. This was however illusive and for many years this was not uncovered. In the late 1960s and early 1970s however it was established that aspirin, and other related NSAIDs, interacted with the prostaglandin pathways[362]. This work was led by John Vane at the University of London and ultimately led to the award of the Nobel Prize in Physiology or Medicine in 1982.

Calor, dolor, rubor and tumor: heat, pain, redness and swelling are the four classical signs of inflammation as described by Celsus, the Roman encyclopaedist in the 1st century AD. These signs are all improved through the action of NSAIDs as they are brought about in part through the action of prostaglandins[340]. Prostaglandins are autocrine and paracrine lipid mediators that act to maintain local homeostasis. Following injury and during inflammation they are upregulated significantly before the recruitment of immune cells[340].

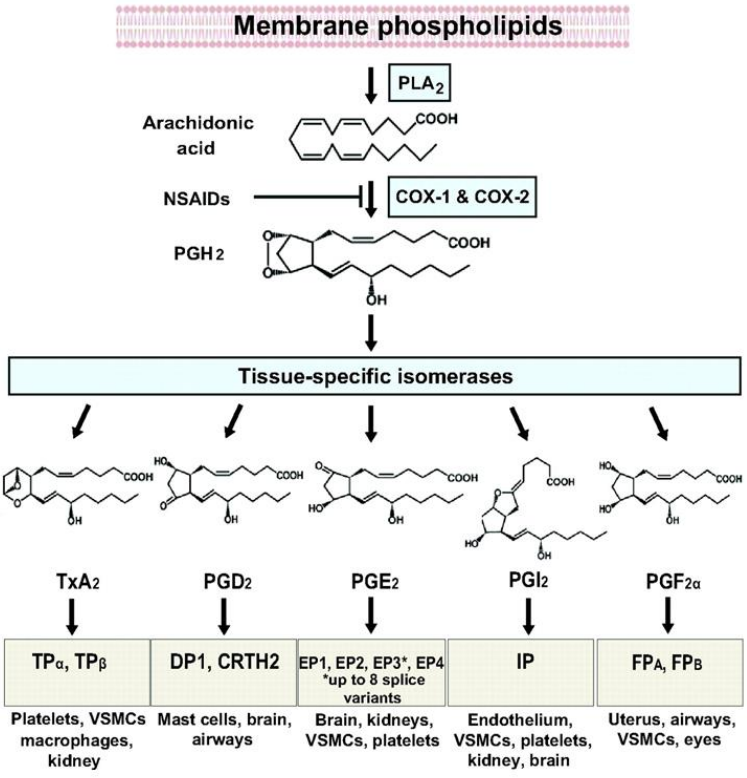

Figure 7-12: The biosynthetic pathway of prostanoids. Reproduced with permission from Ricciotti, E, and Fitzgerald G. Prostaglandins and Inflammation. Arterioscler Thromb Vasc Biol. 2011 May; 31 (5) Figure 1, p986.

Prostaglandins are formed when arachidonic acid, an unsaturated fatty acid, is released from the plasma membrane through the action of phospholipases (Figure 7-12). This is metabolised by the intracellular, membrane bound enzyme cyclooxygenases (COX) of which there are two known isoforms, COX-1 and COX-2[360,363]. COX-1 is expressed by most cells, is constutive, thought to be cytoprotective and serves for several homeostatic functions including epithelial gastric mucosal protection. COX-2 is induced by inflammatory signals, hormones and growth factors. COX-2 is the most important source of prostaglandin formation in inflammation and malignant proliferative diseases[364].

NSAIDs influence prostaglandin synthesis through the competitive inhibition of the active site of the COX enzymes[365]. Table 7-2 lists some of the more commonly used NSAIDs and their mechanism of action.

Table 7-2: Common NSAIDs and their mechanism of action

Action	Drug	Result	Ref
Non-selective COX inhibitor (COX-1 constitutional, and COX-2)	Aspirin (irreversible) Ibuprofen Indomethacin Diclofenac Naproxen	Inhibition of cytoprotective prostaglandins (loss of gastric mucosal protection, worse platelet aggregation). Also inhibition of inflammatory prostaglandins (see below).	366 367
Selective COX-2 inhibitor (Inducible)	Celecoxib Rofecoxib Meloxicam	Inhibition of inflammatory prostaglandins (reduced recruitment of inflammatory cells, sensitization of pain receptors, improved hypothalmatic temperature control).	368

K.1.2 NSAIDs and their use in adhesion formation

In addition to their use in the treatment of inflammation, NSAIDs have shown benefit in adhesion reduction in abdominal and pericardial adhesions in animal models[369,370]. The potential for NSAIDs to be a useful adjunct in the modulation of tendon adhesion following injury and repair was recognised many years ago. In the classic works by Kulick *et al.* published in 1984 and 1986, the outcome from using injectable[371] and oral ibuprofen[372] in primates was evaluated. The initial paper was successful in reducing tendon adhesion in a primate model when ibuprofen was injected at the site of repair. The follow up work, however, using oral ibuprofen suggested that adhesions were indeed

still reduced in the repaired tendon but the ultimate tensile strength was also adversely affected.

It is generally accepted clinically, and in the literature, that NSAIDs probably have a negative impact on bone healing[373-375]. In the literature, particularly in reference to review articles, there is much scepticism about the benefits of NSAID use in tendon healing as the impression is that whilst adhesion may be reduced, so too is mechanical strength. This may be true for some NSAIDs but does not appear to hold true for ibuprofen, as discussed below.

K.1.2 Ibuprofen and its use following tendon injury

Ibuprofen has recently been used by several groups as a part of a multifaceted approach for prevention of tendon adhesion in tendon injury. One study used a tissue engineering approach of a long-term drug delivery system. Modified mesoporous silica nanoparticles were loaded with ibuprofen then electrospun into a polymer scaffold of poly(L-lactic acid) (PLLA)[376] . An *in vitro* drug release profile demonstrated release of approximately 6% in the first six hours followed by a more sustained release occurring with 91% having been released at 100 days. Controls of a PLLA electrospun scaffold, and a co-spun PLLA-ibuprofen scaffold, and no scaffold were used. At four weeks histology showed dense adhesions in the control group and the PLLA scaffold group. Both scaffolds containing ibuprofen demonstrated low levels of adhesion. This was maintained at eight weeks with the exception of the PLLA-ibuprofen scaffold (short term release) which demonstrated some inflammation and adhesion formation. The group postulated this was due to the inflammatory reaction of the PLLA scaffold starting to dissolve and that the ibuprofen release had ceased. The PLLA nanoparticle loaded ibuprofen scaffold demonstrated superior results throughout. Biomechanical analysis revealed little different in ultimate tensile strength of tendons.

Liu *et al.* again used an electrospun fibrous membrane in a drug delivery system[377]. In this study, ibuprofen was loaded into a poly(L-lacticacid)-polyethelene glycol (PELA) biblock co-polymer by co-dissolving the drug and polymer before performing the electrospinning process. *In vitro* drug release studies demonstrated a burst release over the first two days followed by a sustained release over the following days. The drug release is dependent on the polymer degradation. Animal testing in a leghorn chicken

model revealed superior anti-adhesion properties of the PELA-ibuprofen scaffold when compared to controls (both PELA membrane alone, and no scaffold) at 21 days. Biomechanical analysis showed work of flexion was significantly different between both PELA membranes and the surgical control, and between the PELA membrane and PELA-ibuprofen membrane which had the lowest levels of adhesion. No significant different was seen between the maximal tensile strength of the tendons repaired with PELA membranes or surgical controls. These approaches use the combination of a physical barrier (the electrospun fibres) combined with the anti-inflammatory action of the ibuprofen to obtain these results. Liu *et al*.'s approach furthermore has an anti-adhesive tendency due to the polymer choice. In both studies the operated limbs were splinted. The group went on to also use celecoxib loaded membranes with some success[378] and more recently are developing a membrane to release naproxen[379].

An interesting *in vitro* study into the mechanism behind the effect of ibuprofen on tendon healing and adhesion formation was performed[380]. They demonstrated dose-dependant inhibition of migration and spreading of tendon cells both *ex vivo* from tendon explants and *in vitro*. Suppression of mRNA expression and paxillin levels was observed. Paxillin is a cytoskeletal protein found in focal adhesions that occur at sites where cells adhere to ECM. It was suggested that this down-regulation of paxillin is responsible for the anti-adhesion effect of ibuprofen through reduction of fibroblast adhesion related to extrinsic healing. Further work looked at matrix metalloproteinase (MMP) and collagen production using an *in vitro* model of rat tenocytes[381]. MMPs -1, -8 and -13 are collagenases and are able to cleave collagen I in the ECM. MMP-9 is a gelatinase that breaks down collagen IV. Up-regulation of MMP-1,-8, -9 and -13 were seen in response to ibuprofen but there was no effect on the expression of collagen I or III. They proposed this as evidence for impairment of healing in tendons after ibuprofen treatment.

Debate exists in the literature and amongst clinicians as to whether ibuprofen should be given to patients with tendon injuries. The current literature would tend to support its use. To date however, no clinical trial has been done to establish this definitively.

K.1.3 Polymer-drug conjugates

Drug delivery is a vast field of active research, and within that, drug-pendant polymers are also being investigated and are discussed fully in these recent reviews[382-386]. The potential

for drug-releasing polymers has been recognised for many years. It was proposed in 1970s by Ringsdorf and was initially targeting anti-cancer therapeutics[382]. In 1980, review articles by Heller proposed the three mechanisms by which bioerodible polymers could be used for drug release[386,387], see Table 7-3.

Table 7-3: Mechanisms for drug release from bioerodible polymers

Mechanism	Action
1	Solubilisation by cross-link cleavage
2	Solubilisation by hydrolysis, ionization or protonation of pendant groups
3	Solubilisation by back bone cleavage

Many drugs have been conjugated to polymeric carriers for a variety of reasons, including stabilisation in the vasculature, improving solubility or half-life, or to enhance uptake[384]. Whilst this is an active area of research, this has mostly been focused on either incorporating the drug within a polymer or polymer nanoparticle[377,388] or conjugating it to a pre-existing polymer backbone. Using a drug releasing monomer however gives greater versatility for fine tuning drug release and allow for increased efficiency of drug loading[389]. Drug release from polymers was considered back in the 1970s and is discussed fully in these recent reviews[390-392].

K.1.3.1 Drug releasing monomers

The formation of drug releasing monomers whereby the drug is held in place with a labile linker is an attractive, and tailorable, approach to drug release[384,393]. Using this approach the release rates, high level drug loading, and bulk polymer characteristics can be tailored.

The drug release profile through side chain hydrolysis of drug pendant polymers depends on the strength and chemical nature of the bond between the drug and polymer, the polymer structure and the local conditions (in particular local pH). Furthermore, the structure of the monomer unit, including both the length and hydrophobicity, and the distance of the cleaving bond from the polymer backbone all influence the rate of hydrolysis of the drug from the polymer[394-397].

A few groups have investigated the use of ibuprofen releasing monomers in the literature through a hydrolysable ester linkage. Stebbins *et al.* synthesised an ibuprofen-L-malic acid

monomer which was copolymerised with a linear aliphatic diols (1,3-propanediol, 1,5-pentanediol, or 1,8- octanediol) using an enzyme[393]. Drug release from the copolymers was investigated in PBS at 37^{o}C by HPLC. Babazadeh *et al.* synthesised a monomer based on 2-hydroxypropyl methacrylate (HPMA) before copolymerising in solution with either HEMA or methyl methacrylate (MMA)[398]. Drug release was investigated in PBS at 37^{o}C with a range of pHs.

Ibuprofen release from a polymer brush has not been presented in the literature to the best of my knowledge, drug release has been studied however from linear, branched and multi-arm polymer architectures. It may be advantageous as it may be possible to produce high drug loading through the use of high concentrations of drug-releasing monomers, a something that has been challenging in the drug release field[393,399].

K.1.3 Synthesising an ibuprofen-releasing monomer

The ability to incorporate a drug releasing moiety into the modular and versatile scaffold design presented in this thesis would be a useful additional tool for scaffold functionalization. As discussed in Chapter 1, the use of the ARGET ATRP controlled radical polymerisation system allows for the incorporation of a wide variety of monomer units into the resulting polymer brush.

In this Chapter the potential of a hydrolysable ibuprofen releasing monomer unit it investigated with the intention of incorporating it into the 3D scaffold system (Figure 7-13).

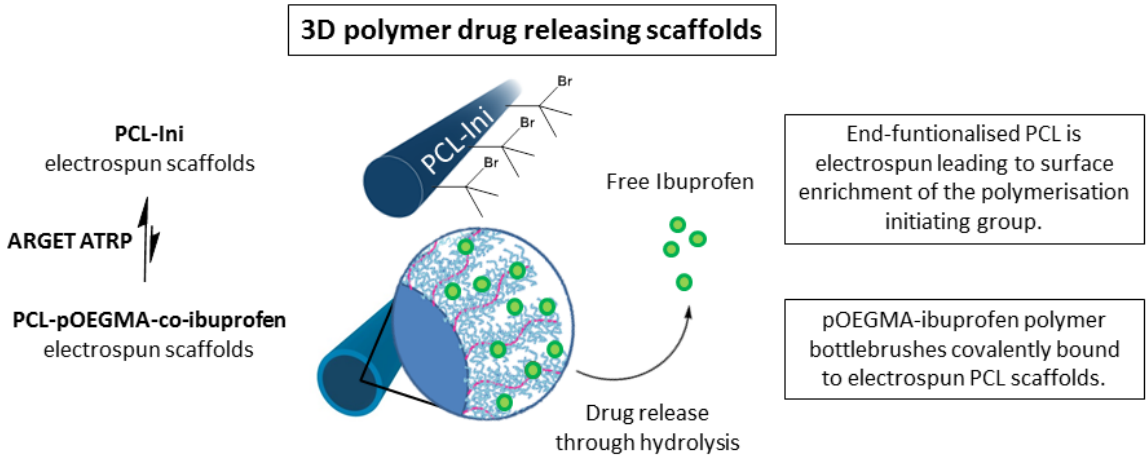

Figure 7-13: A schematic representation of the intended drug releasing monomer within the surface initiated polymer bottlebrush system.

K.2 Materials and Methods

In addition to materials used in previous chapters, further materials and instrumentation are discussed below.

K.2.1 Materials

HPMA and *N*-(2-Hydroxypropyl) methacrylamide (HPMAm) was purchased from Polysciences (Germany) and used as received. All other reagents were supplied from Sigma-Aldrich and were used as received unless specified. Deuterated solvents were used for ^{1}H-NMR and purchased from Merck, Darmstadt, Germany.

K.2.2 Synthesis of ibuprofen releasing monomers via a hydrolysable ester

Monomer units with cleavable ibuprofen were designed and synthesised for polymerisation into the pOEGMA brush. The aim of this was to produce an antifouling surface coating that was capable of ibuprofen drug release to further enhance the anti-adhesion effect of the scaffold following a primary tendon repair. Initially an ester linkage was used as this is a labile linker that can be hydrolysed and is commonly used in the field[392].

K.2.1 Synthesis of HPMAm-Ibuprofen monomer 1

Figure 7-14: The synthesis of HPMAm-ibuprofen

Based on a published protocol[398], ibuprofen (200 mg, 0.97 mmol) and 4-(Dimethyl)aminopyridine (DMAP, 60.7 mg, 0.5 mmol) were inserted into a glass vial and dissolved in 1.9 mL of dry DCM. A septum and parafilm were used to seal the vial before it was cooled and stirred in an ice bath. Whilst cooling, *N,N*-dicyclohexylcarbodiimide (DCC, 200 mg, 0.97 mmol) was dissolved in 1.9 mL of dry DCM, and *N*-(2-Hydroxypropyl) methacrylamide (HPMAm, 121.4 mg, 0.85 mmol) was dissolved in a further 1 mL dry DCM. Septa were applied to the vessels and the solids dissolved. Once the synthesis vial was cold, the DCC was added dropwise through the

septum followed by the HPMAm. The reaction mixture was stirred vigorously for 1 hr before being allowed to warm to room temperature over 24 hours.

The following day the white precipitate *N,N*-dicyclohexylurea (DCU) was filtered off and discarded. Using an extraction funnel the organic layer was sequentially extracted three times by a 10 wt % of sodium bicarbonate ($NaHCO_3$), twice by hydrochloric acid (HCL, 2M) once by UHQ water and finally by a saturated brine solution. The extracted solution was dried using $MgSO_4$ which was then removed by filtration. Removal of the solvent yielded the crude product as a yellow liquid. The product was purified by silica column (ethylacetate/hexane 3:7) and confirmed on ^{1}H-NMR and mass spectrometry.

K.2.2.2 Synthesis of PEGMA-Ibuprofen monomer 2 (peg3ma-ibu)

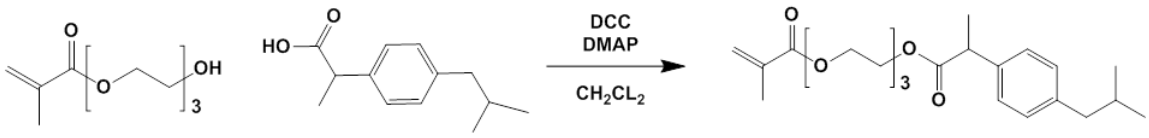

Figure 7-15: The synthesis of peg3ma-ibu.

Based on the reaction scheme used to couple the ibuprofen and the HPMAm, a similar technique was used. In brief, ibuprofen (1.5 g, 7.27 mmol) and DMAP (444mg, 3.6 mmol) were dissolved in dry DCM. The vial was sealed and cooled. DCC (1.5 g, 7.27 mmol) was dissolved in further dry DCM and mono-disperse peg3ma (1.3g, 3.6 mmol) previously isolated using a silica column, was dissolved in further dry DCM. Once the synthesis vial was cold, the DCC was added drop-wise through the septum followed by the peg3ma. The reaction mixture was stirred vigorously for 1 hr before being allowed to warm to room temperature over 24 hours. The following day the DCU was filtered off and discarded.

The product was purified by silica column (ethyl acetate/hexane 1:1, increasing to 100% ethyl acetate) using thin layer chromatography (TLC) to guide fraction collection and confirmed on ^{1}H-NMR using $CDCL_3$. Please see results for peak assignment.

K.2.3 Optimisation of the ARGET ATRP reaction for the ibuprofen-ester-monomers

Polymerisation of monomers with different functional groups affects the ARGET ATRP reaction control and rate. ARGET ATRP co-polymerisations with OEGMA were performed to establish whether the monomer candidates, HPMAm-ibu, HPMA and peg3ma-ibu affected the polymerisation adversely. For each of the monomer units being considered the reaction conditions the impact on the polymerisation was explored and where appropriate the conditions were optimised in solution.

The reaction was initially performed as for the optimised conditions for OEGMA as detailed in chapter 2, section 2.2.3 with 5 mol% of the OEGMA monomer substituted for the test monomer (HPMAm-ibu, HPMA or peg3ma-ibu). Variations in the length of the reaction, temperature, solvent, concentration, molar ratio of reducing agent, the presence of ibuprofen within the reaction mixture, different ligands and the differences between the monomers was explored.

A final monomer and set of reaction conditions were chosen to undertake surface initiated polymerisation of a drug-releasing polymer brush from the PCL-Ini electrospun scaffolds.

K.2.3.1 Co-polymerisation of OEGMA and peg3ma-ibu

Peg3ma-ibu was selected as the best monomer to take forward and explore as a potential drug release candidate and using the optimised conditions, was co-polymerised with OEGMA.

In brief, molar equivalent ratios of the reagents were maintained at monomer:Cu(II) catalyst:TPMA:EBIB:AScA of 150:1:1:0.9:0.15. The monomer component was divided into 75 mol % OEGMA and 25 mol % peg3ma-ibu. The OEGMA (850 mg, 0.0018 mol), peg3ma-ibu (242 mg, 0.0006 mol), Cu(II)Cl (2.12 mg, 15.7 µmol), TPMA (4.57 mg, 15.7 µmol) and EBiB (2.76 mg, 14.1 µmol) were inserted into a round bottom flask containing 8 mm diameter functionalised 17% (w/w) and 9% (w/w) PCL-Ini scaffolds with 10 mL of 50% (v/v) IPA/UHQ water. The flask was sealed with a new rubber septum and parafilm before being introduced into an ice bath to cool before being degassed with bubbling argon for 30 minutes. From a degassed stock solution of AScA in 1:1 (v/v) IPA/UHQ water, the reducing agent (0.42 mg, 2.4 µmol) was added to the reaction mixture using a gas tight syringe. The solution was then

transferred to a pre-warmed silicone oil bath and stirred at 30^{o}C. The reaction was allowed to proceed for 4 hours before being terminated with bubbling oxygen. Monomer to polymer conversion (X%) was determined by ^{1}H-NMR and molecular weights were determined by SEC from the polymer formed by the sacrificial initiator in solution.

Functionalised scaffolds were washed with ethanol in an ultrasonicator for 30 seconds three times before being washed with UHQ water three times and dried in a vacuum dessicator. Polymer in solution, formed from the sacrificial initiator, was purified. Initially, rotatory evaporation was performed to remove the IPA before the sample was freeze dried to remove the excess UHQ water. The remaining polymer (liquid) was dissolved in DCM and precipitated into a 1:1 mixture of hexane and ether in a centrifuge tube. The tube was centrifuged at 5000 rpm for 5 minutes to collect the polymer before the excess solvent was decanted. The purified polymer was dried further using rotatory evaporation to remove any excess solvent and characterised using ^{1}H-NMR to ensure any unreacted monomer had been removed.

K.2.4 Ibuprofen drug release via a hydrolysable ester

Drug release in solution was examined before progressing to release from functionalised scaffold surfaces.

K.2.4.1 Ibuprofen drug release in solution by ^{1}H-NMR

In an initial run, 30 mg of peg3ma-ibu was dissolved in 160 µL of deuterium oxide (D_2O). The solution was divided between four newly purchased glass NMR tubes to give 40 µL and 5 mg of monomer per tube.

Deuterated phosphate buffered saline (dPBS) was made up using 10x concentrated PBS solution diluted using D_2O to the standard concentration. From this dPBS solution buffers at pH 6.0, 7.4 and 8.1 were made in addition to a 0.1M sodium hydroxide (NaOH) solution in D_2O.

To each of the NMR tubes containing the monomer solution, 710 µL of one of the solutions was added. 10% (v/v) DMSO and a further 710 µL dPBS of the required pH was added to the NMR tubes to facilitate the peg3ma-ibu monomer to dissolve. The tubes were immediately sealed with a stopper and parafilm, and labelled. The samples were immediately assessed

using ^{1}H-NMR as a time 0 before being introduced to a water bath where they were maintained at 37^{o}C, during which time ^{1}H-NMRs were regularly taken to assess the monomer.

The ibuprofen release in solution was further observed from p(OEGMA-*co*-peg3ma-ibu) co-polymer. 100 mg of the purified p(OEGMA-*co*-peg3ma-ibu) was dissolved in 400 µL dPBS in a glass vial. Several beads of cuprisorb^{TM} were added to remove any remaining copper from the solution. 80 µL of the polymer solution were added to each NMR tube and the experiment set up and run as above with a further 710 µL of dPBS of pH 6, 7.4 and 8.1 and 0.1M NaOH in dPBS. An immediate ^{1}H-NMR was performed as a time 0 before the tubes were incubated in a water bath at 37^{o}C. Regular ^{1}H-NMRs were performed to assess the ibuprofen release.

K.2.4.2 Ibuprofen drug release from functionalised scaffolds

17% (w/w) PCL-p(OEGMA-*co*-peg3ma-ibu) scaffolds and 9% (w/w) PCL-p(OEGMA-*co*-peg3ma-ibu) scaffolds from the same polymerisation, and having been washed and dried together, and control scaffolds functionalised with a pOEGMA brush but with no peg3m-ibu had a dry weight recorded. Scaffolds were dipped in ethanol before being rinsed in PBS three times to ensure uniform hydration. Excess PBS was wicked away from the scaffolds before they were inserted into 500 µL labelled low binding eppinforf tubes with 300 µL fresh PBS. 150 µL of the supernatant was immediately removed and analysed with a UV/Vis spectrophotometer (Lambda 25, Perkins Elmer, Waltham, USA) in a quartz micro-cuvette. The instrument was set up to scan samples between wavelengths of 350-200 nm at a speed of 480 nm/min. The machine was allowed to warm up for 30 minutes before use and was auto zero'd with PBS prior to use. The UV/Vis spectrophotometer was used to estimate the amount of ibuprofen released from the functionalised scaffolds. Ibuprofen in PBS has a maximum absorbance in the UV region, λ_{MAX} = 264 nm corresponding to the vibrational frequency of the aromatic ring within the ibuprofen compound[400]. Using the associated UV WinLab Data Processor and Viewer software, the absorbance at 265 nm, for the ibuprofen and 320 nm, as a baseline, were isolated and recorded.

Following the reading, the supernatant was returned to the sample, which was sealed, and incubated at 37^{o}C. Regular readings were undertaken to analyse the release of ibuprofen

from the scaffolds. The experiment was performed in triplicate (N = 3). Sample readings were compared to a ladder of ibuprofen in PBS that was generated using a 1 mM solution that underwent 50% (v/v) serial dilutions to 125 µM. A ladder was made up and read at every reading of the scaffolds to check the signal intensity.

K.3 Results and discussion

Ibuprofen pendant monomers were synthesised, characterised and polymerised into pOEGMA brushes both in solution and from functionalised PCL-Ini scaffolds.

K.3.1 Synthesis of ibuprofen releasing monomers via a hydrolysable ester

A monomer with a hydrolysable ester was initially synthesised as this is a labile linker commonly used in the drug release field[395].

K.3.1.1 Synthesis of HPMAm-ibuprofen monomer

HPMAm was initially tried as the monomer to link with ibuprofen through the ester as this monomer is established for use in clinically used drug-polymer conjugates[395,401]. The HPMAm-ibu monomer was synthesised and the product confirmed by ^{1}H-NMR (Figure 7-16) and mass spectrometry (Figure 7-17).

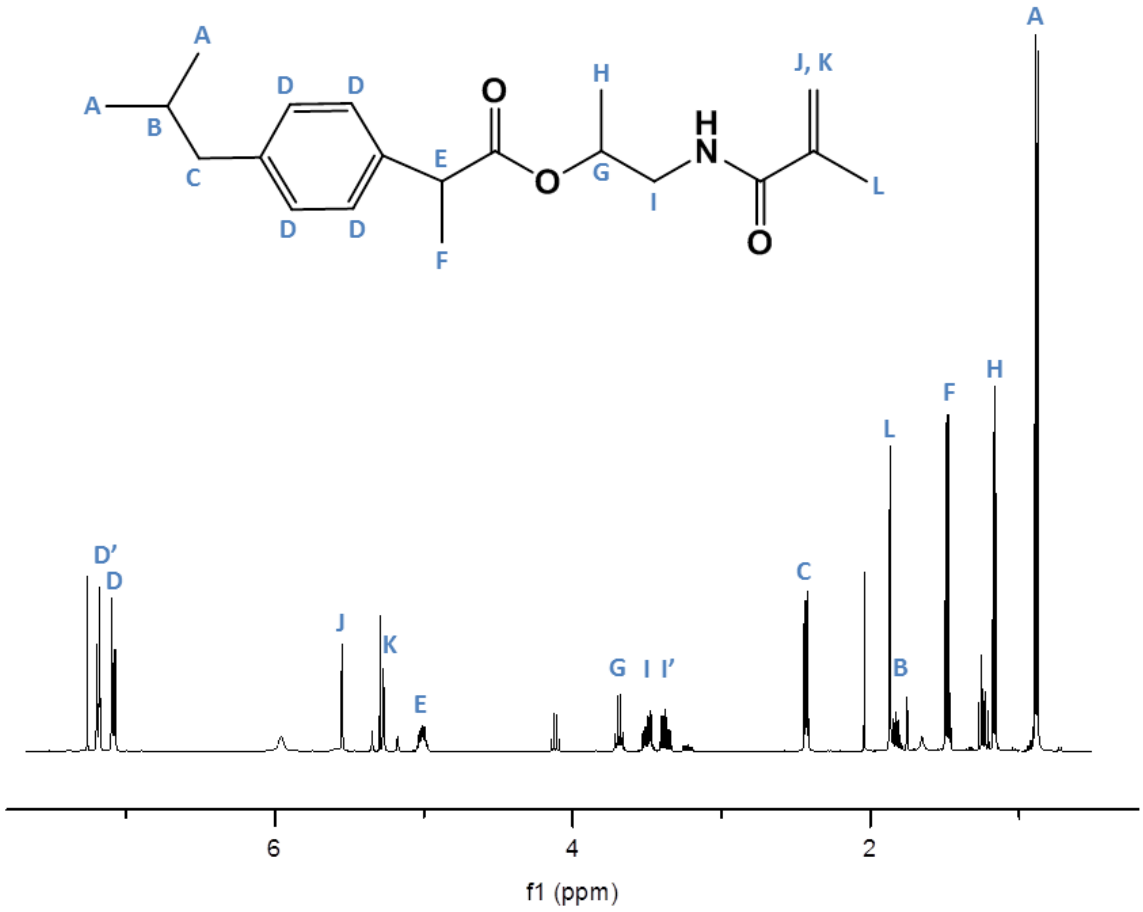

Figure 7-16: ^{1}H-NMR (400MHz, $CDCL_3$) of HPMAm-ibu monomer with peak assignments.

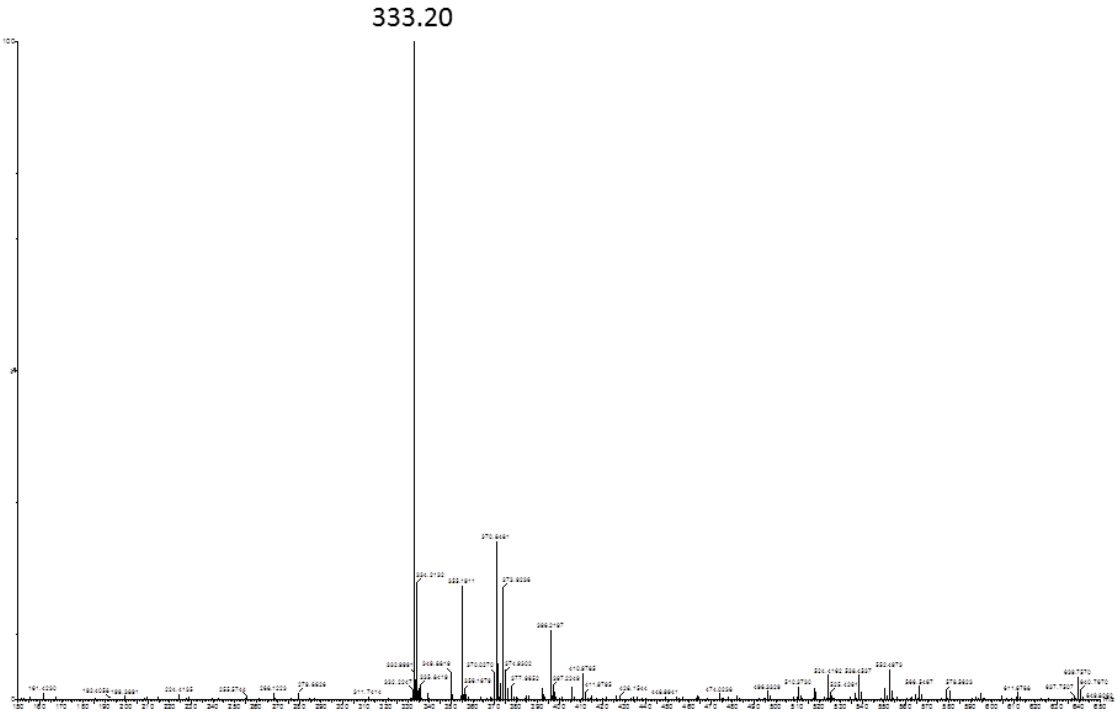

Figure 7-17: Mass spectroscopy for the HPMAm-ibu monomer. Calculated 332.20, found 333.20.

The HPMAm-ibu monomer was then used in several co-polymerisation reactions with OEGMA in solution by ARGET ATRP. It was deemed that the presence of this monomer was having an effect on both the conversion and control of the polymerisation (discussed below in section I.3.2). Due to this effect, an alternative monomer was made. A monomer based on a short methacrylate oligomer of PEG was selected as this was the most structurally similar to the OEGMA being used in the bulk of the polymerisation, the least likely to result in adverse effects on the polymerisation.

K.3.1.2 Synthesis of PEGMA-ibuprofen monomer (peg3ma-ibu)

The peg3ma-ibu monomer was synthesised using a similar method to the HPMAm-ibu monomer. The product was successfully synthesised and confirmed using ^{1}H-NMR (Figure 7-18).

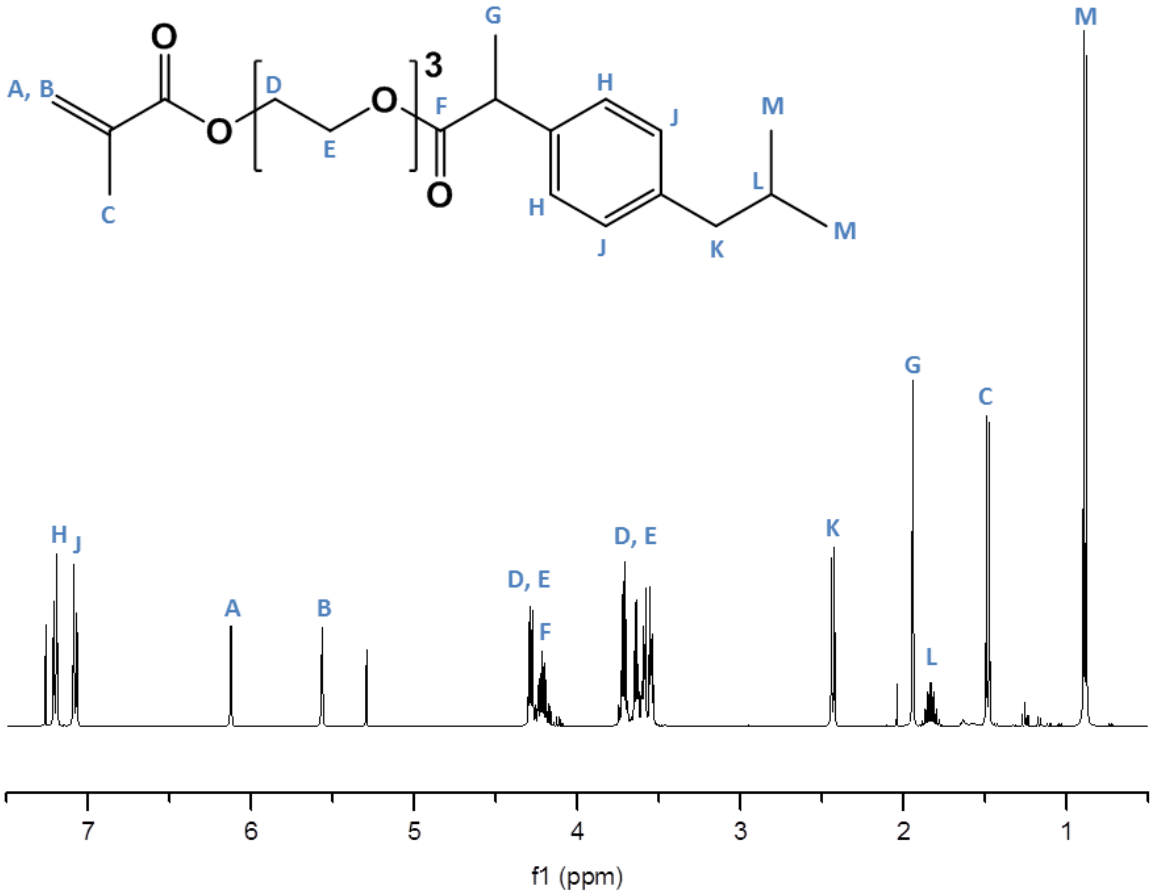

Figure 7-18: ^{1}H-NMR (400MHz, $CDCl_3$) of peg3ma-ibu monomer

K.3.2 Optimisation of the ARGET ATRP polymerisation for the different monomers

Co-polymerisation of HPMAm-ibu with OEGMA was initially undertaken by ARGET ATRP in solution using the SOP used throughout this thesis. It was immediately apparent that the presence of the monomer had an adverse effect on the polymerisation with conversion by ^{1}H-NMR being consistently low (< 50 %) and/or high dispersities found by SEC indicating poor control. Simple variables were tested initially to optimise the reaction including varying time (2 hr vs. 18 hr) and temperature (30, 40 and 50^{o}C) with the resulting polymer X and *Đ* outlined in Table 7-4.

Table 7-4: ARGET ATRP of p(OEGMA-co-HPMAm-ibu) with variations in reaction time and temperature and the corresponding X, *Đ*, and M_n.

Variable		X (%)	M_n	*Đ*
Time	2 hr	40	27100	1.28
	18 hr	37	25200	1.23
Temperature	30°C	50	29300	1.25
	40°C	39	25000	1.17
	50°C	58	32000	1.33

Increasing the time from 2 hours and the temperature from 30°C, as used in the SOP, did not result in a significant improvement of the monomer to polymer conversion and control. More complex variables were then explored to establish whether an improvement could be made.

The percentage of water in ATRP systems has a large impact on the reaction, so the percentage of IPA was varied to establish whether this would improve the polymer characteristics. Polymerisations were undertaken in a range of dilutions of IPA (Table 7-5). The solubility of the HPMAm-ibu monomer compromised the reaction in pure UHQ water and 20% (v/v) IPA as it resulted in rapid precipitation, so these results are interpreted with caution.

Table 7-5: ARGET ATRP of p(OEGMA-co-HPMAm-ibu) with variations in water content of solvent and the corresponding X, *Đ*, and M_n.

Variable		X (%)	M_n	*Đ*
Solvent	90	23	22800	1.19
% (v/v) IPA in UHW	80	36	32700	1.20
water	60	49	45800	1.31
	50	54	51500	1.30
	40	59	52700	1.33
	20	29	50200	1.16
	0	50	86300	1.26

Notes: 0% (v/v) IPA refers to pure UHQ water. Shaded areas, 20% (v/v) IPA and 0% (w/w) IPA represent reactions with some precipitation of the HPMAm-ibu monomer.

The use of 40% (v/v) IPA appeared to produce a marginal improvement in the reaction (X = 59%), so this was used as the solvent from this point forward. The reaction remains poor however when compared to the homopolymerisation of OEGMA, so further optimisation was undertaken. The molar ratio of reducing agent, ascorbic acid, was varied (Table 7-6).

Table 7-6: ARGET ATRP of p(OEGMA-co-HPMAm-ibu) with variations in molar ratios of AScA and the corresponding X, *Đ*, and M_n.

Variable		X (%)	M_n	*Đ*
Molar ratio of AScA	0.05	32	21800	1.22
	0.1	39	31800	1.30
	0.15	70	31800	1.30
	0.2	71	27900	1.26
	0.3	79	42400	1.69
	0.4	77	72800	1.93

The molar ratio of 0.15 AScA, as used throughout this thesis continued to be the optimal amount and was not changed. Whilst the monomer to polymer conversion of the reaction was improved, the control continued to be below that of the optimised OEGMA polymerisation. The possibility of the presence of the ibuprofen in the reaction was explored, as the aromatic ring within the structure may lead to disruption of the reaction process.

Co-polymerisations were undertaken with 30 mol% HPMAm, with no ibuprofen, 30 mol% HPMAm-ibu, and 5 mol% HPMAm-ibu with OEGMA (Table 7-7).

Table 7-7: ARGET ATRP of OEGMA with HPMAm with different mol% of ibuprofen and the corresponding X, *Đ*, and M_n.

Variable		X (%)	M_n	*Đ*
Monomer	30 mol% HPMAm	28	15000	2.26
	30 mol% HPMAm-ibu	37	27500	1.30
	5 mol% HPMAm-ibu	70	31800	1.30

Notes: The 5 mol% HPMAm-ibu is the same data presented in Table 7-6 above for the 0.15 molar ratio AScA as this was undertaken with 5 mol% ibuprofen. It has been included here for comparison.

The co-polymerisation of OEGMA with HPMAm was inferior to the polymerisation with HPMAm-ibu, so the inclusion of the ibuprofen in the reaction does not appear to be deleterious to the reaction. The 5 mol% HPMAm-ibu reaction results in a more optimal polymer, this is also the reaction with the lowest level of HPMAm monomer.

An alternative but similar monomer, HPMA, was tried together with ligand substitution for both the HPMAm-ibu and the HPMA monomers in the co-polymerisation with OEGMA. 30 mol% of the monomers were used compared to the OEGMA to ensure an effect on the polymerisation would be identified. The ligand TPMA has been used until this point (Table 7-

8). 2, 2'-bipyridine (BPY) and *N,N,N',N',N''*-pentamethyldiethylenetriamine (PMDETA) were selected as they represent a range of activities with TPMA being the most active, and BPY being the least active with regard to the activation constant for the copper catalyst.

Table 7-8: ARGET ATRP of OEGMA with HPMAm and HPMA with different ligands and the corresponding X, *Đ*, and M_n.

Monomer	Ligand	X (%)	M_n	*Đ*
HPMAm	TPMA	28	15000	2.36
	BPY	79	38400	3.69
	PMDETA	54	295200	1.49
HPMA	TPMA	50	44400	1.56
	BPY	88	94500	2.58
	PMDETA	37	219100	1.77

Notes: 2, 2'-bipyridine (BPY), *N,N,N',N',N''*-pentamethyldiethylenetriamine (PMDETA). HPMAm TPMA result is from the previous table, but included here for completeness. Shaded areas represent readings that were beyond the calibration limits of the SEC column so appear artificially low.

The use of lower activation ligands, BPY and PMDETA, resulted in the deterioration of the control of the reaction despite improved conversion for BPY. Despite having tried a range of variables the conversion and control of the copolymerisation for both HPMAm and HPMA remain poor and may be a result of the presence of the acrylate group within both monomer units. An alternative monomer unit, based on PEG was tried, peg3ma-ibu.

A drug releasing monomer structurally as similar as possible to the bulk OEGMA monomer was synthesised (peg3ma-ibu). This was done due to the negative impact that the HPMAm and HPMA monomers were having on the control and conversion of the ARGET ATRP polymerisation. This may be due to the reactivity of the different monomers. Acrylate monomers, such as HPMAm and HPMA are discussed in the literature to have lower reactivity ratios than methyl methacrylate monomers, such as OEGMA[402]. It may be therefore that within the polymerisation presented within this thesis that the OEGMA is preferentially being polymerised before the HPMA or HPMAm monomers. The synthesis of a methyl methacrylate drug releasing monomer would remove this variable.

The peg3ma-ibu monomer was co-polymerised with OEGMA using the original reaction conditions in the SOP used in this thesis. This monomer was successfully copolymerised into the OEGMA brush in solution with reproducible results at 20 mol% substitution for the OEGMA. The conversion was low but the control of the reaction was much improved. A

typical copolymer produced had a conversion (X) of 50%, *Đ* 1.06, and M_n 15800. The peg3ma-ibu monomer was taken forward for surface initiated polymerisation and drug release studies.

K.3.3 Ibuprofen drug release via a hydrolysable ester

Once the ibuprofen monomer, peg3ma-ibu, had been selected, a co-polymerisation of OEGMA and peg3ma-ibu was undertaken from 17% (w/w) and 9% (w/w) PCL-Ini scaffolds. A monomer substitution of 10 mol% peg3ma-ibu was made. This reaction gave a conversion (X) of 78% by ^{1}H-NMR which also revealed there was unreacted peg3ma-ibu monomer present in the solution following the reaction. The polymer solution was subsequently dialysed in 4 L of UHQ water with 3 water changes over 12 hours before being assessed on the SEC. The resulting polymer was M_n 20500 with a *Đ* 1.07. The purified polymer was used for the assessment of drug release in solution. The scaffolds were ultrasonicated in ethanol three times, as previously outlined in Chapter 3, before being dried and used for a pilot assessment of drug release.

K.3.3.1 Ibuprofen drug release in solution

The purified p(OEGMA-*co*-peg3ma-ibu) polymer was used to assess the hydrolysis of the ester linkage through the release of ibuprofen by ^{1}H-NMR. Three pHs of 6.0, 7.4 and 8.1 were used for the incubation of the polymer, together with an incubation in NaOH which would result in complete cleavage of the ester linkage and used as a positive control.

The samples were scanned by ^{1}H-NMR regularly over the course of 42 days and the percentage of ibuprofen hydrolysed from the polymer calculated (Figure 7-19). The sample incubated with NaOH demonstrated 38% cleavage at time 0, approximately 30 minutes after the addition of the NaOH, and 100% release at 24 hours. None of the other samples (pH 6.0, 7.4 or 8.1) demonstrated any hydrolysis of the ibuprofen. At day 42 the samples were opened and the pH checked. All pHs had remained stable through the experiment.

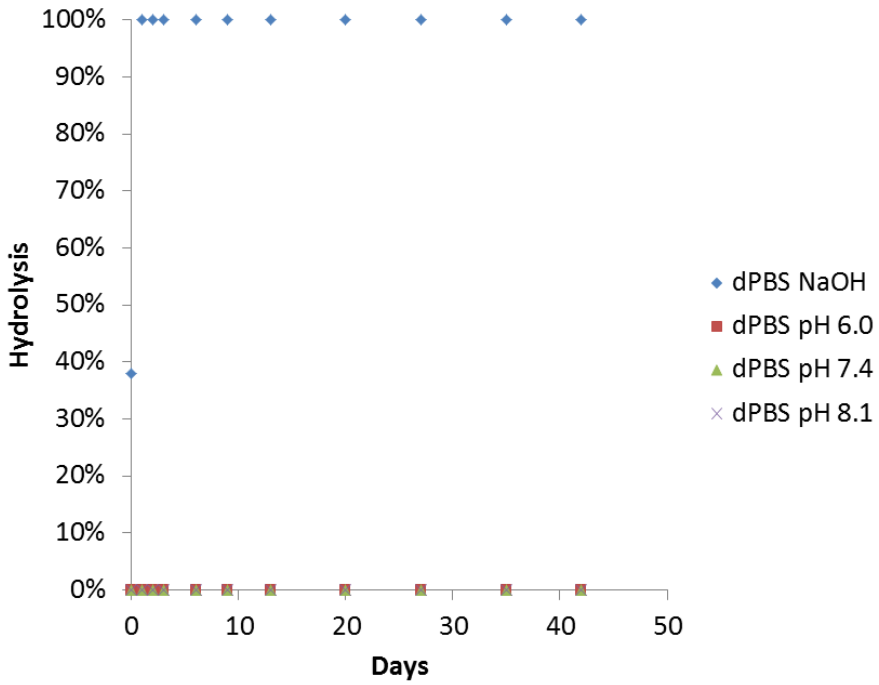

Figure 7-19: Drug release from the p(OEGMA-*co*-peg3ma-ibu) polymer in solution by ^{1}H-NMR.

At this point, 80 µL of 0.1M NaOH was added to each of the samples to assess whether ibuprofen release could be achieved. After 24 hours of incubation with NaOH all samples had 100% ibuprofen release. The hydrolysis of the ibuprofen using the NaOH demonstrates that hydrolysis of the ester linkage and ibuprofen release is possible. This does however demonstrate a high level of stability. It is known form the literature that the rate of hydrolysis of the ester will be dependent on the "R" groups on the ester, in this case, the ibuprofen and the polymer brush. It has been demonstrated that both the hydrophilicity and the size of the R groups impact the rate of hydrolysis. The higher the hydrophilicity, the greater the rate of hydrolysis, and the larger the R group the slower the release, even at higher pH[386]. The polymer brush certainly represents a considerable R group and this may contribute to the stability of this bond. The data suggesting that the ester associated with the polymer brush structure being highly stable is supported by the data presented in Chapter 5. Chapter 5 illustrates the rate of hydrolysis of the ester linkage in a OEGMA monomer with 3 repeating PEG units by ^{1}H-NMR. At 6 weeks (42 days) approximately 10% of the peg3ma is hydrolysed at pH 7.4 and 16% at pH 8.1. This hydrophilic peg3ma monomer demonstrates a faster rate of ester hydrolysis than the p(OEGMA-*co*-peg3ma-ibu) polymer. Chapter 5 also demonstrates that the pOEGMA bottlebrushes are held to the PCL polymer fibres through an ester linkage and following incubation in physiological conditions for 10 weeks does not

result in complete hydrolysis. This contributes to the data suggesting that in this system, the ester linkage is quite stable. Furthermore, the peg3ma-ibu monomer is made up of a unit 3 peg chains long. The OEGMA monomer used in this work has an average peg chain of 9 units. It may be that the ibuprofen has become embedded within the OEGMA brush and inaccessible for bond cleavage, particularly as the ibuprofen itself is highly hydrophobic.

Ibuprofen-polymer prodrugs have been presented in the literature. Babazadeh *et al.* synthesised a monomer based on 2-hydroxypropyl methacrylate (HPMA) before copolymerising in solution with either HEMA or methyl methacrylate (MMA)[398]. Drug release was performed in PBS at 37^{o}C and was measured using UV spectrophotometry, revealing approximately 40% and 14% release at 12 hours for the HEMA and MMA copolymers respectively at pH 7.4. This was reduced at pH 1, 24% and 10%, and faster at pH 10 with approximately 70% and 28% for the HEMA and MMA copolymers at 12 hours respectively. Similarly, Davaran *et al.* produced a series of PEGylated ibuprofen prodrugs that produce a single, linear PEG chain (number average molecular weight 5000) coupled with an ester, a thioester or an amide to an ibuprofen compound[403]. The rate of drug release from the PEG is compared in PBS and human plasma and measured using a UV-vis spectrophotometer. The ester linked ibuprofen-PEG prodrug demonstrated the slowest release of the 3 linkages and is outlined in Table 7-9.

Table 7-9: Ibuprofen release from PEGulated ibuprofen prodrugs[64].

pH	% drug release at 48 hrs
1	10
7.4	12
8.0	14

These linear polymers demonstrate that the ester linkage in this case is labile when compared to the system presented in this thesis. Whilst the systems presented are clearly quite different with regard to monomer type, it is interesting to note that the release from the PEGylated prodrug presented by Davaran *et al*. is significantly slower than that of Babazadeh *et al.* this may be due to the size of the polymer the drug is affiliated to, which would tie in with the findings here.

K.3.3.2 Ibuprofen drug release from functionalised scaffolds

17% (w/w) and 9% (w/w) PCL-Ini scaffolds underwent surface initiated polymerisation through ARGET ATRP and were grafted with p(OEGMA-*co*-peg3ma-ibu) in the same reaction used for the drug release in solution (section K.3.3.1). The polymerisation, as described above, was successful and surface grafting with polymer was established using water contact angle measurements (Figure 7-20). The surface wettability of PCL-pOEGMA scaffolds is very great, water droplets immediately soak into the scaffolds. The PCL-p(OEGMA-*co*-peg3ma-ibu) scaffolds are less hydrophilic than the PCL-pOEGMA. The water droplet completely absorbs into the scaffolds, but it is over the course of several seconds, rather than the immediate effect seen with PCL-pOEGMA. This is expected as the ibuprofen is highly hydrophobic.

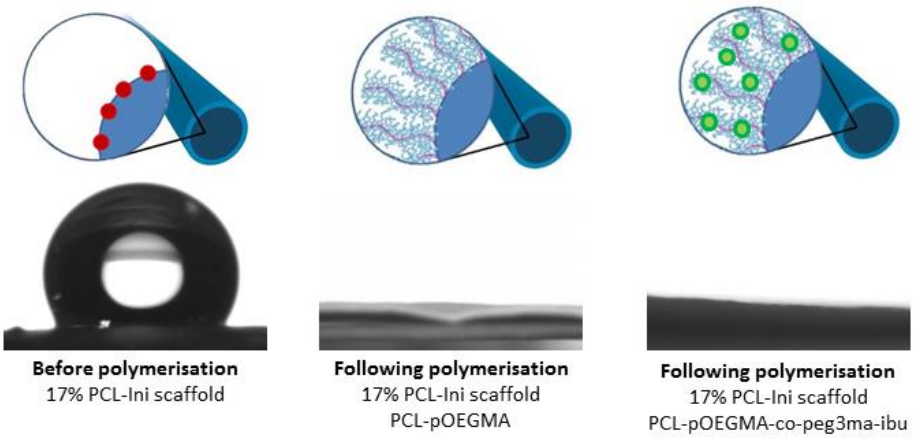

Figure 7-20: Surface grafting of PCL-p(OEGMA-co-peg3ma-ibu) is confirmed with change in water contact angle (right) and compared to PCL-pOEGMA scaffolds (centre).

17% (w/w) and 9% (w/w) PCL-p(OEGMA-*co*-peg3ma-ibu) scaffolds (N = 3 per scaffold type) together with controls (polymerised scaffolds with no ibuprofen) were incubated in individual low bind eppindorf tubes in PBS at 37°C. Periodically 150 µL of the supernatant was removed and scanned using a UV-vis spectrophotometer, before being returned to the tube. A calibration curve of known concentrations of ibuprofen was generated and used to establish the amount of ibuprofen being released from the samples (Figure 7-21).

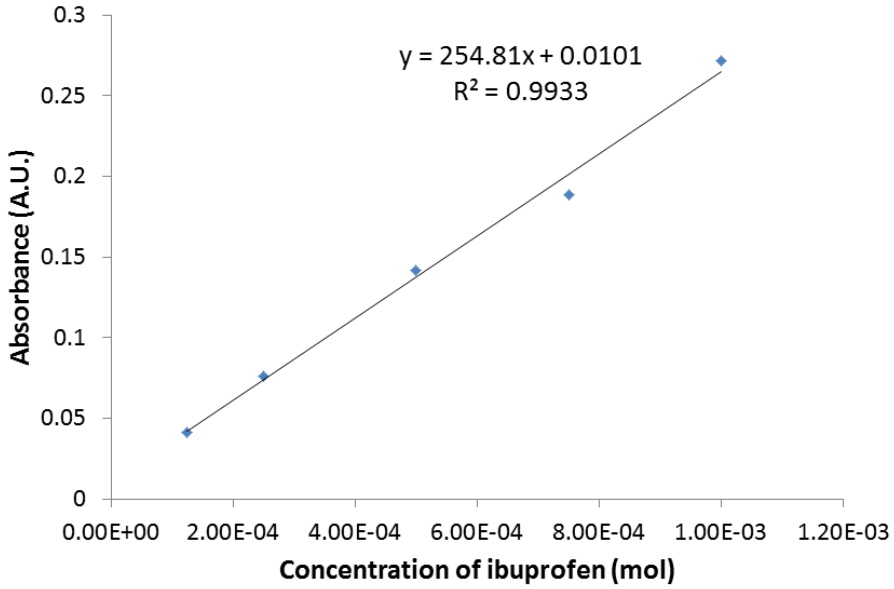

Figure 7-21 Calibration curve of known concentrations of ibuprofen and the absorbance on UV-vis spectroscopy.

The absorbance was directly proportional to the concentration of ibuprofen between 1 mM and 125 μM with an r^2 of 0.9933. This was used to calculate the amount of ibuprofen released from the scaffolds over a 42 day period, which was normalised to the mass of the scaffold. The data from this pilot experiment is somewhat confusing as there appears to be ibuprofen release from the 17% (w/w) PCL-p(OEGMA-*co*-peg3ma-ibu) scaffolds, but very little from the 9% (w/w) PCL-p(OEGMA-*co*-peg3ma-ibu) scaffolds. Furthermore, a positive signal is seen from the 17% (w/w) p(OEGMA-*co*-peg3ma-ibu) scaffolds at time 0, where the PBS had been added and immediately removed and read on the instrument. This might suggest that inadequate washing had occurred with these samples as a burst release would not be expected. On the other hand, these samples had been washed together with the 9% (w/w) PCL-p(OEGMA-*co*-peg3ma-ibu) scaffolds, so should inadequate washing have caused this result, it would be expected to be seen in the 9% (w/w) scaffold data also.

This data must be interpreted with caution and is extremely preliminary, and hence is not included here. Furthermore it is in contrast to the with the ibuprofen degradation from polymer in solution by ^{1}H-NMR, a simpler and more controlled system. It may be that there is some ibuprofen release being seen from the 17% (w/w) PCL-p(OEGMA-*co*-peg3ma-ibu) scaffolds being identified using the UV-vis instrument which is more sensitive that the ^{1}H-NMR, but this may be negligible to the relative amount that remains on the scaffold. Significant further work is required to characterise this system. In the first instance a more labile linkage, such as a thioester could be tried.

K.4 Conclusions

The addition of a monomer unit with a drug delivery moiety would be a valuable addition to the modular and versatile scaffold system presented in this thesis. This Chapter, outlining the pilot work done to date on this monomer reveals that the use of an ester linkage in this system appears to be quite stable within the polymer brush structure. This feature is also seen and discussed in Chapter 5 with regards to the stability of the polymer brushes themselves.

The field of drug-pendant polymers is vast and complex. Significant further work needs to be invested into this system to understand it further and to make the drug-releasing monomer a reality, including the use of physiological fluids rather than PBS, as this will result in a more rapid and accurate drug release that reflects the *in vivo* position.

Appendix L : Permission for reproduction of Figure 7-10 from Ricciotti et al.[340]

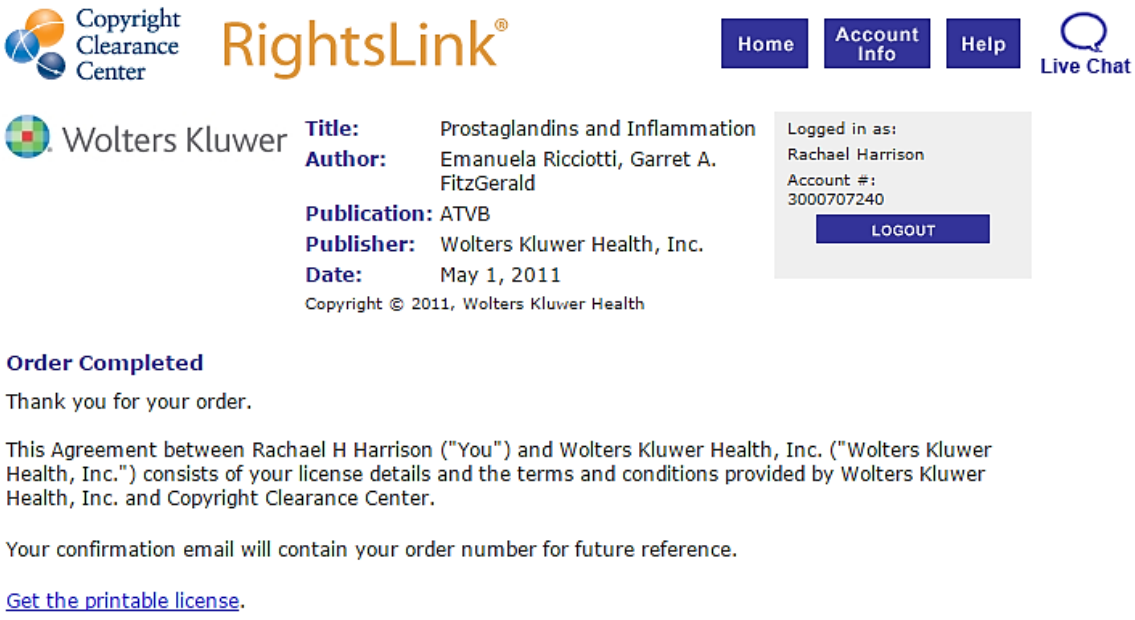

Copyright Clearance Center RightsLink®

Home | Account Info | Help | Live Chat

Wolters Kluwer

Title: Prostaglandins and Inflammation
Author: Emanuela Ricciotti, Garret A. FitzGerald
Publication: ATVB
Publisher: Wolters Kluwer Health, Inc.
Date: May 1, 2011

Copyright © 2011, Wolters Kluwer Health

Logged in as:
Rachael Harrison
Account #:
3000707240
LOGOUT

Order Completed

Thank you for your order.

This Agreement between Rachael H Harrison ("You") and Wolters Kluwer Health, Inc. ("Wolters Kluwer Health, Inc.") consists of your license details and the terms and conditions provided by Wolters Kluwer Health, Inc. and Copyright Clearance Center.

Your confirmation email will contain your order number for future reference.

Get the printable license.

Order Completed

Thank you for your order.

This Agreement between Rachael H Harrison ("You") and Wolters Kluwer Health, Inc. ("Wolters Kluwer Health, Inc.") consists of your license details and the terms and conditions provided by Wolters Kluwer Health, Inc. and Copyright Clearance Center.

Your confirmation email will contain your order number for future reference.

Get the printable license.

License Number	3770830146049
License date	Dec 16, 2015
Licensed Content Publisher	Wolters Kluwer Health, Inc.
Licensed Content Publication	ATVB
Licensed Content Title	Prostaglandins and Inflammation
Licensed Content Author	Emanuela Ricciotti, Garret A. FitzGerald
Licensed Content Date	May 1, 2011
Licensed Content Volume	31
Licensed Content Issue	5
Type of Use	Dissertation/Thesis
Requestor type	Individual
Portion	Figures/table/illustration
Number of figures/tables/illustrations	1
Figures/tables/illustrations used	Figure 1
Author of this Wolters Kluwer article	No
Title of your thesis / dissertation	Engineered Scaffolds for the Preservation of Gliding Tissue Interfaces
Expected completion date	Jan 2016
Estimated size(pages)	200
Requestor Location	Rachael H Harrison Office 2.12 Royal School of Mines Department of Materials Imperial College Prince Consort Road London, United Kingdom SW7 2AZ Attn: Rachael H Harrison
Billing Type	Invoice
Billing address	Rachael H Harrison Office 2.12 Royal School of Mines Department of Materials Imperial College Prince Consort Road London, United Kingdom SW7 2AZ Attn: Rachael H Harrison
Total	0.00 GBP

CLOSE WINDOW

Appendix M : List of publications

Abstracts

1. "Free Radical Polymerization for the Controlled and Facile Production of a Cell Repellent and Antifouling Surface in 2- and 3D Systems" **RH Harrison**, R Chapman, AJ Gormley, LW Chow, JAM Steele, M Mahat, L Podhorska, SP Hettiaratchy, IE Dunlop, MM Stevens. *Tissue Engineering: Part A* (Volume 21, Issue S1 pS-307). 2015

Papers

2. "Modular and Versatile Spatial Functionalization of Tissue Engineering Scaffolds through Fiber-Initiated Controlled Radical Polymerisation" **RH Harrison**, JAM Steele, R Chapman, AJ Gormley, LW Chow, MM Mahat, L Podhorska, RG Palgrave, DJ Payne, SP Hettiaratchy, IE Dunlop, MM Stevens. Advanced Functional Materials (Volume 25, Issue 36 p5748-5757). 2015. Impact factor 10.8.

3. "Tissue Engineering and Regenerative Medicine: a Year in Review" **RH Harrison**, JP St-Pierre, MM Stevens. Tissue Engineering Part B: Reviews. February 2014, 20(1):1-16. Impact factor 4.254.

4. "Micro calcified particles as a natural component of vascular tissue. A new biomineralization process in vertebrates, with implications for vascular calcification research and potentially connecting cardiac diseases with several other pathologies." S Bertazzo, JP St-Pierre, CM Horejs, I Hermann, S Agarwal, H Autefage, S Omelon, JAM Steele, A You, C Kallepitis, A Kinkeldey, M Dean, JD Hutcheson, **RH Harrison**, C Rotich, K Smith, C Brassey, S Evans, J Davies, W Jahnen-Dechent, E Aikawa, AH Chester, MH Yacoub, MM Stevens (*manuscript in preparation*).

Quote from Breaking Bad[404].

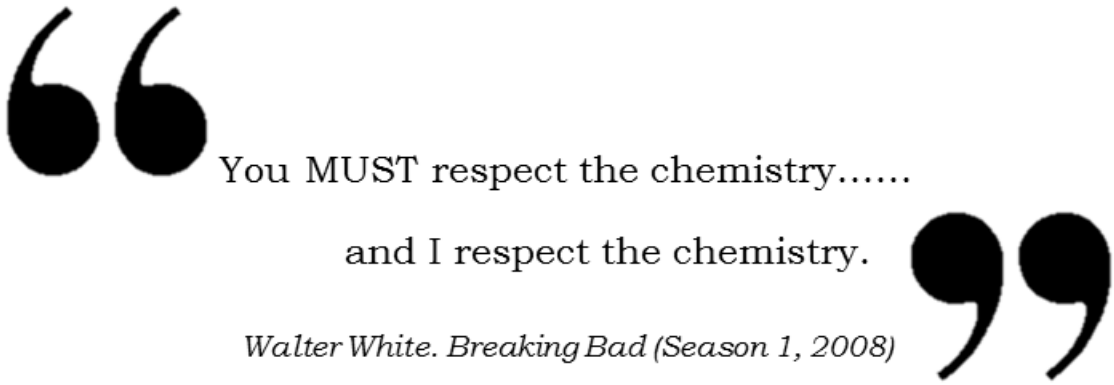

References: Appendix

340 Ricciotti, E. & FitzGerald, G. A. Prostaglandins and Inflammation. *Arteriosclerosis Thrombosis and Vascular Biology* **31**, 986-1000, doi:10.1161/atvbaha.110.207449 (2011).

341 Kakwere, H., Payne, R. J., Jolliffe, K. A. & Perrier, S. Self-assembling macromolecular chimeras: controlling fibrillization of a beta-sheet forming peptide by polymer conjugation. *Soft Matter* **7**, 3754-3757, doi:10.1039/c0sm01237h (2011).

342 Harrison, R. H. *et al.* Modular and Versatile Spatial Functionalization of Tissue Engineering Scaffolds through Fiber-Initiated Controlled Radical Polymerization. *Advanced Functional Materials* **25**, 5748-5757, doi:10.1002/adfm.201501277 (2015).

343 Simmons, R. L., Yu, R. T. & Myers, A. G. Storable Arylpalladium(II) Reagents for Alkene Labeling in Aqueous Media. *Journal of the American Chemical Society* **133**, 15870-15873, doi:10.1021/ja206339s (2011).

344 Kvach, M. V. *et al.* A convenient synthesis of cyanine dyes: Reagents for the labeling of biomolecules. *European Journal of Organic Chemistry*, 2107-2117, doi:10.1002/ejoc.200701190 (2008).

345 McCullen, S. D., Autefage, H., Callanan, A., Gentleman, E. & Stevens, M. M. Anisotropic Fibrous Scaffolds for Articular Cartilage Regeneration. *Tissue Eng. Part A* **18**, 2073-2083, doi:10.1089/ten.tea.2011.0606 (2012).

346 Accardi, M. A. *et al.* Effects of Fiber Orientation on the Frictional Properties and Damage of Regenerative Articular Cartilage Surfaces. *Tissue Eng. Part A* **19**, 2300-2310, doi:10.1089/ten.tea.2012.0580 (2013).

347 M. Kobayashi, Y. T., N. Hosaka, M. Kaido, A. Suzuki, N. Yamada, N. Torikai, K. Ishihara, A. Takahara. Friction behavior of high-density poly(2-methacryloyloxyethylphosphorylcholine) brush in aqueous media. *Soft Matter* **3**, 740-746 (2007).

348 Yamamoto, S., Ejaz, M., Tsujii, Y. & Fukuda, T. Surface interaction forces of well-defined, high-density polymer brushes studied by atomic force microscopy. 2. Effect of graft density. *Macromolecules* **33**, 5608-5612, doi:10.1021/ma991988o (2000).

349 Christopher R. Jacobs, H. H., Ronald Kwo. *Introduction to Cell Mechanics and Mechanobiology*. 1st edn, (Garlands Science, 2012).

350 Natoli, R. *Impact Loading and Functional Tissue Engineering of Articular Cartilage* Ph.D thesis, Rice University, (2008).

351 Komistek, R. D., Kane, T. R., Mahfouz, M., Ochoa, J. A. & Dennis, D. A. Knee mechanics: a review of past and present techniques to determine in vivo loads. *Journal of biomechanics* **38**, 215-228, doi:10.1016/j.jbiomech.2004.02.041 (2005).

352 Strange, D. G. T., Tonsomboon, K. & Oyen, M. L. Mechanical behaviour of electrospun fibre-reinforced hydrogels. *Journal of Materials Science-Materials in Medicine* **25**, 681-690, doi:10.1007/s10856-013-5123-y (2014).

353 Kai, D. *et al.* Mechanical properties and in vitro behavior of nanofiber-hydrogel composites for tissue engineering applications. *Nanotechnology* **23**, doi:10.1088/0957-4484/23/9/095705 (2012).

354 Nair, L. S. & Laurencin, C. T. Biodegradable polymers as biomaterials. *Progress in Polymer Science* **32**, 762-798, doi:10.1016/j.progpolymsci.2007.05.017 (2007).

355 Richardson, T. P., Peters, M. C., Ennett, A. B. & Mooney, D. J. Polymeric system for dual growth factor delivery. *Nat. Biotechnol.* **19**, 1029-1034, doi:10.1038/nbt1101-1029 (2001).

356 Lee, K. Y. & Mooney, D. J. Hydrogels for tissue engineering. *Chemical Reviews* **101**, 1869-1879, doi:10.1021/cr000108x (2001).

357 Goldberg, M., Langer, R. & Jia, X. Nanostructured materials for applications in drug delivery and tissue engineering. *Journal of Biomaterials Science-Polymer Edition* **18**, 241-268, doi:10.1163/156856207779996931 (2007).

358 Sill, T. J. & von Recum, H. A. Electro spinning: Applications in drug delivery and tissue engineering. *Biomaterials* **29**, 1989-2006, doi:10.1016/j.biomaterials.2008.01.011 (2008).

359 Agarwal, S., Wendorff, J. H. & Greiner, A. Use of electrospinning technique for biomedical applications. *Polymer* **49**, 5603-5621, doi:10.1016/j.polymer.2008.09.014 (2008).
360 Vane, J. R. & Botting, R. M. Mechanism of action of nonsteroidal anti-inflammatory drugs. *American Journal of Medicine* **104**, 2S-S8, doi:10.1016/s0002-9343(97)00203-9 (1998).
361 Stone, E. An account of the success of the bark of the willow in the cure of agues. *Phil Trans Roy Soc* **53**, 195-200 (1763).
362 Moncada, S., Ferreira, S. H. & Vane, J. R. PROSTAGLANDINS, ASPIRIN-LIKE DRUGS AND EDEMA OF INFLAMMATION. *Nature* **246**, 217-218, doi:10.1038/246217a0 (1973).
363 Smith, W. L. PROSTAGLANDIN BIOSYNTHESIS AND ITS COMPARTMENTATION IN VASCULAR SMOOTH MUSCLE AND ENDOTHELIAL CELLS. *Berne, R. M. (Ed.). Annual Review of Physiology, Vol. 48. Xii+769p. Annual Reviews Inc.: Palo Alto, Calif., USA. Illus*, 251-262 (1986).
364 Dinchuk, J. E. *et al.* RENAL ABNORMALITIES AND AN ALTERED INFLAMMATORY RESPONSE IN MICE LACKING CYCLOOXYGENASE-II. *Nature* **378**, 406-409, doi:10.1038/378406a0 (1995).
365 Yuan, C. *et al.* Cyclooxygenase Allosterism, Fatty Acid-mediated Cross-talk between Monomers of Cyclooxygenase Homodimers. *Journal of Biological Chemistry* **284**, 10046-10055, doi:10.1074/jbc.M808634200 (2009).
366 Vane, J. R. & Botting, R. M. The mechanism of action of aspirin. *Thrombosis Research* **110**, 255-258, doi:10.1016/s0049-3848(03)00379-7 (2003).
367 Gan, T. J. Diclofenac: an update on its mechanism of action and safety profile. *Current Medical Research and Opinion* **26**, 1715-1731, doi:10.1185/03007995.2010.486301 (2010).
368 Forslund, C., Bylander, B. & Aspenberg, P. Indomethacin and celecoxib improve tendon healing in rats. *Acta Orthopaedica Scandinavica* **74**, 465-469, doi:10.1080/00016470310017802 (2003).
369 Nishimura, K., Nakamura, R. M. & Dizerega, G. S. IBUPROFEN INHIBITION OF POSTSURGICAL ADHESION FORMATION - A TIME AND DOSE-RESPONSE BIOCHEMICAL EVALUATION IN RABBITS. *Journal of Surgical Research* **36**, 115-124, doi:10.1016/0022-4804(84)90076-3 (1984).
370 Vandersalm, T. J., Okike, O. N., Marsicano, T. H., Compton, C. & Espinoza, E. PREVENTION OF POSTOPERATIVE PERICARDIAL ADHESIONS - AN ANIMAL STUDY. *Archives of Surgery* **121**, 462-467 (1986).
371 Kulick, M. I., Brazlow, R., Smith, S. & Hentz, V. R. INJECTABLE IBUPROFEN - PRELIMINARY EVALUATION OF ITS ABILITY TO DECREASE PERITENDINOUS ADHESIONS. *Ann Plast Surg* **13**, 459-467, doi:10.1097/00000637-198412000-00001 (1984).
372 Kulick, M. I., Smith, S. & Hadler, K. ORAL IBUPROFEN - EVALUATION OF ITS EFFECT ON PERITENDINOUS ADHESIONS AND THE BREAKING STRENGTH OF A TENORRHAPHY. *J. Hand Surg.-Am. Vol.* **11A**, 110-120 (1986).
373 Gerstenfeld, L. C. *et al.* Differential inhibition of fracture healing by non-selective and cyclooxygenase-2 selective non-steroidal anti-inflammatory drugs. *JOURNAL OF ORTHOPAEDIC RESEARCH* **21**, 670-675, doi:10.1016/s0736-0266(03)00003-2 (2003).
374 Goodman, S. *et al.* COX-2 selective NSAID decreases bone ingrowth in vivo. *JOURNAL OF ORTHOPAEDIC RESEARCH* **20**, 1164-1169, doi:10.1016/s0736-0266(02)00079-7 (2002).
375 Harder, A. T. & An, Y. H. H. The mechanisms of the inhibitory effects of nonsteroidal anti-inflammatory drugs on bone healing: A concise review. *Journal of Clinical Pharmacology* **43**, 807-815, doi:10.1177/0091270003256061 (2003).
376 Hu, C. *et al.* Long-term drug release from electrospun fibers for in vivo inflammation prevention in the prevention of peritendinous adhesions. *Acta biomaterialia* **9**, 7381-7388, doi:10.1016/j.actbio.2013.03.040 (2013).
377 Liu, S. *et al.* Prevention of Peritendinous Adhesions with Electrospun Ibuprofen-Loaded Poly(L-Lactic Acid)-Polyethylene Glycol Fibrous Membranes. *Tissue Eng. Part A* **19**, 529-537, doi:10.1089/ten.tea.2012.0208 (2013).

378 Jiang, S. *et al.* Down-regulating ERK1/2 and SMAD2/3 phosphorylation by physical barrier of celecoxib-loaded electrospun fibrous membranes prevents tendon adhesions. *Biomaterials* **35**, 9920-9929, doi:10.1016/j.biomaterials.2014.08.028 (2014).

379 Lui YS, L. M., Loo SC. Sustained-release of naproxen sodium from electrospun-aligned PLLA-PCL scaffolds. *Journal of tissue engineering and regenerative medicine*, doi:10.1002/term.2000 (2015).

380 Tsai, W. C. *et al.* Ibuprofen inhibition of tendon cell migration and down-regulation of paxillin expression. *JOURNAL OF ORTHOPAEDIC RESEARCH* **24**, 551-558, doi:10.1002/jor.20069 (2006).

381 Tsai, W.-C. *et al.* Ibuprofen Upregulates Expressions of Matrix Metalloproteinase-1,-8,-9, and-13 without Affecting Expressions of Types I and III Collagen in Tendon Cells. *JOURNAL OF ORTHOPAEDIC RESEARCH* **28**, 487-491, doi:10.1002/jor.21009 (2010).

382 Liu, S., Maheshwari, R. & Kiick, K. L. Polymer-Based Therapeutics. *Macromolecules* **42**, 3-13, doi:10.1021/ma801782q (2009).

383 Uhrich, K. E., Cannizzaro, S. M., Langer, R. S. & Shakesheff, K. M. Polymeric systems for controlled drug release. *Chemical Reviews* **99**, 3181-3198, doi:10.1021/cr940351u (1999).

384 Zhang, Y., Chan, H. F. & Leong, K. W. Advanced materials and processing for drug delivery: The past and the future. *Advanced drug delivery reviews* **65**, 104-120, doi:10.1016/j.addr.2012.10.003 (2013).

385 Dash, T. K. & Konkimalla, V. B. Poly-epsilon-caprolactone based formulations for drug delivery and tissue engineering: A review. *Journal of Controlled Release* **158**, 15-33, doi:10.1016/j.jconrel.2011.09.064 (2012).

386 Heller, J. CONTROLLED RELEASE OF BIOLOGICALLY-ACTIVE COMPOUNDS FROM BIOERODIBLE POLYMERS. *Biomaterials* **1**, 51-57, doi:10.1016/0142-9612(80)90060-5 (1980).

387 Heller, J. Biodegradable polymers in controlled drug delivery. *Critical reviews in therapeutic drug carrier systems* **1**, 39-90 (1984).

388 Panyam, J. & Labhasetwar, V. Biodegradable nanoparticles for drug and gene delivery to cells and tissue. *Advanced drug delivery reviews* **55**, 329-347, doi:10.1016/s0169-409x(02)00228-4 (2003).

389 Kumar, N., Langer, R. S. & Domb, A. J. Polyanhydrides: an overview. *Advanced drug delivery reviews* **54**, 889-910, doi:10.1016/s0169-409x(02)00050-9 (2002).

390 Ringsdorf, H., Schlarb, B. & Venzmer, J. MOLECULAR ARCHITECTURE AND FUNCTION OF POLYMERIC ORIENTED SYSTEMS - MODELS FOR THE STUDY OF ORGANIZATION, SURFACE RECOGNITION, AND DYNAMICS OF BIOMEMBRANES. *Angewandte Chemie-International Edition* **27**, 113-158, doi:10.1002/anie.198801131 (1988).

391 Duncan, R. The dawning era of polymer therapeutics. *Nature Reviews Drug Discovery* **2**, 347-360, doi:10.1038/nrd1088 (2003).

392 Liechty, W. B., Kryscio, D. R., Slaughter, B. V. & Peppas, N. A. Polymers for Drug Delivery Systems. *Annual Review of Chemical and Biomolecular Engineering, Vol 1* **1**, 149-173, doi:10.1146/annurev-chembioeng-073009-100847 (2010).

393 Stebbins, N. D., Yu, W. & Uhrich, K. E. Enzymatic Polymerization of an Ibuprofen-Containing Monomer and Subsequent Drug Release. *Macromolecular bioscience* **15**, 1115-1124, doi:10.1002/mabi.201500030 (2015).

394 Veronese, F. M. & Morpurgo, M. Bioconjugation in pharmaceutical chemistry. *Farmaco* **54**, 497-516, doi:10.1016/s0014-827x(99)00066-x (1999).

395 Larson, N. & Ghandehari, H. Polymeric Conjugates for Drug Delivery. *Chemistry of Materials* **24**, 840-853, doi:10.1021/cm2031569 (2012).

396 Veronese, F. M. *et al.* PEG-doxorubicin conjugates: Influence of polymer structure on drug release, in vitro cytotoxicity, biodistribution, and antitumor activity. *Bioconjugate Chemistry* **16**, 775-784, doi:10.1021/bc040241m (2005).

397 D'Souza, A. J. M. & Topp, E. M. Release from polymeric prodrugs: Linkages and their degradation. *Journal of Pharmaceutical Sciences* **93**, 1962-1979, doi:10.1002/jps.20096 (2004).
398 Babazadeh, M., Sheidaei, M., Abbaspour, S. & Edjlali, L. Synthesis, characterization, and in vitro evaluation of new Ibuprofen polymeric prodrugs based on 2-hydroxypropyl methacrylate. *Scientia pharmaceutica* **81**, 281-296, doi:10.3797/scipharm.1204-14 (2013).
399 Stebbins, N. D., Yu, W. L. & Uhrich, K. E. Linear, Mannitol-Based Poly(anhydride-esters) with High Ibuprofen Loading and Anti-Inflammatory Activity. *Biomacromolecules* **16**, 3632-3639 (2015).
400 Kolhe, P., Misra, E., Kannan, R. M., Kannan, S. & Lieh-Lai, M. Drug complexation, in vitro release and cellular entry of dendrimers and hyperbranched polymers. *International Journal of Pharmaceutics* **259**, 143-160, doi:10.1016/s0378-5173(03)00225-4 (2003).
401 Vasey, P. A. *et al.* Phase I clinical and pharmacokinetic study of PK1 N-(2-hydroxypropyl)methacrylamide copolymer doxorubicin : First member of a new class of chemotherapeutic agents - Drug-polymer conjugates. *Clinical Cancer Research* **5**, 83-94 (1999).
402 Ziegler, M. J. & Matyjaszewski, K. Atom transfer radical copolymerization of methyl methacrylate and n-butyl acrylate. *Macromolecules* **34**, 415-424, doi:10.1021/ma001182k (2001).
403 Davaran, S., Rashidi, M. R., Hanaee, J., Hamidi, A. A. & Hashemi, M. Synthesis and hydrolytic behavior of ibuprofen prodrugs and their PEGylated derivatives. *Drug Delivery* **13**, 383-387, doi:10.1080/10717540500456007 (2006).
404 Gilligan, V. (ed Vince Gilligan) (AMC, 2008).